Faculty of Engineering

Department of Architecture and Built Environment

A novel Hybrid Radiative and Ventilative Cooling System Integrated with Latent Heat Storage for Buildings in Hot-Arid Climates

Rami Zein Elabdein Yousif Zein Elabdein

(BSc, MSc)

Thesis submitted in partial fulfilment of the requirements for the award of the degree of Doctorate of Philosophy in Sustainable Energy Technology

October 2018

Abstract

The use of phase change material (PCM) as potential energy storage for cooling of buildings using night low-temperature air is one of the promising sustainable strategies referred to as “the free cooling of buildings”. Application of this strategy in hot climates is not exploited, and most of the published work has been carried out in moderate and continental climates. Moreover, the free cooling potential is insufficient under extreme summer conditions, owing to the small temperature difference between the PCM and the ambient air in addition to the limited available charging time. Therefore, with the aim of sustaining and enhancing the free cooling potential in such disadvantageous conditions, an innovative hybrid nocturnal radiative and ventilative cooling system using latent heat storage (NRV-LHS) has been proposed in this study. Such a combined system has not been adduced in previous studies.

In this research, the nocturnal radiative and free cooling potential in hot-arid regions is assessed. According to the local climate and thermal comfort conditions of the case study, a paraffin-based RT28HC PCM of a transition temperature range of 27-29 °C was considered. Thermal energy storage (TES) system comprising a number of PCM panels has been proposed and assessed using transient computational fluid dynamics modelling to optimise the geometrical configuration under various inlet air conditions. The proposed PCM storage system has been investigated experimentally to evaluate the charging and discharging behaviour of the PCM for a range of PCM modules arrangements. The operational performance of the hybrid NRV-LHS system has been evaluated experimentally under hot and moderate summer conditions of hot-arid climate for various scenarios of free and radiative cooling operation modes.

The parametric study results have shown that a compact TES system design made of thin PCM modules and narrow air flow channels is more effective in accelerating the PCM charging process. The difference between the PCM transition temperature and the inlet air temperature, along with the air flow rate play a significant role in the heat transfer rate during both transformation phases.

The findings have indicated that the proposed NRV-LHS system has a great potential to operate satisfactorily under the severe summer conditions in hot-arid regions. The system can improve the thermal performance of the free cooling systems by extending the charging period beyond the free cooling range. The system also enhances the heat transfer rate and minimises the effect of PCM supercooling, which contributes positively to the charging effectiveness. For the summer period (May-October), the system could fulfil up to 57% of the cooling load. The estimated COP of the system varied between 5.82 and 9.01. This performance could allow the system to maintain the thermal comfort, leading to substantial energy savings up to 76% compared to conventional air conditioning systems. The outcomes of this research would be beneficial to introduce an appropriate design of PCM-air heat exchangers combined with an air-based nocturnal radiative cooling system, applicable for real implementation in buildings, especially in hot-arid regions.

Acknowledgements

Firstly and foremost, praise be to Allah, as without him, this work would never be accomplished.

My sincere thankfulness and appreciation to my supervisor Dr Siddig Omer for his continuous support and guidance, and for the trust, immense knowledge, and motivation that he provided me. My appreciation also extends to my supervisor Dr Guohui Gan for his support.

My acknowledgement to the University of Nottingham (UK) for the PhD scholarship, and to the University of Khartoum and the Ministry of Higher Education and Scientific Research of Sudan for the financial support and for giving me the opportunity to reach this stage.

My sincere thankfulness to all my friends and colleagues at the University of Nottingham for their support, assistance, and good memories.

My deepest gratitude to all my family, especially my parents, wife, and siblings for their continuous encouragement, and prayers. Also, thankfulness to my immediate family for the beautiful memories throught my study period.

Table of contents

Abstract ..... ***i***

Acknowledgements ..... ***iii***

Table of contents ..... ***iv***

List of tables ..... ***ix***

List of figures ..... ***xi***

List of publications ..... ***xxi***

Nomenclature ..... ***xxii***

Chapter 1 Introduction ***1***

1.1 Introduction 1

1.2 An overview 2

1.3 Hypothesis 5

1.4 Aim and objectives 9

1.5 Novelty and contribution 10

1.6 Thesis structure 11

Chapter 2 Review of Nocturnal Radiative Cooling Strategy ***13***

2.1 Introduction 13

2.2 Passive cooling strategies 14

2.2.1 Heat gain prevention techniques 14

2.2.2 Heat gain modulation techniques 15

2.3 Natural cooling strategies 16

2.3.1 Comfort ventilation 17

2.3.2 Nocturnal ventilative cooling 17

2.3.3 Evaporative cooling 18

2.3.4 Nocturnal radiant cooling 18

2.3.5 Ground cooling 18

2.4 Nocturnal radiant cooling 19

2.4.1 Mechanism of radiant cooling 19

2.4.2 Atmospheric incoming long-wave radiation 20

2.4.3 Potential of radiative cooling 22

2.4.4 Application methods of radiant cooling 23

2.5 Published studies in radiant cooling with lightweight radiators 29

2.6 Discussion of design factors influencing the radiative cooling performance 42

2.6.1 Effect of thermal mass and storage 42

2.6.2 Reduction of convective heat transfer with the ambient air 45
2.6.3 Enhancement of nocturnal radiators emissivity 48
2.6.4 Effect of radiator tilt angle 51
2.7 Summary 52
Chapter 3 Review of Latent Heat Storage based Free Cooling Systems 54
3.1 Introduction 54
3.2 An overview of thermal energy storage (TES) 55
3.2.1 Thermochemical energy systems (TCES) 56
3.2.2 Sensible heat storages (SHS) 56
3.2.3 Latent heat storages (LHS) 57
3.3 Overview of latent heat storage (LHS) for building application 58
3.3.1 Solid-Solid PCM 60
3.3.2 Solid-Gas and Liquid-Gas PCM 60
3.3.3 Solid-Liquid PCM 60
3.4 Methods of PCM application in buildings 69
3.4.1 Impregnation of PCM into the construction materials 69
3.4.2 Integration of PCM into the building envelope 69
3.4.3 Other concepts of PCM applications for building cooling and heating 71
3.5 Research development on PCM based free cooling of buildings 73
3.6 Discussion of the factors affecting performance and application of PCM in free cooling systems 104
3.6.1 Climate conditions 104
3.6.2 PCM transition temperature 104
3.6.3 Encapsulation of PCMs 106
3.6.4 Heat transfer of the PCM-air heat exchangers 108
3.6.5 Stability of PCMs 110
3.6.6 Economic aspect of free cooling systems 110
3.7 Summary 113
Chapter 4 Proposed System Design and Research Methodology 115
4.1 Introduction 115
4.2 Description of the proposed NRV-LHS system design 116
4.2.1 Design concept 116
4.2.2 System components 116
4.2.3 Operation principles 118
4.3 Research methodology 121
4.3.1 Phase I: Literature review and theoretical analysis 121

4.3.2 Phase II: Assessment of night cooling potential 124
4.3.3 Phase III: Design and development of the NRV-LHS system 125
Chapter 5 Evaluation of Night Cooling Potential in Hot-Arid Climate..... 128
5.1 Introduction 128
5.2 Evaluation of free cooling potential 129
5.2.1 Identification of human thermal comfort 129
5.2.2 Microclimate conditions 131
5.2.3 Investigation of building thermal performance 134
5.3 Evaluation of nocturnal radiative cooling potential 142
5.3.1 Applicability of radiative cooling in hot-arid climate 142
5.3.2 System description 144
5.3.3 Modelling of the radiative cooling system 145
5.3.4 Results and discussion of the radiative cooling system 153
5.4 Summary 162
Chapter 6 CFD Modelling of the PCM-Air Heat Exchanger..... 163
6.1 Introduction 163
6.2 PCM selection 164
6.3 Sizing of the TES unit 166
6.4 Geometry description and modelling assumptions 168
6.5 Computational methodology 170
6.5.1 Models and governing equations 170
6.5.2 Boundary conditions 173
6.5.3 Solution methods 173
6.5.4 Initial settings and base case conditions 174
6.6 Independence tests 176
6.6.1 Time independence study 176
6.6.2 Grid independence study 178
6.7 Results and discussion 179
6.7.1 Temperature variation in the PCM-air heat exchanger 179
6.7.2 Influence of inlet air temperature 183
6.7.3 Influence of air flow rate 189
6.7.4 Influence of TES geometrical configuration 193
6.8 Summary 202

Chapter 7 Experimental Investigation of the PCM-Air Heat Exchanger under Steady-state Inlet Air Conditions ***203***
7.1 Introduction 203
7.2 Description of the system 204
7.2.1 TES unit 204
7.2.2 Air circulating fan 208
7.2.3 Air ducting system 209
7.3 Experiment setup and operation 210
7.4 Instrumentation setup and measurements 213
7.5 Experiments procedure and setup 216
7.5.1 Steady-state inlet operating conditions 216
7.5.2 Transient inlet operating conditions 217
7.6 Assessment of the PCM charging and discharging process 218
7.7 Results and discussion of PCM charging 220
7.7.1 Charging process 220
7.7.2 Influence of inlet operating conditions 225
7.7.3 Influence of air channels height 229
7.7.4 Influence of PCM supercooling 232
7.8 Results and discussion of PCM discharging 234
7.8.1 Discharging process 234
7.8.2 Influence of inlet operating conditions 239
7.8.3 Influence of air channels height 243
7.9 A comparison of the experimental and modelling results 247
7.9.1 Results of the PCM charging 247
7.9.2 Results of the PCM discharging 250
7.10 Summary 253
Chapter 8 Experimental Investigation of the PCM-Air Heat Exchanger under transient Inlet Air Conditions ***255***
8.1 Introduction 255
8.2 Experiments procedure and operation setup 256
8.3 Assessment of the PCM charging process 259
8.4 Impact of the surrounding air on the PCM charging 260
8.5 Results and discussion of PCM charging under hot conditions 261
8.5.1 Operation under free cooling mode 261
8.5.2 Operation under radiative cooling mode 264
8.6 Results and discussion of PCM charging under moderate conditions 269
8.6.1 Operation under free cooling mode 269

8.6.2 Operation under radiative cooling mode 272
8.7 Summary 277
Chapter 9 Energy Saving Potential of the NRV-LHS System 278
9.1 Introduction 278
9.2 Performance evaluation 279
9.3 Pressure analysis and fan power consumption 281
9.4 Cooling capacity of the proposed system 283
9.5 Comparison with conventional air conditioning systems 287
Chapter 10 Conclusions and Future Work 288
10.1 Conclusions 289
10.2 Future work 292
References 293
Appendix 326
A: Fan specifications (17106010 Vent-Axia) 326

List of tables

Table 2.1: Classification of the natural cooling strategies and the associated heat sink (La Roche, 2011: p222).....16
Table 2.2: Potential cover materials for radiative cooling. 46
Table 2.3: Optical properties of some surfaces (Moss, 2002: p.70).....49
Table 2.4: Selective surface coating materials and their potential radiative cooling performance at an ambient temperature of 25 °C. 50
Table 3.1: Comparison of required mass and weight of LHS and SHS substances to store **106** kJ with $\Delta T = 15$ K (Hasnain, 1998, Khadiran et al., 2016).....58
Table 3.2: Organic Solid-Liquid PCMs with phase change temperature between 19 and 30 ºC (Tyagi and Buddhi, 2007, Kenisarin and Mahkamov, 2007, Verma and Singal, 2008, Raj and Velraj, 2010, Cabeza et al., 2011, Riffat et al., 2013). 64
Table 3.3: Inorganic Solid-Liquid PCMs with phase change temperature between 19 and 30 ºC (Zalba et al., 2003, Pasupathy et al., 2008, Sharma et al., 2009, Cabeza et al., 2011). 66
Table 3.4: Eutectic PCMs with phase change temperature between 19 and 30 ºC (Zalba et al., 2003, Sharma et al., 2009, Cabeza et al., 2011, Veerakumar and Sreekumar, 2016). 67
Table 3.5: Available commercial PCM within the phase change temperature range 19-30°C. 68
Table 5.1: Comfort temperature ranges for Khartoum adopted by the international standards and Merghani (2001).....131
Table 5.2: Internal load and environmental comfort settings used in DesignBuilder software (CIBSE, 2006:p.1-3). 136
Table 5.3: Assigned construction materials specifications. 137
Table 5.4: Details of the radiative cooling system design and operating conditions. 145
Table 5.5: Air temperature drop and cooling rate obtained by radiative cooling in summer.....162
Table 6.1: Thermo-physical properties of the RT28HC PCM (RUBITHERM).....165
Table 6.2: Coordinates of the monitored points and rakes.....175

Table 6.3: Mesh information. 178
Table 6.4: Solidification time under tested inlet temperatures at an air flow rate of 213 L/s. 184
Table 6.5: Melting time and comfort period maintained under tested inlet air temperatures at an air flow rate of 53 L/s. 188
Table 6.6: Tested air flow rates. 189
Table 6.7: Solidification time under tested air flow rates at an inlet temperature of 23 °C. 190
Table 6.8: Melting time and comfort durations under tested air flow rates at inlet air temperature of 36 °C. 192
Table 6.9: Geometrical details of the tested cases. 193
Table 7.1: Geometrical parameters of the TES system 207
Table 7.2: Inlet air conditions for the charging process. 225
Table 7.3: Inlet air conditions for the discharging process. 239
Table 8.1: Total PCM cooling rate and the corresponding charging period under hot summer conditions. 268
Table 8.2: Total PCM cooling rate and the corresponding charging period under moderate summer conditions. 276
Table 9.1: Suitable conditions for PCM charging in a reference day during summer and transitional months in a hot-arid climate of Khartoum. 279
Table 9.2: Predicted pressure drop and fan power consumption for different air flow rates. 281
Table 9.3: Predicted pressure drop and fan power consumption for different TES configurations. 283
Table 9.4: A comparison of performance for different TES configurations and operating conditions in summer of hot-arid climates (May-June). 284
Table 9.5: Performance of the optimum hybrid cooling system during the overheated months. 286

List of figures

Figure 1.1: Estimated global mean temperature change 1880-2017, updated by (NASA) from (Hansen et al., 2010). 2
Figure 1.2: World fossil fuel consumption since 1880 (Smil, 2016). 3
Figure 1.3: Percentage contributions of world primary energy supply by fuel in the year 2015 (IEA, 2017b: p.6). 3
Figure 1.4: Energy use by sector in Sudan (a hot-arid region) in the year 2015 (AUE, 2015:p. 8). 4
Figure 2.1: Suitable outdoor conditions for natural cooling strategies application (La Roche, 2011: p.223) 17
Figure 2.2: Heat transfer on the roof surface (a) day and (b) night. 19
Figure 2.3: Radiation spectrum of earth, atmosphere, and sun (Hoffman and Simmons, 2008). 21
Figure 2.4: Concrete roof with moveable thermal insulation for radiative cooling of buildings (Givoni, 1994: p.84). 24
Figure 2.5: Lightweight metallic radiator for radiant cooling of buildings (Givoni, 1994: p.86). 26
Figure 2.6: Unglazed solar collector application for radiant cooling of buildings (Givoni, 1994: p.87). 27
Figure 2.7: Test room cooled by an asbestos-cement radiator (Givoni, 1994: p.113). 30
Figure 2.8: Roof radiation trap concept for (a) cooling and (b) heating in buildings (Givoni, 1994: p.117). 31
Figure 2.9: Corrugated metal roof with internal adjustable insulation for radiant cooling of buildings (Givoni, 1994: p.120). 32
Figure 2.10: Test bed with adjustable insulation panel and water-filled bottles as thermal storage for radiant cooling (Gulich et al., 1996). 34
Figure 2.11: Installation of a radiator with water pipes on the building roof (Dimoudi and Androutsopoulos, 2006). 37
Figure 2.12: Calculated velocities and air flow pattern at wind speed 2.7 m/s for different wind shield heights 25, 50, and 100 mm. 38

Figure 2.13: Radiant cooling system proposed by Bagiorgas and Mihalakakou (2008). 39
Figure 2.14: Photographs of the three radiative panels investigated by Tevar et al. (2015). 40
Figure 2.15: Cooling power and energy savings percentages by radiant cooling for different cities in Malaysia (Hanif et al., 2014). 40
Figure 2.16: Monthly average night radiant cooling potential in different cities in India (Panchabikesan et al., 2017b). 41
Figure 2.17: Radiant cooling system coupled with water-filled bags above a metallic roof (Givoni, 1994: p.105). 42
Figure 2.18: Radiant cooling system coupled with roof embedded water pipes (Dimoudi and Androutsopoulos, 2006). 43
Figure 2.19: Radiant cooling system coupled with a water storage tank (Al-Nimr et al., 1998). 44
Figure 2.20: Methods utilised to minimise convective heat transfer with ambient air in radiative cooling systems (Golaka and Exell, 2007, Gentle et al., 2013). 48
Figure 3.1: Classification of thermal energy storage methods (Baylin, 1979: p.2, Mehling and Cabeza, 2008: p.1, Sharma et al., 2009). 55
Figure 3.2: Latent and sensible heat storage variation with temperature (Mehling and Cabeza, 2008:p.3, Gil et al., 2010).....58
Figure 3.3: Classification of the Solid-Liquid PCMs (Su et al., 2015).....61
Figure 3.4: Classes of available PCM based on their melting temperatures range and enthalpy (Baetens et al., 2010). 62
Figure 3.5: PCM integration into buildings' envelope for heating and cooling requirements (Zhang et al., 2007). 71
Figure 3.6: Incorporation of PCM in (a) a trombe wall (Zalewski et al., 2012), and in (b) a solar chimney (Liu and Li, 2015). 72
Figure 3.7: A typical operation of free cooling systems incorporated PCM storage; (a) charging, and (b) discharging (Hed and Bellander, 2006). 73
Figure 3.8: (a) Charging, and (b) discharging of the heat pipe/PCM cooling system proposed by Turnpenny et al. (2000). 75

Figure 3.9: An arrangement of the heat pipe/PCM units below a ceiling fan proposed by Turnpenny et al. (2001).....76
Figure 3.10: Schematic of the NVP system proposed by Yanbing et al. (2003). 77
Figure 3.11: The free cooling system proposed by Zalba et al. (2004); (a) the TES unit configuration, (b) schematic of a real installation, and (c) the temperature change during solidification and melting process. 78
Figure 3.12: Experimental apparatus of the free cooling system proposed by Takeda et al. (2004). 80
Figure 3.13: An underfloor cooling system incorporated packed bed PCM granules proposed by Nagano et al. (2006), (2007).....81
Figure 3.14: The free cooling system proposed by Stritih and Butala (2007); (a) the experimental setup and (b) the PCM storage configuration with fins. 82
Figure 3.15: Operational principles of the free cooling system proposed by Medved and Arkar (2008).....84
Figure 3.16: The real-scale PCM prototypes investigated by Lazaro et al. (2009b); (a) aluminium pouches filled with an inorganic PCM, and (b) aluminium panels filled with organic PCM. 85
Figure 3.17: Experimental setup of the PCM-air heat exchanger with rigid panels developed by Dolado et al. (2011a). 86
Figure 3.18: Experimental setup of the PCM storage proposed by Waqas and Kumar (2011a). 87
Figure 3.19: (a) Schematic of the modular PCM heat exchanger developed by Raj and Velraj (2011), and (b) the temperature contours computed by CFD modelling. 89
Figure 3.20: (a) Experimental setup and (b) the PCM heat exchanger model proposed by Jaber and Ajib (2012).....91
Figure 3.21: (a) Arrangement of multiple PCM slabs, and (b) schematic of the free cooling system proposed by Mosaffa et al. (2013a), (2013b).....92
Figure 3.22: The TES system of rectangular tubes filled with PCM developed by Rouault et al. (2013).....93
Figure 3.23: (a) Night and (b) daytime operation of the free cooling system proposed by Darzi et al. (2013). 94

Figure 3.24: The configuration of the proposed solar air collector and the PCM storage investigated by Waqas et al. (2015).....95
Figure 3.25: Experimental setup of the system proposed by Iten and Liu (2015).....97
Figure 3.26: (a) Tested configurations and (b) flow visualisation results of the system developed by Osterman et al. (2015b). 98
Figure 3.27: Configuration of the LHTES apparatus designed by Mirahmad et al. (2016). 99
Figure 3.28: (a) Schematic and (b) view of the free cooling system proposed by Muthuvelan et al. (2016). 100
Figure 3.29: Experimental setup of the free cooling system proposed by Rajagopal (2014), (2016). 101
Figure 3.30: Experimental setup of the free cooling system proposed by Alam (2017)**.** 102
Figure 3.31: Experimental setup of the free cooling system proposed by Panchabikesan et al. (2017a), (2018). 103
Figure 3.32: Some of the PCM encapsulation techniques available in the market. 107
Figure 3.33: Methods utilised for heat transfer enhancements in PCM applications (Agyenim et al., 2010). 109
Figure 3.34: Cost breakdown for the free cooling systems developed by (a) Zalba et al. (2004), and (b) Osterman et al. (2015a). 112
Figure 4.1: Charging and discharging modes of the NRV-LHS system.....116
Figure 4.2: Main components of the NRV-LHS system.....117
Figure 4.3: Operation principles of the NRV-LHS system.....119
Figure 4.4: Diagram showing the overall research methodology. 121
Figure 4.5: (a) Part of the housing complex, (b) the selected house view. 123
Figure 4.6: Floor plans of the selected house.....123
Figure 5.1: Factors affecting the potential of free cooling of buildings in any location. 129
Figure 5.2: Summer (red) and winter (blue) comfort zone for Khartoum; (a) demarcated by Merghani (2001), and (b) recommended by ASHRAE standards. ..130
Figure 5.3: Monthly data of dry-bulb temperature and the precipitation rate for the site of Khartoum (Khartoum airport meteorological station). 132

Figure 5.4: Average dry-bulb temperature in Khartoum during (a) summer and transitional months, and (b) winter months (Khartoum airport meteorological station). 133
Figure 5.5: (a) Model of the house in DesignBuilder, (b) diagram of sun path over Khartoum. 135
Figure 5.6: Comparison of the ambient air temperature used in the simulation to actual data measured by Khartoum airport meteorological station. 135
Figure 5.7: Annual cooling load of the building under various passive cooling techniques.....138
Figure 5.8: Monthly cooling load of the building. 139
Figure 5.9: Daily cooling load of all building spaces on the average summer day.140
Figure 5.10: (a) Indoor air temperature and (b) cooling load of the selected room on a typical summer day. 141
Figure 5.11: Monthly data of (a) precipitation rate, (b) dew point temperature (c) cloud cover percentage, and (d) wind speed in Khartoum. 143
Figure 5.12: Geometrical configuration of the radiative cooling system. 144
Figure 5.13: Heat transfer balance of the radiative cooling system. 146
Figure 5.14: Variation of the cooling rate per unit area and the outlet air temperature with the radiator emissivity. 153
Figure 5.15: Variation of the cooling rate per unit area and the outlet air temperature with the air flow rate. 154
Figure 5.16: Variation of the cooling rate per unit area and the outlet air temperature with the air duct height. 155
Figure 5.17: Variation of the radiative cooling rate per unit area, the sky temperature, and the outlet air temperature with the cloudiness factor. 156
Figure 5.18: Variation of the cooling rate per unit area, the radiator stagnation temperature, and the outlet air temperature with the wind speed. 157
Figure 5.19: Stagnation temperature of the radiator with and without windscreen for different wind speeds. 158
Figure 5.20: Variation of the radiative cooling rate per unit area, the sky temperature, and the outlet air temperature with the dew point temperature. 159

Figure 5.21: The hourly profile of the air temperature drop by the proposed radiative cooling system during summer in Khartoum. 161
Figure 6.1: Enthalpy-Temperature curve of the RT28HC PCM (RUBITHERM). 165
Figure 6.2: (a) Indoor air temperature and (b) cooling load of the room on a typical summer day. 167
Figure 6.3: Configuration of the modular PCM heat exchanger.....168
Figure 6.4: Details and boundary conditions of the 2D model created in the ANSYS DesignModeler. 169
Figure 6.5: PCM mean liquid fraction at different time-steps during the (a) charging and (b) discharging process. 177
Figure 6.6: Mean liquid fraction of the PCM during a charging phase for different grid sizes. 178
Figure 6.7: Temperature variation at three PCM locations during the charging process. 180
Figure 6.8: Temperature variation after 2 hours of the charging process. 180
Figure 6.9: Temperature variation at three PCM locations during the discharging process. 181
Figure 6.10: Temperature variation after 2 hours of the discharging process. 182
Figure 6.11: Variation of (a) PCM liquid fraction and (b) outlet air temperature for different inlet air temperatures during the charging process. 184
Figure 6.12: Contours of (a) PCM liquid fraction (b) temperature after 4 hours of charging for inlet air temperatures 21, 23, 25, 26, and 27 °C and at air flow rate of 213 L/s. 185
Figure 6.13: Variation of (a) PCM liquid fraction and (b) outlet air temperature for different inlet air temperatures during the discharging process. 187
Figure 6.14: Contours of (a) PCM liquid fraction (b) temperature after 6 hours of discharging for inlet air temperatures 34, 36, and 38 °C and at air flow rate of 53 L/s. 188
Figure 6.15: Variation of (a) PCM liquid fraction and (b) outlet air temperature for different air flow rates during the charging process.....190
Figure 6.16: Variation of (a) PCM liquid fraction and (b) outlet air temperature for different air flow rates during the discharging process. 192

Figure 6.17: Variation of (a) PCM liquid fraction and (b) outlet air temperature during the charging process for different TES configurations. 194
Figure 6.18: PCM solidification time for different TES configurations.....195
Figure 6.19: Contours of temperature distribution in the tested TES configurations after 4 hours of charging at inlet air temperature 23 °C and air flow rate 213 L/s. .196
Figure 6.20: Variation of (a) PCM liquid fraction and (b) outlet air temperature during the discharging process for different TES configurations.....198
Figure 6.21: PCM melting time and comfort duration for different TES configurations.....199
Figure 6.22: Contours of temperature distribution in the tested TES configurations after 4 hours of discharging at inlet air temperature 36 °C and air flow rate 53 L/s. 200
Figure 7.1: A 3D view of the experimental PCM cooling storage system. 204
Figure 7.2: The CSM unit produced by Rubitherm GmbH (RUBITHERM). 205
Figure 7.3: Details of the proposed TES unit.....206
Figure 7.4: Photographs of the stainless steel supporting frame with PCM shelves. 207
Figure 7.5: Details of the three tested PCM modules arrangements.....208
Figure 7.6: Photographs of the (a) axial flow fan and (b) the fan speed controller.208
Figure 7.7: Photographs of (a) the regulating damper and (b) the divergent duct with air guides. 209
Figure 7.8: Insulation of the TES system.....210
Figure 7.9: Rig connection with the environmental chamber. 211
Figure 7.10: A schematic and a photograph of the experiment setup. 212
Figure 7.11: Photographs showing the measurement tools; (a) Type K a stick probe thermocouple, (b) Type K a copper probe thermocouple, (c) Gauge pressure transducer, (d) DT 800 Data tacker, (e) a handheld van anemometer. 214
Figure 7.12: A drawing showing the positions of thermocouples and pressure sensors. 215
Figure 7.13: Plan of the experiments under steady-state inlet operating conditions. 217
Figure 7.14: Heat transfer balance of the PCM-air heat exchanger. 218

Figure 7.15: Variation of the PCM modules temperatures during the charging process at four locations along (a) the 4th-row modules "middle" (b) the 8th-row modules "top". 221
Figure 7.16: Air temperature variation in the test rig during the charging phase. .. 223
Figure 7.17: Surrounding air temperature during charging experiments of the three tested TES configurations. 224
Figure 7.18: Heat exchange rate with the surrounding during charging experiments of the three tested TES configurations. 224
Figure 7.19: Impact of inlet air temperature on PCM charging; variation in (a) the outlet air temperature, and (b) the PCM cooling rate. 226
Figure 7.20: Impact of air flow rate on PCM charging; variation in (a) the outlet air temperature, and (b) the PCM cooling rate. 227
Figure 7.21: PCM solidification period under operating conditions of the charging process. 228
Figure 7.22: Impact of air channels height on PCM charging; variation in (a) the outlet air temperature, and (b) the PCM cooling rate. 230
Figure 7.23: Sensitivity of PCM solidification time to the air channels height under various (a) inlet air temperatures, and (b) air flow rates. 231
Figure 7.24: The supercooling at PCM-mid3 under adopted (a) inlet air temperatures, and (b) air flow rates. 233
Figure 7.25: Variation of the PCM modules temperatures during the discharging process at four locations along (a) the 4th-row modules "middle" (b) the 8th-row modules "top" 235
Figure 7.26: Air temperature variation in the test rig during the discharging phase. 237
Figure 7.27: Surrounding air temperature during discharging experiments of the three tested TES configurations. 238
Figure 7.28: Heat exchange rate with the surrounding during discharging experiments of the three tested TES configurations. 238
Figure 7.29: Impact of inlet air temperature on PCM discharging; variation in (a) the outlet air temperature, and (b) the PCM heating rate. 240

Figure 7.30: Impact of air flow rate on PCM discharging; variation in (a) the outlet air temperature (b) the PCM heating rate. 241
Figure 7.31: PCM melting period under operating conditions of the discharging process. 242
Figure 7.32: Comfort duration under operating conditions of the discharging process. 243
Figure 7.33: Impact of air channels height on PCM discharging; variation in (a) the outlet air temperature, and (b) the PCM heating rate. 244
Figure 7.34: Sensitivity of PCM melting time to the air channels height under various (a) inlet air temperatures, and (b) air flow rates. 245
Figure 7.35: Influence of air channels height on the comfort level period under various (a) inlet air temperatures, and (b) air flow rates. 246
Figure 7.36: Details, boundary conditions, and measurement locations of the tested geometry in ANSYS software. 247
Figure 7.37: Charging process; (a) PCM temperature at PCM_A, (b) PCM temperature at PCM_B, and (c) Outlet air temperature. 249
Figure 7.38: Discharging process; (a) PCM temperature at PCM_A, (b) PCM temperature at PCM_B, and (c) Outlet air temperature. 251
Figure 8.1: Ambient temperature profiles of typical days in peak summer and transitional months (case study for Khartoum). 256
Figure 8.2: Plan of the experiments under transient inlet operating conditions. 257
Figure 8.3: Hourly profile of the air temperature reduction obtained by the radiative cooling system. 258
Figure 8.4: Variation of heat exchange rate with the surrounding during the charging experiments under (a) hot and (b) moderate summer conditions. 260
Figure 8.5: Temperatures variation with the time under hot summer conditions (free cooling mode). 262
Figure 8.6: Variation of (a) charging effectiveness, and (b) PCM cooling rate under hot summer conditions (free cooling mode). 263
Figure 8.7: Temperatures variation with the time under hot summer conditions (radiative cooling mode). 265

Figure 8.8: Variation of charging effectiveness at different air flow rates under hot summer conditions (radiative cooling mode).....267
Figure 8.9: Variation of the PCM cooling rate at different air flow rates under hot summer conditions. 268
Figure 8.10: Temperatures variation with the time under moderate summer conditions; (a) charging during first night hours, and (b) charging during last hours (free cooling mode). 270
Figure 8.11: Variation of (a) charging effectiveness, and (b) PCM cooling rate under moderate summer conditions (free cooling mode).....271
Figure 8.12: Temperatures variation with the time under moderate summer conditions (radiative cooling mode). 273
Figure 8.13: Variation of charging effectiveness at different air flow rates under moderate summer conditions (radiative cooling mode).....274
Figure 8.14: Variation of the PCM cooling rate at different air flow rates under moderate summer conditions (free and radiative cooling modes comparison).....275
Figure 9.1: Predicted pressure drop and fan power consumption for different air flow rates. 282
Figure 9.2: A comparison of energy produced and energy consumed by the system for different TES configurations and operating conditions.....285
Figure 9.3: Contribution of cooling systems to the building cooling load during summer months (May-October).....286
Figure 9.4: A comparison of electrical energy consumption between the hybrid NRV-LHS system and conventional AC systems. 287

List of publications

Zeinelabdein R., Omer S., & Gan G. Critical review of latent heat storage systems for free cooling in buildings. *Journal of Renewable & Sustainable Energy Reviews*; 2018, 82 (3): 2843-2868. https://doi.org/10.1016/j.rser.2017.10.046

Zeinelabdein R., Omer S., Mohamed E., & GAN, G. Free cooling using phase change material for buildings in hot-arid climate. *International Journal of Low-Carbon Technologies*; 2018, 13, 327-337. https://doi.org/10.1093/ijlct/cty037

Zeinelabdein R., Omer S., & Gan G. Experimental performance of latent thermal energy storage for sustainable cooling of buildings in hot-arid regions. *Journal of Energy and Buildings*, 2019.

Mohamed E., Riffat S., Omer S. & **Zeinelabdein R.** A comprehensive investigation of using mutual air and water heating in multi-functional DX-SAMHP for moderate cold climate. *Journal of Renewable Energy*, 2019, 130**,** 582-600. https://doi.org/10.1016/j.renene.2018.06.075

Zeinelabdein R., Omer S., & Gan G. Experimental analysis of a PCM-Air heat exchanger for building cooling in hot-arid climates. *In:* 17th International Conference on Sustainable Energy Technologies - SET2018, 21-23rd August 2018, Wuhan, China.

Zeinelabdein R., Omer S., Mohamed E., Amaireh I., & Gan G. Free cooling based phase change material for domestic buildings in hot arid climate. *In:* 16th International Conference on Sustainable Energy Technologies - SET 2017, 17-20th July, 2017, Bologna, Italy. http://eprints.nottingham.ac.uk/48436/

Amaireh I., Gan G., Omer S., **Zeinelabdein R.**, Feasibility of Double-Skin Façades for Multi-storeys Office Buildings in Amman/Jordan: An insight into Thermal performance for both summer and winter Peak Conditions. *In:* 16th International Conference on Sustainable Energy Technologies - SET 2017, 17-20th July 2017, Bologna, Italy. http://eprints.nottingham.ac.uk/48438/

Alabdullatief A., Omer S., **Zeinelabdein R.,** & Alfraidi S, 2016. Green roof and louvers shading for sustainable mosque buildings in Riyadh, Saudi Arabia. *In:* 1st International Conference on Mosque Architecture, 5-7th December 2016, University of Dammam, Saudi Arabia. http://eprints.nottingham.ac.uk/48270/

Nomenclature

A	area	m²
C_{n}	cloudiness factor	
Cp	specific heat capacity	kJ/kg. K
D	characteristic dimension	M
D_h	hydraulic diameter	M
dt	temperature difference	K
d	thickness	M
E_{fan}	total energy consumption	Wh
$\bar{f}$	charging effectiveness	
g	gravitational acceleration	m/s²
H_{channel}	height of the air channel	Mm
h_{si}	heat transfer coefficients at the inside surface	W/m² K
h_{so}	heat transfer coefficients at the outside surface	W/m² K
h_{A}	convective heat transfer coefficient due to the wind	W/m² K
L	length	M
$\dot{m}$	air mass flow rate	kg/s
Nu	Nusselt number	
n	cloudiness index	
P	power	W
p	pressure	Pa
Pr	Prandtl number	
Q_{useful}	useful energy	Wh
$Q_{\mathrm{air,in}}$	air inlet energy	W
$Q_{\mathrm{air,out}}$	air outlet energy	W
Q_{PCM}	heat absorbed/released by the PCM	W
Q_{exch}	heat exchange rate with the ambient	W
Q_{rad}	long-wave radiation heat exchange rate	W
Q_{conv}	convective heat exchange rate	W
Q_{cond}	conduction heat exchange rate	W
$R°$	total radiation energy	W/m²
Re	Reynolds number	
RH	relative humidity	%
T_{sky}	sky temperature	°C
T_r	radiator temperature	°C
T_{solidus}	solidus temperature of PCM	°C
T_{liquidus}	liquidus temperature of PCM	°C
T_{amb}	ambient air temperature	°C
T_{surround}	air temperature around the test rig	°C

T_{TES}	temperature of the thermal energy storage	°C
T_{dp}	dew point temperature	°C
$T_{\mathrm{air,out-initial}}$	initial outlet air temperature	°C
$T_{\mathrm{air,out-rad}}$	outlet air temperature from radiative cooling system	°C
$T_{\mathrm{air,in}}$	inlet air temperature	°C
$T_{\mathrm{air,out}}$	outlet air temperature	°C
T_{st}	stagnation temperature	°C
t	time	s, min, hr
U	thermal transmission coefficient	W/m² K
U_{x}	overall uncertainty of the experiment	
u, v	velocity of fluid	m/s
$\dot{V}$	air volume flow rate	L/s
W	width	M
Z	height	M
ΔQ_{air}	heat transferred from the air	W
Δp	pressure drop	Pa
Δx	the sensitivity of the variable x	

Greek symbols

α	wind shear exponent	
β	liquid fraction	
γ	kinematic viscosity	m²/s
ε	emissivity	
η	efficiency	%
λ	thermal conductivity	W/m K
ρ	density	kg/m³
σ	Stefan-Boltzmann constant	W/m² K^4
τ	infrared transmittance	

Abbreviations

2D	Two-Dimensional
AC	Air-conditioning
ACH	Air change rate per hour
ASHRAE	American Society of Heating, Refrigerating and Air-Conditioning Engineers
CFD	Computational Fluid Dynamics
CIBSE	The Chartered Institution of Building Services Engineers
COP	coefficient of performance
CSM	compact storage modules
EC	Environmental chamber

HPC	High-Performance Computing
HTF	Heat Transfer Fluid
HVAC	Heating, Ventilation, and Air Conditioning
LHS	Latent heat storage
NRV-LHS	Nocturnal radiative and ventilative cooling system incorporating latent heat storage
PCM	Phase Change Material
rad	radiative
SHS	Sensible heat storage
TCES	Thermo-chemical energy systems
TES	Thermal Energy Storage

Subscripts

air	air
amb	ambient
c.sky	clear sky
ins	insulation
ref	reference
r	radiator
wall	Duct wall

Chapter 1
Introduction

1.1 Introduction

This chapter begins by providing a general overview of the recent global energy utilisation and its association with climate change. It then introduces the research problem, states the aim, the objectives and the novelty of the study, and concludes by outlining the thesis structure.

1.2 An overview

Nowadays, a universal concern has been directed towards the environmental issues to protect the earth from the climate change, as the global warming has become the coming danger that threatens the life on the planet earth (Nejat et al., 2015). According to (NASA) estimations, the rise in the earth's global mean temperature is estimated at around 0.6 °C in the year 2000 and is jumped to around 0.9 °C in the year 2017 (Figure 1.1).

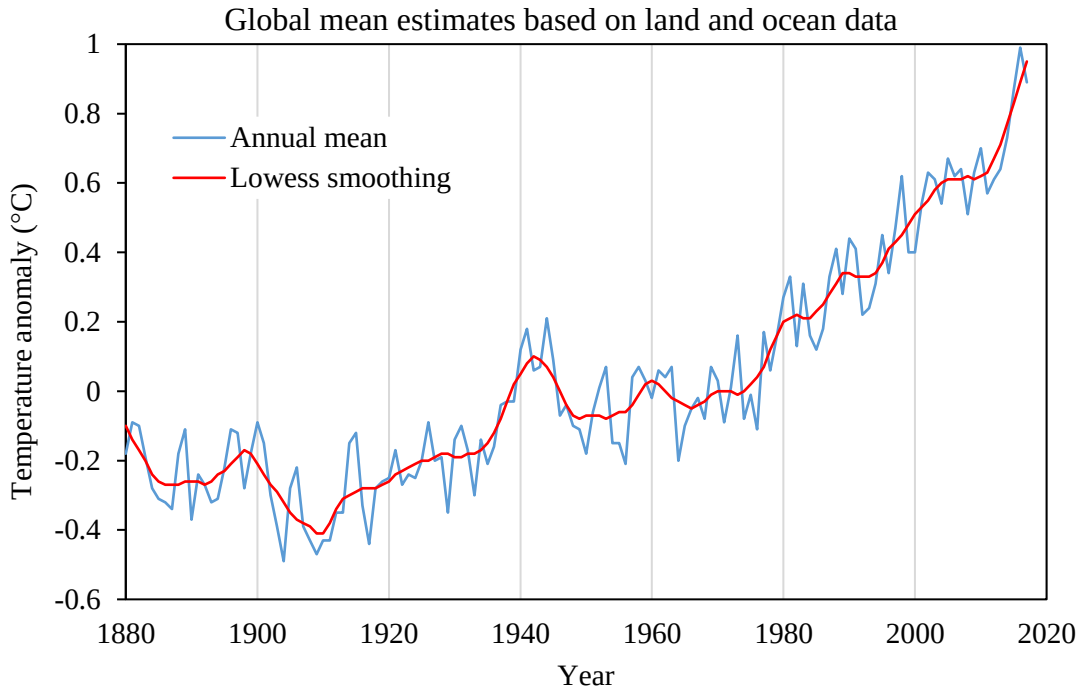


Figure 1.1: Estimated global mean temperature change 1880-2017, updated by (NASA) from (Hansen et al., 2010).

Fossil fuels combustion in the form of coal, oil, and natural gas are the primary cause for the carbon dioxide emissions, which primarily contribute to the global warming (Hu et al., 2018a). According to Smil (2016), the recent concentrations of the greenhouse gases in the atmosphere are vastly higher than at any time before and are expected to continue to rise in future due to the intensive and increasing use of fossil energy as a result of worldwide economic growth and urban development (Figure 1.2). The global temperature is predicted to continue rising significantly if the emissions are not curbed.

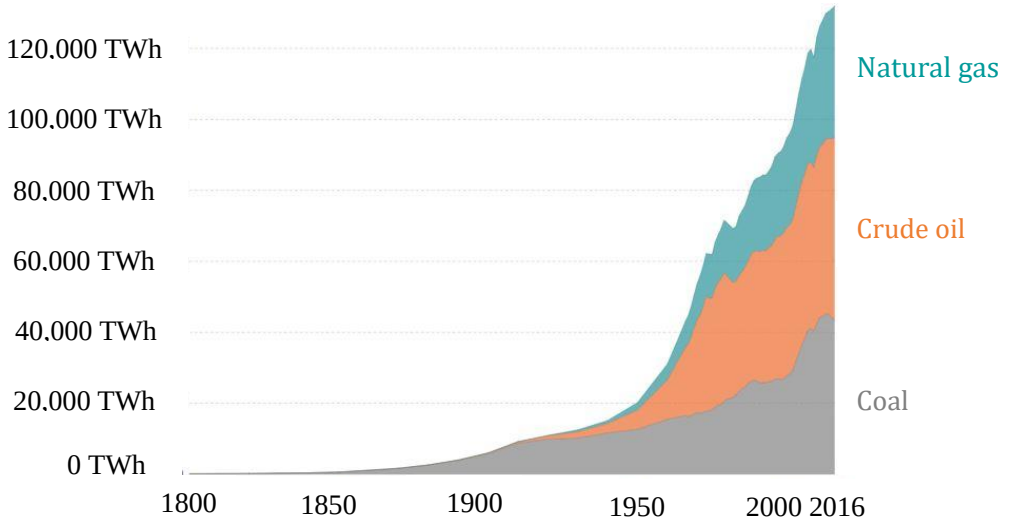


Figure 1.2: World fossil fuel consumption since 1880 (Smil, 2016).

The global annual consumption of all forms of primary energy has increased more than 10-fold during the past century (Boyle, 2004: p.6). According to the IEA (2017b), the percentage contributions of various energy sources to world primary energy consumption in the year 2015 are shown in Figure 1.3. Fossil fuels contribution was approximately three-quarters of the total (81.4%), while the renewable energy sources share was around 13.7%. Thus, a substantial consciousness has recently augmented towards switching to clean and abundant energy sources and to adopt energy-saving techniques in all kinds of sectors.

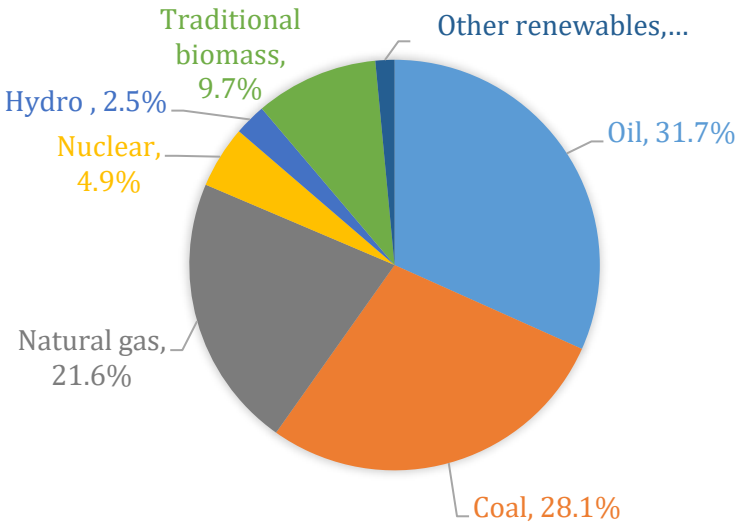


Figure 1.3: Percentage contributions of world primary energy supply by fuel in the year 2015 (IEA, 2017b: p.6).

Buildings (residential and commercial) have the dominant contribution to the global energy use by around 36% of the total in 2015 and are responsible for over 30% of the CO_2 emissions (Nejat et al., 2015). In hot-arid countries, energy consumption in buildings is even much higher, for instance, according to the Arab Union of Electricity (AUE, 2015:p. 8) statistics, buildings in Sudan (as a typical hot climate country) account for around 69.5%, where about 56.5% of the total use is by the residential buildings (Figure 1.4). A large amount of energy consumption in buildings is for indoor thermal comfort provision. According to IEA (2017a), this situation is expected to augment significantly in future, due to the predicted growth in population, growing need for buildings and provision of comfort conditions, and the rise of indoor occupation time due to change in the lifestyle (Pérez-Lombard et al., 2008).

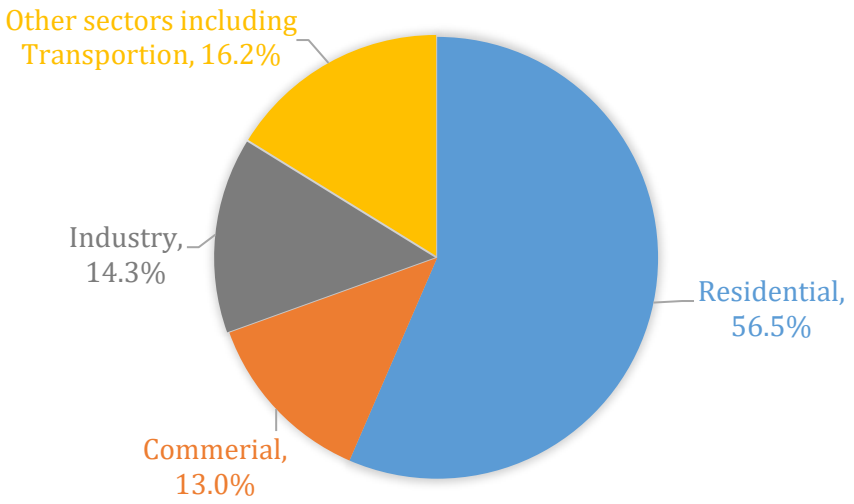


Figure 1.4: Energy use by sector in Sudan (a hot-arid region) in the year 2015 (AUE, 2015:p. 8).

Heating, ventilating, and air conditioning (HVAC) systems are widely used as indoor climate regulators to maintain thermal comfort and improve indoor air quality in buildings. These systems are accountable for most of the energy consumption in buildings, having a negative impact on human health and the environment. They all cause a considerable impact on the energy supply and demand balance (Boyle, 2004:p.6). Thus, sustainable and environmentally friendly alternative strategies are vastly needed to avert or lower the use of these conventional systems in buildings.

1.3 Hypothesis

In some hot-arid regions where there is a small temperature difference between the daytime indoors and the night-time outdoors (Zalba et al., 2004), the natural cooling due to temperature drop at night can be admitted into the building interior to provide instantaneous cooling or can be stored for later use. The lower the night ambient air temperature, the higher the cooling potential (Carrilho da Graça et al., 2002). The use of buildings interior mass to store the cooling from the ambient night air is referred to in the literature as night cooling. While the phenomenon of storing the cooling in a specialised thermal energy storage medium to be retrieved when it is needed is referred to as free cooling of buildings (Waqas and Din, 2013). Some studies show that the free cooling concept is much applicable for locations with a significant diurnal temperature variation typically between 12 and 15 K (Givoni, 1994, Takeda et al., 2004).

Thermal energy storage (TES) systems play a crucial role in the continuous operation of free cooling technology (Dincer and Dost, 1996). TES mechanisms are classified into sensible, latent, and thermo-chemical storages or a combination of these (Sharma et al., 2009).

Sensible heat storage (SHS) aims to store heat by increasing the temperature of a storage substance without any phase change process. SHS substances are available, inexpensive, and well developed. However, the disadvantages are the low thermal storage capacity, the non-isothermal behaviour during the charging and discharging phases, and the non-suitability for most practical applications with a narrow temperature range (Agyenim, 2007, Ding, 2014).

Thermo-chemical energy storage systems (TCES) make use of absorbed and released heat during dissociating and synthesising the chemical compound in totally reversible endothermic chemical reactions (Liu et al., 2010). TCES systems have high energy density at a constant temperature, stable storage, and wide temperature ranges (Ding and Riffat, 2013). However, the expensive cost and limited experience in their long-term operation are the major disadvantages.

Substances used for latent heat storage (LHS) are known as phase change materials (PCM), which can be defined as substances that store and release heat as they undergo a phase change by rearranging their microstructure (Riffat et al., 2015). The use of PCM for building cooling and heating applications has attracted enormous attention over the past decades, owing to the effectiveness and the superiority of these substances compared to other TES substances (Fang et al., 2016, Mohamed et al., 2017). Unlike SHS materials, PCMs have gained growing interest worldwide as efficient lightweight TES substances for building applications (Zalba et al., 2004). PCMs have the advantage of a large energy density and possess an isothermal performance as they absorb and discharge heat at almost a constant temperature or within a narrow temperature range, which makes these substances appropriate for maintaining the thermal comfort day and night (Pasupathy et al., 2008, Regin et al., 2008). Compared to TCES systems, PCMs have energy densities lower by around five times. However, the lower complexity and cost make the PCM energy storage more reliable (Fernandez et al., 2010, Pardo et al., 2014, Liu et al., 2016c).

The incorporation of PCM as specialised storage in free cooling systems was launched two decades ago by Turnpenny et al. (2000) and (2001). The first studies exploring the concept of free cooling in hot-arid climates have been carried out by Waqas and Kumar (2011a) and (2011b). Over the last 20 years, various designs of free cooling systems have been developed using different types of PCM candidates and a range of TES configurations to provide thermal comfort in buildings. Recent development in the free cooling technology has been reported in several published reviews including (Thambidurai et al., 2015, Alizadeh and Sadrameli, 2016, Iten et al., 2016, Zeinelabdein et al., 2018). The literature revealed that the cooling potential of free cooling systems using PCM energy storage varies with the local climate conditions and the specifications of the PCM substance. It has been reported that the inlet temperature and flow rate of the heat transfer fluid (HTF) are the main operational parameters affecting the PCM charging and discharging behaviour. There is a lack of data regarding the free cooling systems under variable inlet air conditions. Additionally, further detailed parametric analyses on the PCM energy storage geometrical configurations are still required, as this influences the charging and the discharging processes.

The majority of the studies in this area are carried out in the moderate and continental climates where the prevalent ambient air temperatures are in the range 20-25 °C (Panchabikesan et al., 2017a), under such conditions, the free cooling has shown good potential. On the other hand, regions with a high demand for cooling reaching around eight months a year, the case of hot-arid regions, have given less attention. Some studies exploring the concept of free cooling in the hot-arid climate have been carried out by Waqas and Kumar (2011a) and (2011b), but generally speaking, published work is scarce for this climate.

In hot-arid regions, the ambient air temperature in the moderate summer months is capable of fulfilling the thermal comfort requirements during the night-time and also during the daytime if a sufficient TES is allocated. Conversely, during the extreme summer months, some studies (Stritih and Butala, 2011, Waqas and Kumar, 2011a) predicted a low effectiveness for the free cooling systems operation, as the ambient air temperatures most of the night are higher compared to the PCM operating temperature range, and hence, it is difficult to provide the daytime cooling.

Natural cooling techniques such as evaporative cooling, radiative cooling, and ground cooling are some of the solutions to complement the free cooling systems. Evaporative cooling assisted free cooling systems have been investigated in many studies including (Jaber and Ajib, 2012, Panchabikesan et al., 2017a, Panchabikesan et al., 2018). The use of ground cooling and radiative cooling to aid enhancing the charging performance of the free cooling systems has not been considered in the previous research, and there is a need for such studies.

Nocturnal radiative cooling is a process of exchanging heat with the cold sky during clear nights. Radiative cooling depends primarily on the microclimate and can be harnessed effectively under the low humidity and clear sky conditions, which generally characterise the hot-arid regions. In such locations, surfaces that directly face the sky, such as buildings roofs, could considerably cool down at night below the ambient temperature by long-wave radiation exchange (Givoni, 1994, Santamouris, 2007).

Radiative cooling in buildings could be applied via several methods depending on the type of radiating surface. These may include high mass radiating roofs with external moveable insulation, specialised lightweight metallic radiators, and unglazed solar collector radiators (Givoni, 1994: p.80-88). Based on many requirements including the time in which the indoor cooling is required and the desired mode of heat transfer between the TES medium and the indoor space, an air-based system using lightweight metallic radiator may be adopted for building cooling. The produced cooling on the radiator surface could be used to lower the temperature of the ambient air before it enters the PCM modules during the charging phase. Simultaneously, the air could be used for instantaneous cooling, considering air supply at an appropriate velocity.

In this study, the nocturnal radiative cooling has been proposed to aid the free cooling storage during the charging phase, when the available night cooling is not sufficient during peak summer conditions in hot-arid climates.

1.4 Aim and objectives

The prime aim of this research is to enhance the night cooling storage capacity of the free cooling systems through the integration of radiative cooling technology for applications during peak summer periods of hot-arid climates, in order to maintain all-day thermal comfort and thus, lowering the energy consumption of buildings in these climates.

The objectives to fulfil the above aim are:

- Carry out a comprehensive and critical review of the recent progress and development in the free cooling technology to identify the challenges and explore potential opportunities and strategies to enhance the utilisation of free cooling in hot-arid regions.
- Evaluate the free cooling potential under hot-arid climate conditions by assessing the thermal comfort of a typical microclimate, the climate conditions and the building energy demand using Energy-Plus simulation model.
- Evaluate the nocturnal radiative cooling potential under hot-arid climate conditions by optimising a system design based on a roof integrated metallic surface with appropriate air channels, using numerical model.
- Investigate the thermal performance and optimise the design of a modular PCM energy storage in the integrated system by conducting a numerical parametric analysis of the geometry under various operating conditions.
- Investigate the charging and discharging behaviour of the PCM energy storage through a laboratory test under constant and dynamic inlet air conditions.
- Carry out potential energy saving assessment.

1.5 Novelty and contribution

The novelty of this work is the provision of a sustainable cooling of buildings in hot-arid climates by integrating radiative cooling with the free cooling to enhance the charging performance of the PCM energy storage under the peak summer of hot-arid climate. It should be stressed that after a careful review of the literature, there is no previous study addressing such a combination which is aimed at enhancing the night cooling in hot-arid climate.

The contribution and usefulness of this study are summarised as follows.

- The present research is recent and could contribute to the progress and enhancement of the free cooling technology. The outcomes are beneficial for producing an optimum design for modular PCM-air heat exchangers applicable for commercialisation and real implementation in buildings, based on the parametric study on the TES geometrical configuration and the operating conditions.
- At a building-scale, the proposed system could improve the occupants' comfort, permit significant energy savings, and contribute positively to the environmental protection by reducing the operation time and energy use of the conventional HVAC systems.
- At a large-scale, wide application of the proposed system has the potential to offset the peak load to the periods of natural cooling availability at the night-time. This could lessen the need for capital investment in new electricity generating plants, which in turn will reduce the CO_2 emissions to the environment.
- The current study will add knowledge to the literature database, due to the scarceness of such work based on the PCM energy storage for free cooling targeting the hot-arid regions, and in particular, the domestic buildings in the selected climates.

1.6 Thesis structure

The thesis is divided into nine chapters and includes the following;

Chapter 1 provides a general background on the current energy status worldwide, introduces the problem statement, aim and objectives, and the novelty of the research. It concludes with the thesis structure.

Chapter 2 initially overviews the passive and natural cooling strategies for buildings applications, with a focus on the nocturnal radiative cooling technology. The chapter discusses the cooling mechanism, the different application methods, and the operating principles. A comprehensive review of the nocturnal radiative cooling systems based on lightweight metallic radiative surfaces is provided. The key design considerations and the potential enhancement opportunities in the thermal performance are highlighted and discussed.

Chapter 3 begins by overviewing the thermal energy storage classifications and the associated advantages and disadvantages, with the main focus on the latent heat storage systems. It addresses the possible methods of PCM application in buildings, highlighting on their merit and providing a succinct review of the most recent research in the PCM energy storage systems based free cooling of buildings. It also discusses the significant aspects influencing the performance of free cooling systems and the enhancements that could be applied. The chapter concludes by summarising the key achievements of the free cooling systems applications based on the reviewed work.

Chapter 4 comprises two main sections; the first section describes the proposed nocturnal radiative and ventilative cooling system incorporating latent heat storage (NRV-LHS), highlighting the working principles and the technical characteristics of the system. The second section discusses the adopted methodology to achieve the aims and objectives of the study and the investigation tools utilised to assess the system performance.

Chapter 5 comprises two main sections; the first section evaluates the potential of the free cooling technology in the hot-arid regions through identifying the thermal comfort zone, analysing the local climate data, and examining the building energy performance using DesignBuilder simulation software. The second section evaluates the potential of the nocturnal radiative cooling based on roof integrated lightweight metallic radiator. Detailed calculations are carried out to investigate the impact of a variety of operating and design parameters.

Chapter 6 studies the thermal performance of a proposed PCM energy storage system for free cooling applications via computational fluid dynamics modelling, using ANSYS Fluent software. The detailed description of the TES unit design and sizing including the PCM selection are revealed. The computational methodology is explained, and independence studies are carried out. The computed results under different operating conditions and TES geometrical configuration are presented and discussed.

Chapter 7 investigates the thermal performance of a laboratory-scale PCM-air heat exchanger. It begins by describing the TES unit configuration, the experiment setup, the instrumentation and measurement setup, and the tests procedure and conditions. The experimental results are discussed for various inlet air conditions and when varying the stacking arrangement of the PCM modules. The chapter concludes by comparing the results of the modelling and the experiments for model validation.

Chapter 8 examines the potential operational performance of the proposed NRV-LHS system experimentally. The charging performance results are discussed under the moderate and hot summer conditions of the hot-arid climate of Khartoum, under both nocturnal ventilative and radiative cooling strategies.

Chapter 9 assesses the energy saving potential of the proposed hybrid NRV-LHS system in comparison with conventional air conditioning systems.

Chapter 10 comprises the main conclusions, design guidelines and recommendations derived from the overall study. Moreover, suggestions for further development of the proposed system are drawn.

Chapter 2

Review of Nocturnal Radiative Cooling Strategy

2.1 Introduction

This chapter provides a general overview of the passive and natural cooling strategies for buildings. It mainly focuses on the nocturnal radiative cooling by discussing the cooling mechanism and the application methods, highlighting the operating principles, cooling potential, merits, and demerits. The chapter also provides a thorough review of the nocturnal radiant cooling systems in the literature based on lightweight metallic radiative surfaces. The design factors and considerations that govern the thermal performance of the radiative cooling systems are discussed. The outlook and future research are also considered.

2.2 Passive cooling strategies

Passive cooling strategies, also known as bioclimatic architectural design methods, refer to the means utilised to defend the building against the climate threats through prevention and modulation of heat gain (Moore, 1993, Al-Obaidi et al., 2014). These strategies were widely investigated, and plenty of data are available in many published reviews (Sadineni et al., 2011, Pacheco et al., 2012, Oropeza-Perez and Østergaard, 2018).

2.2.1 Heat gain prevention techniques

Prevention of heat gain involves the following considerations;

- **Microclimate and site design,** which largely influence the building thermal performance. Therefore, the building should respond to the local climate and the urban configuration; the adjacent buildings, and vegetation (Santamouris and Asimakopoulos, 1996: p.7-8).

- **Building's orientation, form, and layout** have a significant impact on the building thermal behaviour, as these determine the exposure of the external surfaces and the interior space to the solar radiation, wind, and daylighting. Moreover, these parameters have control of the heat gain/loss rate according to the ratio of the exposed surface area to the space volume (Givoni, 1994: p.22-25).

- **Building's envelope design** greatly governs the interaction between the indoor and outdoor environment. The main aim is to limit the heat gain during the summer period by balancing the need for ventilation, daylighting and thermal protection of the building. This requires an appropriate selection of building materials and design for all building envelope components; walls, floors, roof and windows (Okba, 2005).

- **Solar radiation control,** which aims to protect the indoor space from the incident solar radiation by using shading elements on the glazing and the

external opaque components of the building, based on the summer and winter requirements (Okba, 2005, Kamal, 2012).

- **Colour of building external surfaces** has an enormous influence on the indoor temperature in buildings based on the solar radiation intensity and characteristics of the surfaces related to incident heat radiation, and its impact also extends to the urban context, leading to significant changes in the outdoor temperature (Akbari, 2009). Low albedo colours at the outer surfaces could be useful in reducing buildings cooling load (Santamouris, 2007).

- **Behavioural and occupancy pattern**, which are simple methods involving effective adaptation actions such as; adjusting the activity level, dressing according to weather conditions, opening and closing of windows/curtains, and moving to the cooler spaces (Santamouris and Asimakopoulos, 1996: p.7-8).

- **Internal heat gain control**, which could be achieved through proper design and operation of the internal heat sources; the artificial lighting, equipment, and occupants (Santamouris and Asimakopoulos, 1996: p.7-8).

2.2.2 Heat gain modulation techniques

Modulation of the heat gain could be realised through the use of the building thermal mass, which is typically included in the walls, internal partitions, and floors that have been fabricated using high heat capacity materials. Thermal mass in a simplified manner is the capability of a material to absorb and store the heat during the daytime and release it later to the ambient (Davies, 2004). Appropriate use of thermal mass in buildings moderates the indoor temperature by averaging the outdoor day/night temperature pattern. Hence, thermal mass is more beneficial where a large diurnal temperature variation exists (Braun, 1990). For effective operation, the application of thermal mass should be accompanied by the use of other passive and/or natural cooling strategies such as having appropriate building orientation, glazing area, shading, ventilation method, and insulation level, in order to control the incoming solar radiation and the heat gain/loss (Reardon et al., 2011: p.178).

2.3 Natural cooling strategies

Natural cooling of buildings is meant by dissipating heat from the internal space to the natural heat sinks of a lower temperature. The natural heat sinks involve the ambient air (sensible or latent), the sky, the water, and the earth. Application of the bioclimatic architectural design techniques is considered a precondition for the effective operation of natural cooling systems in buildings (Samuel et al., 2013).

Natural cooling techniques are more associated with the human thermal comfort by expanding the comfort zone in the given space rather than elimination of the entire cooling load. The use of natural means does not exclude the use of assistive renewable energy systems or major mechanical systems for advancing the efficiency of the natural cooling systems (Santamouris and Asimakopoulos, 1996: p.5-6).

According to Givoni (1994: p.3-4), natural cooling systems could be classified according to the sinks where the heat is dissipated, as shown in Table 2.1.

Table 2.1: Classification of the natural cooling strategies and the associated heat sink (La Roche, 2011: p222).

Natural cooling system	Heat sink
Comfort ventilation	Ambient air
Nocturnal ventilative cooling	Ambient air
Nocturnal radiant cooling	Sky
Direct evaporative cooling	Ambient air
Indirect evaporative cooling	Ambient air
Ground cooling	Earth

The application of natural cooling strategies in buildings depends on the specific site and the microclimate conditions. The psychometric chart in Figure 2.1 demonstrates the conditions in which the natural cooling strategies can be harnessed to provide comfort.

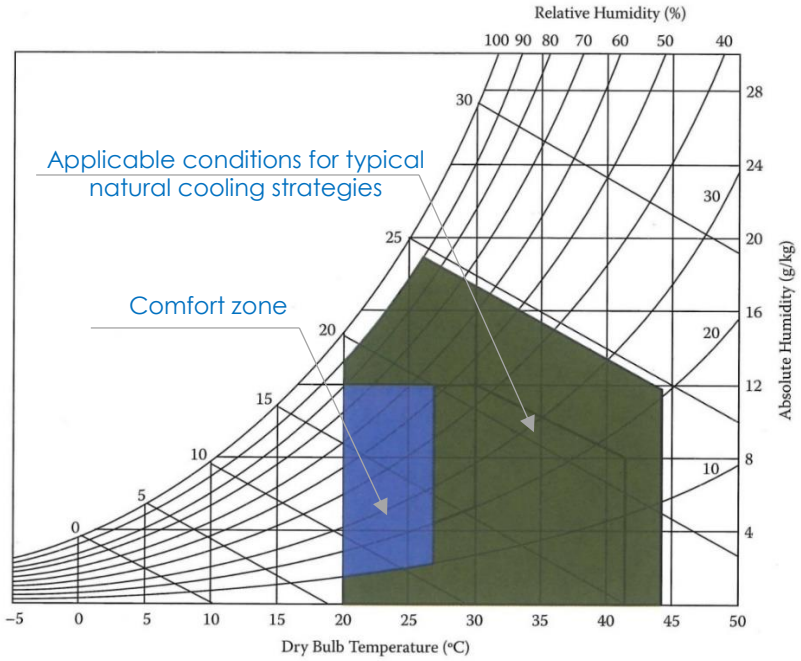


Figure 2.1: Suitable outdoor conditions for natural cooling strategies application (La Roche, 2011: p.223)

2.3.1 Comfort ventilation

Comfort ventilation is the simplest and most common method to enhance human thermal comfort, mainly throughout the daytime (Blondeau et al., 1997). Comfort ventilation is applicable for regions with a diurnal temperature range of about 10 K and a maximum outdoor temperature between 28 ºC and 32 ºC and (typical conditions of warm-humid climate). This strategy varied with the occupants' acclimatisation and comfort expectations (Givoni, 1998).

2.3.2 Nocturnal ventilative cooling

The cold ambient air at night can be introduced to provide direct indoor cooling. In addition, daytime cooling could be provided, if the building interior mass used as cooling storage at night (Carrilho da Graça et al., 2002). Night ventilation coupled with an appropriate thermal mass is applicable for hot-arid regions of a diurnal temperature variation larger than 8 K, night ambient temperature around 20 ºC, and daytime ambient temperature between 30 ºC and 36 ºC (Givoni, 1994: p.17).

2.3.3 Evaporative cooling

Evaporative cooling is a procedure of transforming the hot air into a cool breeze via water evaporation. This strategy aims to decrease the temperature of the ambient air before being admitted into the indoor space either; via direct air movement over a water surface (direct evaporative cooling) or via air movement over a surface that has already been cooled by evaporation (indirect evaporative cooling). In the direct evaporative cooling, humidified air is delivered into the indoor space, while cooling without escalating the humidity level inside the space is attained through the indirect type. The indirect evaporative cooling is applicable for locations where the wet-bulb temperature is 24 ºC, and the maximum dry bulb temperature is 44 ºC (Givoni, 2011).

2.3.4 Nocturnal radiant cooling

Radiant cooling aims to cool the building by long-wave heat radiation to the sky through the building roof or a particular surface without or with a storage mass for daytime cooling. Radiant cooling is primarily influenced by the moisture content of the ambient air and the presence of clouds and can be harnessed successfully under clear sky conditions and relatively low dew point temperatures (the case of hot-arid regions). A detailed discussion of this strategy is provided in sections 2.4-2.6.

2.3.5 Ground cooling

Earth can be utilised as a natural cooling source, taking advantage of its moderate and constant temperature at a certain depth during summer daytime. The ground cooling can be harnessed directly by integrating the building into the ground (entirely or partially) such as earth-covered buildings or indirectly through circulation of a heat transfer fluid inside embedded pipes between a given internal space and the soil, allowing removal of the internal heat (La Roche, 2011: p.263-264). The indirect ground cooling suits regions with a temperate climate, where the soil temperature at two or three-metre depth may be low enough to serve as a cooling source. On the other hand, earth-covered buildings would be most suitable in hot-arid regions with mild winters (Givoni, 1994: p.17).

2.4 Nocturnal radiant cooling

2.4.1 Mechanism of radiant cooling

Indeed, any surface releases radiation in a range of wavelengths relying on its absolute temperature, as a result of molecular and atomic agitation attributed to the internal energy of the object substance. At normal temperature on the ground, the radiation emission is in the spectrum of long-wave (Givoni, 2011).

For surfaces of similar or almost near temperature that face each other, the net radiant gain/loss is small. For instance, this could be between a wall and the surrounding ground or a wall of an adjacent building. Nevertheless, when an ordinary surface faces the sky such as a building roof, the radiant flux is different in this case; the outgoing radiation emitted by a surface on the earth towards the open sky is much stronger than the incoming radiation from the colder atmosphere. This leads to cooling of the surface that faces the sky by radiant heat loss (Givoni, 1994: p.81-82). The ordinary surface is considered as a heat radiator, while the sky is a heat sink. The schematic in Figure 2.2 shows the heat exchange taking place on the roof surface, day and night.

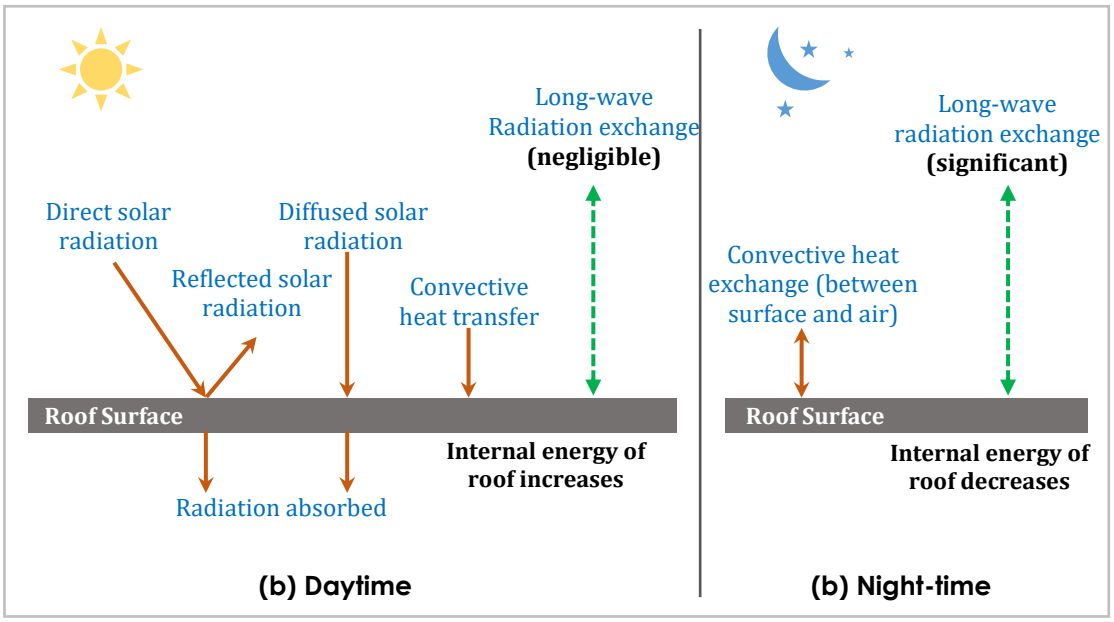


Figure 2.2: Heat transfer on the roof surface (a) day and (b) night.

The emission of long-wave radiation occurs incessantly, day and night. The exposure of the surface to the solar radiation during the daytime results in heating of the surface by absorption, which exceeds the cooling produced by the radiant heat loss (Samuel et al., 2013). That means, as demonstrated in Figure 2.2, the radiative cooling can only be obtained during the night-time. Whereas, the daytime cooling could be achieved through the thermal energy storage means.

2.4.2 Atmospheric incoming long-wave radiation

Surfaces on the earth emit radiation over the range between 5 µm and 30 µm (Givoni, 1994:p.82), with a dominant wavelength of 9.66 µm (Figure 2.3). Whilst, the downward radiation from the atmosphere is varied according to the location and time and is influenced by various atmospheric features. The wavelengths and percentage of radiation absorbed/emitted by various gases on the atmosphere are explained below and exemplified in Figure 2.3 (Granqvist and Eriksson, 1991: p.170).

- Oxygen and Nitrogen, which represent the core components of the earth's atmosphere by around 21% and 78%, respectively, are nearly transparent to infrared radiation.

- Carbon dioxide, which represents only 0.03% of the atmosphere volume, absorbs and emits long-wave radiations around 15 µm. However, its impact on the radiant cooling performance is rather limited, owing to its fixed concentration around the world.

- Ozone, which exists predominantly in the stratosphere, contributes about 1% of the atmospheric radiation and having a maximum radiation emission nearly at a wavelength of 9.6 µm.

- Water vapour, which is considered the most influential environmental factor on the radiation flux between surfaces on the earth and the atmosphere, due to the high emissivity of the water. Water vapour absorbs and emits radiation at the wavelength range between 6.6 µm and 18 µm.

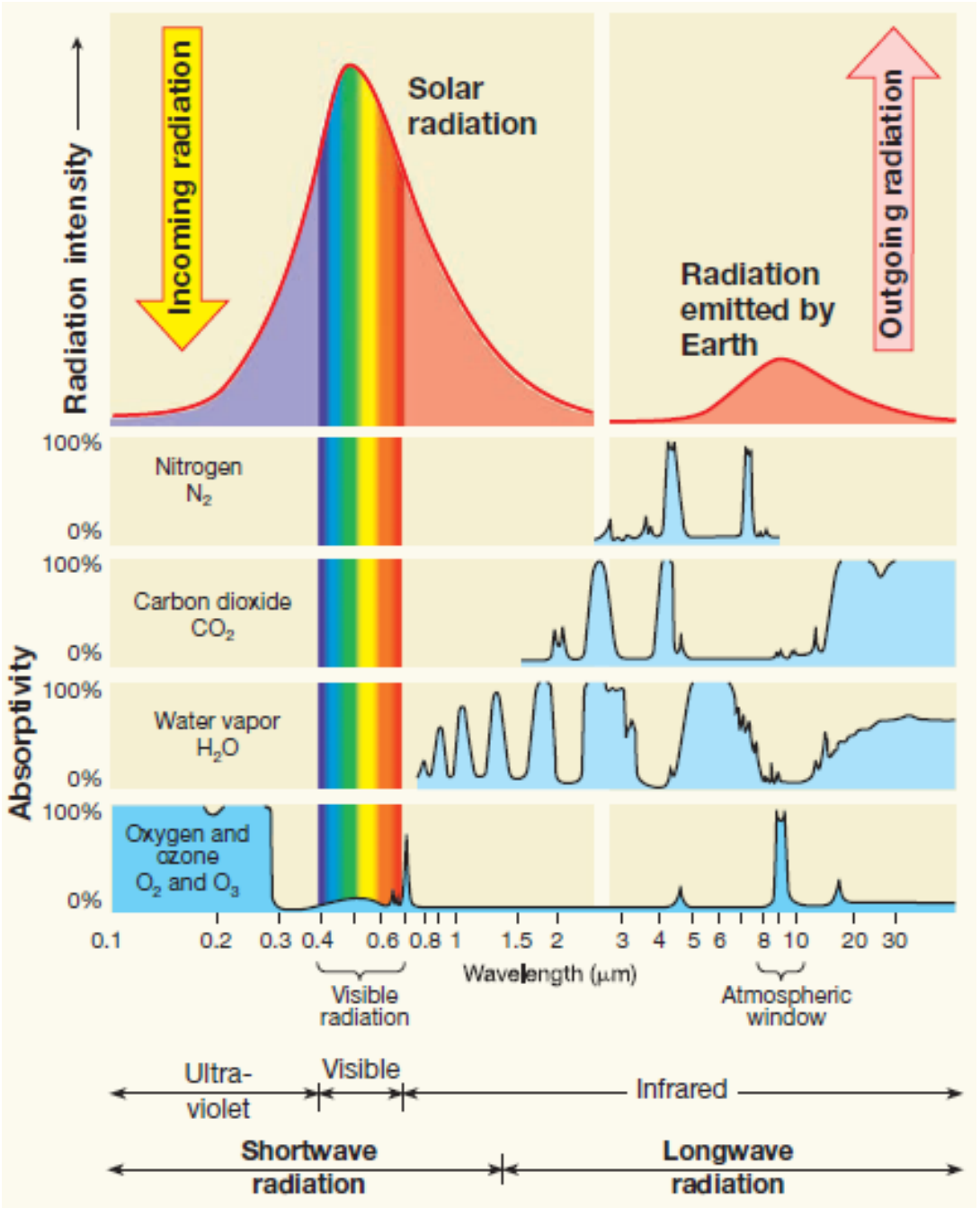


Figure 2.3: Radiation spectrum of earth, atmosphere, and sun (Hoffman and Simmons, 2008).

2.4.3 Potential of radiative cooling

As the moisture content of the ambient air and the presence of clouds have varying concentrations from location to another, several scenarios for the sky radiation ranges can be demonstrated as follows (Orel et al., 1993, Givoni, 1994: p.90);

- Under clear sky conditions and low humidity level, the downward sky radiation is high in the range of 3-8 μm and 13-20 μm. Therefore, the spectrum between 8 μm and 13 μm, where the atmospheric radiation is extremely weak, is referred to as "the sky window", under which, the radiant heat loss to the sky from surfaces on ground reaches the maximum.

- Under cloud cover conditions, the atmospheric radiation reaches the peak, as clouds receive and emit radiation over the entire wavelength ranges, resulting in a radical reduction in the radiant cooling potential.

- When the moisture content of the ambient air increases, the intensity of the downward atmospheric radiation increases accordingly, as water vapour absorbs and emits radiation over the wavelength between 8 μm and 13 μm. In this case, the phenomenon of the sky window disappears.

The balance between the outgoing radiation emitted by a given surface towards the sky and the incoming radiation received by the surface depends mainly on the microclimate conditions. Based on intensive experimental research in different climates, Givoni (1994: p.90) reported that the nocturnal radiant cooling performs the best in the hot-arid regions, where the net radiant heat loss from a given radiator on a building roof can approximately reach 70 W/m² or more under clear sky conditions and low humidity level. However, in the hot-humid regions, the net radiant heat loss is lower, nearly around 40-50 W/m² under the clear sky state, while it is negligible under the overcast sky conditions. Santamouris (2007: p.271-272) denoted that the overall cooling predicted from a nocturnal radiant system is difficult to exceed 150 W/m², even if it operates under the favourable climate conditions of a clear sky and low humidity level.

2.4.4 Application methods of radiant cooling

The implementation of the radiant cooling strategy in buildings could be achieved via various design methods. Santamouris (2007: p.271-277) and Zhang et al. (2018) categorised the application methods according to the working heat transfer fluid into two types; air-based or water-based systems; open or closed loop. Givoni (1994: p.80-88) sorted the radiant cooling techniques based on the radiator type as;

- High-mass radiating roof with external moveable insulation,
- Specialised lightweight metallic radiator, and
- Unglazed solar collector radiator.

In addition to the application methods mentioned above, hybrid systems combine the use of radiative cooling with one or more of the renewable and sustainable energy systems have recently been proposed and tested (Lu et al., 2016).

2.4.4.1 High mass radiating roof with external moveable insulation

The concept is to use the roof as a radiating surface as well as a storage medium. This could be a high-density concrete roof or a steel deck with water-filled bags, which has first been suggested by Hay (1978) and termed the "sky-therm" system. The use of moveable thermal insulation panels directly above the roof is essential for this system (Hay and Yellott, 1969). At night, the insulation panels are moved aside to expose the roof surface to the sky. This allows cooling of the roof by long-wave radiation. In addition, the roof surface cools further via convection by the cooler ambient air. That means high wind velocities on the site are desirable to enhance the cooling of the roof (Figure 2.4a). On the other hand, during the daytime, the insulation panels are used to shade the roof in order to reduce the heat gain by the solar radiation. The cooler ceiling serves as a heat sink absorbing the heat inside the room (Figure 2.4b). Givoni (1994: p.83) pointed out that such systems could obtain a cooling rate up to 120 W/m² in a windy night in the desert regions. The system is capable of providing instantaneous night cooling by conduction through the ceiling and by convection through the warm air close to the ceiling. Accordingly, the use of the high-mass roof itself or a storage

material located at the ceiling surface with the existence of an adequate building's envelope design, are the main requirements to transfer the night cooling to the daytime.

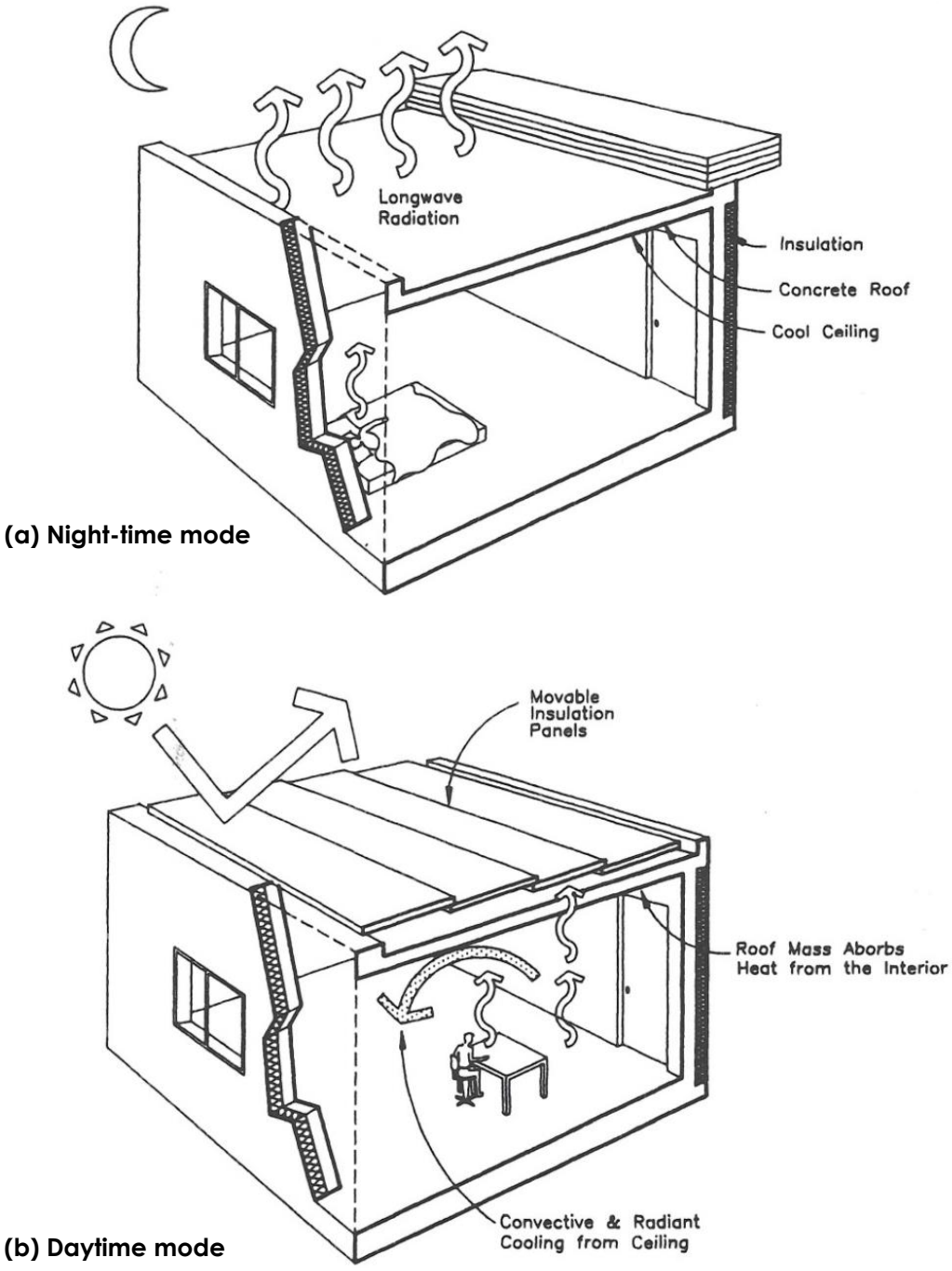


Figure 2.4: Concrete roof with moveable thermal insulation for radiative cooling of buildings (Givoni, 1994: p.84).

2.4.4.2 Specialised lightweight metallic radiator

In this system, a lightweight metallic sheet is placed over a well-insulated building roof with air passages in between. A fan could be used for air flow if needed (Givoni, 1998).

At night, the metal plate cools by long-wave radiation and also gains heat by convection from the ambient air that has a higher temperature until the heat loss and gain reaches the equilibrium, and hence, the radiator temperature stabilises at a certain degree lower than the ambient temperature called the stagnation temperature. The produced coolness would be introduced into the building interior via the ambient air flow through the channel between the roof and the metallic radiator, either depending on the buoyancy of the air in the windy locations or using a fan. However, there are some cooling losses through this transmission process (Figure 2.5a). Conversely, to transfer the produced cooling at night to the daytime, an appropriate storage system is needed. This could be the internal structure mass of the building or a specialised storage medium, considering the closing of building fenestrations to avoid coolness loss to the ambient (Figure 2.5b).

The cooling rate of the lightweight metallic radiators depends mostly on the surrounding wind. At high wind speeds, the convective gain by the radiator increases, leading to a lower cooling production, and vice versa. This type of radiant cooling systems is more beneficial for the buildings occupied during the night-time, such as domestic buildings, and during the daytime on both the heavyweight and lightweight structure buildings by locating a specialised thermal energy storage unit.

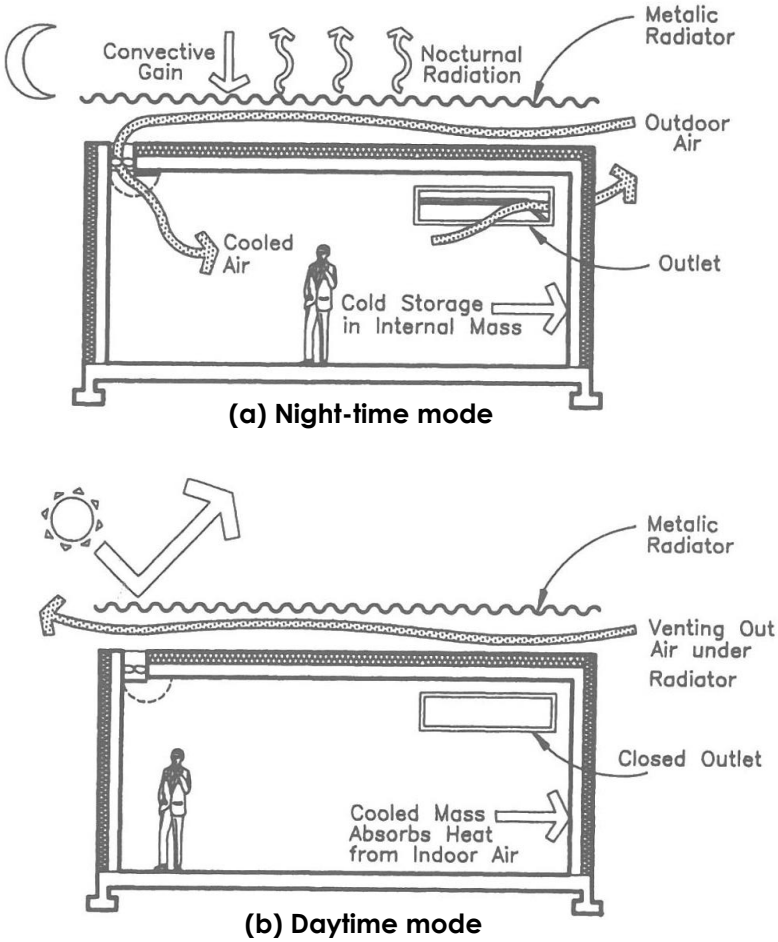


Figure 2.5: Lightweight metallic radiator for radiant cooling of buildings (Givoni, 1994: p.86).

2.4.4.3 Unglazed solar collector radiator

The concept was suggested by McCormick and Landro (1980), which aims to employ the unglazed solar collectors with an optimised slope facing the sky as nocturnal radiators during summer nights. The collectors cool by long-wave radiation, which in turn lead to a cooling of the water circulated in pipes directly attached to the surface, the yielded coolness can be utilised through one of the following methods;

- Circulation of the cooled water in pipes embedded inside the roof slab. The roof works as a thermal storage mass allowing convective and radiative cooling from the ceiling panel to space beneath. Moreover, obstruction of water flow over the radiator is necessary during the daytime (Figure 2.6).

- Circulation of the water to cool a water pond placed over the roof and under the collector. The pond works as a main thermal storage mass, and the heat flow between the pond and the room is by conduction through the roof (Etzion and Erell, 1991).

In addition, unglazed solar collectors can be exploited for domestic water heating in winter by circulation of the water during the daytime.

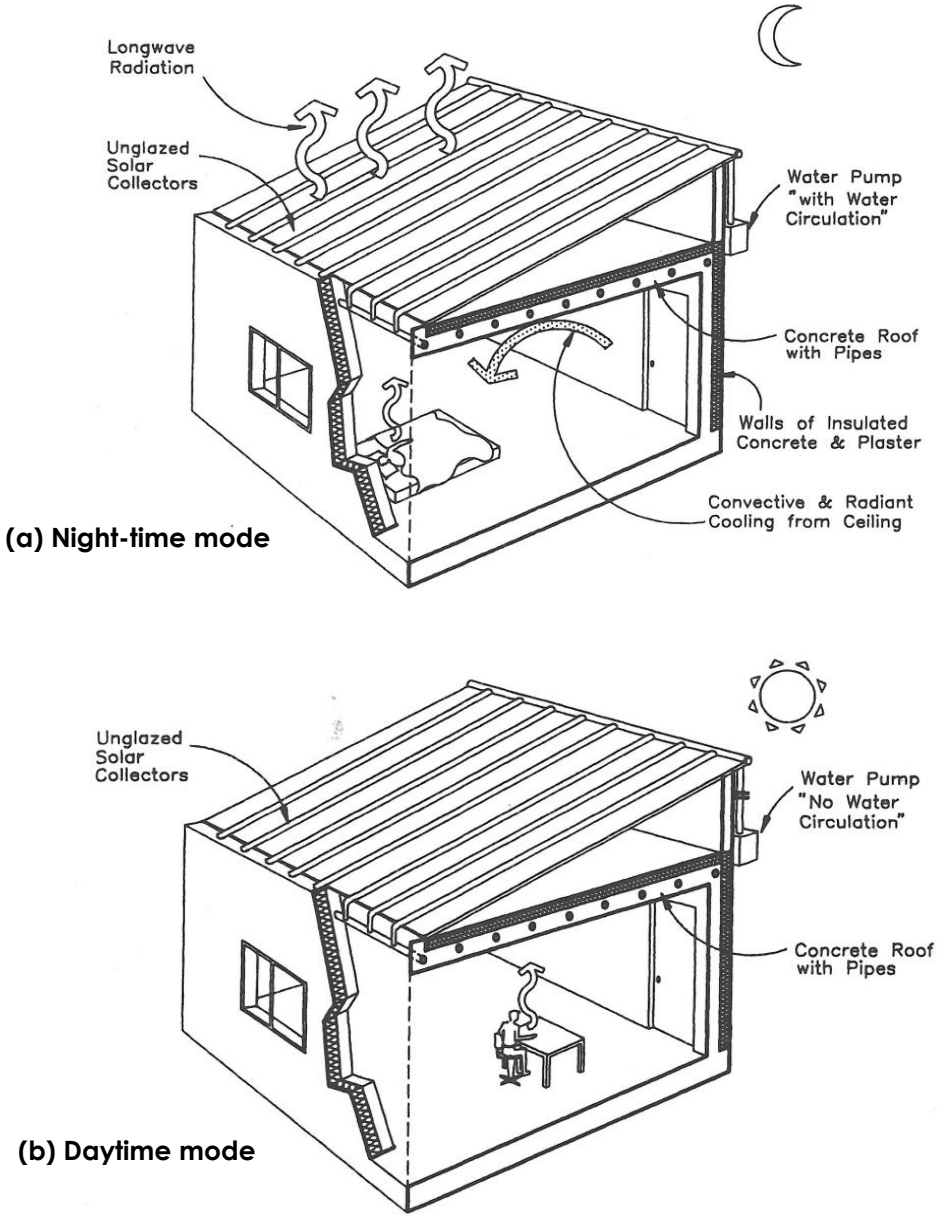


Figure 2.6: Unglazed solar collector application for radiant cooling of buildings (Givoni, 1994: p.87).

2.4.4.4 Hybrid systems incorporating radiant cooling

A range of novel hybrid systems for building applications has been proposed using nocturnal sky radiative cooling towards efficient exploitation of energy resources (Lu et al., 2016). Such systems may include;

- Use of photovoltaic-thermal panels as night cooling radiator with water-based or air-based systems (Eicker and Dalibard, 2011, Sohel et al., 2014, Fiorentini et al., 2015, Lin et al., 2014).
- Integration of direct or indirect evaporative cooling with water-based radiative cooling systems (Farmahini Farahani et al., 2010, Heidarinejad et al., 2010, Farmahini-Farahani and Heidarinejad, 2012).
- Use of heat pipes arrangement as a night cooling radiator (Chotivisarut and Kiatsiriroat, 2009, Chotivisarut et al., 2012).
- Integration with heat pump system (Man et al., 2011, Amir and van Hout, 2019)
- Coupling with phase change material ceiling integrated MPCM slurry storage (Zhang and Niu, 2012).
- A solar desiccant enhanced radiant cooling system (Lu and Yan, 1995, Ali, 2013).
- Solar collector wall for heating and radiant cooling of buildings (Yong et al., 2015).
- A single-phase thermosiphon for cold collection and storage of radiative cooling (Zhao et al., 2017).

2.5 Published studies in radiant cooling with lightweight radiators

The first discussions and analyses of the nocturnal radiant cooling for buildings applications have emerged during the 70s of the previous century (Lu et al., 2016). Since then, a considerable amount of studies investigating the thermal performance of various radiant cooling systems have been published (Panchabikesan et al., 2017b). However, the number of published reviews in the area of nocturnal radiative cooling are quite rare (Vall and Castell, 2017, Family and Mengüç, 2017, Sun et al., 2017, Zeyghami et al., 2018, Lu et al., 2016).

The comprehensive systematic review in this chapter focuses on the performance of air-based and water-based nocturnal radiant cooling systems incorporating lightweight metallic radiative surfaces for building applications. The novel hybrid systems are also highlighted, and areas for future research are suggested, which might allow opportunities to enhance the performance of radiative cooling systems.

Early experimental research on the radiative cooling in buildings was conducted by Givoni and Hoffman (1970), in which the application potential of corrugated asbestos-cement roofs as nocturnal radiators in the desert climate was investigated. A polyethylene windscreen functioning as a radiating surface was stretched above an asbestos roof by about 0.1 m to allow air flow (Figure 2.7). During the night, air circulation was permitted between the room and the channels created on the roof to cool the room, while during the daytime, the air flow was blocked to prevent heat gain. Through the system, the indoor maximum air temperature at night was reduced by around 8-10 K below the maximum outdoor temperature. Whilst, the indoor temperature during the daytime was higher by about 3 K than the night-time temperature. This proves the crucial role of the building's thermal mass in conserving the night coolness for later use. However, a deterioration in the system performance was noticed after one month of operation, which was attributed to the high humidity level and dust accumulation on the windscreen.

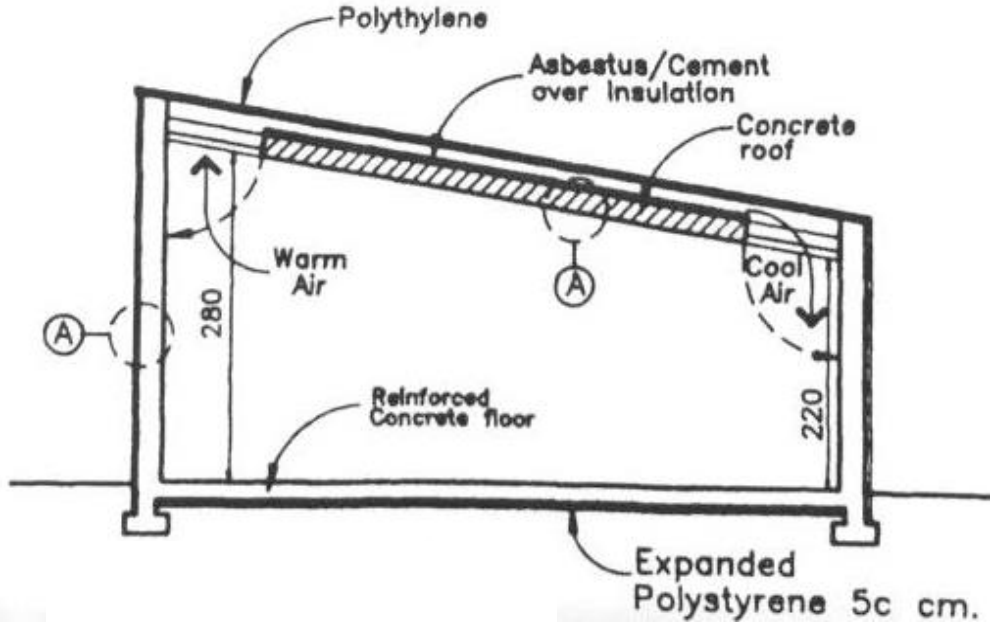


Figure 2.7: Test room cooled by an asbestos-cement radiator (Givoni, 1994: p.113).

In another study, a so-called "roof radiation trap" system for both summer cooling and winter heating in buildings was proposed by Givoni (1977). The nocturnal radiator was a white-painted corrugated metal sheet placed with an inclination above a flat concrete roof of a test cell. Thermal insulation panels were utilised below the radiator with an air passage. Vertical glazing coupled with a movable insulation panel was used in a way to face the sun in winter. In summer; the cooled air during the night is circulated through the channel into the room using a fan. The cooling produced could be used for instantaneous indoor thermal comfort or can be stored for later use. The operable panel is kept closed during the daytime to prevent the solar gain (Figure 2.8a). In winter, the operable panel is opened during the daytime to allow solar penetration through the glazing into the concrete roof, which has a dark colour coating. The heat stored in the massive roof could be transferred into the room by radiation through the ceiling (Figure 2.8b). The results have shown that the radiator temperature was lower than the ambient temperature by 7-8 K at night. The drop achieved in the outlet air temperature was between 1/3 and 2/3 of the temperature drop obtained in the radiator, based on the length of the air channel and the air flow rate.

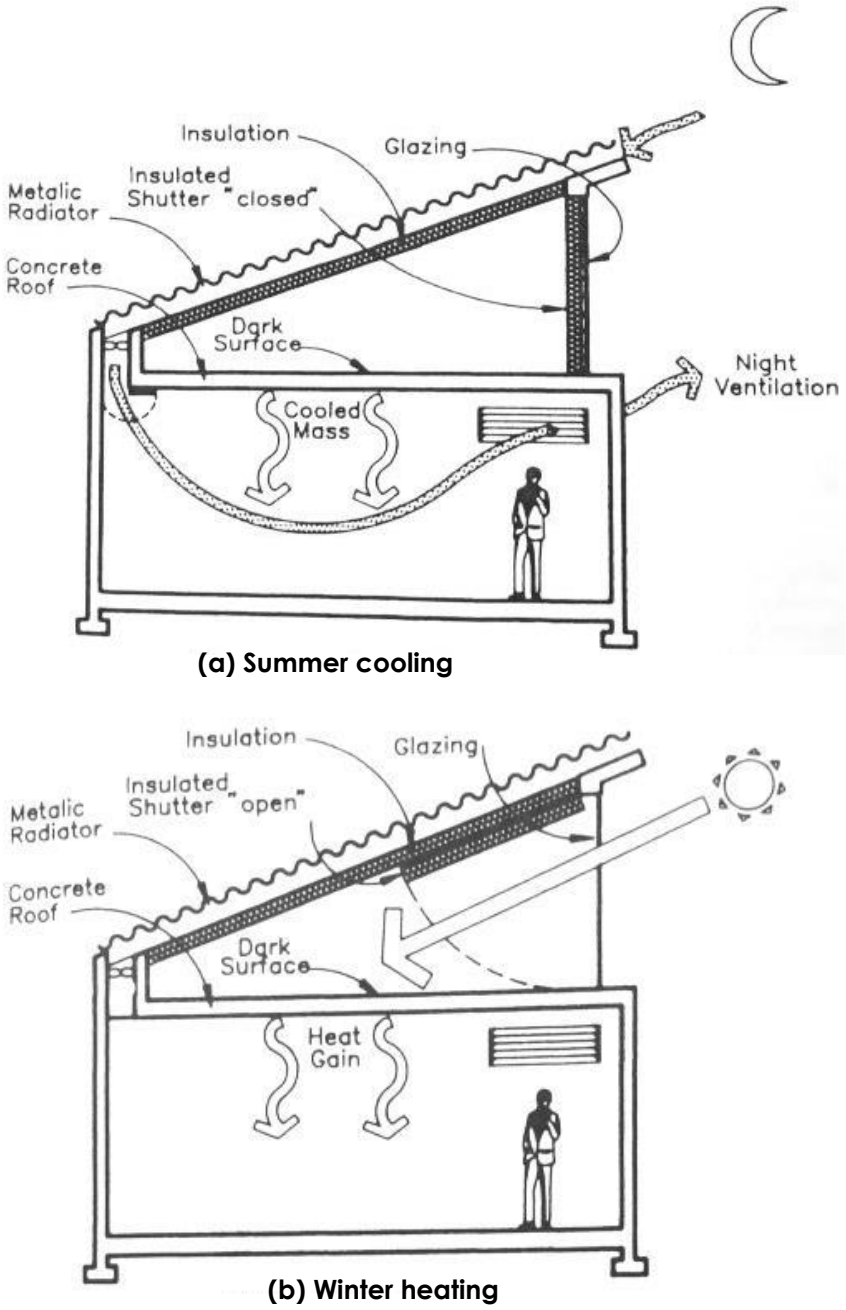


Figure 2.8: Roof radiation trap concept for (a) cooling and (b) heating in buildings (Givoni, 1994: p.117).

Mostrel and Givoni (1982) have conducted long-term experiments to assess the performance of a single windscreen applied to a metallic radiator in the desert climate of Palestine. Under favourable climate conditions of a clear sky, low humidity, and low wind speed, the drop in the radiator temperature below the ambient air temperature

was about 6-8 K through an exposed radiator, and this has been enhanced to 9-11 K with the use of a single layer of polyethylene film. In windy conditions when the function of the windscreen is most needed, the temperature reduction was 30-40% lower for all cases.

The concept of coupling the corrugated metal roof with internal adaptable insulation panels has been suggested by Givoni (1994: p.119-120). Buildings with corrugated metal roofs are very prevalent in many developing countries, especially in hot-arid regions. These lightweight roofs can provide sufficient cooling during the night-time, resulting in comfortable indoor conditions often better than in buildings with high-mass roofs. However, during the daytime, such roof usually heats the room beneath to a temperature higher than the ambient air temperature, if it is not coupled with thermal insulation. Insulation installed directly below the metal roof without an air barrier can profoundly reduce the night cooling effect. However, a ceiling made of insulating material could be used to separate the space into living space and an attic. These panels are opened at night to allow heat dissipation from the interior space to the cooled roof and the sky by long-wave radiation (Figure 2.9a). The ceiling could be closed throughout the daytime to prevent the heat flow into the living space from the attic (Figure 2.9b). Inexpensive insulation can be utilised since it is not exposed to the outside weather conditions. Another advantage is that the concept could be applied to the existing buildings as well.

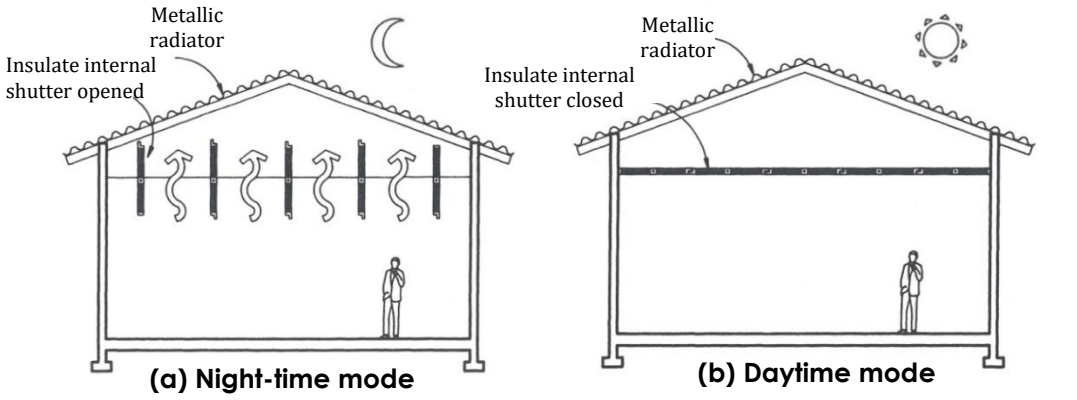


Figure 2.9: Corrugated metal roof with internal adjustable insulation for radiant cooling of buildings (Givoni, 1994: p.120).

In the hot-humid climate of Haifa, Givoni (1994: p.110-111) compared the stagnation temperature of two insulated asbestos-cement panels with different colours; grey and white. Both radiators experienced a temperature reduction by about 5-6 K below the ambient air. Based on the findings of the experiment, the authors have inferred that outcomes from radiant cooling systems can be promising under humid conditions if the sky is clear, while the radiant cooling performance was not significantly affected by the colour of the radiator, unlike during the daytime. Consequently, a radiator that can cool down satisfactorily at night could be exploited as a solar collector for heating purposes during the daytime, based on the climate conditions and the design considerations.

Gulich et al. (1996) have evaluated the potential of radiant cooling and the effectiveness of thermal mass under hot-arid climate conditions, using a well-insulated test bed (1.0 m × 1.0 m × 0.95 m) with internally adjustable insulation panels. The metal roof and the exterior walls were painted white. Water-filled plastic bottles used as thermal mass were located at the floor level, as shown in Figure 2.10. The ceiling panels are controlled following the sunrise and sunset using an electro-mechanical system. The tests were carried out considering three modes of ceiling panels positions; (I) closing of the panels all day, (II) opening of the panels during the night-time only, and (III) opening of the panels during the night-time in conjunction with mechanical ventilation for the attic. The results demonstrated that case III allowed the best performance with a maximum drop in indoor air temperature of 6.9 K compared to the maximum outdoor temperature. The temperature drop was almost equal around 5.4 K in cases I and II. The use of thermal mass at the floor level was not very effective, as measured temperatures at a higher level were much lower than between the storage mass modules. It is worth mentioning that the test conditions were not the same for all cases, as the experiments were conducted sequentially under varied durations. The results were introduced as averages for the test periods, though some tests have lasted for more than a month.

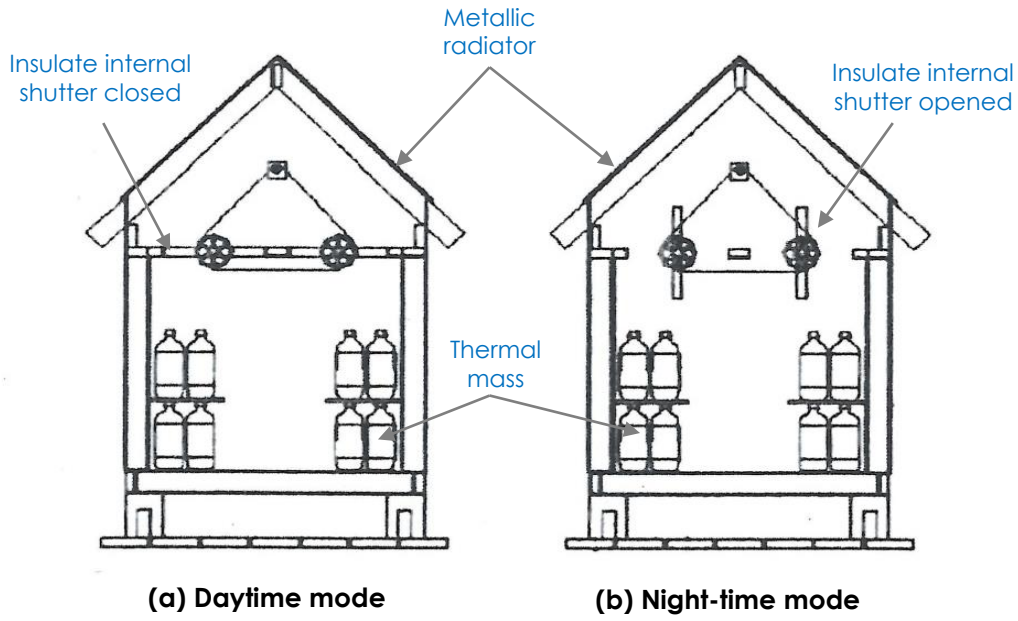


Figure 2.10: Test bed with adjustable insulation panel and water-filled bottles as thermal storage for radiant cooling (Gulich et al., 1996).

Mihalakakou et al. (1998) have examined the thermal performance of a lightweight metallic radiator numerically under the humid subtropical climate of Legnano, Italy. The system comprises a steel plate (14 m × 7 m) covered with a single windscreen of polyethylene, positioned horizontally above the roof of the building with a 0.3 m air gap. The radiator temperature and the cooling produced were calculated for two representative nights in June; one with a clear sky and another with a 60% cloud cover. The calculated data were used to predict the indoor air temperature of an existing building modelled in TRNSYS software. The results predicted a cooling power 29.7-55.8 Wh/m² under favourable weather conditions and 26.7-44.9 Wh/m² under cloudy conditions, depending on the ambient wind speed. Enhancing the area of the radiator by 50% led to an indoor air temperature reduction by 4.3-6.1 K and 2.2-3.4 K in the clear and cloudy nights, respectively.

Using the test bed constructed by Gulich et al. (1996), shown in Figure 2.10, LaRoche and Givoni (2001) investigated the impact of thermal mass configuration on the radiant cooling performance. Concrete bricks were employed as a storage mass and placed in various locations inside the test bed including; floor and wall placement at different heights. The temperature was measured at the surface of the thermal storage mass, the attic space, and at two selected points above the floor level. The measurements taken during the daytime indicated that the air temperature in the attic space was always higher than the ambient air temperature, while, the indoor air temperature of the test bed was largely lower and relatively close to the temperature of the brick mass. The maximum temperature drop for the thermal storage mass below the ambient temperature was around 12 K. Since the experiments have been carried out at different times, the authors have developed formulae to predict the indoor air temperature based on the daily average outdoor temperature to allow direct comparisons. The results have revealed that thermal mass at a high level on the walls possessed a lower temperature compared to that located on the floor or at a low level on the wall. However, the impact of internal gains was not considered, which might increase the indoor temperature in the real conditions.

LaRoche and Givoni (2002) studied the impact of thermal insulation level of the building on the radiant cooling performance through experimenting several insulation placements on the internal walls of the test bed considered in (Gulich et al., 1996). The storage mass temperature and air temperature in the attic and two levels inside the test room were measured to monitor the temperature swings and distribution. The primary variable in this study is the conductive heat loss coefficient (UA), which depends upon several factors including; the infiltration/ventilation rate, heat gain through glazing surfaces, and the insulation level. The first two factors were not considered, since the test bed does not have windows. In the case of the highly insulated room ($UA = 2.4$), the indoor air temperature decreased by 7.9 K from the outdoor average maximum temperature, while with the low insulation level ($UA = 8.1$), the indoor average temperature remained close to the outdoor during the night and lower by around 3-5 K during the daytime. It is inferred from the study that the building envelope has a great role on the radiant cooling system systems performance, especially during the

daytime if the cooling is transferred. Low insulation level might lead to a large indoor temperature fluctuation, while high insulation level could result in nearly stable temperatures. In the case of long night hours when the radiant cooling potential is high, low insulation levels can be acceptable.

Dimoudi and Androutsopoulos (2006) monitored the performance of a water-based prototype roof component for radiative cooling under real weather conditions for 22 days during summer (June-July) in Greece (Figure 2.11). The water is circulated at night through pipes attached to the radiator and embedded in the concrete roof of the building. The cooling stored in the roof would be realised according to the load profile of the building via heat radiation and convection to the ceiling. The efficiency of the radiator (η_{rad}) was evaluated based on the inlet and the outlet radiator pipes water temperature ($T_{rad,in}$ and $T_{rad,out}$, respectively), and the stagnation temperature (T_{stag}) using equation (2.1).

$$\eta_{rad} = \frac{T_{rad,in} - T_{rad,out}}{T_{rad,in} - T_{stag}} \tag{2.1}$$

The results have shown that the investigated system showed a good potential for cooling load reduction in the considered building. The efficiency was considerably reduced with the enhancement of the water flow rate and vice versa. The authors have stated that the applicability of radiative cooling systems is higher in locations with uniform building heights without dense texture. However, it should be indicated that experiment took place in a period characterised with quite steady weather conditions of minimum and maximum ambient air temperatures 17.1 °C and 34.9 °C, i.e. the extreme summer conditions were not investigated.



Figure 2.11: Installation of a radiator with water pipes on the building roof (Dimoudi and Androutsopoulos, 2006).

Using CFD modelling validated with an experiment, Golaka and Exell (2007) investigated the influence of wind shields in lowering the convective heat transfer with the ambient wind in the nocturnal radiators for building cooling in the tropical climate of Thailand. The results have implied that the application wind shield has a significant influence on both convective and radiative heat exchange of the radiator. Wind shields of small height (25 mm) enhanced the convective heat transfer coefficient slightly, whereas, that of a large height (50-100 mm) provided an appropriate drop in the convection rate (Figure 2.12). This was attributed to the turbulence increase over the surface in the case of the small height shields, while the higher wind shields triggered a separation of the main airflow from the radiating surface. Moreover, the increase in the wind shield height interferes with the radiative cooling from the radiative surface. Therefore, the authors have recommended avoiding wind shields at very low wind speeds less than 1 m/s, and at velocities greater than 2 m/s for wind shields of a height 100 mm.

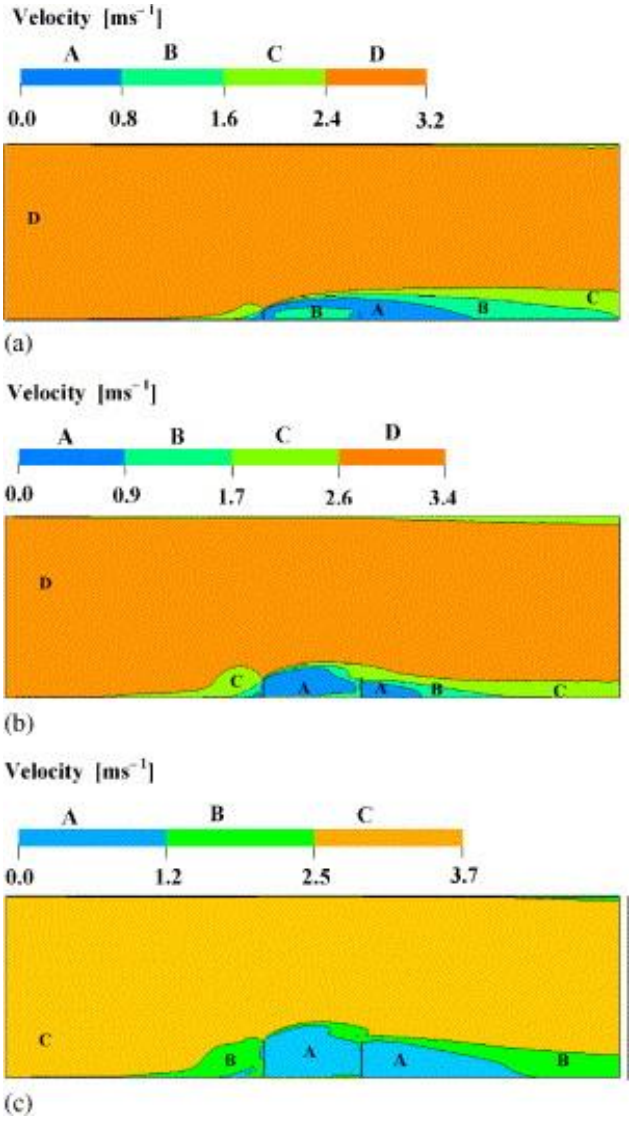


Figure 2.12: Calculated velocities and air flow pattern at wind speed 2.7 m/s for different wind shield heights 25, 50, and 100 mm.

Bagiorgas and Mihalakakou (2008) proposed a radiant cooling system consisting of a flexible aluminium duct of 100 mm diameter employed as a radiator. The top and bottom surfaces of the cylindrical-shape duct were pressed to obtain a flat appearance. The radiator was placed on a metallic surface over a roof of an educational building in Agrinio in Greece using a design shown in Figure 2.13. Ambient air is drawn through the duct into an indoor office space using a fan only operated at night. Two painted radiators with emissivity 0.93 and 0.71 were tested. The experiment was carried out for a continuous 30 days in August and September, and the findings have shown a good agreement with the calculated results for the outlet air temperature. The

performance of the radiator with a high emissivity coating (0.93) was the best. The indoor air temperature of the room equipped with the radiant cooling system was lower by around 2.5-4 K compared to an adjacent room without a cooling system, under similar test conditions. The system showed a high potential of maintaining the thermal comfort day and night during the experiment period. However, experiments under extreme summer condition may be necessary to assess the viability of the proposed system, especially, for comfort provision during the daytime.

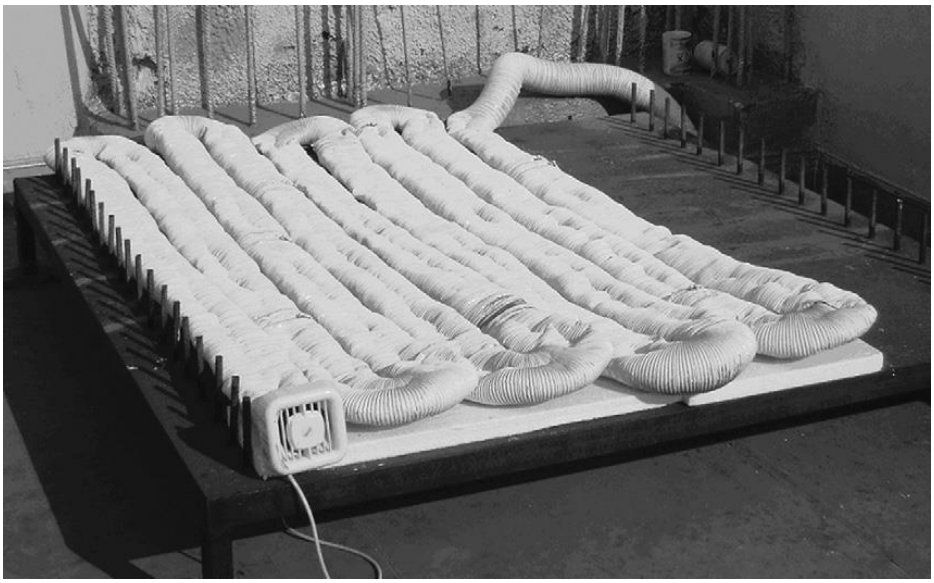


Figure 2.13: Radiant cooling system proposed by Bagiorgas and Mihalakakou (2008).

An experimental study has been carried out by Bathgate and Bosi (2011) to evaluate the use of zinc sulphide and polyethylene as a cover-top for radiative panels for the cooling applications. The thermal performance of both investigated materials was nearly similar. However, zinc sulphide was found to be a highly durable and more appropriate transparent material in the 8-13 µm wave band compared to polyethylene. On the other hand, less expensive techniques to produce large zinc sulphide tiles requires further development.

(Sima et al., 2014) assessed the night radiant cooling potential in the Czech Republic utilising CFD and TRNSYS simulations and substantial enhancement was reported in the indoor air temperature during working hours of a tested office building.

Tevar et al. (2015) developed a mathematical model to evaluate the radiant cooling potential. The model was validated with experiments of three radiator prototypes (Figure 2.14) with different emissivity 0.9, 0.5, and 0.02 by which, cooling power of 63.7, 42.2, 7.5 W/m², respectively, was obtained. The authors pointed out that the developed model can predict the performance of radiative cooling systems, and thus, could be integrated with the available models to simulate the thermal performance of building systems.

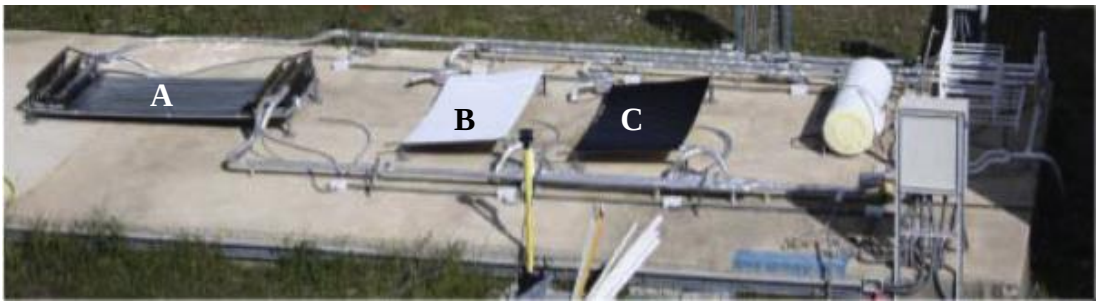


Figure 2.14: Photographs of the three radiative panels investigated by Tevar et al. (2015).

The potential of a radiative cooling system in ten different locations in Malaysia has been evaluated numerically by Hanif et al. (2014). The study has reported potential savings of up to 11% in the cooling power consumption under all tested climate conditions (Figure 2.15).

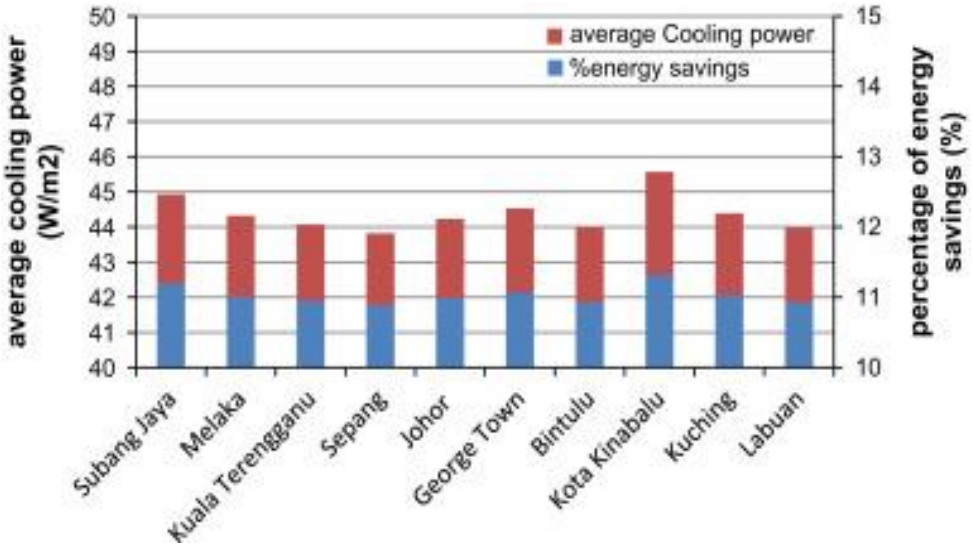


Figure 2.15: Cooling power and energy savings percentages by radiant cooling for different cities in Malaysia (Hanif et al., 2014).

Panchabikesan et al. (2017b) evaluated the cooling potential for various natural cooling strategies including the radiative cooling for five selected Indian cities with different climate conditions. The calculations were performed only for the months where the maximum ambient air temperature exceeds comfort, i.e. ≥28 °C. Based on the theoretical analysis, locations with low humidity level, low cloud cover, and a considerable diurnal temperature variation have demonstrated great potential for radiant cooling application. It is predicted a maximum radiant cooling power of 85 W/m² and a minimum of 48 W/m², with the high potential during the period March-May (Figure 2.16).

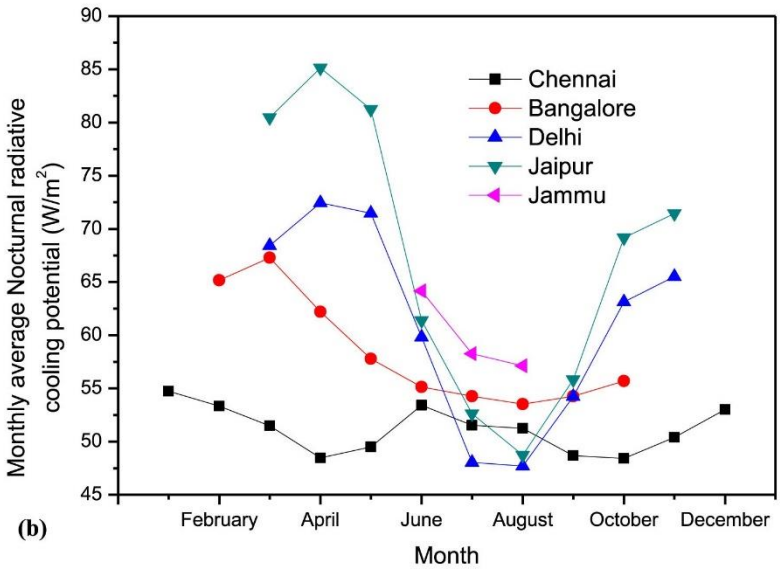


Figure 2.16: Monthly average night radiant cooling potential in different cities in India (Panchabikesan et al., 2017b).

2.6 Discussion of design factors influencing the radiative cooling performance

2.6.1 Effect of thermal mass and storage

The coupling between the nocturnal radiator and thermal mass has a significant impact on the cooling rate and duration maintained in the indoor space (Etzion and Erell, 1991). In addition to the use of the building structure as a storage mass, other methods are utilised to incorporate the thermal mass in the radiant cooling systems.

The use of water-filled plastic bags above a radiative roof (usually a metal deck) with movable insulation panels that cover the solar radiation during the daytime was first proposed by Hay (1978). The cold-water bags and the ceiling act as a heat sink during the daytime absorbing the heat generated inside the building. However, such a system requires to be located directly above the targeted space to be cooled (Figure 2.17).

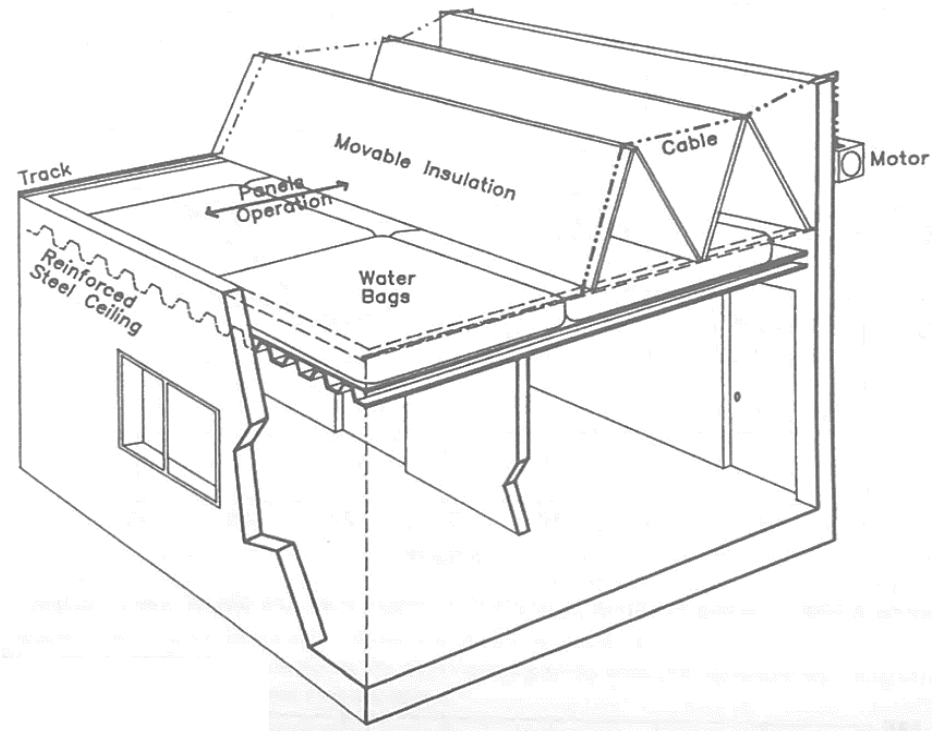


Figure 2.17: Radiant cooling system coupled with water-filled bags above a metallic roof (Givoni, 1994: p.105).

The use of the ceiling panel as thermal storage by embedding water pipes inside the concrete roof was also considered. The circulated fluid absorbs the internal heat and radiates it to the ambient via the radiant panel above the roof (Figure 2.18). This system does not require an installation of the radiative panels directly above the targeted space to be cooled (Dimoudi and Androutsopoulos, 2006).

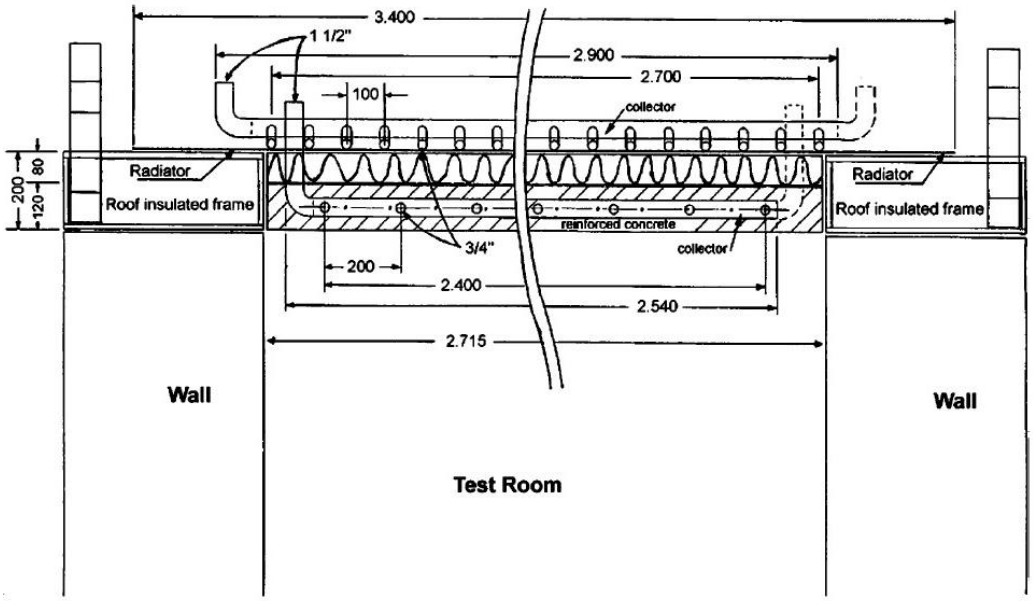


Figure 2.18: Radiant cooling system coupled with roof embedded water pipes (Dimoudi and Androutsopoulos, 2006).

The use of roof ponds is one of the techniques used to cool the space directly below during the night-time (Erell and Etzion, 2000). Such systems require a ceiling with a high thermal conductance. A metal roof could perform better, where its temperature could be approximately similar to that of the water, all the time. However, the practicality would be a concern (Runsheng et al., 2003 and, Kharrufa and Adil, 2008, Sharifi and Yamagata, 2015). The major requirements for such systems are the existence of a structural system capable of affording the mass of the water, and the use of appropriate waterproofing, which results in a high cost. Moreover, it is difficult to use the system to cool the spaces that are not immediately below the roof pond (Santamouris, 2007: p.278).

The coupling of specialised thermal energy storage based on sensible heat substances in the radiative cooling systems has also been investigated. Such systems could be;

- A water-based system (Figure 2.19), where the water cooled by a radiative cooling panel is usually circulated through a water storage tank using pipes with or without mixing of fluid (Al-Nimr et al., 1998).

- An air-based system, utilising packed-bed rocks, water container, etc. as a storage medium. At night, heat is absorbed from the storage by drawing the air cooled using a radiative cooling panel. During the daytime, cooling is discharged via warm air circulation through the storage (Al-Nimr et al., 1999).

The main obstruction of such systems is the heavy substance's weight and hence, space required to accommodate the storage medium since sensible heat materials have small energy densities. Therefore, hybrid radiative cooling systems incorporating PCM as specialised storage are more beneficial for thermal performance enhancement and practical application.

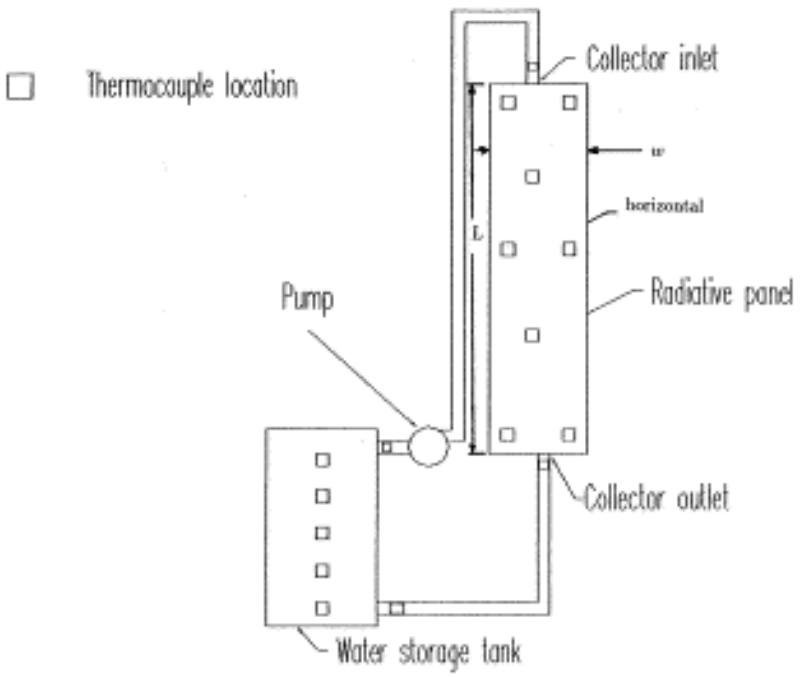


Figure 2.19: Radiant cooling system coupled with a water storage tank (Al-Nimr et al., 1998).

2.6.2 Reduction of convective heat transfer with the ambient air

Under suitable night conditions of clear sky and low humidity level, the stagnation temperature of a lightweight radiator can be well lower than the ambient air temperature due to the radiant heat exchange. However, a convective gain from the surrounding air would take place, which will increase at high wind velocities. In order to reduce the convective gain, two methods have been reported in the literature as follows;

2.6.2.1 Use of windscreen

Application of windscreens is one of the sufficient techniques utilised to decrease the convective heat gain from the ambient air without considerably obstructing the long-wave radiation emission (Givoni, 1994: p.95). A layer made of a material with high transparency in the infrared radiation spectrum can be stretched over the radiator to insulate it from the surrounding air. Materials that could be used as windscreens in radiative cooling systems are rather limited (Lu et al., 2016). The currently available materials and their characteristics are listed in Table 2.2. However, their appropriateness as a convection cover differs widely (Bathgate and Bosi, 2011).

According to previous studies (Bathgate and Bosi, 2011, Lu et al., 2016), it has been indicated that the most investigated and widely used convective cover to date is polyethylene, as it is a very thin, low cost, and low-density material with a 70-75% transparency to long-wave radiation. A typical application of polyethylene film over a radiative surface is shown in Figure 2.20a. Clark and Blanpied (1979) initially measured the characteristics of a polyethylene film windscreen under different climatic conditions, and it was found that it possesses a radiation transmissivity of 0.75, a reflectivity of 0.10, and an emissivity of 0.15. Although the windscreen reduces around 25% of the emitted radiation, a considerable drop in the radiator temperature is obtainable. Based on an experimental investigation, Givoni (1994: p.96) has concluded that the effect of utilising a single layer or a double layer of polyethylene windscreen on the radiant cooling performance is small. This is because the convective gain minimised by a double windscreen is usually balanced by the drop in the long-

wave radiation emission. Compared to an exposed radiator, the results have shown that the temperature drop obtained through a covered radiator was double at high wind speeds and only about one third at low wind speeds.

Table 2.2: Potential cover materials for radiative cooling.

Substance	Transmittance (8-13 µm)	Toxicity	Cost	Reference
Polyethylene	73% (100 µm thick)	Non-toxic	Low	(Clark and Berdahl, 1980)
HDPE mesh	80% (100 µm thick)	Non-toxic	Low	(Gentle et al., 2013)
Zinc selenide (ZnSe)	70% (7.1 mm thick)	Hazardous by skin contact	High	(Harris, 1999:p.32)
Zinc sulphide (ZnS)	64% (4 mm thick)	Low	High (for high purity)	(Harris, 1999:p.32, Bathgate and Bosi, 2011, Bosi et al., 2014)
Tefzel (C-F polymer)	10% (200 µm thick)	Non-toxic	Low	(Bathgate and Bosi, 2011)
Silicon	47% (0.6 mm thick)	Non-toxic	High	(Hull, 1999:p.677)

Ali et al. (1998) investigated the impact of ageing, thickness, and colour of a polyethylene film windscreen applied to a radiative panel on the optical properties and the nocturnal cooling performance. It was found that the colour of the polyethylene film had no substantial impact on its optical properties and hence, on the nocturnal radiant cooling performance. Reducing the thickness of the polyethylene film from 50 µm to 25 µm enhanced the transmissivity and the radiant cooling potential by 8.6%. However, too thin films are subject to flutter by the wind if it is not appropriately stretched. Significant degradation in the transmissivity of the polyethylene film from 0.72 to 0.42 in the sky window wavelength range was observed after 100 days of ageing, resulting in a cooling drop by 33.3%. Therefore, the authors recommended replacing polyethylene films with new ones periodically.

Bathgate and Bosi (2011) and Bosi et al. (2014) concluded that the zinc sulphide substance (ZnS) was found durable, stronger, and impervious to damage by ultraviolet radiation, and therefore, more suitable as a windscreen than polyethylene. The authors also stated that the vulnerability of polyethylene to damage by solar ultraviolet radiation reduces its impracticality for long-term use.

Gentle et al. (2013) carried out an experimental and simulation study to improve the performance of polyethylene using a stabilised high-density polymeric mesh (HDPE). An enhanced night sky radiative cooling performance was achieved compared to conventional polyethylene films. The authors reported that the developed HDPE was mechanically strong, retractable, applicable for large areas application, and durable for many years over the conventional polyethylene film.

According to many studies (Mostrel and Givoni, 1982, Ali et al., 1998, Bosi et al., 2014), the following general aspects appeared to restrict the performance of some windscreens, mainly the polyethylene, based on the climate conditions;

- Condensation on the top surface of the windscreen, which caused by the stagnant air between the windscreen and the radiator which cooled to the dew point temperature. In such case, the windscreen loses its transparency and acts as an ineffective radiator.

- Accumulation of dust and airborne pollutant on the windscreen. A regular removal is required. Otherwise, a substantial reduction in the radiant cooling performance could occur. This problem can exacerbate in the presence of the condensation on the surface of the windscreen.

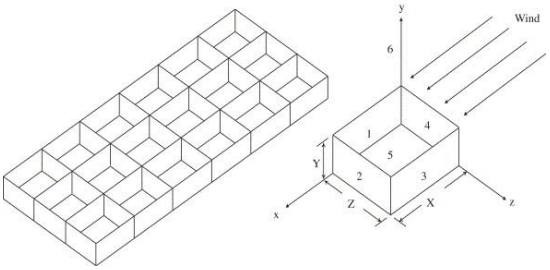
2.6.2.2 Use of windshields

Wind shields (Figure 2.20b), constructed from a material reflective in the infrared spectrum while obstructing the air movement around the radiator surface, are employed to reduce the natural convective gain (Martin, 1989). Based on numerical and experimental studies, wind shields were found more advantageous in locations with high wind speeds and should be avoided in the case of low wind speed, as it

interferes with the radiant heat exchange with the sky, particularly, when large heights of shields are utilised (Golaka and Exell, 2007).

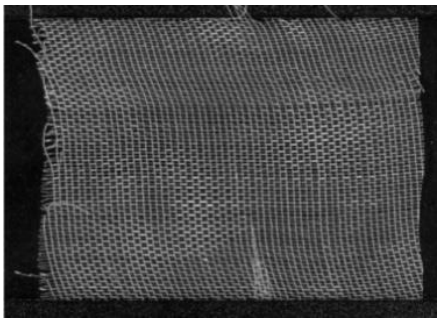


(a) Polyethylene film cover



(b) Wind shield





(c) HDPE and polymeric mesh

Figure 2.20: Methods utilised to minimise convective heat transfer with ambient air in radiative cooling systems (Golaka and Exell, 2007, Gentle et al., 2013).

2.6.3 Enhancement of nocturnal radiators emissivity

The radiant heat flux depends upon the emissivity of the radiative panel. Materials with high emissivity value should be used. If the radiator will be used as a solar collector, the effect of the absorptivity has to be taken into account. Table 2.3 illustrates characteristics relating to heat radiation for several common surfaces. The table provides a general indication since the emissivity factor of the material varies with temperature (Moss, 2002: p.70). It can be stated that most of the ordinary building materials are good radiators, have an emissivity of around 0.9. When metallic radiators are utilised, coating with high emissivity layers should be considered, as these layers act like a radiator in this case.

Table 2.3: Optical properties of some surfaces (Moss, 2002: p.70).

Material/Surface	Emissivity	Reflectivity in the solar range
Brick and stone	0.9	0.1
Aluminium, polished	0.04	0.96
Aluminium, anodised	0.72	0.28
Cast iron	0.8	0.2
Copper, polished	0.03	0.97
Copper, anodised	0.86	0.14
Galvanised steel	0.25	0.75
Paint, metal based	0.5	0.5
Paint, gloss white	0.95	0.05
Paint, matt black	0.96	0.04

The effectiveness of radiant cooling systems can be improved through the use of selective surfaces, which are the surfaces or materials that have a potential to reach lower temperatures compared to that of non-selective ones (Granqvist and Eriksson, 1991: p.170). Such surfaces should possess a high emissivity for long-wave radiation in the spectrum of sky window between 8 µm and 13 µm and a high reflectivity to all other long-wave bands (from clouds, CO_2, dust, etc.) and short-wave spectrum (solar radiation between 0.4 µm and 3 µm), so that the radiative cooling can be harnessed throughout the daytime (Granqvist and Hjortsberg, 1981). Therefore, it is challenging to obtain a substance that satisfies these conditions.

According to Wien's law, most of the radiation emissions from buildings are within the spectrum of the sky window, since the temperature of building surfaces in hot regions is generally in the range 15-60 °C. Therefore, numerous researches have been carried out on the selective surfaces for radiant heat transfer enhancement. However, a limited number of materials have been examined as potential selective radiator surfaces in several studies (Catalanotti et al., 1975, Miller and Bradley, 1979, Landro and McCormick, 1980, Granqvist, 1981, Berdahl, 1984, Eriksson et al., 1985, Nilsson and Niklasson, 1995, Diatezua et al., 1995, Al-Nimr et al., 1998, Dobson et al., 2003, Hu et al., 2018b). Some of the available selective surfaces are listed in Table 2.4, with

their potential cooling performance at an ambient temperature of 25 °C, assuming sky temperature similar to the ambient (in reality are different), an ideal transmittance windscreen, and neglecting the convection and conduction influences.

The numerical and experimental investigations of the selective surfaces for sky radiation have presented promising outcomes up to date. Among all materials considered, the anodised aluminium has a good performance compared to a black body (Table 2.4) and may be considered a practical and an economical selective radiator surface (Bathgate and Bosi, 2011). However, some practical issues and technical difficulties need to be tackled. If high-quality selective coatings are produced at a reasonable cost, the practical application might need means for maintaining the optical properties of the substances that are affected by exposure to the ambient conditions. Furthermore, similar to windscreens, selective surfaces may suffer from condensation problems and accumulation of dust and airborne pollutant on the top surface (Santamouris, 2007: p.281-282).

Table 2.4: Selective surface coating materials and their potential radiative cooling performance at an ambient temperature of 25 °C.

Selective surface material	**Net radiative power at 25 °C (W/m²)**	**Reference**
Black body	74.1 (calculated)	(Bathgate and Bosi, 2011)
Anodised Aluminium	66.6	(Bathgate and Bosi, 2011)
Silicon nitride	63.8	(Eriksson et al., 1985)
Anodised Aluminium + magnesium oxide	62.3 (calculated)	(Bathgate and Bosi, 2011)
Silicon oxy-nitride	61.8	(Diatezua et al., 1995)
Anodised aluminium (Anocoil)	55.1	(Bathgate and Bosi, 2011)
Silicon oxide	32.5	(Granqvist and Hjortsberg, 1981)

2.6.4 Effect of radiator tilt angle

All the previous studies acknowledged that the use of a nocturnal radiator on a horizontal position with an unobstructed view makes the most of the radiative cooling by maximising the net radiant loss to the sky. However, an inclination of the radiator may be required for several purposes such as; placing the radiator on a pitch-roof, using the radiator as a solar collector tilted according to the latitude, or for water drainage purpose (Erell and Etzion, 1996).

The temperature difference among surfaces on or near the ground is relatively small, and therefore, the radiant exchange is also small, while the considerable radiant loss will be toward the cooler sky. Accordingly, the radiator inclination will result in receiving a higher amount of downwards radiation, since the view factor to the sky reduces and the radiator becomes more revealed to the warmer regions of the sky near to the horizon (Santamouris, 2007: p.282). Therefore, it is essential to optimise the tilt angle of the radiator, so the output from the system could exceed the losses yielded by the radiator inclination.

Clark and Berdahl (1980) have found that tilting a radiator surface by 30° from the horizontal reduces its long-wave radiation emission by 15% in comparison to a similar surface on a horizontal position. Martin (1989) has pointed out that, although inclination of a radiator by 45° augments the received radiation from the upper atmosphere by about 4-6% based on the climatic conditions, a reduction up to 20% in the cooling power might occur.

2.7 Summary

Nocturnal radiative cooling is a sustainable method aimed at dissipating heat to the cold sky through the long-wave radiation exchange. Radiative cooling systems for buildings applications can fulfil the immediate night cooling requirements and during the daytime in the case of being coupled with appropriate thermal energy storage. Most of the previous studies have reported substantial cooling potential and energy savings by investigating the performance of various radiative cooling systems in different climates.

The following remarks have been drawn from the reviewed previous research;

- The nocturnal radiative cooling potential depends mainly on the local climate conditions and also on some of the system design parameters. The applicability is high in locations with clear sky conditions, low humidity, low wind speed, and high diurnal temperature variations such as temperate and hot-arid regions. To get the most out of this strategy, selection of surfaces with high emissivity to long-wave radiation and high reflectivity to solar radiation, positioning the surface horizontally, and using appropriate radiator covers with high transparency to long-wave radiation within the sky window are the most significant design considerations.

- Most of the current research focuses on the enhancement of the radiative cooling potential through two main aspects; firstly, the development of selective radiative surfaces and coatings with optimum optical properties that are designed to radiate infrared radiation in the 8-13 μm wavelengths and to reflect radiation outside this band. It should be underlined that the available selective surfaces and suitable material are limited, and hence, further improvement in the optical performance of the current substances and searching for new materials are highly required. Secondly, the use of windscreens and wind shields to reduce the convective gains that significantly reduce the radiative cooling potential. Accordingly, an exploration of suitable materials as radiators covers (windscreens) has become a motivating area for

research, owing to the limited options and some drawbacks associated to radiation transmissivity, durability, cost, etc.

- In addition to the conventional application in buildings, hybrid systems incorporating nocturnal radiative cooling with some renewable and sustainable energy systems have been considered. The researchers attempted to use photovoltaic-thermal (PVT) collectors as nocturnal radiators, and investigate the integration of radiant cooling with solar collector walls, thermal energy storage, heat pipes, direct and indirect evaporative cooling, and desiccant cooling, etc. However, published researches are quite scarce and mainly attempted to predict the feasibility of the proposed concepts through simulation and a limited number of prototype testing.

- Although the physics and fundamentals of the nocturnal radiative cooling are well established, the technology is still in the stage of the experimental work and the performance monitoring. A shift towards the real and broad implementation is subject to tackling of the current challenges and practical issues relevant to optical properties and covering of the radiative panels. Currently, intensive work is underway to produce reliable commercial radiative cooling components.

Chapter 3

Review of Latent Heat Storage based Free Cooling Systems

3.1 Introduction

The objectives of the present review were to provide a comprehensive discussion on the recent development in free cooling systems incorporated latent heat storage and to identify the significant parameters influencing the system thermal performance and application to get a clear picture of possible opportunities and strategies that can be applied to enhance the efficiency of the technology. The chapter begins by overviewing the thermal energy storage systems, highlighting the classifications and the associated advantages and disadvantages, with more focus on the latent heat storage and the application methods in buildings. The chapter provides a succinct review in chronological order for the most recent research in free cooling systems based PCM storage and ends with discussing the major factors affecting the system performance and the suitable enhancements that can be applied.

3.2 An overview of thermal energy storage (TES)

Thermal Energy Storage (TES) systems can be utilised for both short and long-term storages for high or low-temperature energy (Dincer and Dost, 1996, Dincer et al., 1997, Pinel et al., 2011). In principle, TES mechanisms are classified into sensible heat, latent heat and thermo-chemical energy storages or a combination of these (Baylin, 1979:p.2, Mehling and Cabeza, 2008:p.1). The recent development in properties and features of the TES have been reported in many published reviews (Hariri and Ward, 1988, Tatsidjodoung et al., 2013). It is crucial to have an understanding of the different TES technologies and their pros and cons in order to select the most appropriate storage system for a particular application (Prieto et al., 2016). Figure 3.1 demonstrates a general classification of thermal energy storage methods.

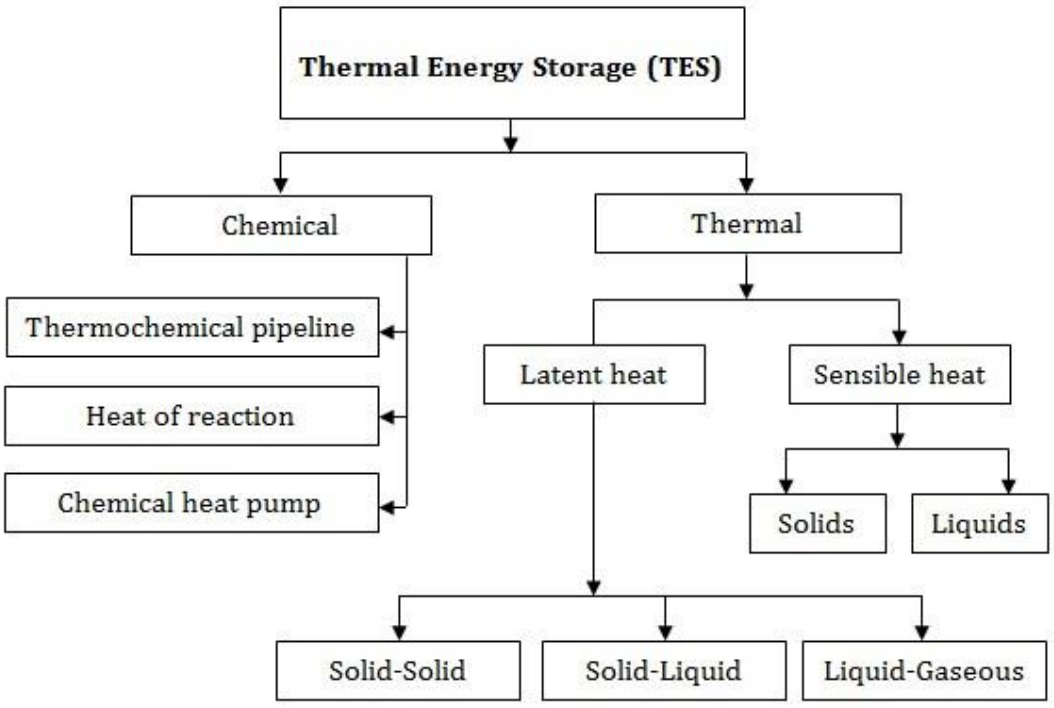


Figure 3.1: Classification of thermal energy storage methods (Baylin, 1979: p.2, Mehling and Cabeza, 2008: p.1, Sharma et al., 2009).

3.2.1 Thermochemical energy systems (TCES)

Thermochemical energy systems (TCES) make use of generation and release of heat during dissociation and synthesising of chemical compounds in a reversible endothermic chemical reaction (Kerskes, 2016:p.246). TCES systems have the advantage of high energy density at a constant temperature, long-term and stable storage, wide temperature ranges, and easy transportation (Cot-Gores et al., 2012, Ding and Riffat, 2013). However, some of the disadvantages are poor heat and mass transfer property under high-density conditions. They are also expensive, and there is limited experience in their long-term operation (Kalaiselvam and Parameshwaran, 2014:p.63). The research in reversible thermochemical reactions is still under development, and some technical and economic barriers need to be tackled before a broader implementation of the technology (H Abedin and A Rosen, 2011).

3.2.2 Sensible heat storages (SHS)

Sensible heat storages (SHS) make use of increasing temperature of a storage substance without any phase change process (Zhang et al., 2016a). The ratio of the heat stored to the temperature rise is the heat capacity of the storage medium (Paksoy, 2007:p.257). SHS substances can be classified into liquid SHS such as water and oil or solid SHS such as rocks, metals, and masonry materials. Since gases have very low heat capacity, they are not usually suitable for cold or heat storage (Mehling and Cabeza, 2007:p.257). Water can be considered the best of all ordinarily used substances, as it has the highest volumetric heat capacity (4187 kJ/m^3 K), which is almost double of that of the concrete and much larger than that of other masonry materials. Typically, a mass of concrete could compensate for the volumetric heat capacity of the water, since the density of concrete is almost double of that for the water. SHS systems are very well developed and are readily available in the literature. More details about thermal properties of a range of SHS substances commonly used in buildings are available in references (Dincer, 2002, Chiras, 2002, Baggs and Mortensen, 2006, Szokolay, 2014). The shortcomings are the limited storage capacity, bulkiness, and the non-suitability for most practical applications with a narrow

temperature range due to the large temperature variation of the charging and discharging periods (Agyenim, 2007, Ding, 2014).

3.2.3 Latent heat storages (LHS)

Latent heat storages (LHS) on the other hand store energy by making use of the phase changing process of a substance by melting or vaporisation without a significant temperature change. Such materials are referred to as phase change materials (PCM) (Dincer and Rosen, 2002:p.141).

The use of LHS as thermal energy storage has attracted enormous attention over the past decades owing to the effectiveness and the superiority of these substances compared to other TES materials (Fang et al., 2016, Mohamed et al., 2017). In general, LHS substances have energy densities higher than SHS and lower by around five times than those of the TCES. However, the lower complexity and effective cost make the LHS more practical compared to TCES (Fernandez et al., 2010, Pardo et al., 2014, Liu et al., 2016c). The latent heat transfer is approximately an isothermal process as PCMs absorb and discharge heat at almost a constant temperature or within a narrow temperature range which is more applicable for maintaining thermal comfort compared to SHS (Regin et al., 2008, Pielichowska and Pielichowski, 2014). Another essential advantage of LHS is their easy integration where other SHS substances are difficult to be installed particularly in existing buildings and lightweight structures (Brun et al., 2013). This is because PCMs are capable of enhancing the mass effect with much lighter weight and volume estimated at 5-14 times compared to conventional SHS systems which require a large space for the energy storage accommodation (Hasnain, 1998, Cui and Riffat, 2011). Table 3.1 compares the required weight and volume of some LHS and SHS substances to store 10^6 kJ of energy at a temperature rise of 15 K during heat storage (Hasnain, 1998, Khadiran et al., 2016).

Moreover, LHS can be used as appropriate storage or can be added to enhance the performance of SHS systems (Pasupathy et al., 2008). On the other hand, the performance of LHS systems is limited mainly by the low thermal conductivity and the lack of thermal stability of PCMs (Zhang et al., 2016b). The cost of PCMs is

relatively high at present compared to SHS. Nevertheless, they are widely available in various forms and temperature range. The current prices are predicted to drop in the near future due to extensive research carried out on PCMs nowadays in addition to the increasing number of PCM manufacturers around the world (Waqas and Din, 2013).

Table 3.1: Comparison of required mass and weight of LHS and SHS substances to store 10^6 kJ with $\Delta T = 15$ K (Hasnain, 1998, Khadiran et al., 2016).

	Sensible heat storage		**Latent heat storage**	
	Rock	**Water**	**Organic PCM**	**Inorganic PCM**
Required weight of storage (kg)	67,000	16,000	5,300	4,350
Required volume of storage (m³)	30	16	6.6	2.7

3.3 Overview of latent heat storage (LHS) for building application

Latent heat storages (LHS) aim to use the stored heat by altering the physical state of a substance from one state to another by melting or vaporization (solid to liquid or liquid to gas and vice versa) at desired operating temperature range which is almost constant for pure substances, and this is one of the advantages of LHS (Abhat, 1980, Mondal, 2008, Mahlia et al., 2014, Xu et al., 2014, Jacob and Bruno, 2015). Figure 3.2 shows a variation of latent and sensible heat storage with temperature.

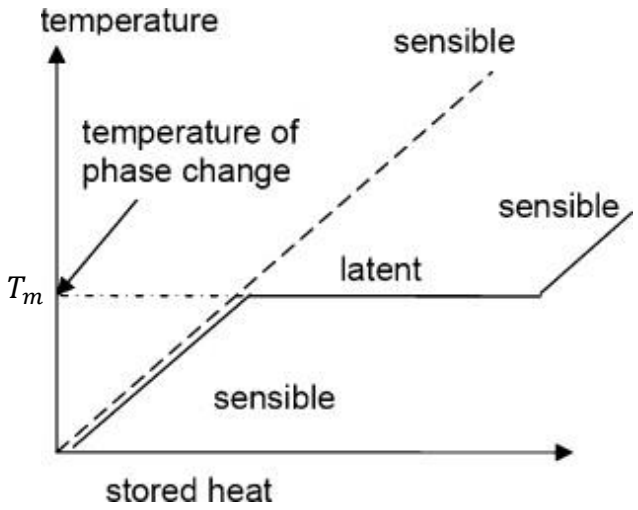


Figure 3.2: Latent and sensible heat storage variation with temperature (Mehling and Cabeza, 2008:p.3, Gil et al., 2010).

The storage capacity of LHS with a solid-liquid PCM (Q_{LHS}) is given as a function of the heat of fusion per unit mass (Δh_m) and the specific heat (C_p) by equation (3.1) (Lane and Shamsundar, 1983);

$$Q_{LHS} = \int_{Ti}^{Tm} m\, C_{pi}\, \Delta T + m\, a_m\, \Delta h_m + \int_{Tm}^{Tf} m\, C_{ps}\, \Delta T \qquad (3.1)$$

where; C_{pi} is the average specific heat between the melting temperature (T_m) and the initial temperature (T_i), C_{ps} is the average specific heat between the final temperature (T_f) and T_m , and a_m is the fraction of the melted material.

The selection criteria for latent heat storage substances have been highlighted through several studies (Lorsch et al., 1975, Abhat, 1983, Soares et al., 2013, SOCACIU et al., 2014, Vats and Vaish, 2014, Alva et al., 2017). All these studies agreed that PCMs should have desirable thermo-physical, chemical, kinetic, and economic properties. In the case of thermo-physical properties, a suitable phase change temperature in the desired operation limit and a high enthalpy of fusion are the two main influential requirements when selecting a PCM for a particular application. A desirable PCM also has to possess other thermo-physical properties including; high thermal conductivity, high specific heat, high density, congruent melting, small volume change during phase transition and low vapour pressure at operational temperatures to minimise the containment defects. Chemically, the PCM should be stable for long-term usage, non-corrosive to encapsulation, non-toxic, non-flammable, non-explosive, compatible with construction and container materials, and exhibiting no degradation after a large number of cycles. In the case of Kinetic properties, PCMs are required to possess a high nucleation rate to avoid supercooling, a sufficient solidification rate to meet demands of heat retrieval from the storage system, and the melting and the solidification should be at a nearly constant temperature and phase segregation. From the economic side, the PCM should be abundant and cost-effective.

Although there are a large number of PCM products in the market, it is difficult to identify a substance that satisfies all the selection criteria to operate as superior thermal storage; and this issue should be handled through a careful design of the system.

Latent heat storage can be achieved through Solid-Solid, Solid-Gas, Liquid-Gas, and Solid-Liquid phase transformation. However, solid-liquid and solid-solid PCMs are the only two of practical interest (Wang et al., 2000). Characteristics and performance of these classifications are as follow.

3.3.1 Solid-Solid PCM

In Solid-Solid PCM substances, the heat is stored when a substance changes from a crystalline to another form. They appear as an alternative solution to overcome the drawbacks of the most utilised Solid-Liquid PCMs that requires adequate encapsulation to prevent the liquid from leaking, this encapsulation lowers the density of the system and escalates the cost of the product. Solid-Solid PCMs may be used without containers. Another positive side is that they have small volumetric expansion compared to Solid-Liquid PCMs which leads to a less stringent container, more design flexibility, and more effective cost. Unfortunately, Solid-Solid PCMs have lower latent heat (Nomura et al., 2010, Cárdenas and León, 2013). Examples of most promising Solid-Solid LHS used as possible candidates for space heating and process heat applications are; pentaerythritol [$C_5H_{12}O_4$], pentaglycerine [$CH_3{-}C-(CH_2{-}OH_3)$], neopentyl glycol[$(CH_3)_2-C-(CH_2{-}OH)_2$], and their mixtures (Lane and Shamsundar, 1983). Noting that, trombe wall with such substances can exhibit much better thermal behaviour compared to a customary concrete trombe wall (Sharma et al., 2009).

3.3.2 Solid-Gas and Liquid-Gas PCM

Solid-Gas and Liquid-Gas PCM have the highest latent heat. However, they are limitedly used for heat storage as such systems require large volume containers which lead to complexity and impracticality, and so they are not widely used for thermal energy storage (Liu et al., 2010, Cárdenas and León, 2013).

3.3.3 Solid-Liquid PCM

Solid-Liquid PCMs have relatively smaller latent heat compared to Solid-Gas and Liquid-Gas PCMs. However, their small volume change (10% or less) makes the

system cost-effective, and these are commonly applied in thermal energy storage systems (Mehling and Cabeza, 2007:p.258). Solid-Liquid PCMs are the most examined and commercially produced type amongst all the LHS family, and hence, a large number of candidates are available in a wide range of operating temperatures.

Abhat (1983) in his major study of LHS substances produced a classification for PCM which has largely been used and cited by some researchers. Solid-liquid PCMs can be classified based on their chemical composition into three main categories; organic compounds, inorganic compounds, and eutectics as illustrated in Figure 3.3. Another general classification of substances that can be used as latent heat storage was given in (Mehling and Cabeza, 2007, Mehling and Cabeza, 2008) based on their typical melting temperature range and enthalpy as shown in Figure 3.4.

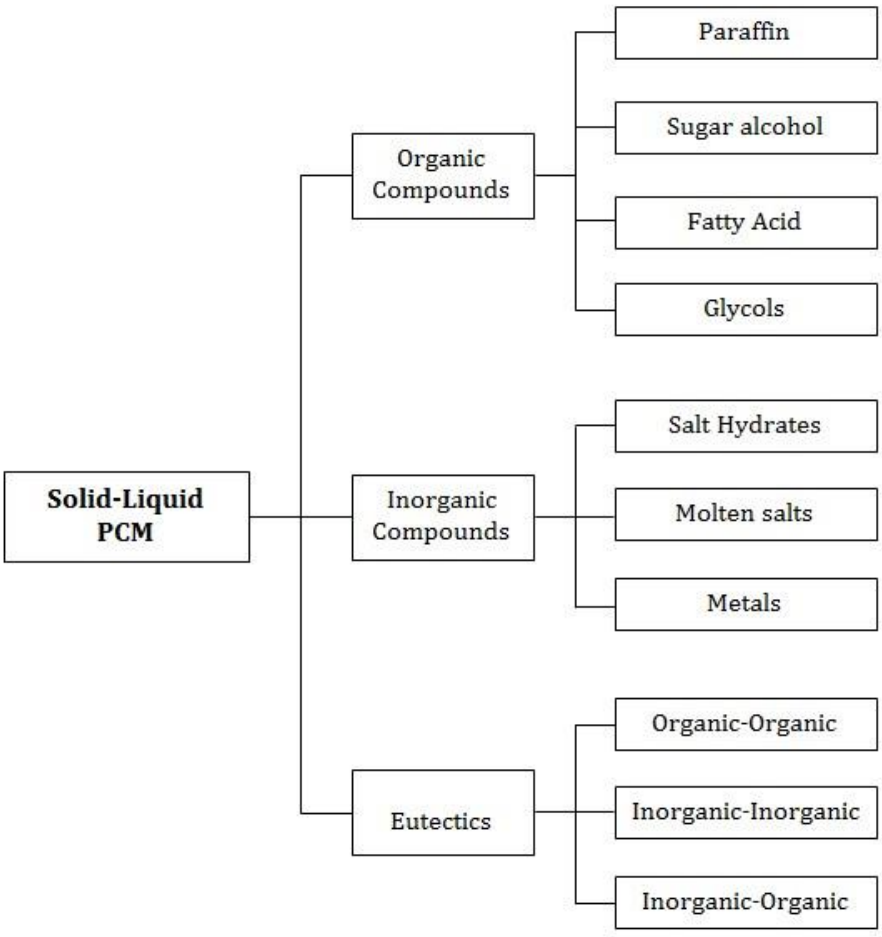


Figure 3.3: Classification of the Solid-Liquid PCMs (Su et al., 2015).

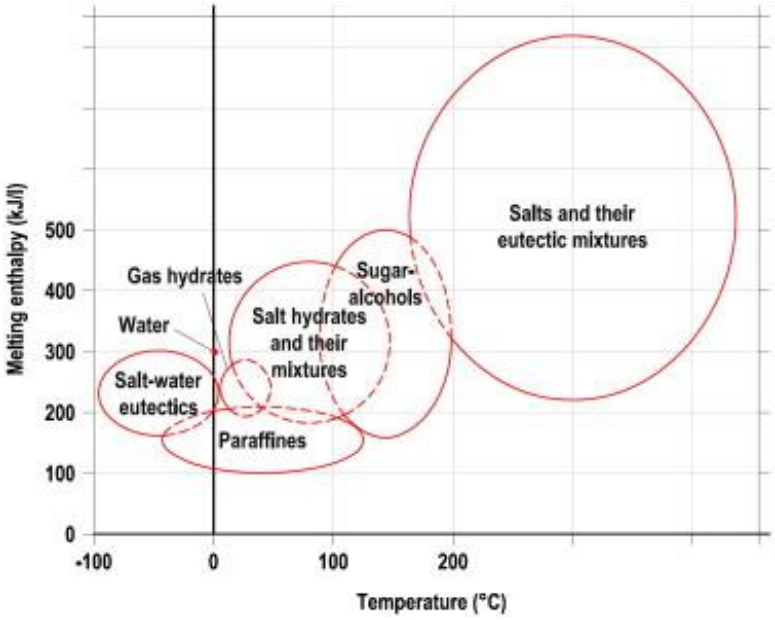


Figure 3.4: Classes of available PCM based on their melting temperatures range and enthalpy (Baetens et al., 2010).

3.3.3.1 Organic Solid-Liquid PCMs

The organic Solid-Liquid PCMs are generally chemically stable, available in a wide range of temperature, and having a high latent heat of fusion. In addition, these compounds show almost less or no supercooling during the charging state. They also show little degradation of the latent heat of fusion, congruent melting, and they are non-corrosiveness and are usually compatible with other construction materials. The organic PCMs can be divided into paraffin and non-paraffin (Kuznik et al., 2011).

Paraffin organic PCMs belong to a group of saturated hydrocarbons with the same characteristics and molecular formulas $[C_nH_{2n+2}]$, which consists of a mixture of straight hydrocarbon chains known as n-alkanes. Noting that, the more the carbon atoms are in the paraffin formula; the higher the melting temperature of the PCM (Su et al., 2015, Shao et al., 2015). Paraffin waxes are safe, inexpensive, reliable, non-corrosiveness and available in a large range of melting temperatures up to around 70 ^{o}C. They also have a reasonable storage density ranging from 120 kJ/kg to about 210 kJ/kg, a low vapour pressure, and no segregation throughout the phase change. The Differential Scanning Calorimetry (DSC) analysis carried out by Baetens et al. (2010) has shown no any indication for significant degradation of thermal properties of the

paraffin waxes after a high number of thermal cycles. Conversely, Paraffin waxes show some unfavourable properties including; low thermal conductivity level (around 0.2 W/m K), relatively large volume alteration, moderate flammability, and incompatibility with the plastic containers.

Non-paraffin organics such as fatty acid, glycols, esters and sugar alcohol generally have favourable thermal properties during both melting and freezing transitions. Amongst all, Fatty acids; which are compounds of carbon (C), hydrate (H), and oxygen (O) with the general formula of $[CH_3(CH_2)_{2n}.COOH]$ where n is the atomic numbers; are the most interested type. Fatty acids have a melting/freezing temperature range of approximately 16-65 ºC and relatively high heat of fusion between 155 and 180 kJ/kg. The most widespread fatty acids are sorted into six groups; Caprylic, Capric, Myristic, Palmitic and Stearic with respectively 8 up to 18 carbon atoms per molecule. Although fatty acids are the most commonly used group of non-paraffin family due to their desirable characteristics, they are flammable at high temperatures and there is a shortage of substances with transformation temperature around the human thermal comfort (Feldman et al., 1989, Rozanna et al., 2005, Baetens et al., 2010, Yuan et al., 2014, Su et al., 2015). Sugar alcohol organics in particular have a phase transformation temperature almost over 100 ºC, then, they can be applied in solar plants and for waste heat recovery at temperatures below 200 ºC (Nomura et al., 2010). Although non-paraffin PCMs represents the largest group of the LHS, they are two to three times more expensive than paraffin. They are also instable at high temperature, having varying toxicity, and mild corrosive (Abhat, 1983, Hasnain, 1998).

Significantly, organic Solid-Liquid PCMs are widely consumed due to their apparent advantages; still, the low thermal conductivity, the substantial volume alteration, and the moderate flammability should be handled carefully by adequate system design and selection of proper container. PCM substances having melting/solidification temperature in the range of 20-30°C are considered suitable for building use in the literature. Examples of some organic Solid-Liquid PCM candidates suitable for space heating and cooling in buildings are tabulated in Table 3.2.

Table 3.2: Organic Solid-Liquid PCMs with phase change temperature between 19 and 30 ºC (Tyagi and Buddhi, 2007, Kenisarin and Mahkamov, 2007, Verma and Singal, 2008, Raj and Velraj, 2010, Cabeza et al., 2011, Riffat et al., 2013).

PCM Compound	Melting temp. (ºC)	Heat of fusion (kJ/kg)
Butyl stearate	19	140
Propyl palmitate	19	186
Paraffin C_{16}–C_{18}	20–22	152
Polyethylene glycol E 600	20–25	146
Dimethyl sabacate	21	120-135
Octadecyl 3-mencaptopropylate	21	143
Paraffin C_{17}	21.7	213
n-Heptadecane	22	215
Paraffin C_{13}–C_{24}	22–24	189
Octadecyl thioglyate	26	90
Lactic acid	26	184
1-Dodecanol [CH_3 $(CH_2)_{11}$ OH]	26	200
Vinyl stearate	27–29	122
Paraffin C_{18}	28	244
n-Octadecane	28.2	245
Methyl palmitate	29	205
Methyl stearate	29	169
Capric acid	30.1	158

3.3.3.2 Inorganic Solid-Liquid PCMs

Inorganic solid-liquid PCMs include salt hydrates, molten salts, and metallic alloys. They usually have a high latent heat of fusion and a volumetric latent heat storage capacity approximately equivalent to a double of the organic compounds (Sharma et al., 2009). Inorganic compounds also have a small volume alteration during the melting phase, a relatively high thermal conductivity (around 0.5 W/m K) and an inexpensive cost compared to organic PCMs. However, supercooling, decomposition and corrosion are the common drawbacks which may influence the properties of PCM

and hence reducing the system efficiency at the long-term (Abhat, 1983). Table 3.3 includes some inorganic compounds suitable for building heating and cooling.

Salt hydrates are the oldest and most investigated PCM group. They can be regarded as mixtures of inorganic salts and water creating a typical crystalline solid of general formula $[A.nH_2O]$ where A represents the salt component. Varying chemical composition of salts is used to accomplish the required phase change temperature. The solid–liquid transition of salt hydrates is basically a dehydration of hydration of the salt, although this process resembles melting or solidification thermodynamically. At the melting phase, the hydrate salt either melts to salt hydrate and fewer moles of water or to anhydrous salt and water, noting that, the melting manner varies among the compositions and can be regarded as congruent, incongruent or semi congruent melting (Rbiradar and Chougale, 2015, Su et al., 2015).

Salt hydrates; besides their excellent thermal properties; are generally inflammable, slightly toxic, economical and compatible with plastic containers. However, incongruent melting represents the major problem faced when applying salt hydrates for energy storage. It can be attributed to the insufficiency of the released water of crystallisation to dissolve all the existent crystalline salt. The hydrate or anhydrous salt usually remains at the lower part of the container due to the density difference and hence reduces the opportunity of its recombination with water during the following solidification phase. This may lead to an irreversible melting/freezing of salt hydrate continuation in decreasing with each load-unload cycle. This problem can be treated via different methods including; mechanical stirring, the addition of thickening agents and adjustment of the chemical compositions (Abhat, 1983, Sharma et al., 2009).

Other common problems associated with the application of salt hydrates are supercooling and phase segregation. Supercooling of the liquid phase before the crystallisation occurrence can be minimised by adding nucleating agents, by retaining some crystals in a small cold zone to act as nuclei or by utilising rough heat exchanging surface on container walls to promote nucleation. Salt segregation can be avoided via utilising thickening agents, rotating storage devices and direct contact heat exchange (Hasnain, 1998).

Molten salts and some metallic PCMs have a high heat of fusion per unit volume, a high thermal conductivity, low specific heat, a small volume change and a large phase change temperature (Cárdenas and León, 2013). Based on their availability of high transformation temperature, they are usually used for solar power generations applications and waste heat recovery at temperatures above 200 ºC (Nomura et al., 2010).

Table 3.3: Inorganic Solid-Liquid PCMs with phase change temperature between 19 and 30 ºC (Zalba et al., 2003, Pasupathy et al., 2008, Sharma et al., 2009, Cabeza et al., 2011).

PCM Compound	Melting Temp. (ºC)	Heat of fusion (kJ/kg)
$FeBr_3 \cdot 6H_2O$	21-27	105
$Mn\ (No_3)_2 \cdot 6H_2O$	25.5	148
$CaCl_2 \cdot 6H_2O$	29.7	192
$LiNO_3 \cdot 3H_2O$	30	189
$LiNO_3 \cdot 2H_2O$	30	296
Gallium	30	80.3

3.3.3.3 Eutectic PCMs

Eutectics usually comprise two or more low melting temperature components which melt and solidify congruently to create a mixture of the components' crystals during the solidification. The key advantage of eutectics over other classes of PCMs is that their melting points can be manipulated via a combination of various weight proportions of components (Sharma and Sagara, 2005).

Eutectic PCMs are largely welcomed in buildings for heating and cooling requirements due to their high volumetric thermal storage density, single melting temperature and to the advantage of melting and freezing congruently. However, there is limited availability of thermos-physical properties data of eutectic PCMs. Also, some fatty eutectics have a very strong odour which makes it undesirable to be operated as PCM wallboard (Thambidurai et al., 2015). Examples of commonly used eutectics of organic and inorganic compounds in buildings are listed in Table 3.4.

Table 3.4: Eutectic PCMs with phase change temperature between 19 and 30 ºC (Zalba et al., 2003, Sharma et al., 2009, Cabeza et al., 2011, Veerakumar and Sreekumar, 2016).

PCM Compound	**Melting temp. (ºC)**	**Heat of fusion (kJ/kg)**
65.5% Capric + 34.5% Lauric acid	18-19.5	140.8
61.5% Capric acid + 38.5% Lauric acid	19.1	132
45% Capric + 55% Lauric acid	21	143
75.2% Capric acid + 24.8% Palmitic acid	22.1	153
26.5% Myristic acid + 73.5% Capric acid	22.4	152
34% $C14H_{28}O_2$ + 66% $C_{10}H_{20}O_2$	24	147.7
50% CaC_{l2} + 50% MgC_{l2} $6H_2O$	25	95
66.6% $CaC_{l2}\cdot 6H_2O$ + 33.3% $Mgc_{l2}\cdot 6H_2O$	25	127
Octadecane + docosane	25.5-27	203.8
Octadecane + heneicosane	25.8-26	173.93
13.4% Stearic acid + 86.6% Capric acid	26.8	160
48% CaC_{l2}+4.3% NaCl + 0.4% KCl+47.3% H_2O	26.8	188
50% CH_3CONH_2 + 50% NH_2CONH_2	27	163
Triethylolethane + urea	29.8	218
47% $Ca(NO_3)_2\cdot 4H_2O$ + 53% $Mg(NO_3)_2\cdot 6H_2O$	30	136
60% $Na(CH_3COO)\cdot 3H_2O$ + 40% $CO(NH_2)_2$	30	200.5

According to the literature (Agyenim et al., 2010, Waqas and Din, 2013, Kousksou et al., 2014), there are many popular international manufacturing companies produce PCMs across the world such as (RUBITHERM) in Germany, (EPS) in the UK, (Climator) in Sweden, (PLUSS) and (TEAP) in India, and (Cristopia) energy systems in France. Table 3.5 includes thermo-physical specifications of various commercial PCMs with melting/solidification temperature within the range of 19-30 °C.

Table 3.5: Available commercial PCM within the phase change temperature range 19-30°C.

PCM	Classification of PCM	Melting temp. (°C)	Enthalpy (kJ/kg)	Density L/S (kg/l)	Specific heat L/S (kJ/kg K)	Conductivity L/S (W/m K)	Maximum operation temp. (°C)
(RUBITHERM)							
RT21	Paraffin	21	155	0.77/0.88	2.0	0.2	40
RT21 HC	Paraffin	21	190	0.77/0.88	2.0	0.6	45
RT22 HC	Paraffin	22	190	0.70/0.76	2.0	0.2	50
RT24	Paraffin	24	160	0.77/0.88	2.0	0.2	55
RT25	Paraffin	25	170	0.76/0.88	2.0	0.2	55
RT25 HC	Paraffin	25	230	0.77/0.88	2.0	0.2	65
RT26	Paraffin	26	180	0.75/0.88	2.0	0.2	60
RT28 HC	Paraffin	28	250	0.77/0.88	2.0	0.2	50
SP21 E	Inorganic	21-23	170	1.4/1.5	2.0	0.6	45
SP24 E	Inorganic	24-25	180	1.4/1.5	2.0	0.6	45
SP25 E2	Inorganic	24-26	180	1.4/1.5	2.0	0.6	45
SP26 E	Inorganic	25-27	180	1.4/1.5	2.0	0.6	45
SP29 Eu	Inorganic	29-31	200	1.5/1.55	2.0	0.6	60
(EPS)							
A22	Organic	22	145	0.785	2.22	0.18	250
A22H	Organic	22	216	0.82	2.85	0.18	400
A23	Organic	23	145	0.785	2.22	0.18	280
A24	Organic	24	145	0.79	2.22	0.18	280
A25	Organic	25	150	0.785	2.26	0.18	280
A25H	Organic	25	226	0.81	2.15	0.18	400
A26	Organic	26	150	0.79	2.22	0.21	280
A28	Organic	28	155	0.789	2.22	0.21	280
A29	Organic	29	226	0.81	2.15	0.18	300
S19	Salt hydrate	19	160	1.52	1.9	0.43	60
S21	Salt hydrate	22	170	1.53	2.2	0.54	60
S23	Salt hydrate	23	175	1.53	2.2	0.54	60
S25	Salt hydrate	25	180	1.53	2.2	0.54	60
S27	Salt hydrate	27	183	1.53	2.2	0.54	60
S30	Salt hydrate	30	190	1.304	1.9	0.48	60
(Climator)							
ClimSel C21	Salt hydrate	21-26	134	1.4	N.A.	0.75-0.93	N.A
ClimSel C24	Salt hydrate	24-27	140	1.4	N.A.	0.75-0.93	N.A
ClimSel C28	Salt hydrate	27-31	170	1.4	N.A.	0.72-0.98	N.A
(PLUSS)							
OM21	Organic	21	250	0.924 (S)	N.A.	0.14/0.21	120
FS21R	Organic	20.6	183	0.887 (S)	N.A.	0.10/0.30	120
FS21	Organic	20-21	130	0.87 (S)	N.A.	0.10/0.30	120
OM29	Organic	29	229	0.87 (S)	3.9 (L)	0.17/0.29	120
FS29	Organic	28-29	189	0.87 (S)	3.4 (S)	0.45 (S)	120
HS21	Inorganic	18-22	185	1.40 (L)	3.4 (L)	0.59/0.82	80
HS22	Inorganic	22-23	185	1.54/1.84	3.0/2.2	0.56/1.13	80
HS 24	Inorganic	24-25	185	1.51/1.8	2.3 (L)	0.55/1.05	80
HS 29	Inorganic	29	190	1.53/1.83	2.3 (L)	0.38/0.47	80

S= Solid, L= Liquid, and N.A. = Not Available.

3.4 Methods of PCM application in buildings

The first studies of exploiting PCM for space cooling and heating have been conducted since 1975 (Telkes, 1975, Barkmann and Wessling, 1975). Currently, PCM products are largely available in several forms such as powder, granule or rubber and in a wide range of container types such as tubes, spheres or panels, etc. This diversity provides a variety of integration means in buildings as follows.

3.4.1 Impregnation of PCM into the construction materials

PCMs can be impregnated into the conventional structural components by several methods such as; direct incorporation by simply mixing a powder or a liquid PCM with the construction materials, in this case, no additional equipment is required, but a risk of leakages and decomposition problems is predicted (Hawes et al., 1993, Voelker et al., 2008, Ascione et al., 2014, Karaipekli et al., 2016).

Another procedure is called immersion, which could be achieved via dipping the construction material into a melted PCM and let the PCM penetrates into the object pores. However, some studies showed that this technique might have an insufficient impact on long-term use due to leakage drawbacks.

Moreover, some macro-encapsulated PCMs can be added to the building structures to avoid the material leakage and to reduce the unsafe impression on the structure components (Zhou et al., 2012). For instance, it was reported that concrete included 5% microencapsulated PCMs can save energy up to 12% (Hunger et al., 2009).

3.4.2 Integration of PCM into the building envelope

A wide range of encapsulated PCM inside different configurations and types of containment such as; plastic bags, aluminium foils, PVC panels, etc. can be integrated into the external and internal fabric of the building such as walls, floors, plaster, ceiling, windows, paint, etc. to increase their thermal mass effect (Zalba et al., 2003, Pomianowski et al., 2013). Several concepts of PCM integration into the building envelope for heating and cooling requirements in the literature are presented in Figure 3.5.

The key advantages of using PCMs in building fabric is that no loss and no additional cost results from energy transportation as the PCM storage delivers the energy directly to the targeted space (Rodrigues, 2009:p.126, Geetha and Velraj, 2012). Incorporating PCMs into the building fabric has been explored through various configurations in different researches and reported as a potential technique of lowering energy consumption in buildings;

PCM in walls and wallboards was investigated in (Feldman et al., 1995, Banu et al., 1998, Darkwa and Kim, 2004, Kuznik and Virgone, 2009, Lai et al., 2010, Hasse et al., 2011, Kuznik et al., 2011, Memon, 2014, Kong et al., 2014, Panayiotou et al., 2016). PCM in floors and under floors was handled for heating requirements in (Xu et al., 2005, Zhang et al., 2006). While PCM use in upper ceiling space is also widely applied as it represents the most exposed surface to the internal space, unlike walls and floors which may usually be covered by furniture or other fittings, besides; higher temperatures exist closer to the ceiling above. PCM integration into the building ceiling was examined in the references (Koschenz and Lehmann, 2004, Pasupathy and Velraj, 2008, Abuelnuor et al., 2017).

Another interesting method is to integrate the PCM into windows and shutters to absorb the excess heat and to reduce the direct and indirect solar gains; such concept was considered in (Ismail and Henrıquez, 2002, Merker et al., 2002, Mehling, 2004, Weinläder et al., 2005, Fokaides et al., 2015, Silva et al., 2016). PCM panels are also used in ventilated double skin facades to minimise the energy demand for space heating and cooling (de Gracia et al., 2015, Luo et al., 2017).

According to Akeiber et al. (2016), although PCM can be integrated into any component of the building envelope, the wall installation is the most common approach detected in the literature (80%) due to ease setup and incorporation.

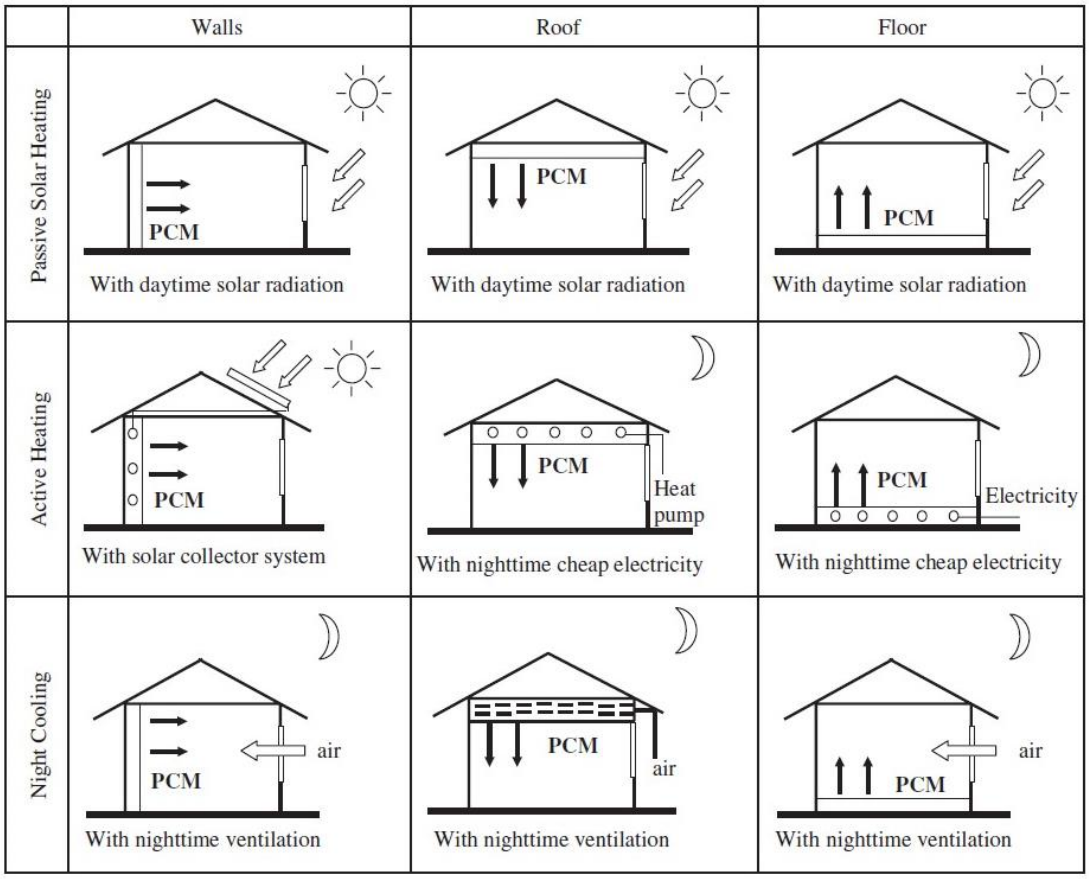


Figure 3.5: PCM integration into buildings' envelope for heating and cooling requirements (Zhang et al., 2007).

3.4.3 Other concepts of PCM applications for building cooling and heating

There are many other methods of PCM incorporation in buildings for both cooling and heating purposes (Hossain et al., 2015). PCMs can be used in a trombe wall providing the same performance with much lighter weight. Such studies have been considered in (Telkes, 1978, Castellón et al., 2009, Rabani et al., 2013). PCMs are usually utilised in solar-PV applications as a passive temperature regulator (Huang et al., 2004, Huang et al., 2006, Ma et al., 2015, Hasan et al., 2016). PCMs can also be incorporated in solar chimneys replacing the conventional storage material and storing the solar energy gained from the absorber (Amori and Mohammed, 2012, Liu and Li, 2015). Figure 3.6 shows an example of the PCM application in a trombe wall and solar chimneys.

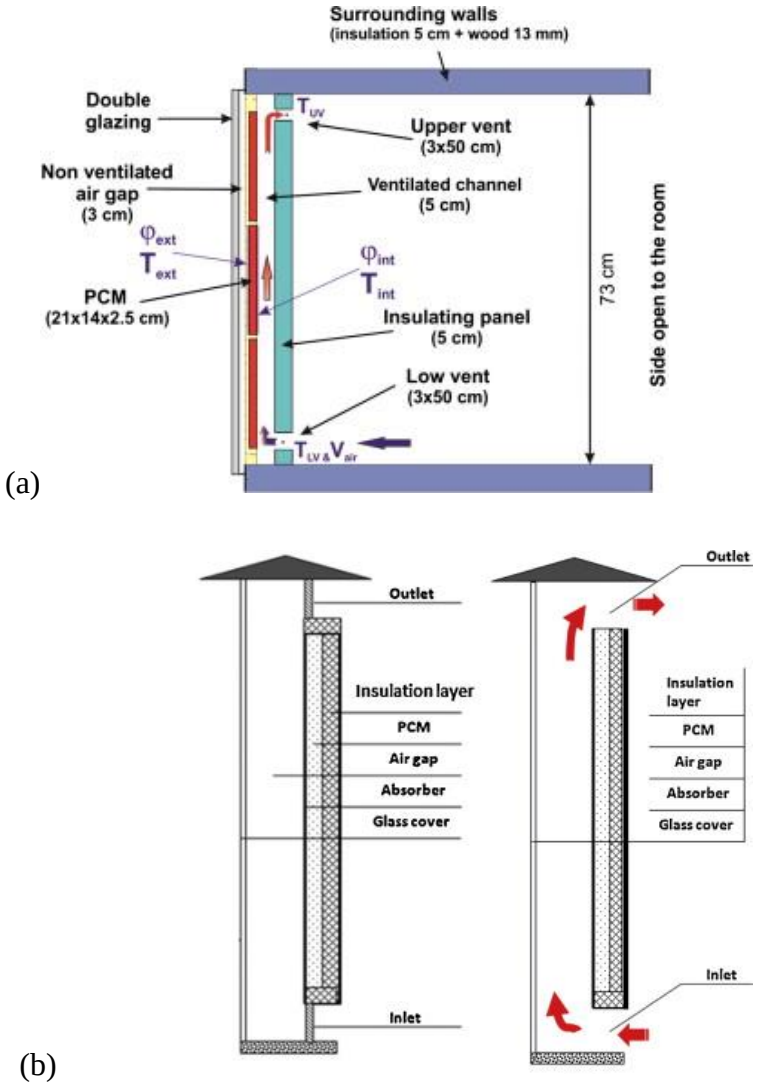


Figure 3.6: Incorporation of PCM in (a) a trombe wall (Zalewski et al., 2012), and in (b) a solar chimney (Liu and Li, 2015).

Another method is the application of PCM as specialised storage located in the room interior envelope. In this case, the storage unit is combined with any passive or active heating and/or cooling systems by allowing circulation of the heat transfer fluid across the storage unit to store the heat/cold energy in the PCM (Rodrigues, 2009, Iten et al., 2016). This concept has the advantage of simple integration into the interior space compared to the other methods as the PCM unit can easily be added, removed or retrofitted without affecting the building structure. PCM storage combined with active systems for space cooling and heating was discussed in (Tyagi et al., 2012, Chaiyat, 2015, Tyagi et al., 2016, Mosaffa and Farshi, 2016, Promoppatum et al., 2017). PCM specialised storage based free cooling system is covered in the following section.

3.5 Research development on PCM based free cooling of buildings

Phase change materials are promising sustainable technologies which could be used to store the cold energy available during nights in sufficient latent heat storage for later utilisation during the daytime. The charging process takes place by circulating the cold ambient air through the PCM storage removing its heat, and the PCM starts to freeze. This process continues until the outdoor temperature goes down below the PCM operation temperature (Figure 3.7a). On the other hand, the stored cold energy will be discharged once the indoor temperature exceeds the upper limit of the comfort zone through the circulation of the hot air through the PCM storage. The passing air rejects the heat to the PCM which begins to melt. The exit air becomes cold and then will be introduced into the indoor space (Figure 3.7b).

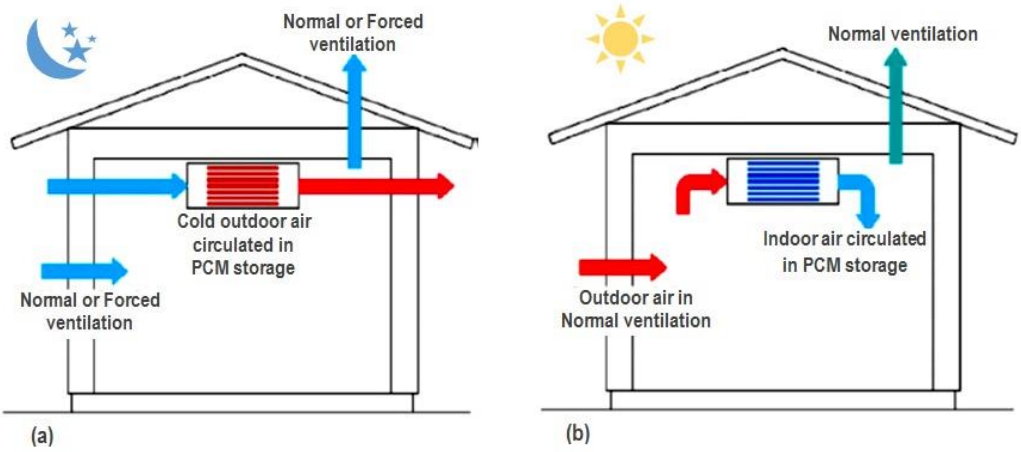


Figure 3.7: A typical operation of free cooling systems incorporated PCM storage; (a) charging, and (b) discharging (Hed and Bellander, 2006).

The researchers have investigated LHS systems based free cooling of buildings for over 25 years. Various designs of cooling and ventilation systems have been developed using different types of PCMs and a wide range of heat exchanger configurations. Any PCM heat exchanger utilised in free cooling contains the following three main components; an appropriate PCM with a phase change temperature within the desired range, where most of the absorbed heat will be stored as a latent heat; a convenient container for the storage medium for adopting the volume alteration throughout the

phase change process; and a proper heat exchange surface to transmit the heat from the energy supply to the PCM and from the PCM to the load (Sharma et al., 2009).

There have been a considerable number of published reviews in the area of LHS (Pomianowski et al., 2013). The majority of these articles have focused on reviewing the development of the PCM substances, the heat transfer enhancement, the mathematical modelling developed for the latent heat problem, and the application of PCM in buildings by addressing the integration methods (Sharma and Sagara, 2005, Pasupathy and Velraj, 2006, Wang et al., 2009, Zhu et al., 2009, Baetens et al., 2010, Agyenim et al., 2010, Cabeza et al., 2011, Dutil et al., 2011, Osterman et al., 2012, Parameshwaran et al., 2012, Zhou et al., 2012, Rao et al., 2012, Al-Abidi et al., 2012, Liu et al., 2012, Pomianowski et al., 2013, Soares et al., 2013, Al-Saadi and Zhai, 2013, SOCACIU et al., 2014, Kalnæs and Jelle, 2015, Konuklu et al., 2015, Souayfane et al., 2016, Akeiber et al., 2016, Kenisarin and Mahkamov, 2016, Navarro et al., 2016a, Navarro et al., 2016b, Wahid et al., 2017, Patel et al., 2017, Saffari et al., 2017, Milián et al., 2017, Kylili and Fokaides, 2017). However, there have been few reviews that focused on PCM incorporation in free cooling of building technology, although this area has been investigated for over 25 years and numerous systems have been developed and assessed. Only few review publications have targeted PCM application in free cooling include (Raj and Velraj, 2010, Waqas and Din, 2013, Kamali, 2014, Thambidurai et al., 2015, Alizadeh and Sadrameli, 2016, Iten et al., 2016, Zeinelabdein et al., 2018).

The first serious discussions on free cooling technique incorporating LHS was carried out two decades ago by Turnpenny et al. (2000). In this work, a system with embedded heat pipes inside the PCM units was designed and developed for storing the night coolness to be discharged throughout the next daytime. A low powered fan located below the storage unit was used to draw the air from the room over the exposed part of the heat pipes as shown in Figure 3.8. A salt hydrate Na_2SO_4 $10H_2O$ with 21 ºC freezing/melting temperature was used for this research, and 1.5% borax nucleating agents were added to reduce the supercooling effect. The heat pipes with attached fins were applied to enhance the heat exchange between the air and the PCM and hence avoiding the need for complex heat exchange configurations on the outer surface of

the PCM, as this allows simple retrofitting for the system. Theoretical modelling and experimental work were performed to assess the potential of this design. An average heat transfer rate of 40 W from the air to PCM was obtained over a melting duration of 19 h, when the temperature difference between air and the PCM melting point was 5 K. Accordingly, the authors suggested an alternative design for the fins attached to the heat pipes inside the PCM unit in order to increase the heat exchange rate and to shorten the transformation period, hence decreasing the number of PCM units needed to cool one room.

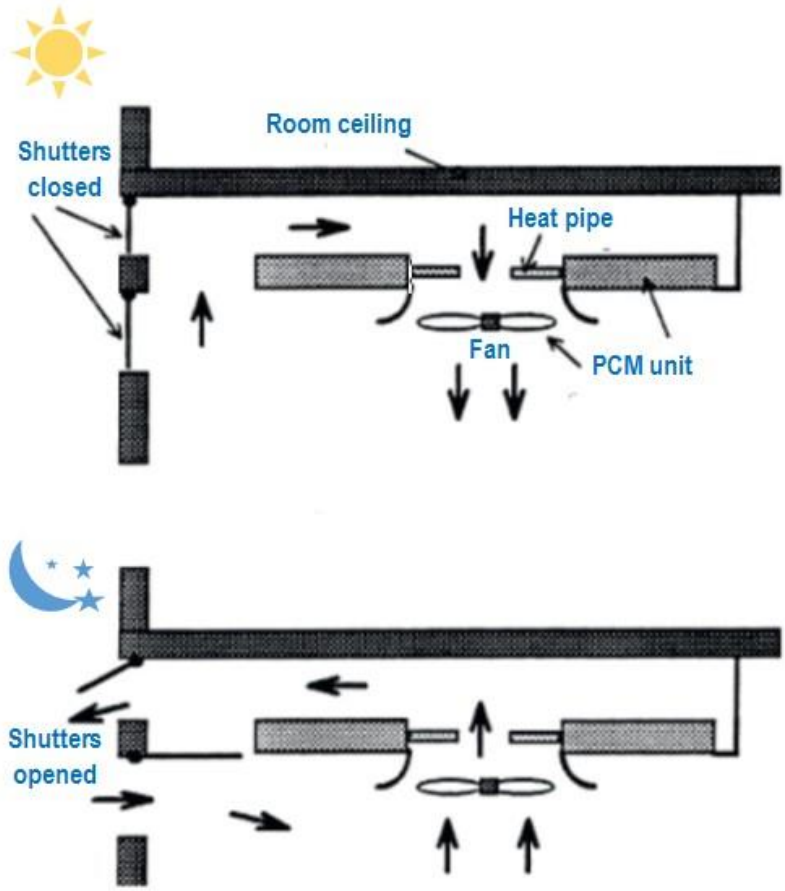


Figure 3.8: (a) Charging, and (b) discharging of the heat pipe/PCM cooling system proposed by Turnpenny et al. (2000).

Turnpenny et al. (2001) improved the same system that provided in their previous study (Turnpenny et al., 2000). The authors assessed the potential of a full-scale prototype cooling system to cool a room under UK summer conditions. A ceiling fan with a 1.20 m sweep diameter was used over a series of PCM units with embedded

heat pipes arranged in a circular layout (Figure 3.9). At night, the cold ambient air is directed through the heat pipes by the ceiling fan; the air becomes hotter and then exhausted to the outdoors. During the day, vents are closed, and the ceiling fan is kept "ON" in order to enhance the room air convection with the PCM storage. The results showed that the developed storage system combined with night ventilation had provided a heat transfer rate of 200 W, which is sufficient for cooling demand in typical UK summer conditions as stated by the authors. It is also mentioned that the system can deliver substantial energy saving and cost benefits compared to conventional air conditioning systems and other alternatives such as chilled beams. In addition, a major decrease in the percentage of CO_2 emissions can be achieved by exchanging the AC devices by free cooling units. A reduction in the CO_2 emissions by around 430 tons per year was predicted by fitting the proposed free cooling system in 2000 office buildings in the UK, as the applied HVAC systems utilise around 10% of the total fossil fuel.



Figure 3.9: An arrangement of the heat pipe/PCM units below a ceiling fan proposed by Turnpenny et al. (2001).

In another major study, Yanbing et al. (2003) have developed a mathematical model in order to examine the thermal performance of a proposed night ventilation with the PCM packed bed storage (NVP) system (Figure 3.10). The mathematical results were validated using an experimental work carried out for a real test room during a summer period of Beijing/China. The utilised PCM is a type of fatty acid compounds developed by the authors. It has a melting temperature range of 22-26 ºC and a latent heat capacity of 190 kJ/kg. A total mass of 150 kg was used in this test. An acceptable reduction in indoor temperature to the comfort limit was achieved throughout the test

period (24 June to 4 July) compared to a similar room without a cooling system. Cooling discharging rates up to 1000 W during night-time and up to 300 W during the daytime were obtained. The overall coefficient of performance (COP) of the experimental installation was 80.

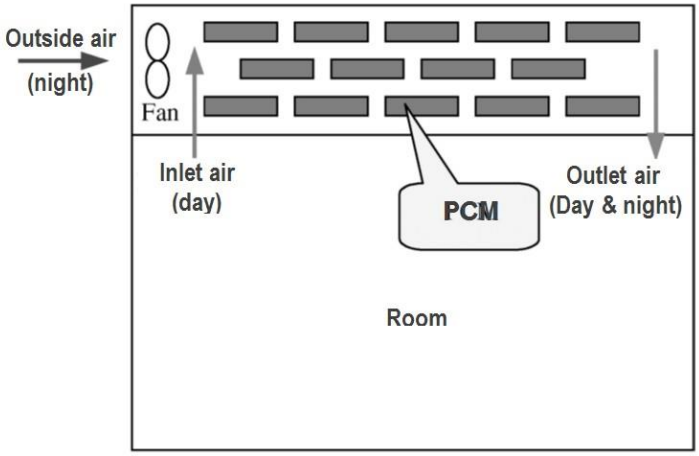


Figure 3.10: Schematic of the NVP system proposed by Yanbing et al. (2003).

An experimental prototype for free cooling applications was constructed and investigated by Zalba et al. (2004). The authors used a commercially available flat plate PCM packs with a melting temperature range 20-25 ºC incorporated inside a shell created with a couple of plates of polystyrene material with an air cavity in between to ensure lowest thermal losses (Figure 3.11a). A parametric study was performed to investigate the performance of the empirical model under different parameters, and the best results were then utilised to design an actual free cooling system. The statistical analysis demonstrated that; lower thickness of encapsulation, higher flow rate and a larger variation of the inlet air temperature and the phase change temperature, all together have a high impact on solidifying the PCM in a short period. Also, all these parameters have an evident influence on the PCM melting, but the inlet temperature has the dominant control rather than the encapsulation thickness while augmenting the air flow diminishes the melting time substantially. Based on the best results obtained from the parametric study, the authors designed a cooling system with a loading capacity of 3 kW using eight tested modules of RT25 and C22 PCMs to cool an industrial room (Figure 3.11b). The changes in air temperature throughout the PCM

modules are presented in Figure 3.11c. A feasibility evaluation proved that the proposed system is technically feasible and the economically beneficial compared to conventional cooling systems.

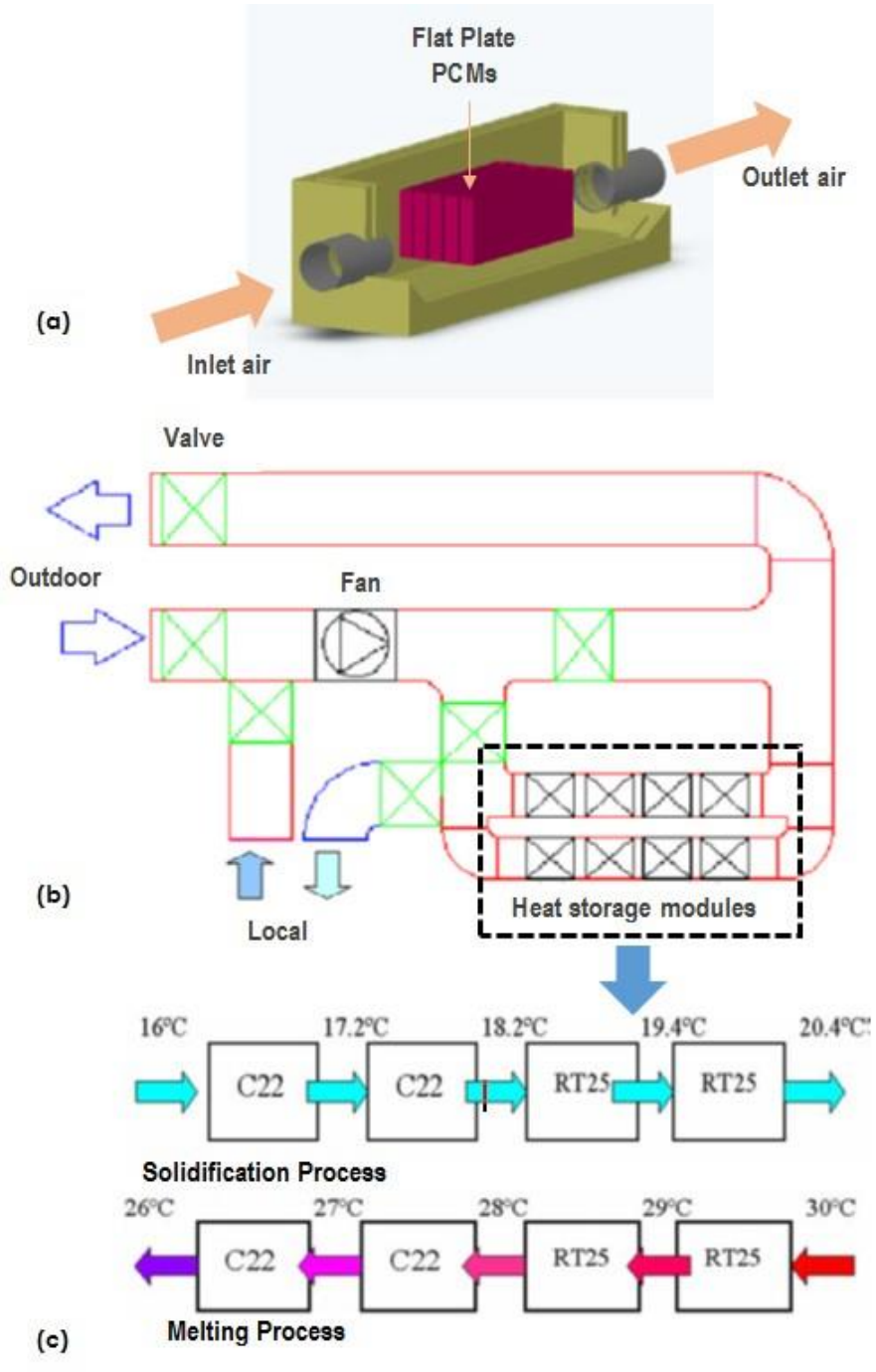


Figure 3.11: The free cooling system proposed by Zalba et al. (2004); (a) the TES unit configuration, (b) schematic of a real installation, and (c) the temperature change during solidification and melting process.

Marín et al. (2005) have examined the same experimental setup developed by Zalba et al. (2004), but instead of using pure PCM, graphite matrixes were embedded with the PCM inside the flat plate container in order to enhance the heat transfer rate. The system was analysed using a numerical model and validated experimentally. The results were compared to other from a system without a graphite matrix. The findings revealed that; reducing the thickness of the PCM with graphite components by 30% has provided similar solidification/melting response time to that provided by the pure PCM by only half of the fan power consumption. Furthermore, a significant decrease in the PCM phase change time up to 50% was achieved in the enhanced design with a minimal reduction in energy storage approximated by 12-20%.

Takeda et al. (2004) also have developed a full-size experimental ventilation apparatus based on a system proposed by Nagano et al. (2004). The system consists of a rectangular duct 140 mm × 140 mm × 900 mm built to allow direct heat exchange between the ventilation air and the contained packed bed of PCM granules as shown in Figure 3.12. The PCM granules are commercially available Rubitherm GR of 1-3 mm particle diameter and comprise 65% ceramic materials and 35% paraffinic hydrocarbon by weight. The phase change temperature of the PCM is within the range of 22.5-25 ºC. The outlet air temperature from the storage system was measured for various inlet temperatures to simulate the alteration of ambient air temperature. The results showed that the exit air temperature always remains consistent within the limit of PCM phase change during the discharging phase. Moreover, the proposed cooling device was integrated into a household ventilation system, and the room temperature was set at 26 ºC. The ventilation load was calculated via a simulation tool for a summer season of eight cities in Japan to explore the influence of air temperature on the system performance. A decrease in ventilation load ranged from 42.8% to 62.8% was achieved. The authors also have stated that the benefits from the system depend significantly on diurnal temperature variation rather than on average temperature.

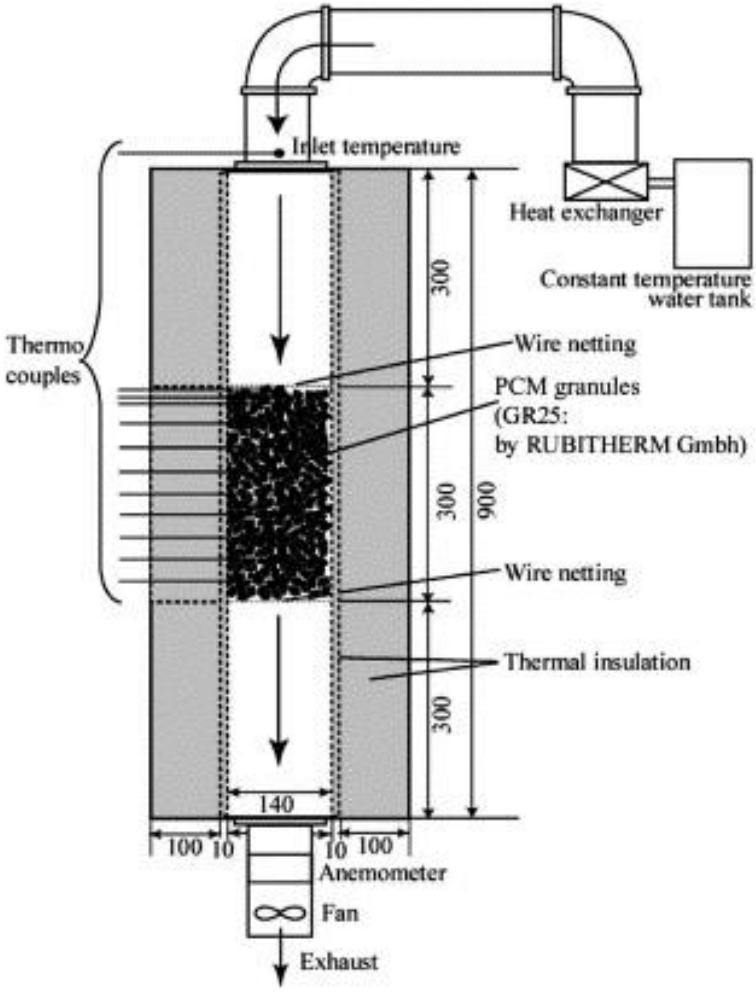


Figure 3.12: Experimental apparatus of the free cooling system proposed by Takeda et al. (2004).

Nagano et al. (2006), (2007) have proposed a floor-supply air conditioning system via impregnating a packed bed latent heat storage into the building mass to enlarge its thermal storage capacity (Figure 3.13). A small-scale experimental model with a floor area of 0.5 m² was built for this study, and a 30 mm depth of granules containing PCMs were embedded directly in the room floor. The utilised PCM was made of foamed glass beads and paraffin wax and has a melting/solidification temperature around 20 °C. During the night, cold air from an air conditioner is circulated inside the cavity below the floor which allows charging of cold energy to the floorboard, concrete slab, and PCM packed bed. During the daytime, the accumulated cold energy is released to the interior space through the porous of the floor board. The charging and discharging were performed similarly to a schedule of air conditioning operation over 24 h duration

in a typical office building, and the indoor temperature was set at 28 ºC. Each night the system has stored about 1.79 MJ/m² of cooling which is capable of limiting the operation of the AC system for only three hours throughout the daytime and lowering the daily cooling load by 89%. The authors stated that increasing the amount of PCM can fulfil the daytime total cooling demand of the tested office space.

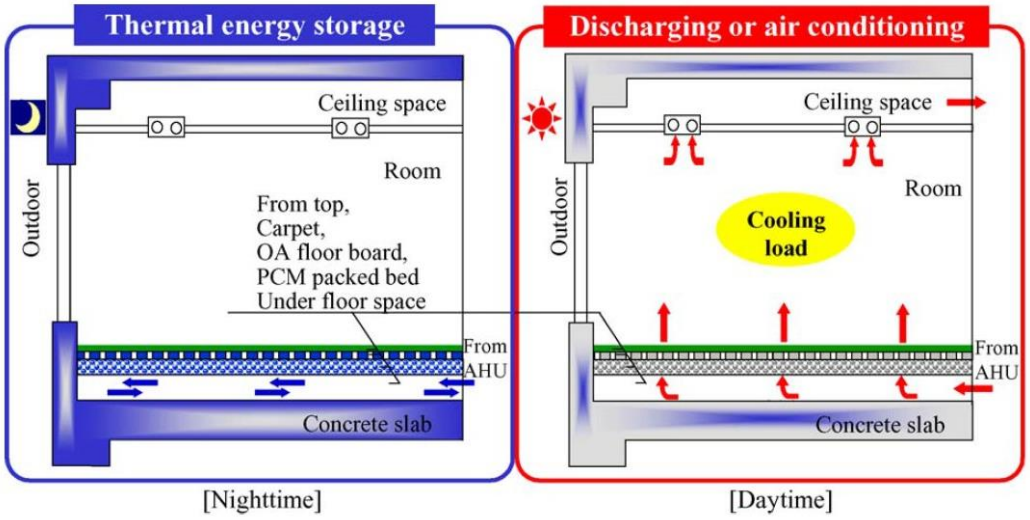


Figure 3.13: An underfloor cooling system incorporated packed bed PCM granules proposed by Nagano et al. (2006), (2007).

An experimental setup was designed by Stritih and Butala (2007), (2011) to evaluate the heat transfer within a proposed PCM cold storage system based on free cooling as shown in Figure 3.14a. About 3.6 kg of commercially available PCM (paraffin Rubitherm RT20) with a melting temperature of 22 ºC was placed inside a metal box designed with a configuration to allow simple integration into the building ceiling. The metal duct was externally insulated to suppress the surrounding cold transfer. Aluminium fins were used externally and internally at both top and bottom sides of the metal box to enhance the thermal performance (Figure 3.14b). Air temperatures and heat flux as a function of time were calculated for several air speeds and inlet temperatures utilising a numerical model. The experimental measurements and modelling results showed a good agreement. The indoor air temperature was reduced from 27 ºC to 24 ºC for more than 2.5 h with at 7.8 l/s flow rate. Moreover, energy savings between 14% and 87% were predicted based on the selected parameters.

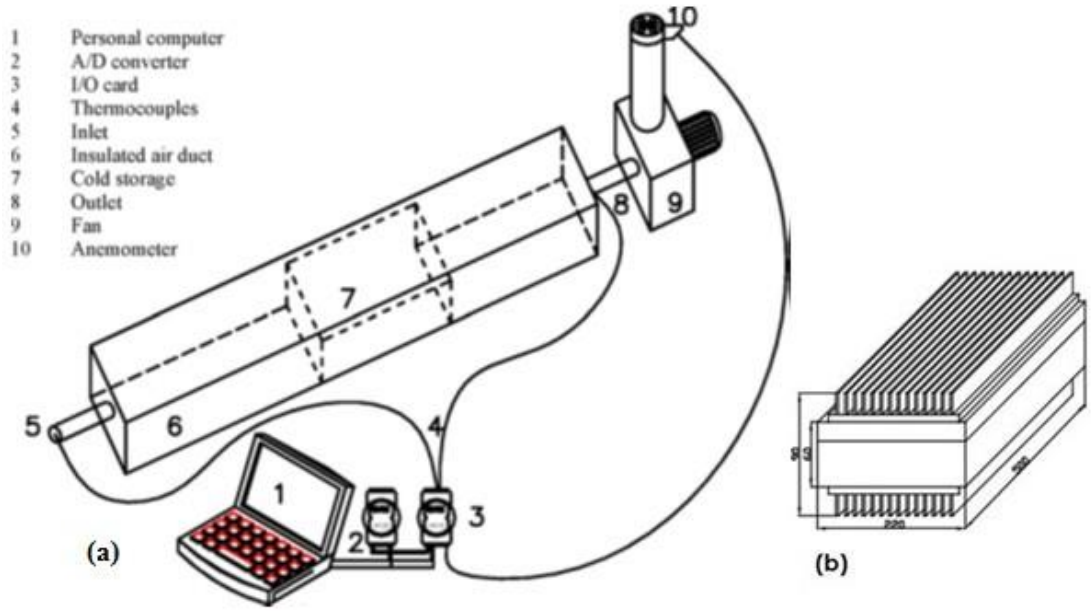


Figure 3.14: The free cooling system proposed by Stritih and Butala (2007); (a) the experimental setup and (b) the PCM storage configuration with fins.

To eliminate and lower the use of conventional air conditioning systems in buildings; Arkar and Medved (2005) proposed a free cooling system which consists of a cylindrical latent heat thermal energy storage (LHTES) device filled with spherical balls of paraffin PCM. The authors introduced a numerical model considering the inconsistency of the spaces among the spheres and the velocity of the fluid due to a small tube to sphere diameter proportion. The proposed LHTES device was investigated by integrating it into a mechanical ventilation system of an existing house in Slovenia (Arkar and Medved, 2007, Arkar et al., 2007). The concept was tested and compared to other cooling techniques using TRNSYS simulation tool. The findings indicated that the free cooling device could accomplish better comfort conditions and a noticeable reduction in the size of the mechanical system. A 6.4 kg of the PCM per square metre of floor area is sufficient to achieve the thermal comfort in the tested house. The authors also mentioned that the developed LHTES device could be utilised for winter heating when it is combined with an air-based solar collector or a ventilated facade.

Another major study was conducted by Medved and Arkar (2008) who assessed the free cooling potential under different climatic conditions of six European cities. The same packed bed cylindrical LHTES device that developed in (Arkar and Medved, 2007, Arkar et al., 2007) was applied to a building mechanical ventilation system. The utilised PCM was commercially available RT20 paraffin with a relatively large phase change temperature range (12 K). The size of the LHTES system was optimised according to the cooling degree hours (CDH) which represents the maximum free cooling potential estimated by the following formula (3.2);

$$CDH = \sum_{i=0}^{2208} (T_a - T_o)\,\delta \qquad (3.2)$$

where; δ =1 h, when T_a>T_o, and δ = 0 h, when $T_a \leq T_o$. The air flow is fully regulated by a control unit based on the inlet ambient air temperature (T_a) and the outlet air temperature (T_o). When $T_o > T_a$; often during the night; the interior space was ventilated directly by the ambient air which is within the thermal comfort range for the selected cities, and a separate air circulation was provided to solidify the PCM (Figure 3.15b). While in the case of $T_a > T_o$; mostly during the daytime; the room was ventilated through the PCM unit extracting the accumulated cold (Figure 3.15a). For the studied climates (continental) it is found that the PCM with a larger phase change temperature range (12 K) is more advantageous than the PCM with a narrow temperature range (4 K). The authors also stated that the optimal melting temperature of PCM is almost equivalent to the average temperature of the hottest month or only ± 2 ºC to guarantee an effective performance. The ideal ratio between the mass of the PCM and the air flow rate has to be between 1.0 and 1.5 kg/m³/h in order to meet around 85%-95% of the maximum CDH.

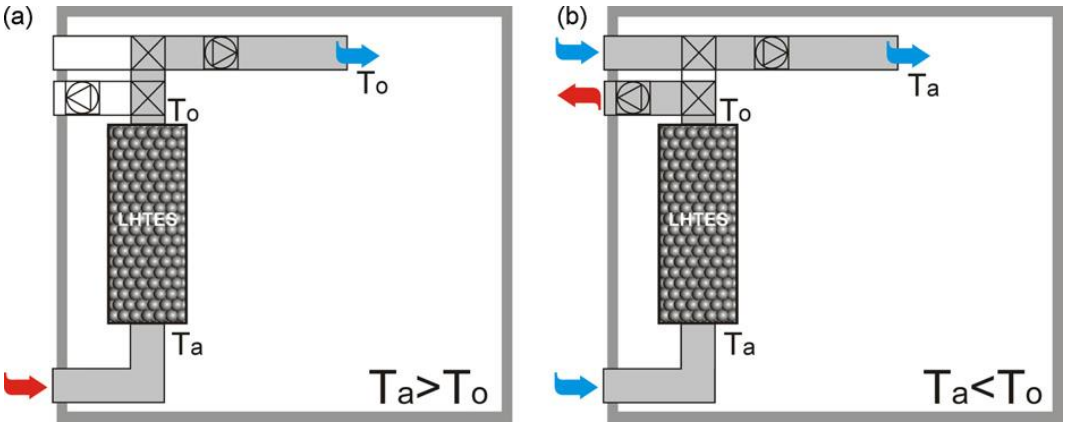


Figure 3.15: Operational principles of the free cooling system proposed by Medved and Arkar (2008).

Based on the results obtained by Zalba et al. (2004), an experimental setup was designed by Lazaro et al. (2009b) to examine the thermal behaviour of two real-scale prototypes of PCM-air heat exchanger for free cooling purposes; one was designed utilising aluminium pouches filled with inorganic PCM (Figure 3.16a), and the other type was designed utilising aluminium panels filled with organic PCM (Figure 3.16b). An air conditioner was employed to simulate various operation modes. A feasibility study was performed for different inlet air temperatures and air flow rates. The results indicated that, although the aluminium panels with organic PCM have a lower conductivity and a smaller stored energy, a higher cooling power and a shorter melting time (nearly half) was obtained due to the thickness stability, in contrast to the aluminium pouches which displayed high container expansions and PCM leakage during the phase change. Based on these findings the authors proved that it is better to enhance the heat exchanger design rather than escalating the conductivity level to ensure satisfactory outcomes, as increasing the conductivity in most cases results in additional costs.

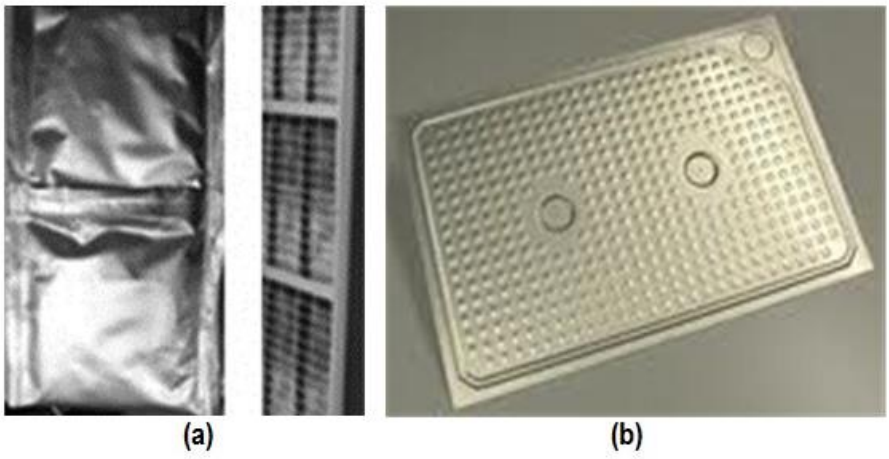


Figure 3.16: The real-scale PCM prototypes investigated by Lazaro et al. (2009b); (a) aluminium pouches filled with an inorganic PCM, and (b) aluminium panels filled with organic PCM.

Based on the satisfactory performance of the second prototype (aluminium panel with organic PCM) that evaluated in (Lazaro et al., 2009b), it was selected for further implementation by Lazaro et al. (2009a). An empirical model consists of 18 PCM modules was built to evaluate the technical viability of the proposed cooling system. The authors reported that utilising a modular design concept is beneficial to assess the technical viability of the tested configuration for different applications, as it is possible to size the number of PCM modules and the average phase change temperature based on the needed cooling power, favourable indoor temperature and duration required to maintain this temperature. Moreover, a selection criterion for PCM melting temperature was investigated according to the cooling load; it was found that PCM with a melting point lower than the required indoor temperature should be selected in case of high cooling demands, while PCM with a melting point closer to indoor objective temperature is suitable for the low cooling demands.

An experimental setup used to investigate the full thermal cycling of a real-scale PCM-air heat exchanger was developed by Dolado et al. (2011a). Commercially available macro-encapsulated paraffin RT27 in rigid aluminium slabs was used. Figure 3.17 shows the experimental setup of the conducted study. The key findings showed that the continuous thermal cycling of the designed storage unit is a repetitive procedure and no deterioration was observed regarding the properties of the PCM. A full

solidification of the PCM was realised in less than three hours for a temperature variation of 8K between the inlet air and the PCM average phase change point with an air mass flow between 0.4 and 0.5 kg/s. Average heat flux up to 4.5 kW and 3.5 kW for one h were achieved for the melting and solidification phases, respectively. Another work related to this study had been carried out in parallel by the same authors in (Dolado et al., 2011b). The computed results of the experimental study were utilised to validate the results of a developed numerical model for the tested PCM-air heat exchanger. The authors reported that the developed numerical model could be employed as a designing tool for these sorts of PCM-air heat exchangers in various applications.

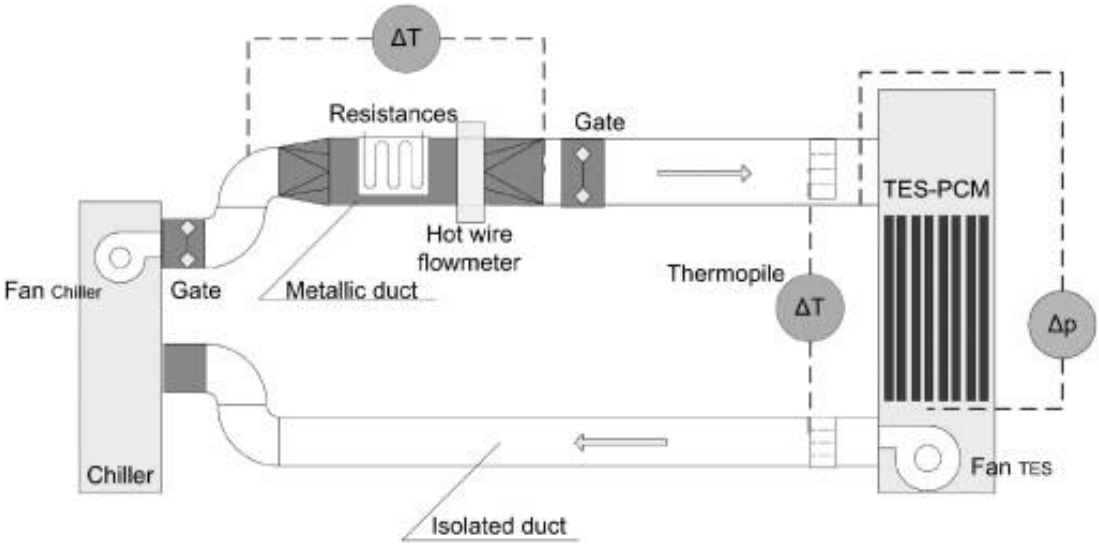
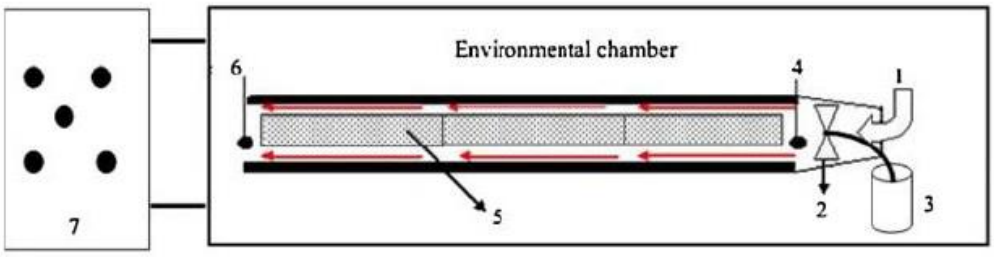


Figure 3.17: Experimental setup of the PCM-air heat exchanger with rigid panels developed by Dolado et al. (2011a).

The first investigation of free cooling systems under hot and arid climate conditions was carried out in 2011 by Waqas and Kumar (2011a). A prototype storage unit was built using three PCM containers and tested inside a controlled environmental chamber as illustrated in Figure 3.18. The utilised PCM was a commercialised type of salt hydrates (SP29, Rubitherm GmbH) with a phase change temperature range of 28-29 ºC, encapsulated inside a galvanised steel container (0.5 m × 0.5 m × 0.01 m). Three inlet air temperatures 20 ºC, 22 ºC and 24 ºC were tried for the charging of the PCM and 36 ºC, 38 ºC and 40 ºC for the discharging phase. The key findings indicated that; the examined PCM storage could be allocated to maintain the indoor daytime

temperature within the acceptable ranges via extraction of the accumulated cold energy at night. Moreover, increasing the inlet charging temperature from 22 ºC to 24 ºC has led to an approximately 55% extra time required for full solidification of the PCM, while decreasing the inlet temperature from 22 ºC to 20 ºC saved about 33% of the required time for the complete solidification. Augmenting the air flow rate from 4.0 to 5.0m³/h lowered the solidification period by around 16%. The authors also concluded that low inlet air temperature and high flow rates are useful during the charging phase to assure a complete solidification of the PCM in a short time, while, lower flow rates are beneficial for the cold energy discharge throughout the daytime.



1: Air inlet to storage unit. 2: Fan. 3: Fan speed controller. 4: Air inlet temperature sensor. 5: storage material (PCM). 6: Air outlet temperature sensor. 7: Control panel for chamber AC, heater and fan.

Figure 3.18: Experimental setup of the PCM storage proposed by Waqas and Kumar (2011a).

Using a numerical method, Waqas and Kumar (2011b) have assessed the behaviour of a flat plate air-based PCM storage system for free cooling in the summer season of Islamabad, Pakistan. The modelling results were validated with the results of a previous experimental study conducted by Halawa et al. (2005) considering the use of the same inlet temperature data and the simulation time. The findings generally showed close agreement between both approaches. However, the numerical model predicts higher outlet air temperatures at the start time of the melting phase simulation and lower values at the rest time. The numerical calculations indicated early completion of the solidification process than that appeared during the experiment. The authors came out with these conclusions; the proposed cooling system is capable of bringing the hot daytime temperature well to the comfort range in the investigated hot and dry region. The cooling capacity was maximised when selecting a PCM with a melting point equal to the comfort temperature of the hottest summer month.

Raj and Velraj (2011) have developed a modular storage unit for free cooling application in locations with low diurnal temperature variation. The storage unit consists of a number of modules placed vertically over each other with spacers above and below each module. The designed module was a PCM encapsulated inside a 750 mm diameter shell containing several tubes for air flow (Figure 3.19a). CFD modelling was performed for one module and two air spacers to study the temperature distribution, air flow, and heat transfer phenomena in the proposed heat exchanger. Temperature contours in Figure 3.19b indicated that uniform temperatures about 22 °C are dominant at the inlet side of the spacer and constant temperature of around 26 °C was maintained around the PCM walls of the inner tube. The temperature increase is higher at the lower velocity of 0.1 m/s compared to that of 2.0 m/s due to the increase in air mass flow. A steady-state analysis was performed to determine the pressure drop throughout the module and spacers and to recognise the flow and temperature variation of the passing air across the module; this analysis is beneficial for selecting the geometrical and air flow parameters for a given surface temperature and inlet conditions. A transient analysis was also carried out to determine both; the solidification features of the PCM and the geometrical dimensions of the modular design. Comparing the output of CFD simulations to the experimental findings indicated that, the scanning rate of the DSC analysis should be made according to the cooling/heating rate of the selected application to attain the accurate phase change temperature range for the selected PCM; otherwise, incompatible results of phase change temperature between theoretical and practical applications may be expected. The authors also noticed that the provided spacers enhanced the retention time of the air and resulted in better heat transfer, especially at lower air speeds. A supercooling was observed on the PCM adjacent to the inner ring of the tubes when the area between the two tubes reaches the solidus temperature, which was attributed to the diminution of the heat transfer surface area for the given PCM module, accordingly, lessening the distances between the tubes is suggested. In addition, incomplete phase change at the outer boundaries of the PCM module was detected. Thus, reducing the outer diameter of the module design is advocated by the authors.

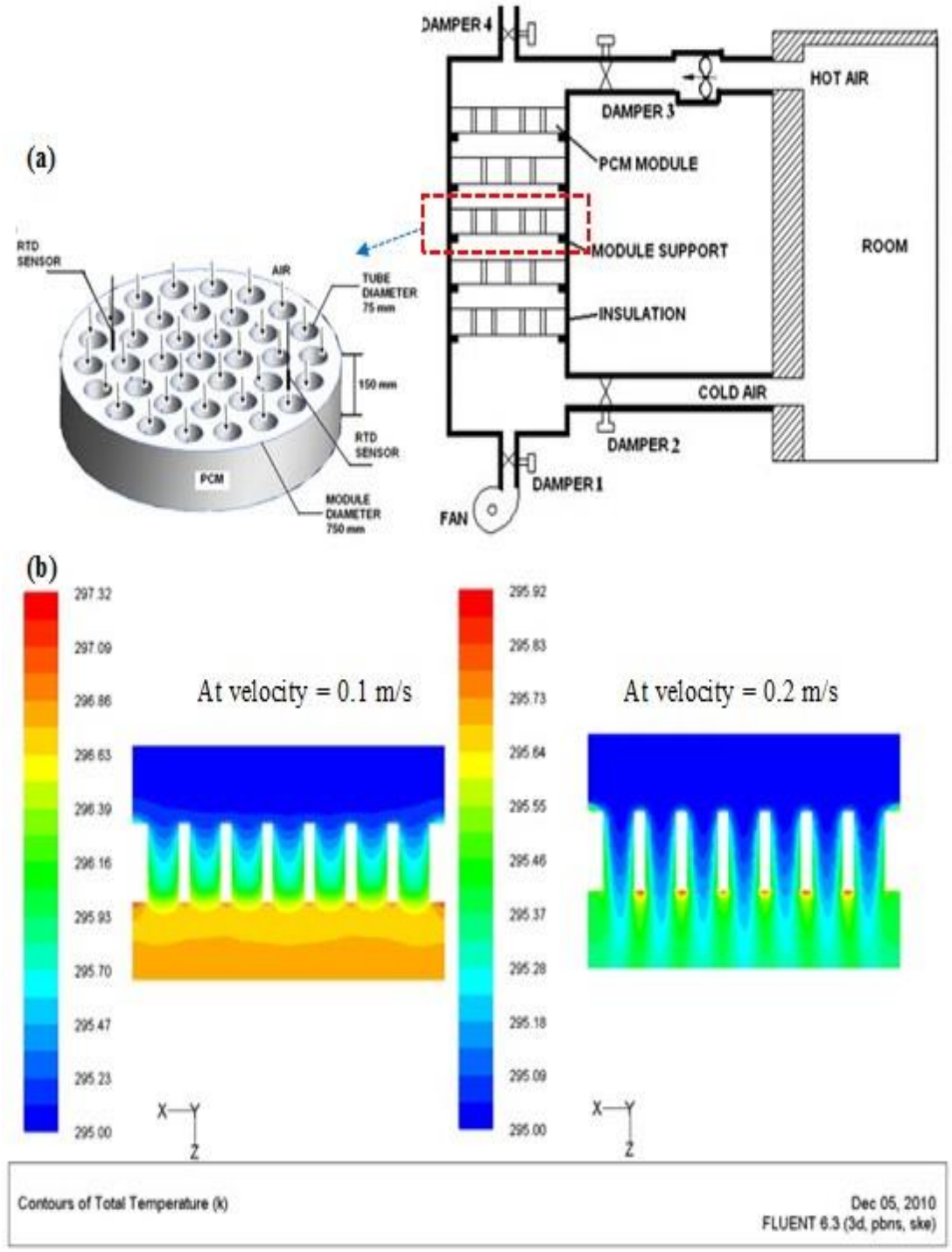


Figure 3.19: (a) Schematic of the modular PCM heat exchanger developed by Raj and Velraj (2011), and (b) the temperature contours computed by CFD modelling.

Bulut and Aktacir (2011) have thought about free cooling as a supportive application for the air conditioning device. They investigated the potential of free cooling for an all-air HVAC system under the climate conditions of Istanbul, Turkey, via analysing the hourly dry-bulb temperature data of 16 years period. The authors reported that free cooling or so-called economiser cycle could be used as a part of the HVAC system to supply comfort temperature with minimum operating costs. This can be accomplished when benefiting from the available natural coolness to fulfil part of the energy load during favourable outdoor climate conditions. It was found that free cooling capacity in the meant location varies with the supply air temperature and months. Significant energy savings can be realised during the transition months; yet, the free cooling concept seems to be non-beneficial during summer months excluding durations in which outside temperatures are less or equal to the high supply air temperature.

A novel cooling using PCM named Indirect Evaporative and Storage Unit (IESU) was developed and optimised by Jaber and Ajib (2012) for residential application under a Mediterranean climate of Amman, Jordan. The proposed cooling system comprises an indirect air cooler combined with a PCM heat exchanger as shown in Figure 3.20a. The heat exchanger was made of a rectangular corrugated flat tube filled with PCM layers, and passages for air flow from two directions were created (Figure 3.20b). The utilised PCM was a commercial type of salt hydrates with a phase change temperature of 20 ºC. A parametric study was carried out to investigate the effect of various parameters related to the PCM storage configuration and the operating conditions on the IESU thermal behaviour. It was found that the influence of heat exchanger length is greater than the width effect and the cooling load increases as distances between plates increased due to the decreasing number of PCM modules. An optimised design was found and can provide a total savings of 80% of the annual cooling demand with a payback period of 7.8 years.

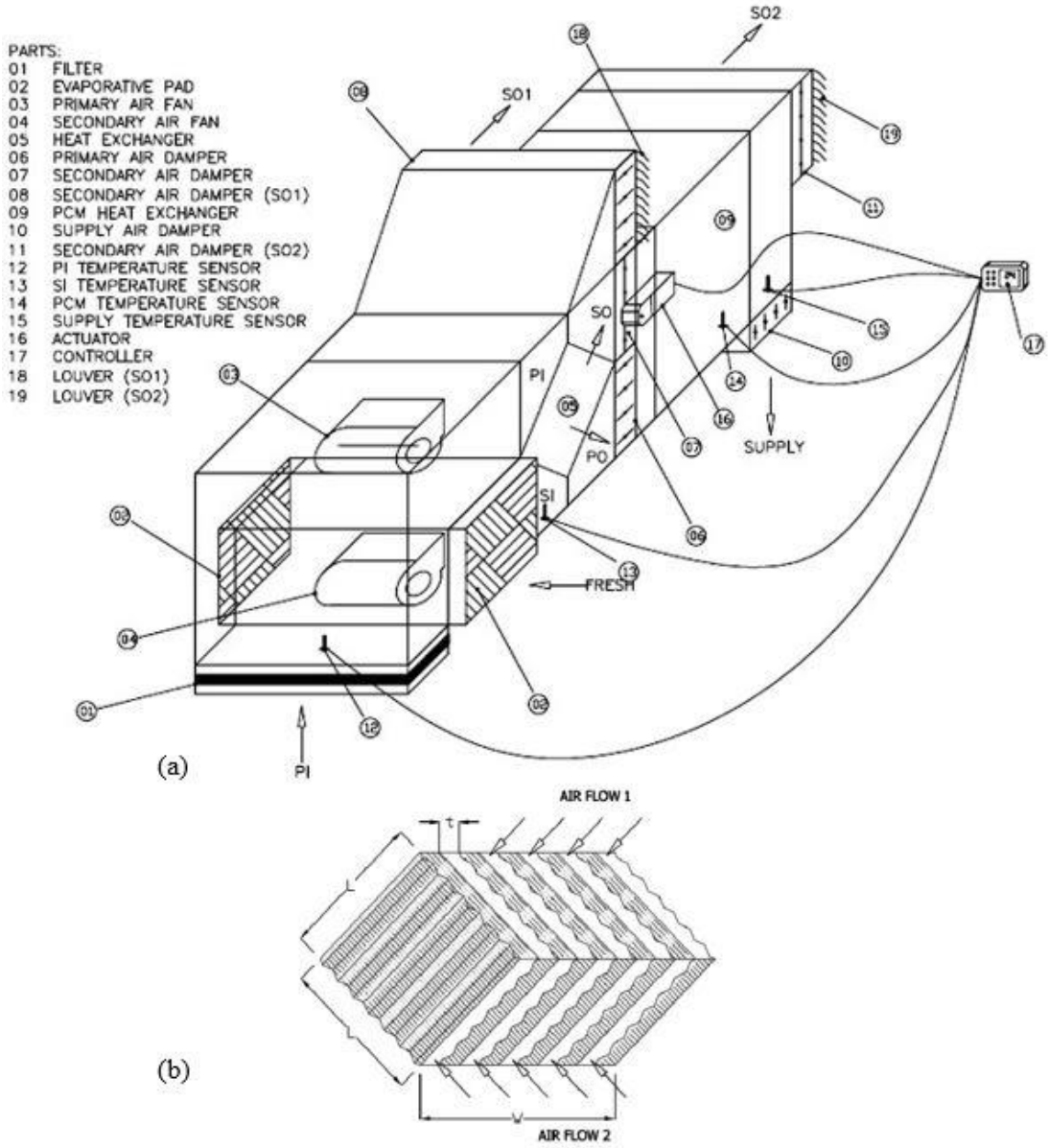


Figure 3.20: (a) Experimental setup and (b) the PCM heat exchanger model proposed by Jaber and Ajib (2012).

Mosaffa et al. (2013a), (2013b) have studied the thermal behaviour of a multiple PCMs for the free cooling application (employing more than one PCM type to store and release the heat). The storage medium comprises several slab units of PCM, each unit includes multiple PCMs, and these units were arranged parallel to each other creating rectangular tunnels in between for the air flow (Figure 3.21a). The schematic of the whole proposed system is shown in Figure 3.21b. During the charging phase, the circulation of the ambient air occurs from the side of the PCM with the lowest phase

change temperature to the higher ones, while reverse flow takes place during the discharging phase in order to enhance the heat transfer between the PCM and the stream of air flow. A two-dimensional mathematical investigation using the effective heat capacity method was performed to study the thermal performance of the cooling system, and the computed results were validated experimentally showing a satisfactory agreement. The thermal comfort was accomplished by the system for the climate of both; Tabriz/Iran (Mosaffa et al., 2013b) and Eindhoven/Netherlands (Mosaffa et al., 2013a) with a COP above 7.0 which is considerably better than that for conventional air conditioners. From the feasibility study; the highest COP was achieved for the PCM slab with a shorter length and a thinner thickness, and the optimal design parameters to maintain the outlet air temperature below 20°C for around 8 h were determined by the authors to be 3.2 mm high and 1.30 m long for the air channel, and 9 mm thickness for the PCM slab.

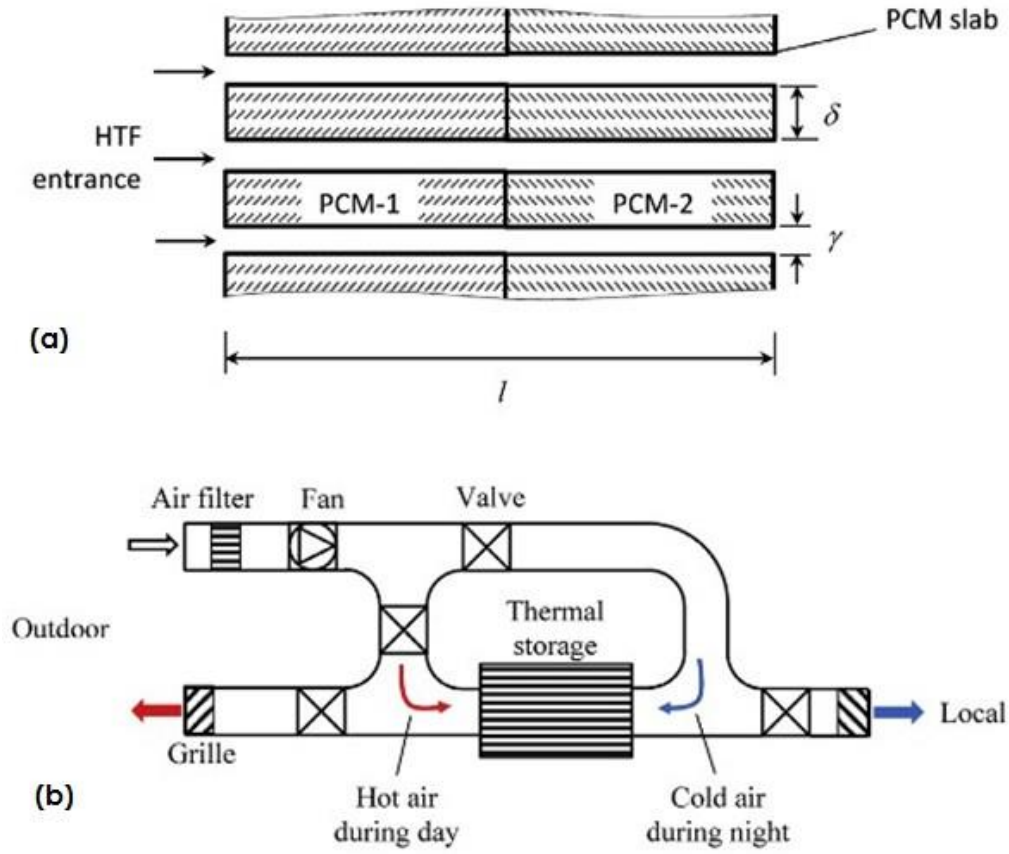


Figure 3.21: (a) Arrangement of multiple PCM slabs, and (b) schematic of the free cooling system proposed by Mosaffa et al. (2013a), (2013b).

A TES system consisted of a bundle of rectangular tubes filled with a commercial RT28HC PCM was developed by Rouault et al. (2013) for free cooling application in buildings (Figure 3.22). The system was investigated numerically to analyse the effect of the arrangement of the PCM tubes on the system efficiency. The feasibility study revealed that tubes of vertical section slightly displayed better performance compared to horizontal ones, the authors also stated that heat exchange improvement techniques are required to enhance the cooling power of the system.

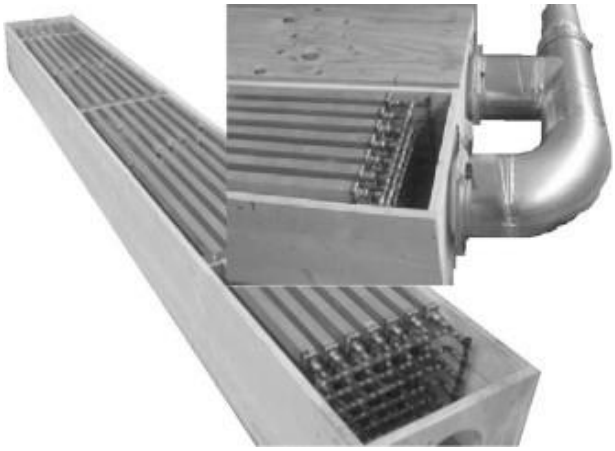


Figure 3.22: The TES system of rectangular tubes filled with PCM developed by Rouault et al. (2013).

Darzi et al. (2013) have studied the impact of mass flow rate and thickness of PCM plates under different indoor room temperatures (i.e. different Stefan number) for free cooling application in buildings. The schematic of the system is shown in Figure 3.23. A commercially available kind of salt hydrates PCM (SP22A17) produced by Rubitherm was used. The authors used numerical simulation to monitor the developments of melt fraction and temperature distribution inside the PCM plates in respect of time, as it is difficult to monitor these parameters experimentally. The findings revealed that increasing the Stefan number (St); computed from equation (3.3); causes the increase of the cooling power and the exit air temperature from the storage unit, while, increasing the mass flow rate maximises the cooling power and allows a faster melting process. It was also stated that the thickness of the PCM plates has a significant impact on the thermal behaviour of the PCM heat exchanger and it has a linear relation with the PCM melting duration for the considered configuration.

$$St = \frac{C_p(T_i - T_m)}{L} \quad (3.3)$$

where; T_m is the average melting temperature, T_i is the inlet temperature, and L is the latent heat of fusion of the PCM. The Stefan number varies only with inlet temperature for the same PCM.

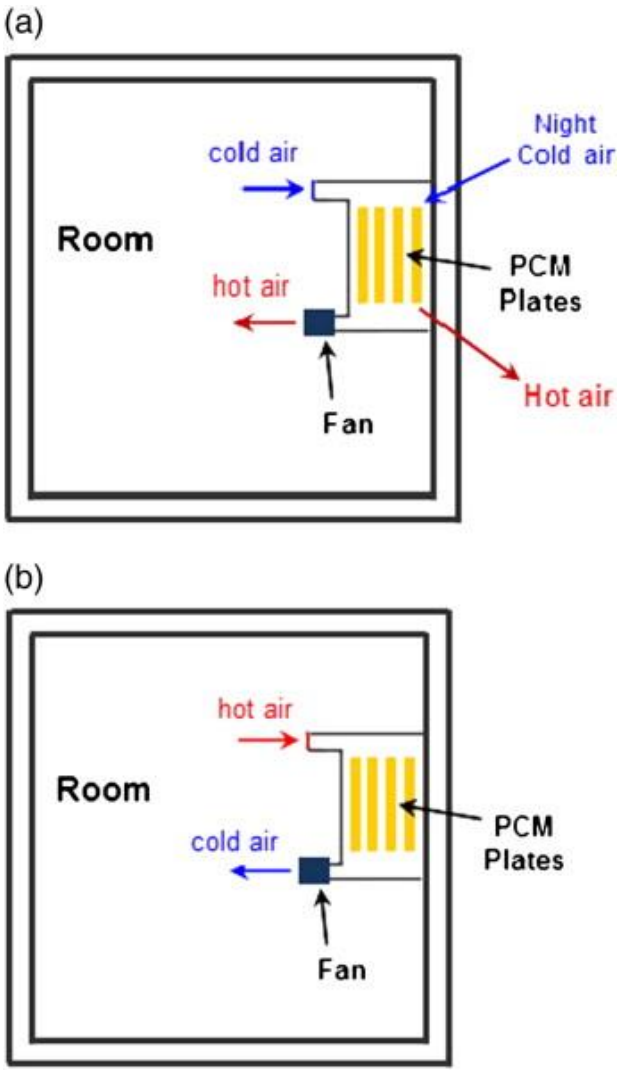


Figure 3.23: (a) Night and (b) daytime operation of the free cooling system proposed by Darzi et al. (2013).

Rajagopal et al. (2014) have studied the potential of free cooling technology in Bangalore city in India based on weather data analysis of the city for one year, and on the estimated cooling load of a considered ten storeys commercial building. The primary objective was to come out with some recommendations to get the most out of

the free cooling strategy. The study revealed that free cooling can maintain the year-round thermal comfort in the considered building and location without any need for supportive mechanical systems.

Waqas et al. (2015) have published a paper in which they coupled the free cooling system that investigated in (Waqas and Kumar, 2011b) with a stand-alone solar air collector to allow operation of the PCM heat exchanger for both summer cooling and winter heating in buildings in hot dry and cold dry climate of Islamabad, Pakistan. A commercial PCM of salt and paraffin mixture with a phase change range 23-27 ºC was utilised. For heating requirements, the received solar energy during winter daytime was absorbed using a flat-plate glazed solar air collector. The collector heats the air before it is being directed by a fan through the PCM storage to be extracted during the cold night hours. The configuration of the solar air collector and the PCM storage is shown in Figure 3.24. The authors have found that a PCM with a transformation point of approximately 27.5 ºC in the middle of the summer comfort represents the appropriate solution for the whole year comfort in the considered location. The optimum performance achieved in summer is when utilising a PCM with a melting temperature of 29 ºC; this increases the cooling capacity by 15% and reduces the heating capacity by only 3% compared to a PCM with a 27.5 ºC melting point. A PCM with a melting temperature of 21 ºC was found suitable for enhancing the system performance in winter conditions. Bearing in mind that; the melting temperature of the PCM (29 ºC) which supplies the maximum cooling in summer can be used in winter but not vice versa.

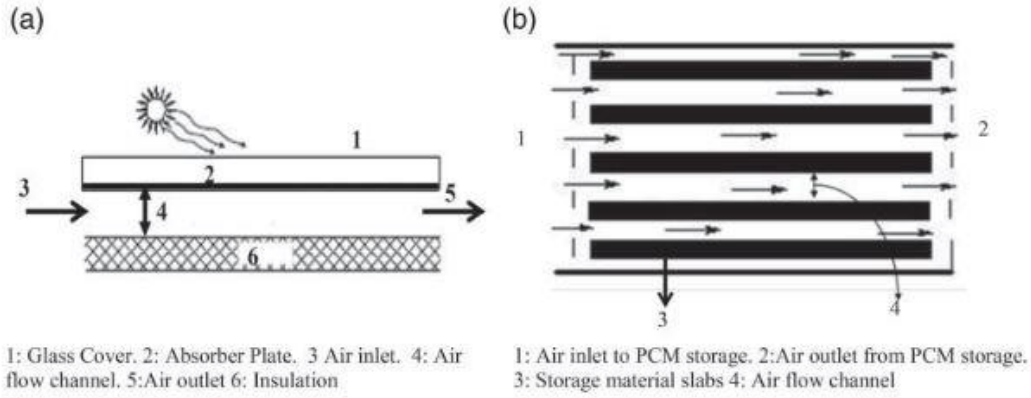
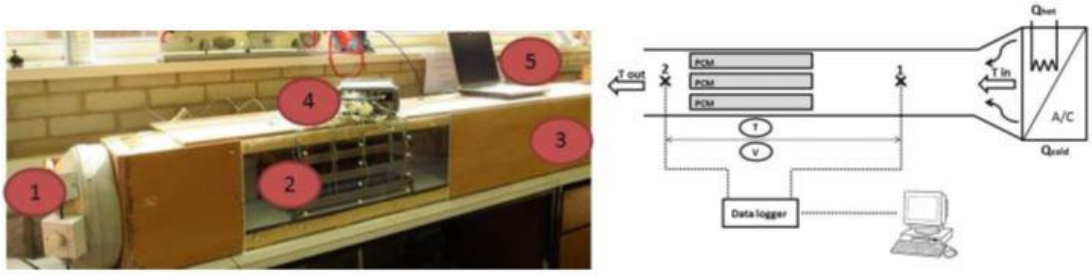


Figure 3.24: The configuration of the proposed solar air collector and the PCM storage investigated by Waqas et al. (2015).

Borderon et al. (2015) have carried out a numerical simulation to investigate the thermal behaviour of a flat plate PCM storage incorporated in a ventilation system for summer comfort in a retrofitted house under a climate of four cites in France (Trappes, Lyon, Nice, and Carpentras). A paraffin-based PCM of latent heat of fusion 170 J/g was considered and tested under different melting temperatures between 21 and 25°C. TRNSYS software was used to model the house, and this has been coupled with MATLAB simulations for the PCM/air system modelling. The results showed that the crystallisation of the PCM at night is only partial in most of the studied cases, which indicates a non-optimal use of the system. Therefore, air flow enhancement was recommended to achieve better performance. Making use of 700 kg of PCM and considering a comfort temperature of 26°C, the number of discomfort hours in the summer season can be reduced to only 2.6% for Trappes city and less than 8% for Lyon city. The results are less impressive in Nice, due to the small daily amplitude of the temperature experienced in this climate, which results in a low charging process. In the case of Carpentras city, a significant improvement in the summer comfort was accomplished. However, an additional amount of PCM is required, and thus a system feasibility analysis must be considered.

An experimental study for a PCM storage incorporated into a ventilation system was conducted by Iten and Liu (2015) for summer comfort in buildings in Mediterranean countries, namely Portugal. The storage unit contains three rectangular metallic modules filled with R25 PCM and kept inside an insulated wooden duct, in addition, a cooling/heating unit was used as a climate controller (Figure 3.25). The effect of temperature and velocity of the inlet air was evaluated for both transformation phases. Under their test conditions, the authors have found for all tested cases that the inlet air velocity has the dominant impact on both phases. Enhancing the inlet air velocity decreases the solidification time linearly and the melting time non-linearly. On the contrary, the impact of the inlet air temperature is more visible during the melting process. Accordingly, the temperature and velocity of the air inlet have to be carefully optimised for the entire running cycle of both charging and discharging phases.



(1) Exhaust fan; (2) PCM modules; (3) Heating/Cooling unit; (4) Data acquisition; (5) PC

Figure 3.25: Experimental setup of the system proposed by Iten and Liu (2015).

Osterman et al. (2015b) have performed a parametric study to evaluate the heat transfer of a PCM storage system for free summer cooling of buildings. The system was also adjusted by adding a solar collector to evaluate its capability for winter heating (Osterman et al., 2015a). Compact storage modules (CSM) plates filled with paraffin RT 22HC PCM by Rubitherm was used for the analysis. The PCM modules were investigated in both vertical and horizontal arrangements, and a perforated plate was placed in front of the plates to keep a uniform air circulation among the plates as shown in Figure 3.26a. The TES system was investigated numerically using Fluent, and the obtained data were validated with experimental results. The air flow was measured by an anemometer and monitored through visual monitoring of smoke streaming among the modules as shown in Figure 3.26b. The results confirm the satisfactory design of the perforated plate for flow regulation. The pressure drop varied from 2.1 mbar to 13.3 mbar, which denotes that the spacing between the modules does not have a substantial influence on the fan power consumption. Based on the analysis, the authors advised decreasing the module thickness to enhance the required time for the phase change.

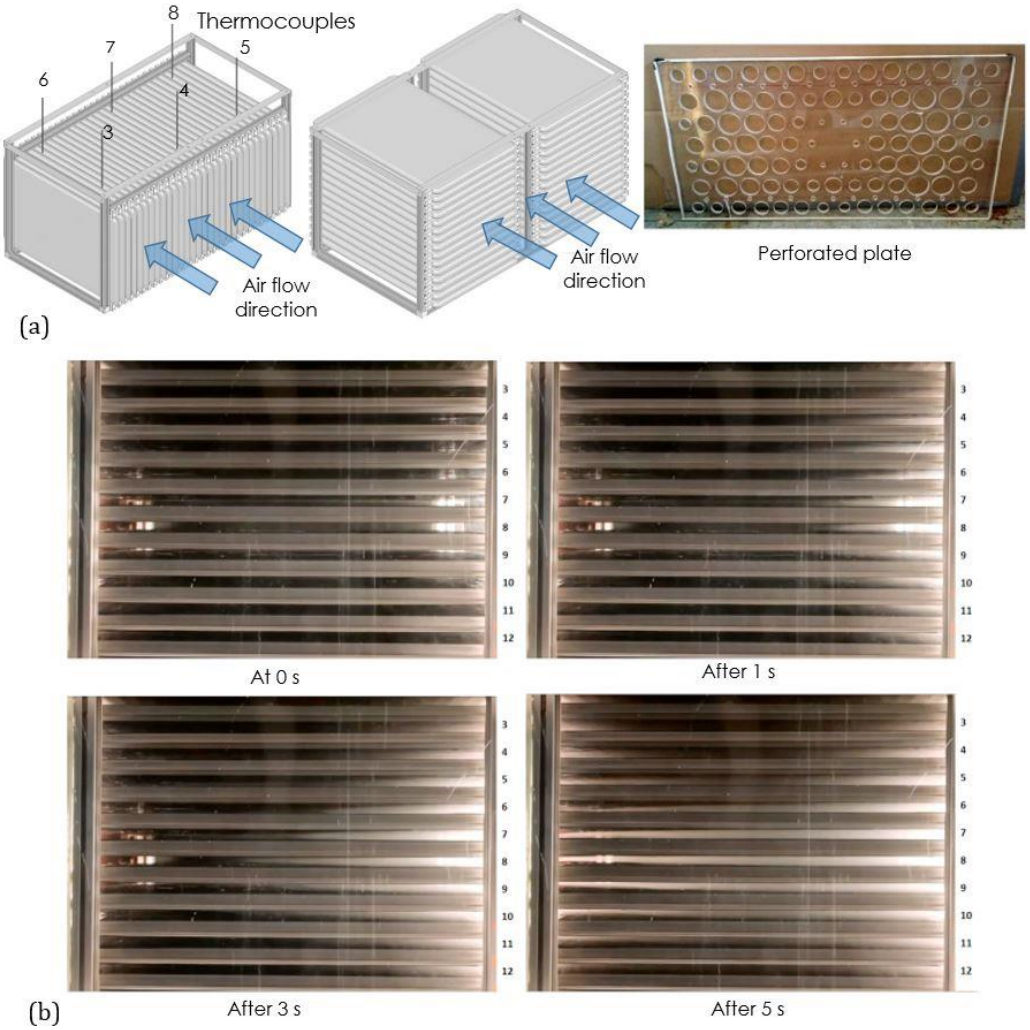


Figure 3.26: (a) Tested configurations and (b) flow visualisation results of the system developed by Osterman et al. (2015b).

A small-scale PCM heat exchanger unit was investigated numerically and experimentally by Mirahmad et al. (2016) for controlling the indoor temperature fluctuation inside a greenhouse prototype. The proposed latent heat storage system contains flat slab arrangement of 200g of PEG1000 PCM was encapsulated inside aluminium pouches with different dimensions corresponding to the PVC tunnel of circular cross-section that packed in it (Figure 3.27). The effect of inlet air temperature and velocity was studied finding that higher temperature variation of the inlet air and the PCM can shorten the phase termination and improve the efficiency, whereas, higher air velocities can reduce the phase duration and efficiency. Applying the

considered LHS cooling device into a greenhouse decreased the indoor temperature by around 10 K during the hottest hours of the day.

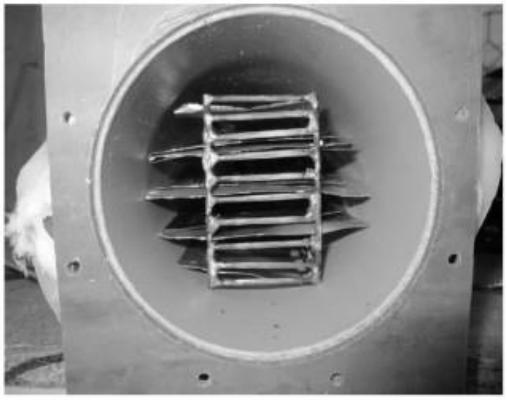


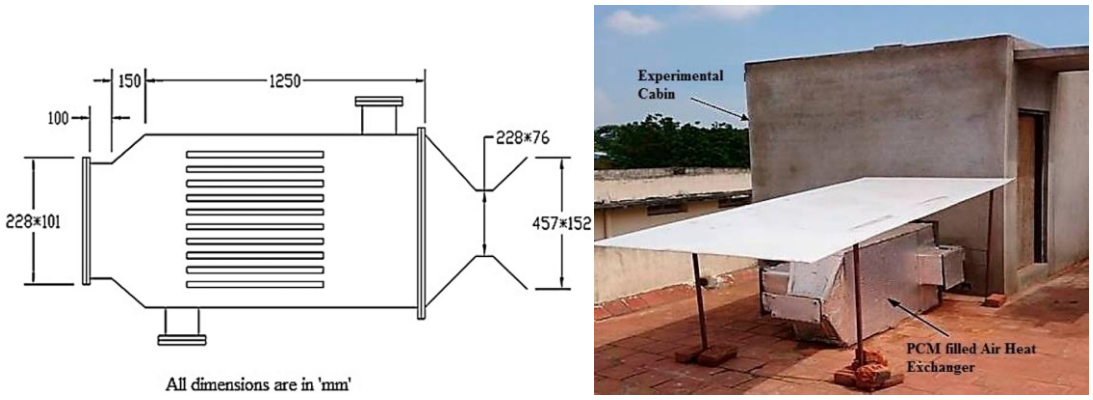
Figure 3.27: Configuration of the LHTES apparatus designed by Mirahmad et al. (2016).

Muthuvelan et al. (2016) have also carried out an experimental investigation to evaluate the thermal performance of a flat plate modular PCM heat exchanger for free cooling application in Pune city in India. The heat exchanger comprises ten modules of PCM with an overall weight of 76 kg made of a commercial HS 29 PCM with a phase change range 17-29 ºC. The outer housing was insulated with polystyrene of a 25 mm thickness. The system was designed for a free cooling capacity of 0.5 kW. A room with dimensions 2.5 m × 2.5 m × 2.5 m was constructed to monitor the indoor temperature based on air supplied by the system. The schematic of the PCM heat exchanger and view of the system along with the cabin is demonstrated in Figure 3.28. The required air flow rate ($\dot{m}_{air}$) to charge the PCM was estimated using equation (3.4);

$$\dot{m}_{air} = \frac{m_{PCM} \times (L)}{C_p \times \Delta T \times dt'} \tag{3.4}$$

where; m_{PCM} is the mass of the PCM, L is the latent heat of fusion of the PCM, C_p is the air specific heat, ΔT is the temperature difference between the PCM and ambient air, and dt' is the duration expected for the full charging. The findings indicated that an average temperature drop of 2.5 K inside the cabin can be obtained. The design is only applicable for locations with an ambient temperature above the comfort by about

5 K during the discharging period. However, the use of air conditioning is still needed in the considered location. The authors suggested reducing the heat losses to enhance the performance, and if the system is combined with an evaporative or a nocturnal radiative cooling mean may entirely eliminate the usage of air conditioning systems.



(a) (b)

Figure 3.28: (a) Schematic and (b) view of the free cooling system proposed by Muthuvelan et al. (2016).

Rajagopal et al. (2016) have analysed the thermal behaviour of a fabricated PCM heat exchanger device (1.20 m × 0.415 m × 0.410 m) with 11 PCM modules for free cooling application in Bangalore city, India. The system was used to fulfil the cooling load of the commercial building considered in (Rajagopal et al., 2014). A commercial RT27 paraffin PCM of a melting temperature range of 25-28 ºC was selected according to the available diurnal temperature variation on the site. During the charging phase; various inlet temperatures (19, 20, 21, and 22 ºC) and inlet air velocities (3.0, 4.0 and 5.0 m/s) were considered using an environmental chamber. While during the discharging phase different internal loads between 0.5 kW and 3.0 kW were tried to vary the temperature of the indoor air used for cold extraction. The system was evaluated experimentally and numerically using CFD simulation. The experimental setup and the configuration of the heat exchanger are demonstrated in Figure 3.29. The authors found that augmenting inlet temperature from 19 ºC to 22 ºC increased the charging duration by around 60% with an only small variation of air velocity. Thus, it is advisable to accelerate the charging at a time of lower temperatures rather than using high air velocities as it will be ineffective after a certain level. This will offer

the advantage of lower power consumption by the fan. A reduction of 2.0-3.5 K in air temperature inside the room equipped with the free cooling device was achieved, compared to a room without cooling system when the internal heat load was maintained at the lowest (0.5 kW) level and the highest level (3.0 kW), respectively. Thus, the internal heat load appears to have a substantial impact on the performance, and it is advised to be reduced to the lowest level.

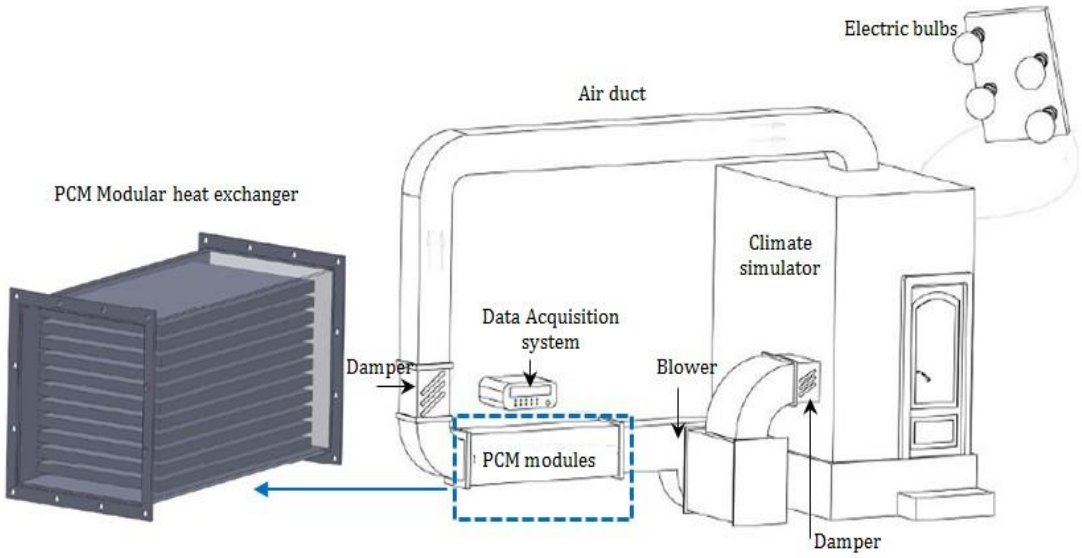


Figure 3.29: Experimental setup of the free cooling system proposed by Rajagopal (2014), (2016).

A comparative study has been carried out by Alam (2017) to evaluate the efficiency of two means of PCM application in buildings; a ceiling integrated PCM for passive cooling, and a separate PCM storage unit for free cooling applications as shown in Figure 3.30. The study was performed using Energy-Plus and CFD simulation tools, and the results were validated with relevant experimental data. The results indicated that the free cooling application of the PCM is more efficient in decreasing the indoor temperature by up to 1.8°C than the ceiling application which resulted in a temperature drop by only 0.5°C for a considered residential building under typical summer conditions of Melbourne, Australia. The authors have also reported that more than the required amount of the PCM was utilised in this study.

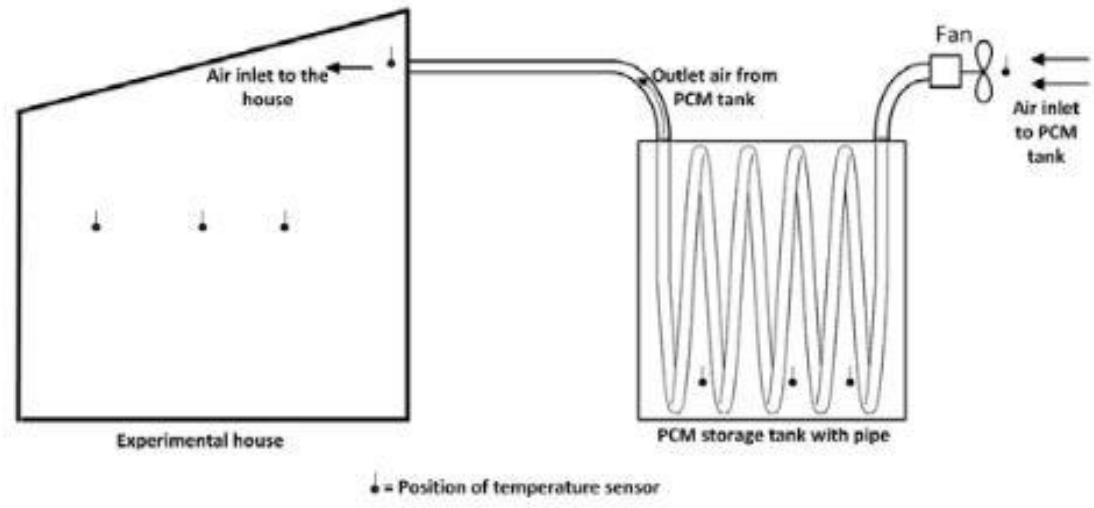


Figure 3.30: Experimental setup of the free cooling system proposed by Alam (2017).

An evaporative cooling assistive the free cooling system has been investigated by Panchabikesan et al. (2017a). The proposed system was a small-scale rig with spherically encapsulated PCM in a cylindrical tank with water spray nozzles operated at the air inlet as shown in Figure 3.31. The experiments were carried out under the real hot-arid climate conditions of Pune, India, using HS29 PCM of a transition temperature of 27–29 °C. The experiments were carried out under the real hot-arid climate conditions of Pune city, India, using HS29 PCM of a transition temperature of 27–29 °C. The results have shown that the PCM remained in the liquid phase even after 8 hours due to the high charging air temperature with the stand-alone free cooling system. While with the combined system with the evaporative cooling, the PCM was fully solidified. It is noticed that the charging performance was better at low relative humidity levels and vice versa. The proposed combined system indicates the potential of cooling storage in the PCM irrespective of the local ambient temperature in the targeted hot-arid location.

Using the same experimental model in (Panchabikesan et al., 2017a), another experimental work has been conducted by Panchabikesan et al. (2018) under the real moderate/temperate climate conditions of Bangalore city, India, using RT 28HC PCM with a transition temperature 25.6–27.1 °C. The authors reported a drop in charging period around 28.7% and 34.8% at the adopted inlet air velocities 2 and 1.5 m/s,

respectively. The proposed hybrid system allowed a complete solidification of the selected PCM at a quicker rate. It is also evident from the results that the increase in the inlet air velocity has a significant impact on the free cooling system performance, while the impact is marginal in the case of the integrated system with the evaporative cooling unit.

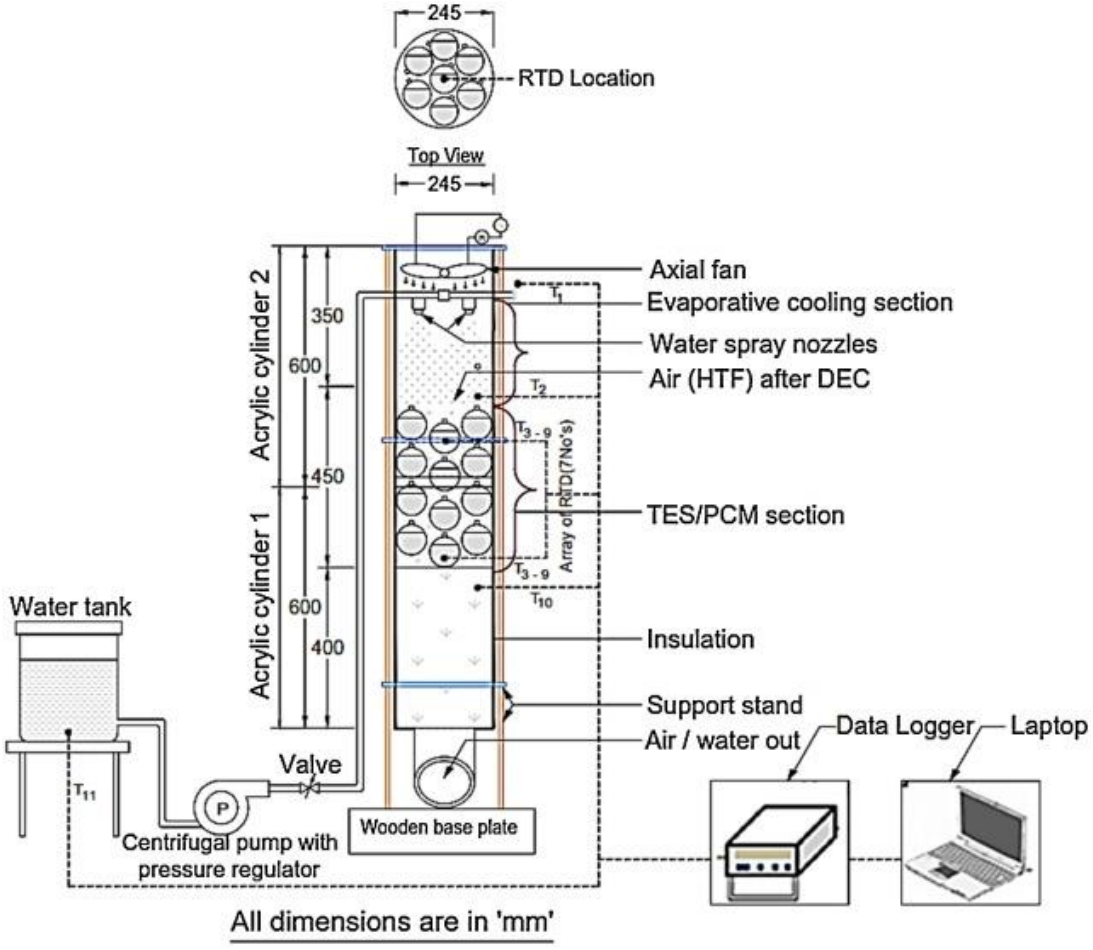


Figure 3.31: Experimental setup of the free cooling system proposed by Panchabikesan et al. (2017a), (2018).

3.6 Discussion of the factors affecting performance and application of PCM in free cooling systems

Based on the current review, this section highlights some critical observations regarding factors with significant impact on thermal performance and application of free cooling technologies. These factors include; climate conditions, PCM transformation temperature, encapsulation of the PCM, heat transfer problems (due to low thermal conductivity, incongruent melting, and supercooling of PCMs) and the stability of the PCM. The economic feasibility of the free cooling systems is also an important factor and should be taken into consideration. Discussion of these factors allows researchers to get a clear picture of potential opportunities to tackle the challenges and possible strategies to enhance the performance of the technology, and accordingly, areas for future research are suggested.

3.6.1 Climate conditions

The free cooling concept is site-specific and climate dependent. In any location, nocturnal ventilative cooling depends mostly on the amplitude of diurnal temperature variation rather than the average outdoor temperature. It is well established that, free cooling based latent heat storage performs effectively in locations with diurnal temperature swing ranging between 12 and 15 K, a typical of desert climates (Raj and Velraj, 2010). Any diurnal temperature variation below this necessitates careful design considerations coupled with a proper selection of the PCM properties (Zalba et al., 2004). It should be stressed that the coupling of PCM storage with passive ventilation systems such as wind catchers or other natural cooling strategies such as evaporative cooling and ground cooling may represent an interesting area for future research.

3.6.2 PCM transition temperature

Several approaches regarding the selection criteria of PCM transformation temperatures for free cooling technology have been reported in the literature (Medved and Arkar, 2008, Butala and Stritih, 2009, Raj and Velraj, 2010, Osterman et al., 2012). The phase change temperature of a PCM considered for the free cooling system should be in the range to provide maximum and quick crystallisation of the PCM

throughout the night charging, and in the same way, should be closer to the indoor design temperature (Yanbing et al., 2003).

Raj and Velraj (2010) have stated that PCM with a particular phase change temperature may not fit well in the outdoor temperature swing throughout the entire year for some climates, and in particular, the hot climate. This suggestion is also supported by Medved and Arkar (2008) who mentioned that a PCM with a range of transformation temperatures is recommended due to its capability of absorbing heat in a variety of inlet air temperatures, and accordingly able to operate throughout the outdoor temperature swing for a more extended period of the year. For buildings in hot regions, PCMs with higher melting/solidification temperatures are much appropriate for cooling enhancement. It has been added that the optimum phase change temperature can be estimated as a function of PCM peak melting temperature (T_p) and the average outdoor temperature (T_a) from this simple equation (3.5);

$$T_p = T_a + 2K \tag{3.5}$$

Butala and Stritih (2009) have proposed a temperature range between 19 and 24 ºC for the PCM application in hotter climates. They have stated that this range will result in a temperature between 23 and 27 ºC for the exit air from the storage medium during the discharging period, which is considered acceptable for the hottest summer period. Osterman et al. (2012) have recommended that, most of the PCMs utilised as thermal energy storage in buildings should possess phase change temperatures within the range of 20-32 ºC to maintain the comfort conditions in most climates, and the proper selection of the PCM transformation temperature must be coupled with the existing appropriate passive or active heating/cooling systems.

In general, it is difficult to find a single PCM that suits the whole year comfort requirements due to the considerable seasonal variation predicted in most locations. Thus, a transition temperature within the comfort limit of the overheating period can be an appropriate solution for different climates. Otherwise, a combination of phase change materials may be used to provide a larger operating temperature range.

3.6.3 Encapsulation of PCMs

PCM encapsulation is one of the ways which enables integration of PCM into buildings, and also prevents PCM leakage as well as protecting the PCM from interaction with the external environment and hence determines its long-term operation. In addition, PCM containers can assist in avoiding some PCM drawbacks such as flammability in the case of paraffin (Rodriguez-Ubinas et al., 2012).

The properties of PCM container play a central role in the performance of the storage system. PCM encapsulation influences the thermal conductivity and hence the time lapse of the freezing/melting phase. The PCM container should be strong, corrosion resistant, thermally and structurally stable, have easy handling features and have a sufficient surface area for heat transfer (Riffat et al., 2013, Chandel and Agarwal, 2017).

There are a variety of PCM encapsulation techniques proposed and utilised by different researchers (Cabeza et al., 2011, Salunkhe and Shembekar, 2012), and offered by companies with various configurations and manufacturing materials. Some of these include aluminium panels, aluminium pouches, metal or spherical plastic balls, flat plates, plastic bags, different forms of plastic tubes, cylindrical pipes, PVC panels, shells, granules, etc. as illustrated in Figure 3.32.

PCM encapsulation can be classified into micro and macro-encapsulation according to the container size. In micro-encapsulation; very small particles varying from 1 to 1000μm in size will be contained inside solid and thin shells. These micro-components can be combined in any matrix compatible with the enclosed shell. In the case of macro-encapsulation, PCM from millilitres to many litres will be packaged in various containers' configurations such as aluminium panels and pouches, and in most cases, the container itself acts as a heat exchanger surface (Waqas and Din, 2013, Jamekhorshid et al., 2014).

Micro-encapsulation is capable of providing more application opportunities in buildings, enhancing the heat transfer through enlarging the heat exchange surface, reducing the interaction between the PCM and the outer environment and controlling

the volume alteration. However, the cost of the micro-encapsulated PCM is higher than macro-encapsulated one, and some micro-encapsulations may influence the mechanical strength of the construction materials (Schossig et al., 2005, Tyagi et al., 2011, Giro-Paloma et al., 2016, Liu et al., 2016a).

On the other hand, macro-encapsulation has the advantage of preventing the leaking of PCM and suits the application of the PCM inside walls and partitions of the building. Conversely, some macro-encapsulations may reduce the heat transfer rate during the solidification process (Farid et al., 2004, Rodriguez-Ubinas et al., 2012).

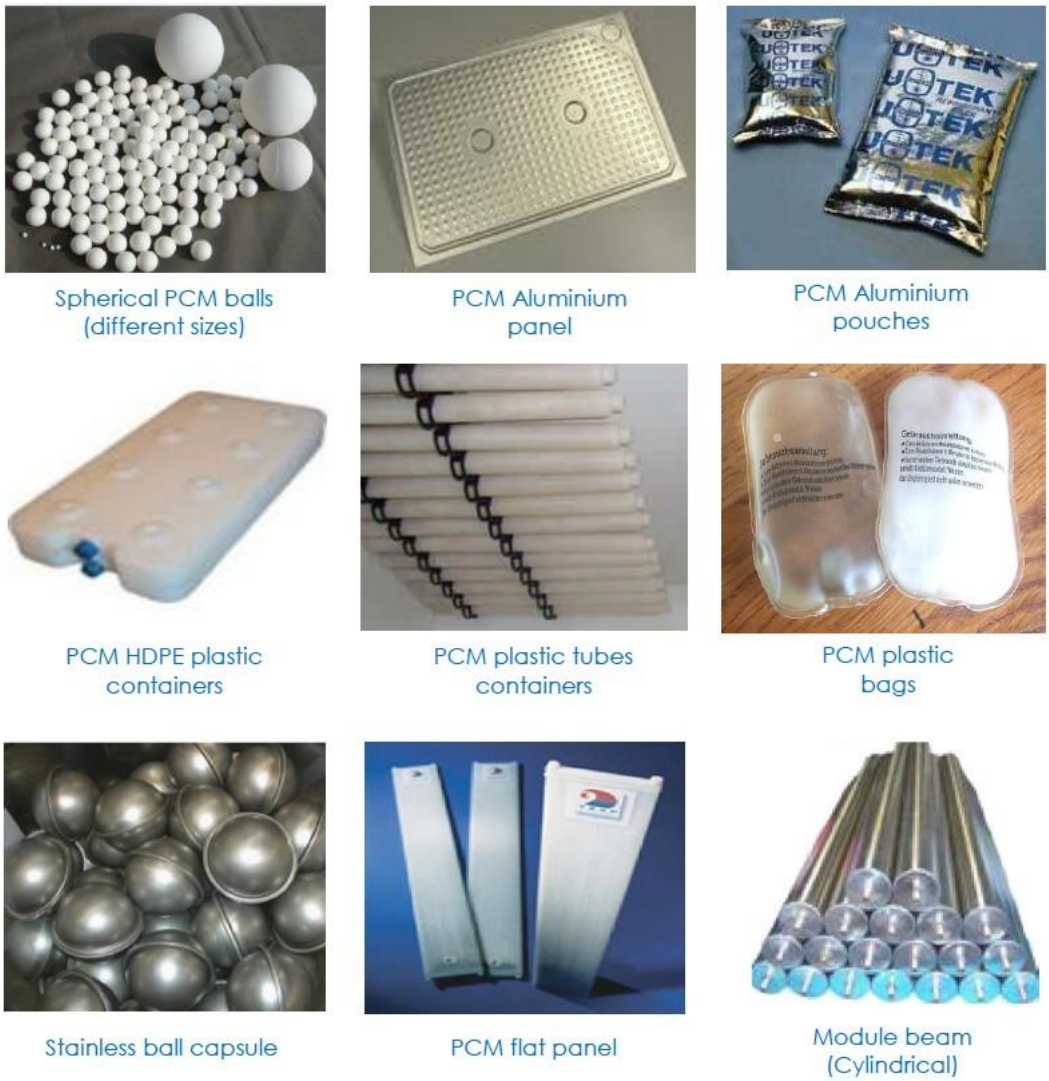


Figure 3.32: Some of the PCM encapsulation techniques available in the market.

3.6.4 Heat transfer of the PCM-air heat exchangers

Many factors limit the utilisation of PCMs for cooling and heating in buildings, including the low thermal conductivity of the most available PCMs, the incongruent melting, and the supercooling problems. Accordingly, comprehensive research has currently been carried out by some researchers and PCM companies to overcome these drawbacks and enhance the thermal behaviour of the PCM.

The majority of studies carried out on phase change materials have reported poor thermal conductivities (Agyenim et al., 2010), and therefore, the heat transfer performance used in free cooling is low (Velraj et al., 1999, Solomon and Velraj, 2013). Promoting the conductivity level to enhance the melting and crystallisation process during the charging and discharging periods has been investigated widely in the literature (Mesalhy et al., 2005, Ibrahim et al., 2017). A review of theoretical and experimental research to advance the PCM conductivity was presented in (Liu et al., 2016b). Adding substances with large thermal conductivities; such as copper, aluminium, nickel, stainless steel and carbon fibre in different configurations such as fins, honeycomb, wool, brush, etc.; is considered as one of the practical techniques for enhancing the heat transfer rate (Figure 3.33) (Fan and Khodadadi, 2011). For instance; a series of axial metal planes perpendicular to the longitudinal pipe to increase the heat transmission between the air and the PCM unit were utilised by Abhat (1983). Application of finned tubes has been reported by Costa et al. (1998). Aluminium fins used inside and outside upper and lower metal box filled with PCM was investigated by Butala and Stritih (2009), (2010). Metal matrix structures with PCMs were extensively investigated in (Satzger et al., 1998, Py et al., 2001, Marín et al., 2005) to increase the conductivity level with a minimum reduction of energy stored. Furthermore, other benefits such as diminishing the supercooling of salt hydrates and lowering the volume alteration of paraffin can also be realised as well by this method.

Another efficient method for enhancement of heat exchange rate is utilising arrangements with multiple PCMs which depends mainly on the temperature difference between the circulated air and the PCM melting temperature. When using

a single PCM, this variance has reduced in the direction of the air flow, however, packing multiple PCMs with melting temperature in a decreasing order during the discharging phase and in an increasing order throughout the charging phase can keep an appropriate or nearly constant temperature difference in the flow directions. This concept leads to approximately steady heat flux, hence, enhancing the performance of the storage system (Jegadheeswaran and Pohekar, 2009, Mosaffa et al., 2013b). For example, a significant increase in heat transfer rate with multiple PCMs was achieved by Farid and Kanzawa (1989) and Gong and Mujumdar (1996) relative to a single PCM.

In conclusion, although these methods have enhanced the heat transfer within the storage system, they may generally increase the PCM weight and cost of the system.

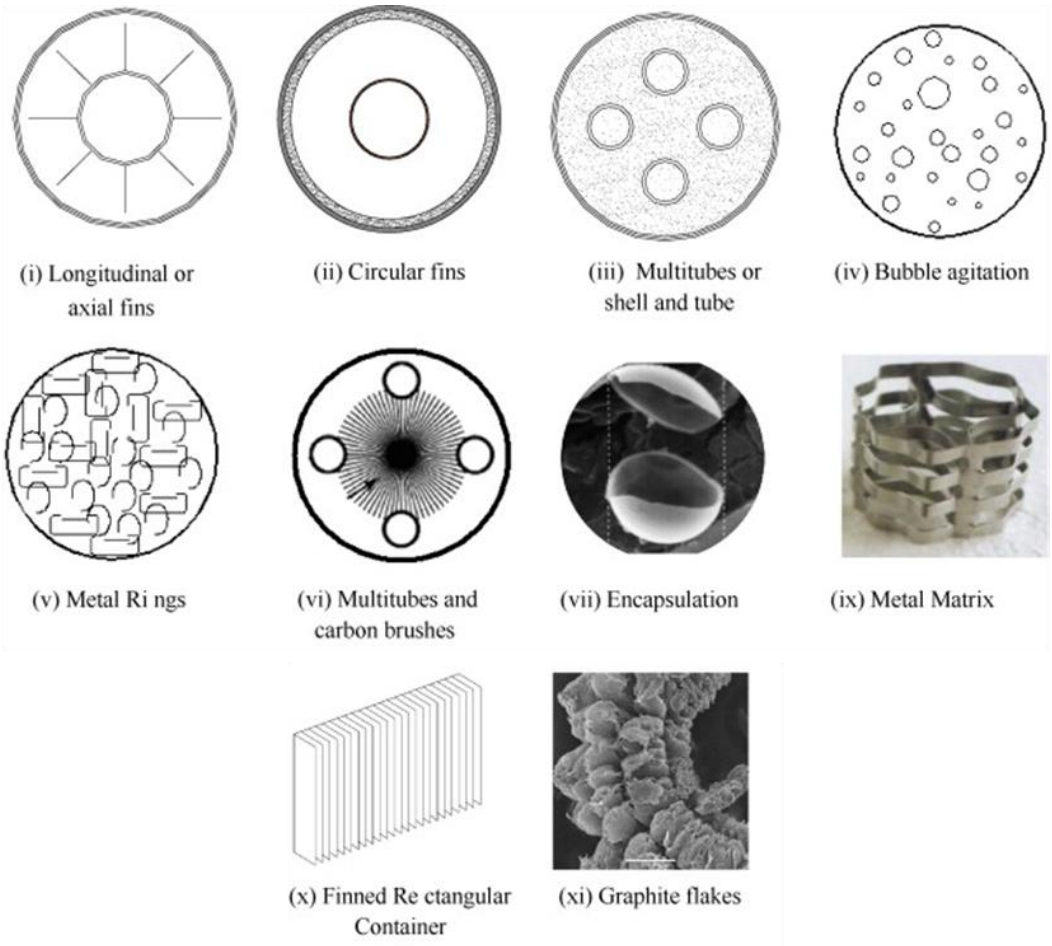


Figure 3.33: Methods utilised for heat transfer enhancements in PCM applications (Agyenim et al., 2010).

3.6.5 Stability of PCMs

Stability of the PCM is another crucial factor that affects its operation for a long-term duration in buildings. The stability problem could be attributed to two key factors; insufficient stability of the PCM properties as a result of thermal cycling and/or the corrosion between the substance and the container (Oró et al., 2012). Thermal stability of PCMs can be recognised by assessing the thermo-physical properties of the PCM after a number of repeated thermal cycles. Therefore, this factor has to be considered when selecting a PCM for a given purpose in order to avoid any system deterioration. A comprehensive review of thermal stability for various PCM groups can be found in (Rathod and Banerjee, 2013). Numerous researches have been carried out to examine the durability of some organic and inorganic materials including (Sharma et al., 1999, Shukla et al., 2008, Zhou et al., 2012, Silakhori et al., 2013, Solé et al., 2014). For example, thermal cycling tests were performed to assess the stability of some chosen organic and inorganic PCMs by Shukla et al. (2008). Their findings indicate that the inorganic PCMs show inappropriate performance after some cycles compared to the organic types which demonstrate good thermal properties after up to1000 cycles.

3.6.6 Economic aspect of free cooling systems

The economic feasibility is a key issue that has not been adequately addressed in most of the studies conducted in the free cooling application, though it was reported that most of the developed storage systems had exhibited high energy efficiency and promising outcomes. According to Kamali (2014), the initial cost of a PCM based free cooling system is estimated to be around 10% higher than a conventional air conditioning system of equivalent capacity, even though the technology has not yet been fully commercialised. However, running costs may be far lower, if the system is appropriately sized.

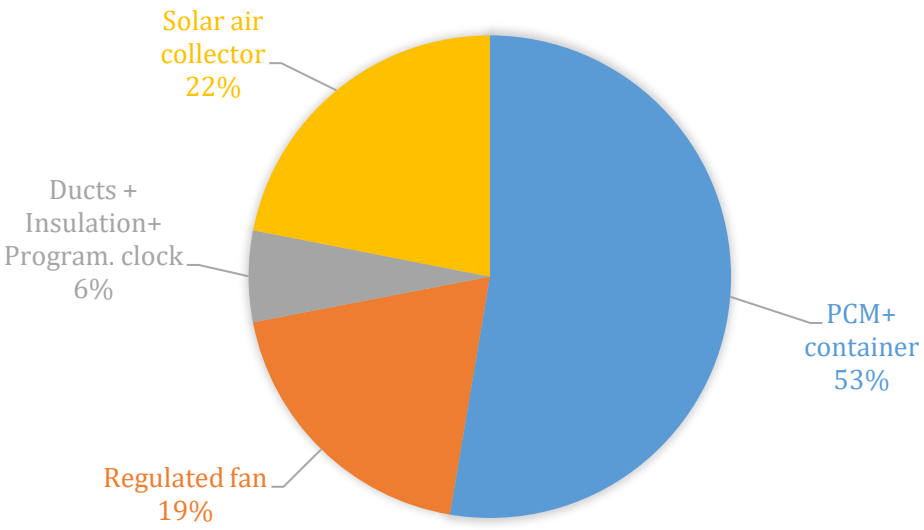
Jaber and Ajib (2012) have assessed the technical and economic feasibility of a free cooling system shown in Figure 3.20 in comparison to an operation of a standard air conditioning system. A free cooling system with an initial cost of €5671 was developed to fulfil the entire annual cooling demand of a typical residential building in Jordan (Mediterranean climate). However, its running cost exceeded the annual

energy saving, i.e. the size of the system is not economically feasible. An optimised design based on a conducted parametric study was then introduced covering around 80% of the total cooling load with an initial cost decreasing to around €1195. The Payback Period (PB) for the optimised system was estimated at 7.8 years. It is important to underline that the high initial cost may be attributed to the usage of two fans as an indirect evaporative cooling is incorporated. The PCM share in the initial cost is not known, as the authors have not provided a cost breakdown.

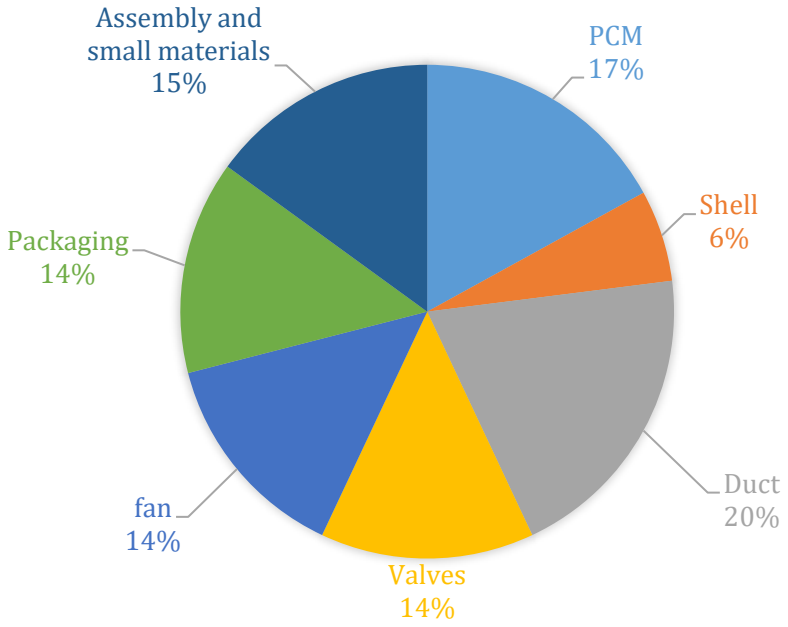
An economic analysis has been carried out by Zalba et al. (2004) for their developed free cooling system. The chart in Figure 3.34a shows the ratio of each component of the total cost. It is clear that about 17% of the whole cost goes to the storage material (PCM). It is also reported that the power consumption by the free cooling system is almost lower by 94% compared to conventional air conditioning systems with similar capacity. However, 9% additional cost is required for the storage unit with an approximate payback period of 3-4 years.

Osterman et al. (2015a) have presented the cost details of their TES system that utilised for both heating and cooling in buildings. A reference office building with 4 m × 3 m × 2.8 m was considered. According to the authors, the overall initial cost was estimated at €1140 which is approximately double that of a conventional air-conditioner. The share of all equipment in the entire cost is presented in Figure 3.34b. It is clear that half of the cost goes to the PCM panels (Aluminium containers filled with 40 kg of paraffin RT22HC PCM). However, if the system is operated for cooling purpose only, the capital cost can be lowered by nearly 20% compared to that of the solar collector.

Both studies reported in (Zalba et al., 2004) and (Osterman et al., 2015a) agreed that the largest fraction of the capital cost had been expended in PCM substance and its encapsulation. The variation in percentages can be attributed to many other factors including differences in the size of the systems and type of PCM utilised. Additionally, the costs of free cooling systems could be decreased, if the PCM production was largely commercialised. Osterman et al. (2015a) stated that the reduction in PCM price could take place if TES is mass fabricated.



(a)



(b)

Figure 3.34: Cost breakdown for the free cooling systems developed by (a) Zalba et al. (2004), and (b) Osterman et al. (2015a).

3.7 Summary

Free cooling systems incorporating latent heat storage are promising sustainable systems best applicable for locations with a diurnal temperature variation of 12-15 K. Most of the reviewed studies indicated that such systems can bring the indoor temperature well to the comfort zone, and significant energy savings exceeding 50% could be realised in all investigated climates compared to conventional air conditioning systems.

The major conclusions drawn from the review are;

- The most critical parameter that affects the free cooling performance is the PCM transformation temperature, as any improper selection of the phase change temperature neither wholly solidifies nor melts the PCM during charging and discharging phases, resulting in inadequate cold energy storage. The low thermal conductivity of PCMs is another factor that represents a key barrier for application as it slows down the solidification and melting processes. Consequently, PCMs with higher thermal conductivities must be chosen and the use of heat transfer enhancements is highly advised.

- In all proposed systems air was the heat transfer fluid. Most of the studies recommend enhancing the air flow rate during the charging period to accelerate the PCM solidification, which can also be enhanced by enlarging the surface area per unit volume of the PCM. An air flow rate 3 or 4 times higher for charging than that for discharging was found appropriate for sufficient cooling storage.

- The magnitude of the utilised PCM storage has varied significantly among most of the studies; PCM weights range from 6.4 to 30 kg/m² of floor area have been reported based on the local climate conditions, cooling load, proposed system, etc.

- The majority of the free cooling studies have been conducted in moderate and continental climates and very limited in hot and arid regions where the demand for cooling is extremely high. This draws attention to the need for conducting more research on free cooling technologies in hot-arid climate conditions.

- Despite a large number of researches on the PCM application for energy storage in buildings, the real case applications documenting the potential and behaviour of PCMs in real operation conditions are quite rare. It should also be noted that no studies are being performed to evaluate the long-term performance of the technology. The barrier to the PCM application in actual buildings may be attributed to their major drawbacks such as; segregation, supercooling, low thermal conductivity, high cost and to the limited number of PCM manufacturers available around the world. Accordingly, the concept of free cooling using PCM energy storage is still under development, and more research is needed to convey the concept from the theoretical and experimental stage to the real implementation phase.

Chapter 4

Proposed System Design and Research Methodology

4.1 Introduction

This chapter comprises two parts; the first part describes the proposed hybrid night radiative and ventilative cooling system using latent heat storage (NRV-LHS) through addressing the design concept, the main components, and the working principles. The second part discusses the overall methodology adopted to achieve the aim and objectives of the study.

4.2 Description of the proposed NRV-LHS system design

4.2.1 Design concept

The proposed innovative NRV-LHS uses night radiative and ventilative cooling concept combined with latent heat storage for the purpose of maintaining thermal comfort at a lower energy consumption rate, and hence reducing dependence on the conventional air conditioning systems. The radiative cooling panels are located externally on the roof of the building facing the sky, while the TES system is situated internally at the ceiling of the room. The diagram in Figure 4.1 describes the general concept of the NRV-LHS system, showing the charging and discharging modes and the air circulation lines (day 'blue' and night 'green').

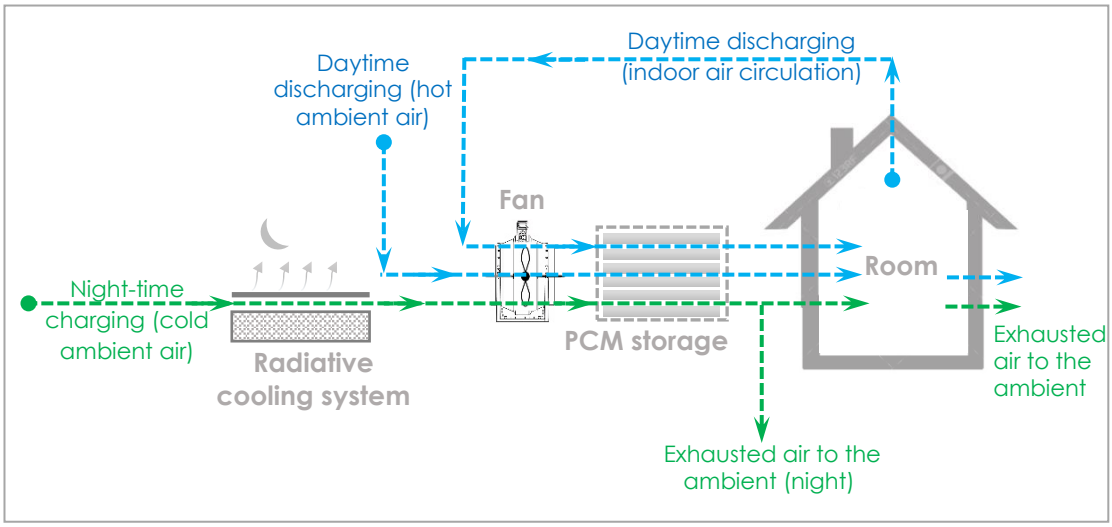


Figure 4.1: Charging and discharging modes of the NRV-LHS system.

4.2.2 System components

The main components of the NRV-LHS system which are integrated into the building are shown in Figure 4.2. The system components can be divided into those related to the radiative cooling system (external components) and those related to the thermal energy storage unit (internal components). A fan coupled with a variable speed controller is employed to blow the air through the system.

The radiative cooling system is based on a lightweight nocturnal radiator panel. The radiator consists of a rectangular flat sheet of galvanised steel. The surface seeing the sky is coated with high emissivity paint and covered with a single layer windscreen to lessen the influence of convective gain from the wind. The radiator is positioned horizontally above the building roof and consists of parallel longitudinal purlins to allow air flow through the channels and to support the radiator structure.

The PCM storage unit is based on a flat-plate configuration and comprises a set of macro-encapsulated PCM modules stacked over each other with air passages in between and are placed inside a rectangular enclosure made of aluminium sheets. The ducting system is equipped with operable regulating dampers, shutters, diffusers and air filters. The adjustable flaps and the fan controller allow the system operation with the external and internal air. The enclosure is covered entirely with high-density insulation, and plasterboard finishing can be used to harmonise with the interior design.

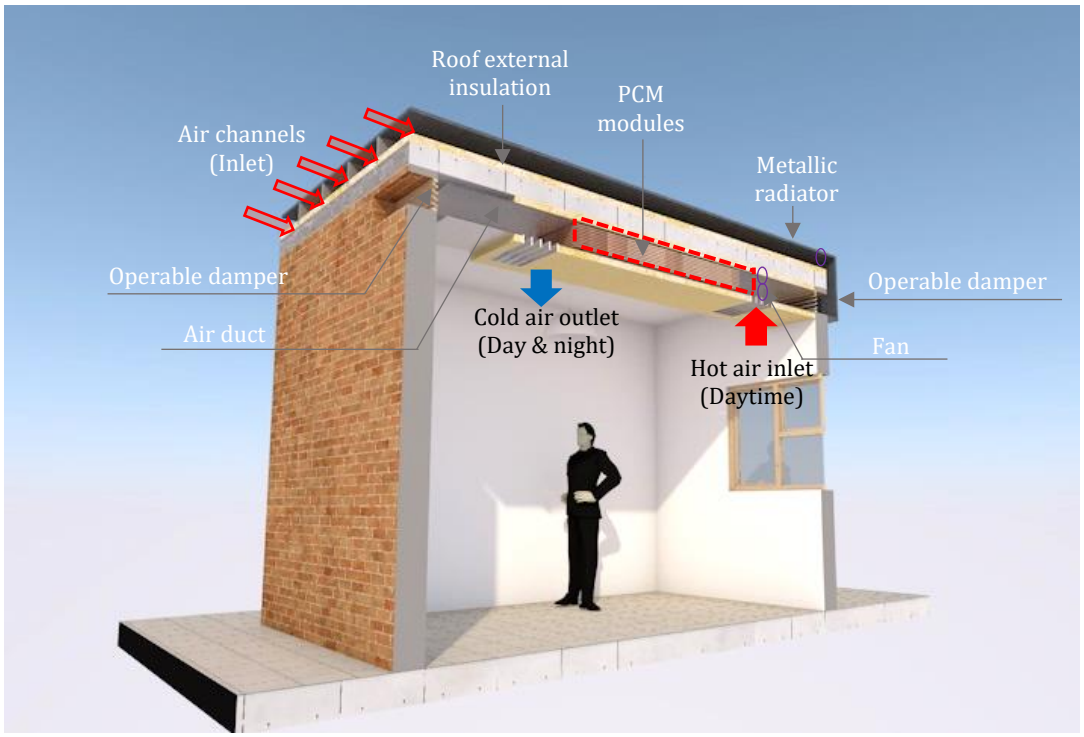


Figure 4.2: Main components of the NRV-LHS system.

4.2.3 Operation principles

The NRV-LHS system runs under two modes of operation as follows (Figure 4.3).

4.2.3.1 NRV-LHS charging mode

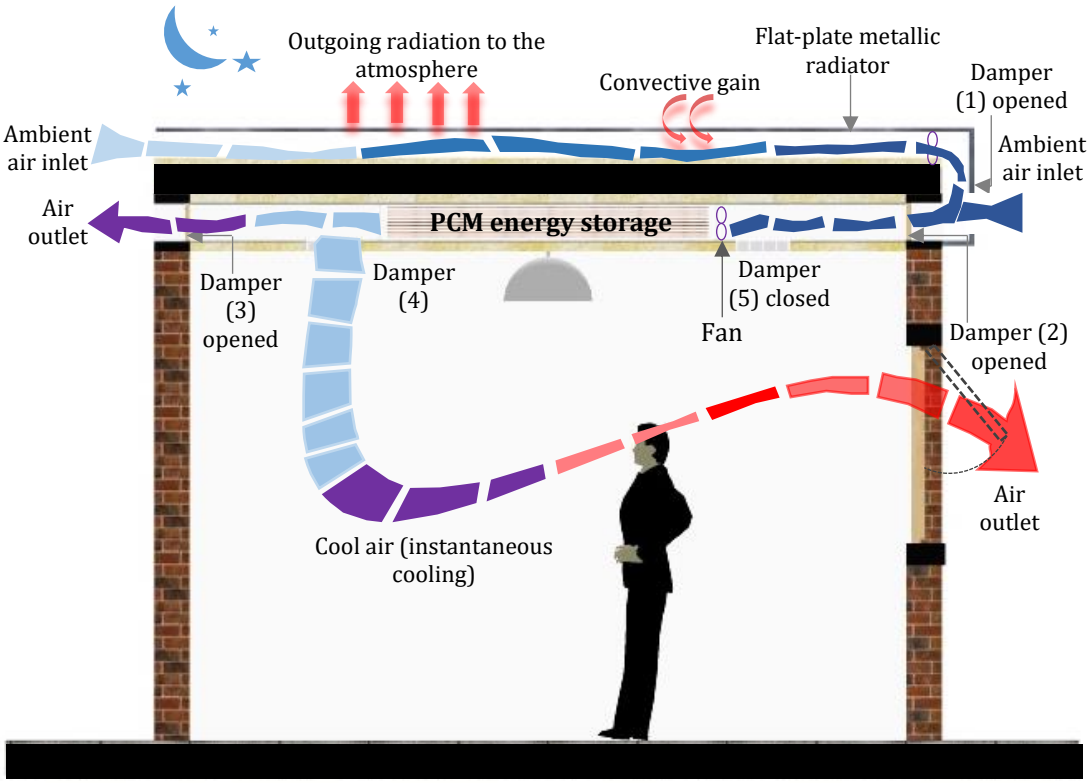
At night, the metallic radiator cools down by losing heat to the sky through radiation exchange. The ambient air is cooled by convection when passing through the channels of the cold radiative surface. The cold air flows through the PCM modules, cooling down the PCM which begins to solidify. Based on the cooling requirements and the climate conditions, the air could be admitted into the indoor space to provide instantaneous cooling or exhausted to the ambient. This process takes place continuously throughout the night until the PCM is fully solidified. The stored cooling in the PCM will be used to offset the cooling load during the daytime (Figure 4.3a).

Occasionally, a mixed operation mode by mixing the air cooled by the radiative cooling system with the ambient air could be allowed under favourable conditions at night to enhance the PCM charging process. Moreover, the system could be operated using the cold ambient air only, when the radiative cooling is not available.

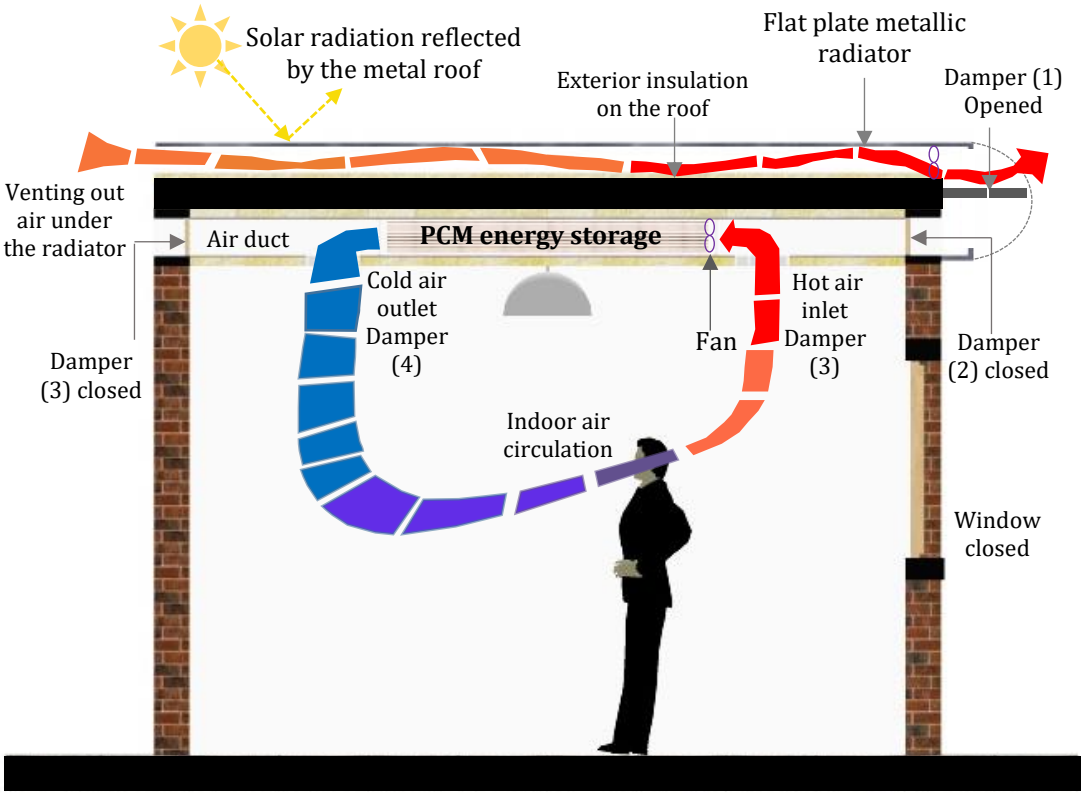
4.2.3.2 NRV-LHS discharging mode

When cooling is required, probably during the daytime, the cooling stored in the PCM is discharged either through an indoor air circulation or via admission of fresh ambient air, depending on the operating conditions. The flowing air dissipates heat to the PCM while its temperature drops to the comfort level (Figure 4.3b).

During the daytime, ambient air flow through the channels below the radiator would be allowed to avoid heat gain through the radiative surface.



(a) Night-time (charging mode)



(b) Daytime (discharging mode)

Figure 4.3: Operation principles of the NRV-LHS system.

The proposed NRV-LHS is a novel cooling system aims to offset the peak load time to the time of free cooling availability and is much applicable for building cooling applications in hot-arid regions. The proposed system has been investigated numerically and experimentally to evaluate its thermal performance.

The key feature of the NRV-LHS system is its capability to enhance the thermal performance of conventional free cooling systems by expanding the charging period, enhancing the heat transfer rate, and therefore, accelerating the PCM solidification process. In addition, the proposed NRV-LHS system possesses the following technical advantages;

- The modular design of the TES unit allows high flexibility to adjust the system capacity based on the cooling requirements.
- The adopted radiative cooling system design is characterised by the simplicity, the use of a lightweight radiator, and the easy installation at the building roof compared to the other radiative cooling systems.
- The radiative cooling system is further useful for buildings occupied during the night hours such as bedrooms in domestic buildings. The concept is also appropriate for application in both; massive and light structures by locating a proper TES medium.
- The TES unit and the air ducting system are configured to suit the installation at the room walls and ceiling and permitting simple intake and supply of the air flow. This is achieved through the use of a number of dampers to regulate the operation of the system.
- The NRV-LHS system allows for flexibility of operation, such as the charging process using a free cooling only mode, a radiative cooling only mode, or a mixed mode. For the cooling discharge, the system permits working by the ambient air or via an indoor air circulation, yet, an automatic control system is required.

4.3 Research methodology

The overall methodology to accomplish the prime aim and objectives of the whole research involves the following three main phases (Figure 4.4).

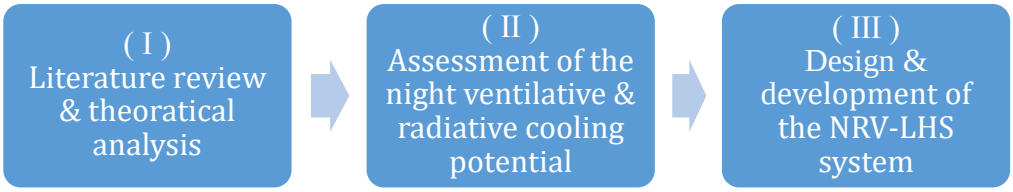


Figure 4.4: Diagram showing the overall research methodology.

4.3.1 Phase I: Literature review and theoretical analysis

This is a significant step to fulfil several objectives such as; exploring and strengthening knowledge about the topic, identifying the research gap, assumptions, and hypothesis, and observing the tendency and progression in the field. This phase has led to the proposed system design and determination of the operating conditions. The reviewed literature covers the following aspects;

4.3.1.1 Literature review on the subject area

This phase aims to review the most recent published work and developed systems relevant to two main areas; the passive and natural cooling strategies of buildings with a concentration on the radiative cooling (Chapter 2), and thermal energy storage with a particular focus on latent heat storage for free cooling of buildings (Chapter 3).

4.3.1.2 Analysis of the case study climate

Microclimate is a critical factor that governs the implementation of nocturnal cooling technologies in buildings. Khartoum city, the capital of Sudan, is one of the hottest and sunniest cities in the world, which features a hot desert climate. Therefore, in this study, the evaluation of the night cooling potential is based on Khartoum climate as a case study for hot-arid regions. Climatic data recorded over 30 years are analysed to determine the design threats and opportunities.

4.3.1.3 Establishment of the comfort zone

Studying thermal comfort inside buildings is crucial as it represents the basis for assessing the potential of natural and passive design strategies (Merghani, 2001). For the present work, the thermal comfort temperature range is the determining factor for measuring the effectiveness of the proposed system, as the discharging performance is assessed based on the thermal comfort period achieved through the system. Therefore, the comfort zone for domestic buildings in hot-arid regions is studied according to the previous studies and the international standards recommendations.

4.3.1.4 Selection of the case study building

Selection of a proper case study is a primary step in assessing sustainable environmental design opportunities. This research targets the residential buildings in hot-arid climate, as this sector has the major contribution to the energy consumption, around 77.2% of the total (Omer, 2002). Most of the energy use in residential buildings is by the air conditioning systems, owing to the high cooling demand, most of the year.

The modern houses' design in Khartoum is considered in this research, as they feature high indoor temperatures above the comfort limit most of the year and experience high energy consumption rates compared to other housing typologies. The adopted house was chosen from one of the major housing developments in Khartoum named Elyasmeen residence, which occupies an area of 98 acres and contains about 595 plots of houses. The adopted house can be considered as a typical for the current houses in Khartoum, as most of the modern houses have almost a similar layout of the indoor spaces and practically adopting similar constructions, but the outer skin design usually differs. Part of the master plan of Elyasmeen complex and the perspectives of the selected house are depicted in Figure 4.5. The house occupies an area of 463 m² and comprises two main storeys; a ground floor used as a reception zone and a first floor made of four bedrooms and living space, in addition to a supplement top floor which includes one bedroom and a large terrace area for outdoor night sleeping. The building layout and spaces dimensions are described in Figure 4.6.



Figure 4.5: (a) Part of the housing complex, (b) the selected house view.



Figure 4.6: Floor plans of the selected house.

4.3.2 Phase II: Assessment of night cooling potential

4.3.2.1 Assessment of night ventilative cooling potential

The free cooling potential in hot-arid regions is assessed based on the analysis of the thermal comfort, the microclimate, and the building thermal performance. Analysis of the thermal comfort and the local climate conditions are used to evaluate the cooling source. The building thermal performance is essential to determine the temperature of the indoor air, since it is used as a heat transfer fluid in the discharging process, and to estimate the cooling load in order to determine the capacity of the TES system.

The thermal performance of the selected house is investigated initially. The impact of a range of bioclimatic design strategies on the thermal performance enhancement is examined, and the model with the best performance is selected for a further study. Application of the bioclimatic design strategies in buildings is considered a precondition for the natural cooling strategies application, such as the nocturnal radiative and ventilative cooling considered in this study. There is a variety of available software which could be used to assess the building energy performance such as TAS, Energy-Plus, IESVE. For this study, the analysis is carried out using DesignBuilder software which employs Energy-Plus simulation model. The Energy-Plus model is selected as it has been widely verified and validated with field-measured data in many studies to ensure its accuracy and only small limitations have been reported (Shrestha et al., 2011, Tabares-Velasco et al., 2012).

4.3.2.2 Assessment of night radiative cooling potential

The potential of a nocturnal radiative cooling strategy for buildings cooling load reduction is assessed. According to the required indoor cooling period (day, night, or both at a time) and the desired mode of heat transfer between the TES medium and the indoor space, an air-based system based on a lightweight metallic radiator integration on the building roof is adopted. This type is also characterised by the simplicity, low cost, practicality, and easy installation at the building roof over other radiative cooling techniques.

In order to optimise the radiative cooling system design under the case study climate conditions, detailed calculations are carried out using a spreadsheet in the Microsoft Excel. The sensitivity of the model to a variety of geometrical and climatic parameters is investigated. The operational behaviour under typical summer conditions in Khartoum is discussed, and the findings are used in the experimental study.

4.3.3 Phase III: Design and development of the NRV-LHS system

The NRV-LHS system design and assessment using computer modelling and experimental testing are carried out as follows;

4.3.3.1 Design of the hybrid NRV-LHS system

The TES system is designed to serve a single room in the selected building. The TES capacity is determined based on an overall cooling load of a room with well-insulated roof and external walls during a typical day of hot summer months in Khartoum (May and June). Selecting an average summer day can be technically and economically beneficial for the whole summer comfort.

The rationale for selecting the PCM thicknesses and the air channel heights is that they are near the optimal for the present case study according to the literature review. The inlet air temperatures for the charging process are selected based on the prevalent ambient temperature during summer nights of the case study. On the other hand, for the discharging process, the inlet air temperatures are selected based on the daytime room temperature under summer conditions, obtained using the Energy-Plus simulation. The air flow rate for the discharging process is selected according to the typical ventilation rates in domestic rooms, in the range 1-4 ACH. While for the charging process, the air flow rate is selected based on the previous studies recommendations (Arkar and Medved, 2007, Medved and Arkar, 2008), i.e. air flow rates of 3-4 times of that used in the discharging process, as this is found appropriate for sufficient cooling storage.

4.3.3.2 CFD modelling of the proposed TES system

One of the essential advantages of the CFD simulation is allowing system optimisation by computing and analysing data that are difficult to be obtained from the laboratory experiments, such as determining the liquid fraction of the PCM domain and temperatures distribution inside a sealed PCM container (Xiang and Gan, 2015). Therefore, the widely-utilised powerful software ANSYS Fluent is used for the optimisation of the system geometrical configuration and the operating conditions.

The CFD analysis is carried out to investigate the solidification and melting characteristics of the PCM and the air flow pattern. The settings, the assumptions, and the computational methodology are all detailed in Chapter 6. A parametric study is conducted to evaluate the impact of various factors on the system thermal performance including the PCM thickness, air channels height, inlet air temperature, and air flow rate.

Under current system design (operating conditions and modelling settings), there is a need for computing resources, substantially higher than a standard computer. Thus, the University of Nottingham high-performance computing (HPC) facility is used to run the simulations. The HPC service allows quick large-scale calculations and provides an opportunity to use more advanced settings, such as refining the geometry meshing and reducing time-steps to increase the accuracy level of the results. Although a simulation case can run for a week in the HPC, the reduction in the computational time is outstanding, approximately more than tenfold compared to a standard computer.

4.3.3.3 Experimental investigation of a laboratory TES unit

The experimental study is carried out in a laboratory environment where an environmental chamber is used to simulate the hot-arid climate conditions. A laboratory-scale TES unit is constructed and connected to the chamber. The temperature and pressure are measured at various locations through the test rig. The experiments setup, the measuring instruments and testing procedure, are detailed in

Chapter 7 and Chapter 8. The experimental work involves the following main investigations;

- PCM charging and discharging processes under steady-state inlet air conditions, in order to assess the impact of the PCM modules arrangement and the operating conditions on the system performance.
- PCM charging process under transient inlet air conditions, in order to assess the operational performance of the system during hot and moderate summer conditions of the hot-arid climate, under various scenarios of free and radiative cooling operation.

The system performance is assessed based on the PCM melting/solidification time, the outlet air temperature delivered by the system, and the heat transfer rate. The experimental results are used to verify and enhance the accuracy of computer modelling.

Chapter 5

Evaluation of Night Cooling Potential in Hot-Arid Climate

5.1 Introduction

This Chapter aims to assess the potential of night cooling strategies; free cooling and radiative cooling; in hot-arid climates, considering Khartoum city as a case study. The free cooling potential is evaluated by considering several parameters including; thermal comfort, climate conditions, and building energy demand. The radiative cooling potential was evaluated taking into the account a system based on a roof integrated metallic surface. Detailed calculations are carried out using an Excel spreadsheet. The sensitivity of radiative cooling performance to a variety of affecting parameters is investigated. The system thermal performance is discussed under summer conditions of Khartoum climate.

5.2 Evaluation of free cooling potential

In order to determine to what extent the natural cooling available at night-time in hot-arid climate is capable of providing whole day thermal comfort in buildings, a number of factors have been studied as shown in Figure 5.1, considering Khartoum climate.



Figure 5.1: Factors affecting the potential of free cooling of buildings in any location.

5.2.1 Identification of human thermal comfort

Thermal comfort conditions vary significantly according to the climate. Hence, many researchers demand countries and regions with various climate conditions to find their own local thermal comfort standards, taking into account people acclimatisation, lifestyle, and experiences (Nicol et al., 1994, Givoni, 1994, Merghani, 2001). There are several studies carried out investigating the human thermal comfort in buildings in hot-arid regions including; Nicol (1974) in Baghdad (Iraq) and Roorkee (India), Heidari and Sharples (2002) in Ilam (Iran), and Merghani (2001) in Khartoum (Sudan). All these studies have presented local thermal comfort zones substantially higher than what have been predicted by the ASHRAE and PMV standards. This supports the rationale for using thermal comfort zones based on local surveys from subjects fully acclimatised to living in hot-arid conditions, as the international standards tend to overestimate locals' thermal sensation.

Merghani (2001) determined the comfort temperature and demarcated the local thermal comfort zone for Khartoum city based on the findings of his major observational study and a fieldwork survey on thermal comfort in residential buildings. The study was based on responses from subjects fully acclimatised to living in Khartoum and utilise many adaptive mechanisms. The analysed data predicted comfort temperatures of 26.45 ºC, 28.8 ºC, and 30.9 ºC for spring, winter and summer seasons, respectively.

The summer and winter thermal comfort limit was compared to those recommended by the international standards (ISO/ASHRAE), as shown in Figure 5.2 and Table 5.1. It is evident that the comfort zone proposed by Merghani (2001) is much wider, including temperatures considered uncomfortable by ASHRAE and ISO standards, and includes more realistic humidity levels, lower than that proposed in ASHRAE. Hence, it has been adopted for this study, as the international standards seem less realistic in specifying the local thermal comfort conditions.

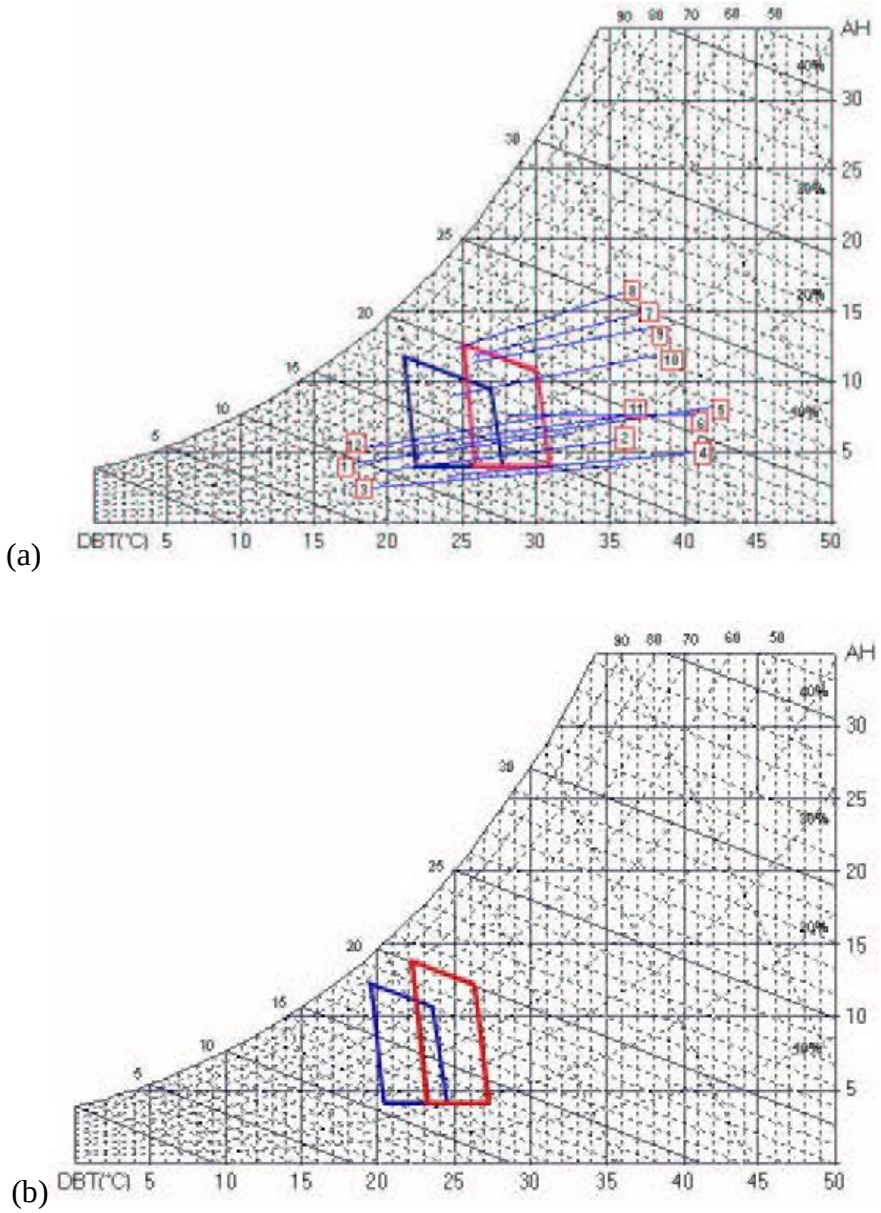


Figure 5.2: Summer (red) and winter (blue) comfort zone for Khartoum; (a) demarcated by Merghani (2001), and (b) recommended by ASHRAE standards.

Table 5.1: Comfort temperature ranges for Khartoum adopted by the international standards and Merghani (2001).

	ASHRAE	**ISO**	**Merghani (2001)**
Summer	23.3-27.2 ºC	23-26 ºC	25.5-30.9 ºC
Winter	20.6-24.4 ºC	20-24 ºC	21.5-27.5 ºC

5.2.2 Microclimate conditions

According to many studies (Raj and Velraj, 2010, Zalba et al., 2004), the successful application of free cooling can be climatically realised in the presence of;

- Suitable diurnal temperature variation, potentially larger than 12 K, and
- Ambient air temperature within or below the PCM transition temperature range during the charging time.

In the current study, Khartoum has been selected as a location representing the hot-arid regions. Khartoum is located at a latitude of 15° 6´N and a longitude of 32° 55´E, and its climate can be classified as a hot desert with very hot summers and warm-dry winters with mild cold nights. Khartoum is characterised by a very long dry season lasts for almost nine months (October-June), and a rainy season (July-September) where occasional precipitations and dust storms are present. The high altitude of the sun and the low proportions of cloud cover make the region exposed to the intensity of insolation (Oliver, 1965).

In this section, the climate data of Khartoum recorded during the period 1961-2000 by Khartoum airport metrological station have been analysed. These data are available from the World Meteorological Organization (WMO, 2016).

The monthly dry bulb temperature data and the precipitation rates throughout the year in Khartoum are demonstrated in Figure 5.3. The temperature typically varies from 16 °C to 42 °C and is rarely below 14 °C or above 44 °C. It is observed that there is a large diurnal temperature variation around 15 K throughout the year. According to the mean maximum temperature profile, periods extending from April to September and from November to February represent the two main seasons summer and winter, respectively. Whereas, March and October are the transitional months. Hence, the overheated period can be considered lasting for eight months involving the transitional months, where a significant demand for cooling exists.

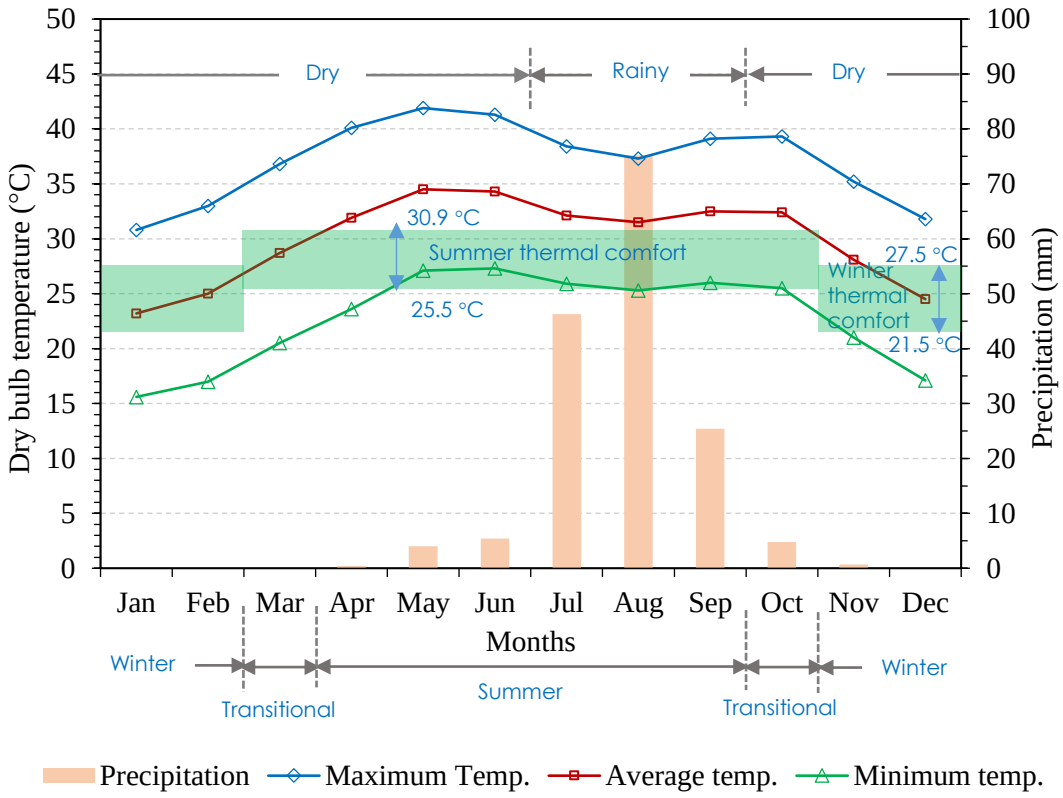
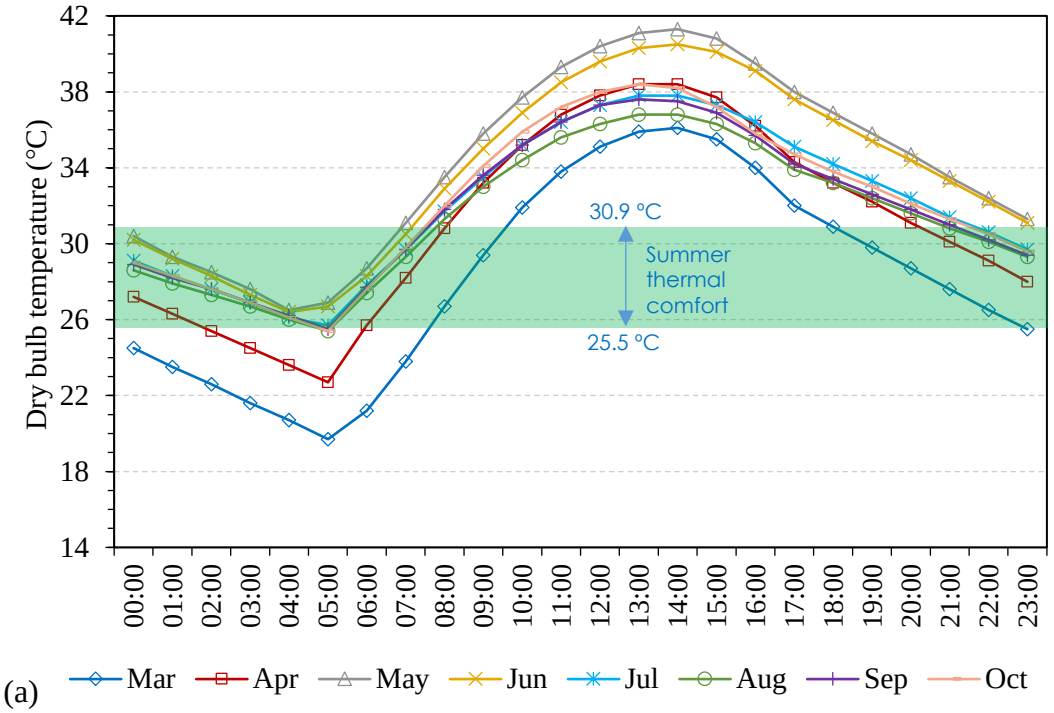
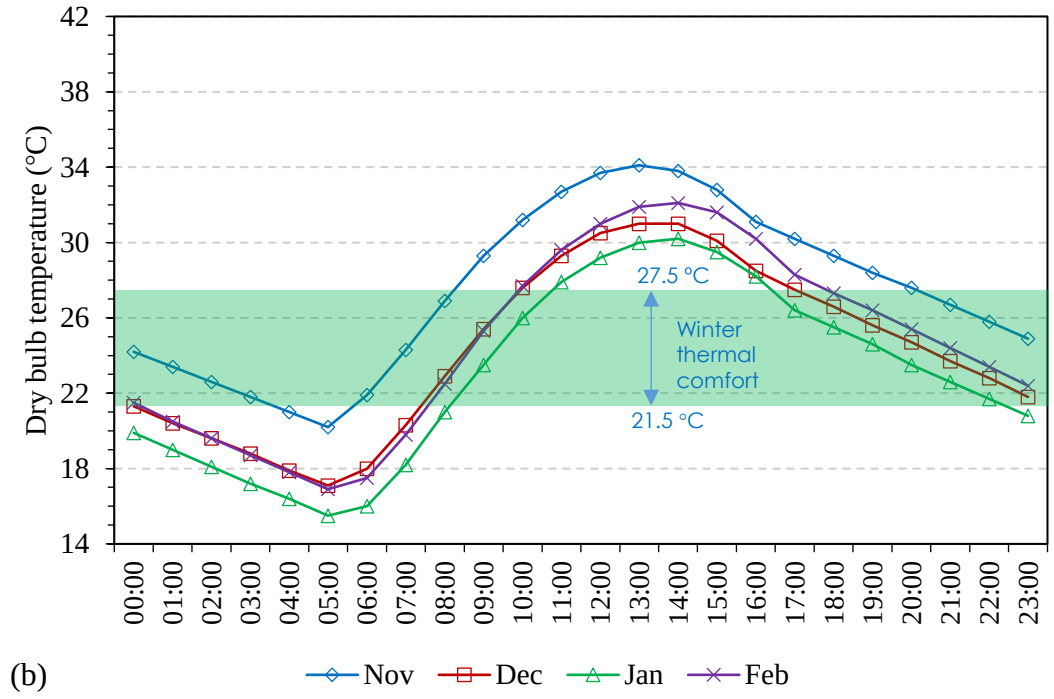


Figure 5.3: Monthly data of dry-bulb temperature and the precipitation rate for the site of Khartoum (Khartoum airport meteorological station).

The diurnal average temperature variation for summer and during the transitional months (March-October) and for winter months (November-February) in Khartoum, along with the thermal comfort limit determined in (Merghani, 2001) are presented in Figure 5.4.



(a)



(b)

Figure 5.4: Average dry-bulb temperature in Khartoum during (a) summer and transitional months, and (b) winter months (Khartoum airport meteorological station).

As shown in Figure 5.4a, the mean outside air temperature at night is well within or below the thermal comfort level by few degrees most of the time. This indicates the potential to provide instantaneous night cooling, besides cooling during the daytime if an appropriate TES unit is employed. However, the charging period during peak summer months (May and June) is relatively short, as the minimum ambient temperatures are higher than the comfort mean temperature for a longer duration. If the PCM transition temperature is selected at the average comfort temperature, this will result in a low temperature difference between the night ambient air and the PCM, leading to a lower TES system performance.

On the other hand, as shown in Figure 5.4b, the comfort zone in winter months lies between the mean maximum and minimum dry-bulb temperature, denoting a need for both cooling and heating. The mean maximum temperature is in the range 30.8-35.2 °C, moderately above the upper band of the winter comfort level. Whilst, the air temperature during the night-time could be cooled considerably between 15.6 and 21 °C. Overall, in hot-arid regions such as Khartoum, the required building cooling and heating in winter are relatively small, and this can be provided using passive cooling and/or heating strategies such as; building shape, thermal mass, conventional ventilation, internal gains, and solar controls.

The dry-bulb temperature profile indicates that May and June are the hottest months in Khartoum. Therefore, the energy performance analysis carried out in this study is based on the average climate conditions of these months.

5.2.3 Investigation of building thermal performance

The purpose of this section is to investigate the thermal performance of the selected house and examine the potential of some passive cooling strategies that could reduce the cooling load requirements. Energy-Plus simulation has been used for this analysis.

5.2.3.1 Input data, assumptions, and settings

A model for the prototype house was created in the DesignBuilder software which employs the Energy-Plus model for simulation as shown in Figure 5.5. The building orientation was set to face towards the south-north direction, no external obstructions

are considered, and the urban terrain was chosen in the local terrain. The model contains 19 thermal zones in addition to a number of non-thermal zones to accommodate the shading elements. The weather data used in the DesignBuilder software were compared to the measured data, recorded by Khartoum airport metrological station for the period 1961-2000 for validation, and a good agreement was observed. An example of the ambient air temperature comparison is shown in Figure 5.6.

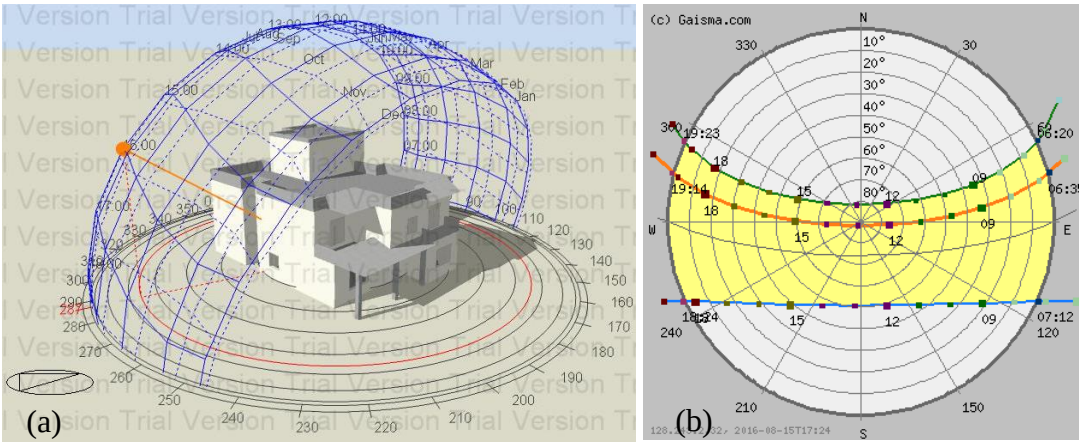


Figure 5.5: (a) Model of the house in DesignBuilder, (b) diagram of sun path over Khartoum.

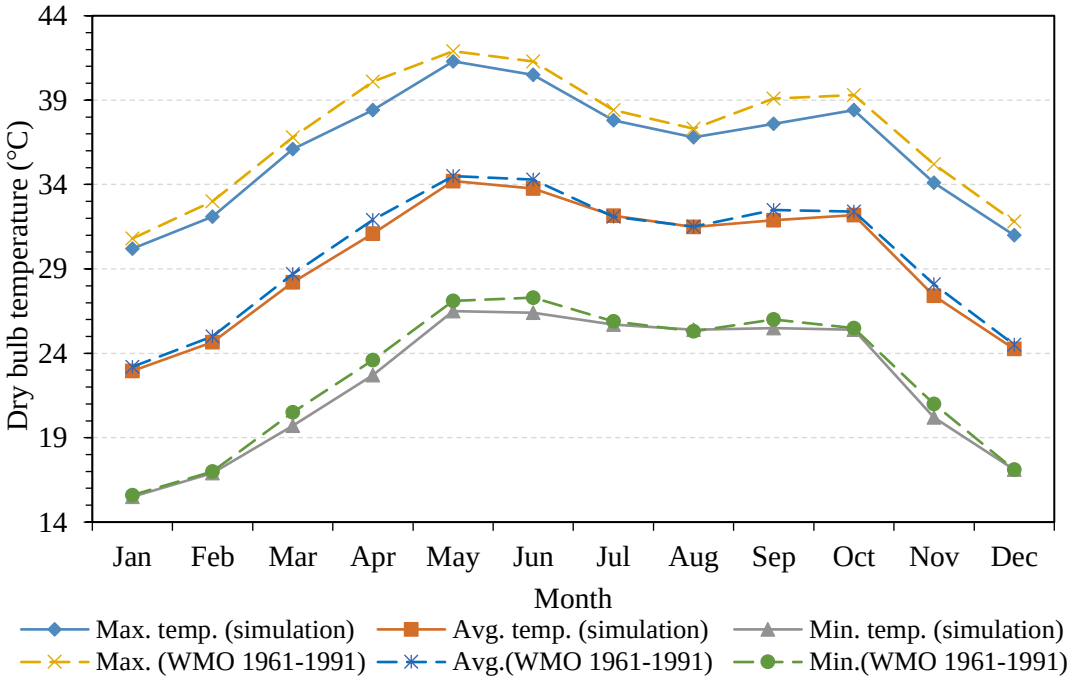


Figure 5.6: Comparison of the ambient air temperature used in the simulation to actual data measured by Khartoum airport meteorological station.

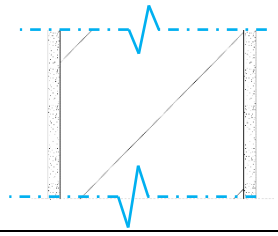
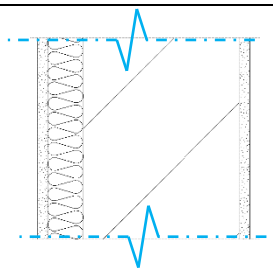
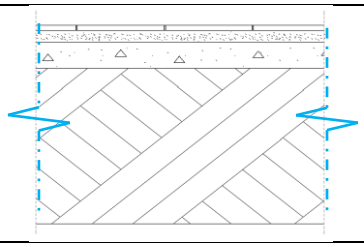
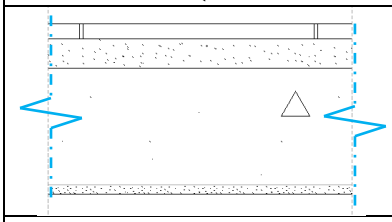
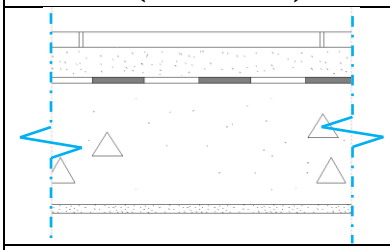
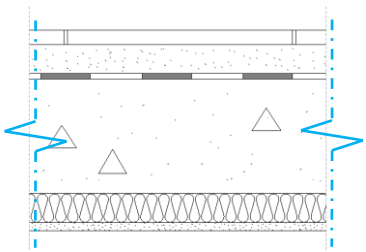
In the case of internal loads and environmental comfort controls, the data used for occupancy and metabolic settings (activity and clothes) were assumed to resemble living style inside houses in Khartoum. The HVAC thermostat set-points were set at 21.5 ºC and 30 °C for cooling and heating, respectively. The RH humidification and dehumidification set-points for cooling and heating were set at 25% and 55%, respectively, based on the comfort zone of Khartoum. The building is considered to be of medium airtightness, setting the air infiltration to a constant rate of 0.3 ACH, and scheduled as always on. Natural ventilation was controlled according to the occupancy schedule by opening 50% of the windows and internal doors area. The luminance level and the minimum fresh air required for each space were set according to CIBSE (2006:p.1-3). The data used for occupancy, metabolic, lighting, and ventilation rate for each building space are summarised in Table 5.2.

Table 5.2: Internal load and environmental comfort settings used in DesignBuilder software (CIBSE, 2006:p.1-3).

Space	Occupancy (No. of people)	Metabolic			Lighting (lux)	Minimum fresh air
		Activity (met)	Summer clothing (Clo)	Winter clothing (Clo)		
Living hall	6	1.1	0.65	1.00	150	1 ACH
Bedroom	2	0.9	1.2	2.50	100	1 ACH
Bathroom	1	1.2	0.25	0.25	150	15 L/s
Kitchen	1	1.6	0.65	1.00	200	60 L/s

The construction materials were specified according to the applied housing constructions specifications in Khartoum. Details of the construction materials assigned to the basic and the enhanced models are presented in Table 5.3.

Table 5.3: Assigned construction materials specifications.

External walls (basic model)		
	Outer 15.0 mm plaster 220 mm Brick outer Leaf 15.0 mm plaster Inner	U-value (W/m^{2}K) 1.932 Thickness (m) 0.250
External wall (enhanced model)		
	Outer 15 mm plaster 220 mm Brick outer Leaf 50 mm Foam-Polyurethane 15 mm Gypsum board Inner	U-value (W/m^{2}K) 0.436 Thickness (m) 0.30
Ground floor (basic and enhanced models)		
	Inner 30 mm Ceramic floor tiles 70 mm Screed 150 mm Cast concrete 900 mm Earth, common	U-value (W/m^{2}K) 1.797 Thickness (m) 1.15
Internal floor (basic and enhanced models)		
	upper 25 mm Ceramic floor tiles 70 mm Screed 150 mm Cast concrete 15 mm Plaster lower	U-value (W/m^{2}K) 1.555 Thickness (m) 0.29
Flat roof (basic model)		
	Outer 25 mm Ceramic floor tiles 70 mm Screed 10 mm Asphalt 150 mm Cast concrete 15 mm Plaster Inner	U-value (W/m^{2}K) 1.896 Thickness (m) 0.30
Flat roof (enhanced model)		
	Outer 25 mm Ceramic floor tiles 70 mm Screed 10 mm Asphalt 150 mm Cast concrete 50 mm Foam-Polyurethane 15 mm Plaster Inner	U-value (W/m^{2}K) 0.435 Thickness (m) 0.35

5.2.3.2 Results and discussion of building energy performance

The simulation has been carried out for an initial base model and several thermally enhanced models with single/multiple passive cooling strategies including the use of roof and external walls insulation, double glazing windows, and shading for glazing surfaces. The models have been investigated under two modes of operation; (i) a free-running mode, where only natural ventilation is activated during favourable outside conditions to monitor the indoor air temperatures, and (ii) an active running mode where the operation of an HVAC is continuous to estimate the required building energy load.

Figure 5.7 compares the annual cooling load of the basic model and when several passive cooling techniques have been applied. It is evident that the wall insulation has the prime role in the cooling load reduction. The model with an insulated roof and walls achieved the maximum cooling load drop (59.8%) compared to the basic model. In contrast, an insignificant drop in cooling load is obtained by using double glazing windows instead of single glazing (3.9%), and when applying shading elements (6.9%). This could be attributed to the sun path directly overhead most of the year in the considered location as shown in Figure 5.5b.

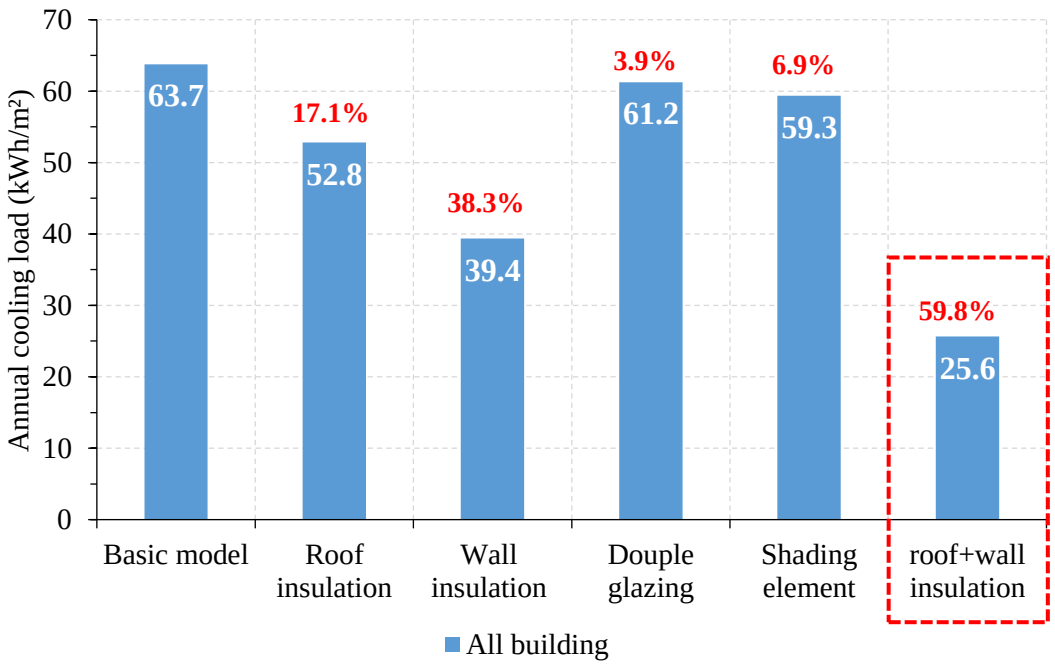


Figure 5.7: Annual cooling load of the building under various passive cooling techniques.

Figure 5.8 compares the monthly cooling load of the basic and the thermally enhanced model with insulated roof and external walls (the best case). It is clear that the original house features a high cooling demand at an average of 12.4 kWh/m² during the peak summer months. The cooling demand of the enhanced model is lower than that for the initial model by more than 50% in all months. In the case of winter months (December-February), a negligible cooling load has been noticed.

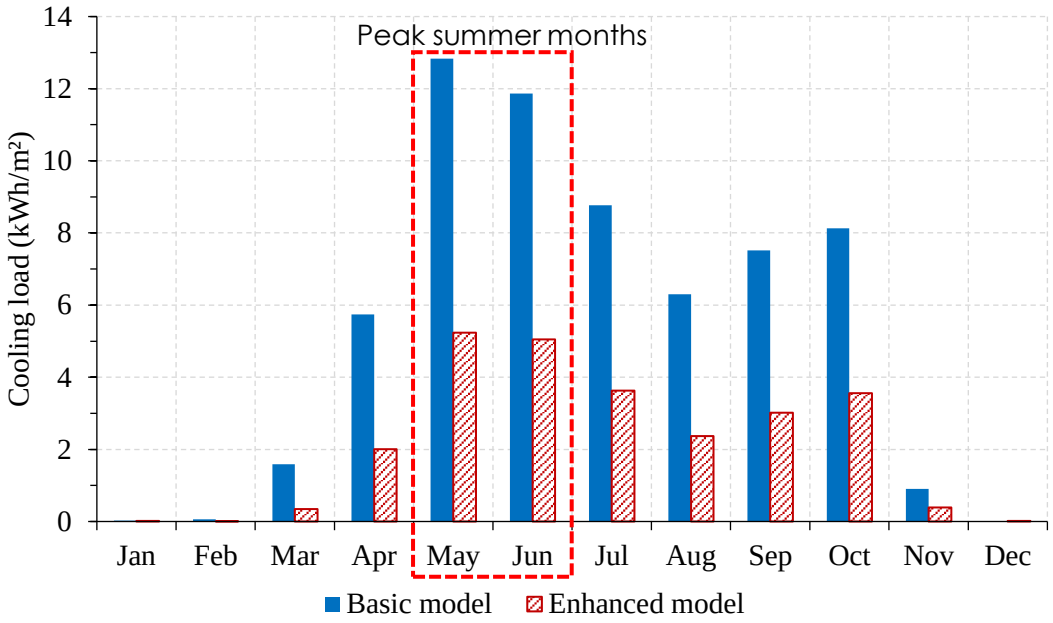


Figure 5.8: Monthly cooling load of the building.

Figure 5.9 details the cooling load of parts of the building on the average summer day. It is clear that the ground floor zones require lower cooling compared to the other floors, owing to the stable comfort temperatures in the adjacent zones on the first floor. The rooms on the first floor experience high cooling loads in the range 537-670 and 225-309 Wh/m² for the basic and the enhanced case, respectively, due to the roof exposure to the sun. The room on the top floor possesses the highest cooling demand, as having the largest exposed surface area to the outdoors. The high cooling demand achieved in the living spaces is attributed to the impact of the large area of glazing, together with internal loads (occupancy, lighting, and equipment). In this study, the sizing of the TES unit was performed based on the cooling load of the south-west room on the first floor level, where its cooling load represents the average for all rooms' load.

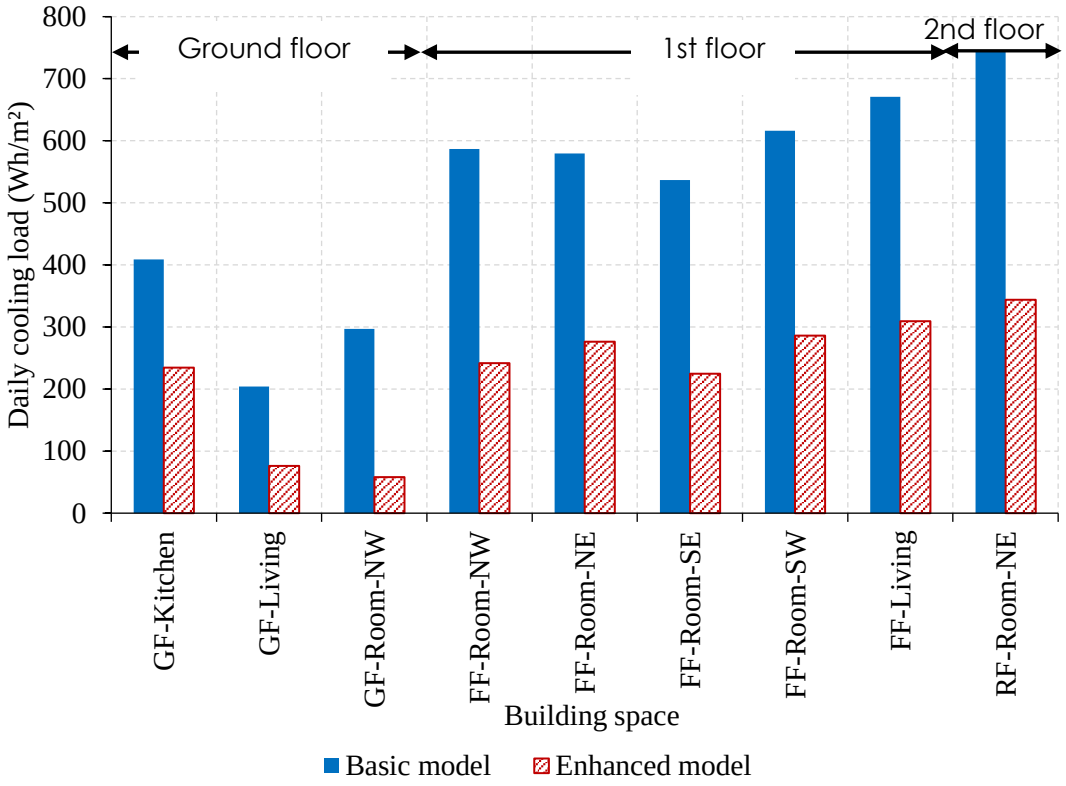


Figure 5.9: Daily cooling load of all building spaces on the average summer day.

Figure 5.10a and Figure 5.10b exhibit the variation in indoor air temperature and cooling load of the adopted room in the typical summer day, respectively. As shown in Figure 5.10a, the use of heavyweight constructions justifies the slight temperature fluctuation inside the room. Throughout the whole day, the basic model features a higher indoor temperature in the range 35.4-37 ºC compared to the enhanced model which exhibits a temperature swing between 34.4 ºC and 36 ºC. The role of the PCM based nocturnal radiative and ventilative cooling system proposed in this study is to bring the indoor temperature down to the comfort level. The lower the difference between the indoor air temperature and the solidus temperature of the PCM, the slower the coolness discharge is. Hence, a longer thermal comfort duration could be maintained, taking into account the important role of the air flow rate.

As shown in Figure 5.10b, the cooling load of the thermally enhanced rooms is lower by 60% than that of the basic room during the night and early morning hours, and by around 25-45% during the daytime hours. The maximum cooling demand of the enhanced room occurs during the afternoon hours (12.00-18.00) with an average of 16

W/m². While for the basic room, it takes place during the evening and night hours (16:00-1:00) with an average of 29 W/m². Therefore, the TES capacity should be carefully selected to afford most of the cooling load. A fan with variable speeds is required to fulfil the varying cooling loads during the day until the next day cycle commences.

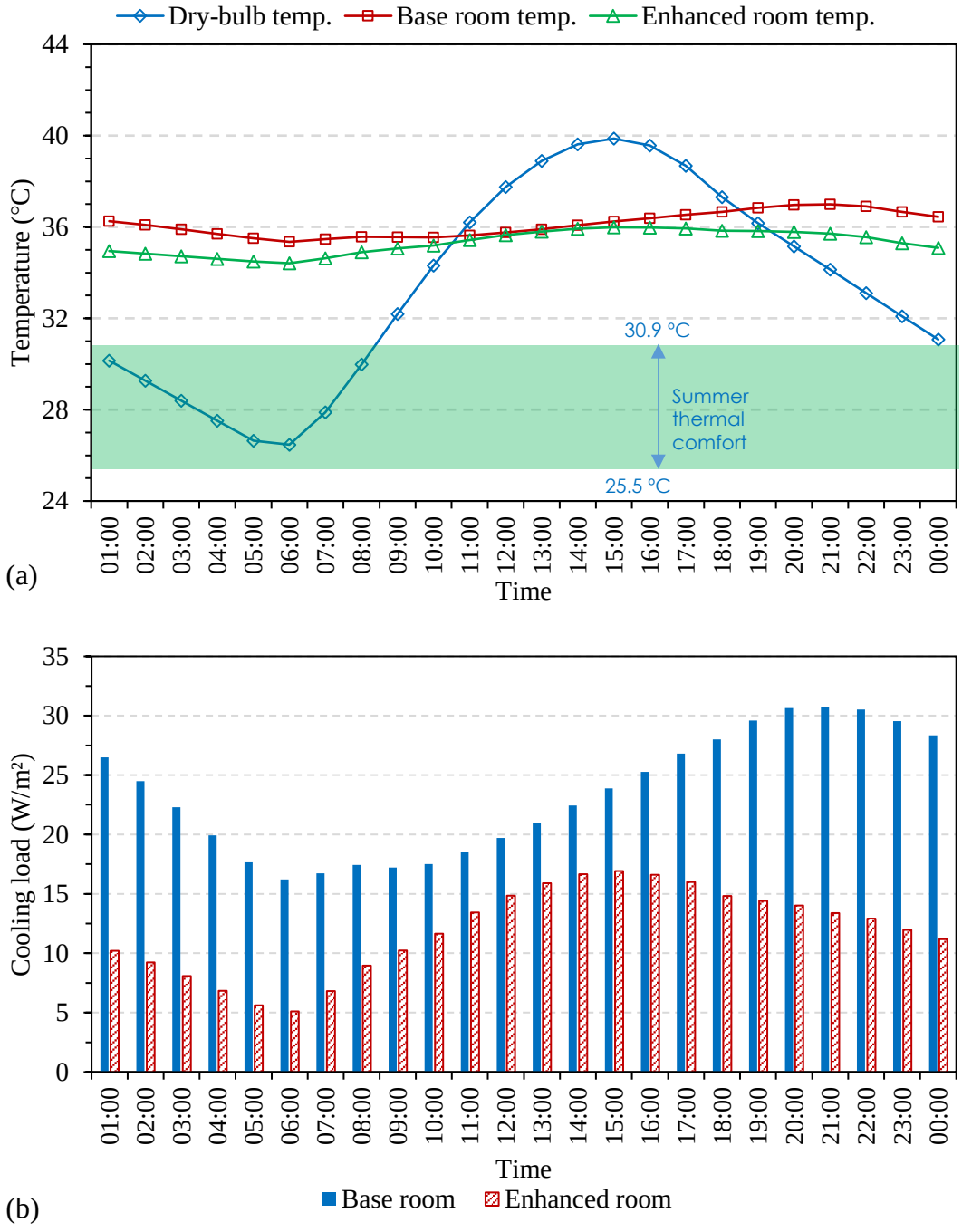


Figure 5.10: (a) Indoor air temperature and (b) cooling load of the selected room on a typical summer day.

5.3 Evaluation of nocturnal radiative cooling potential

This section investigates the potential of nocturnal radiative cooling in hot-arid climate. The proposed system is based on the use of a horizontal flat-plate metallic radiator with a fan-driven air flow which passes through channels between the radiator and the building roof. The climatic suitability is firstly discussed, and the system configuration is described. Detailed calculations are carried out using an Excel spreadsheet. The sensitivity of the model to a variety of geometrical and climatic parameters is investigated.

5.3.1 Applicability of radiative cooling in hot-arid climate

Radiative cooling depends primarily on the microclimate conditions. Cooling by radiative heat dissipation to the upper atmosphere is largely affected by the moisture content of the ambient air and the presence of clouds and is challenging to be harnessed under extreme conditions of these two factors (Givoni, 1994). However, this is not the case for some hot-arid regions, such as Khartoum city, which mostly features clear sky and relatively low dew point temperatures most of the year time. Khartoum climate is characterised by a dry season which extends for about nine months (October-June), and a rainy season which extends from July to September. The total annual rainfall is around 162 mm with the maximum of 75 mm recorded in August (Figure 5.11a). The dew point temperature is usually low, below 7 °C during the dry season and in the range 12-20 °C during autumn (Figure 5.11b). The cloud cover in Khartoum is generally low throughout the year, except during the autumn season. It is less than 22% in the range of clear sky conditions throughout the dry season, and in the range of 23-35% during the autumn season (Figure 5.11c).

In addition to the radiation heat loss to the sky, the coolness of the radiator also depends on the ambient wind speed. The convective heat gain at the radiator increases at high wind speeds leading to a low cooling efficiency. Figure 5.11d shows that Khartoum experiences an average wind speed of 3.9 m/s over the year. In the meteorological stations, wind speed is predominantly measured at the height of 10 m and is much lower within the urban context compared to open sites. In this study, the

wind speed at the height of the building roof was estimated based on the wind profile power law using equation (5.1) (Panofsky and Dutton, 1984);

$$u_z = u_{ref}\left(\frac{Z}{Z_{ref}}\right)^{\alpha} \quad (5.1)$$

where; u_z is the wind speed at a certain height Z, u_{ref} is the known wind speed at a reference height Z_{ref}, and α is the wind shear exponent, an empirically driven coefficient varying depending on the atmosphere stability. According to Panofsky and Dutton (1984), α approximately equals 0.143 for neutral stability conditions.

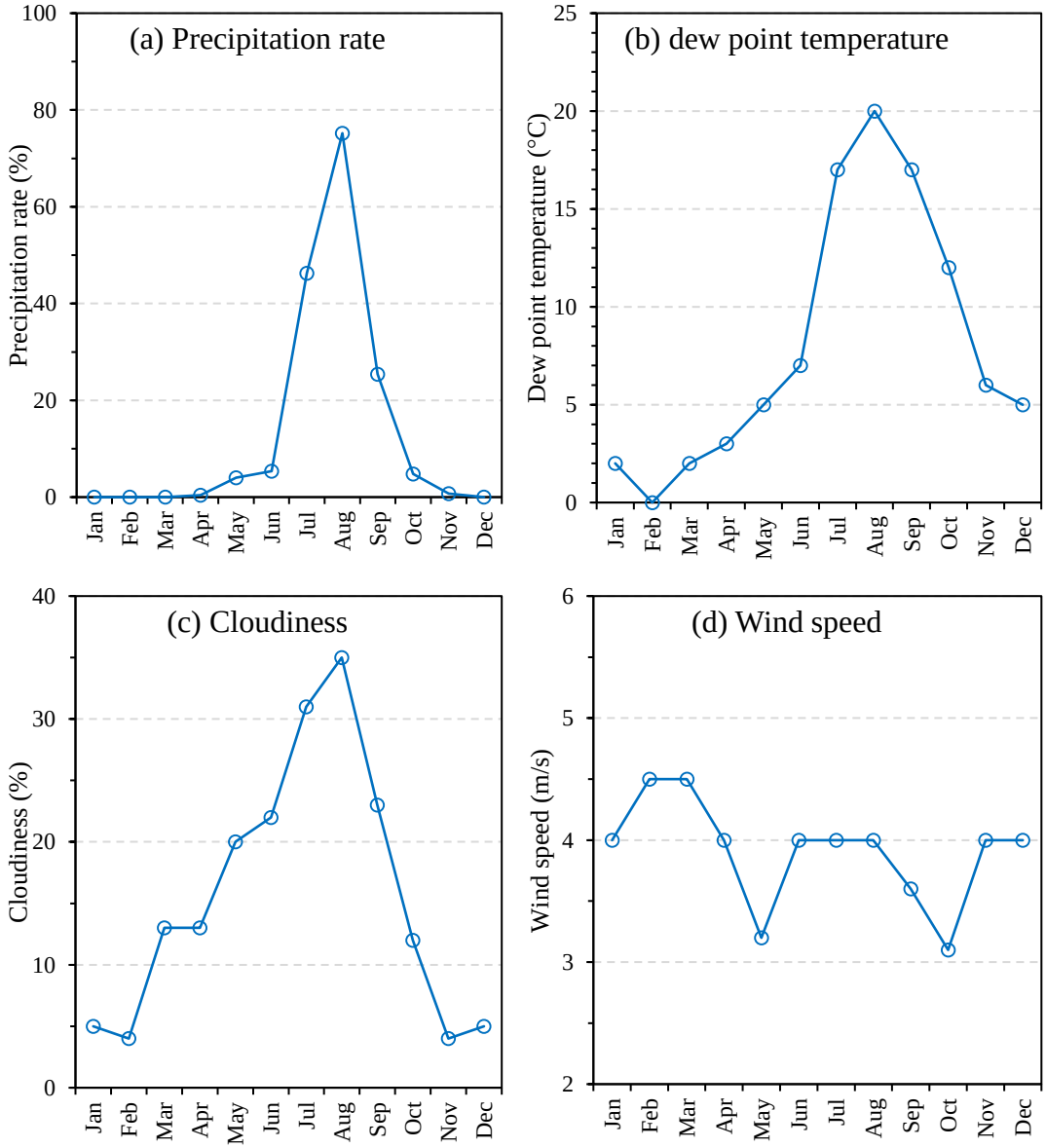


Figure 5.11: Monthly data of (a) precipitation rate, (b) dew point temperature (c) cloud cover percentage, and (d) wind speed in Khartoum.

Overall, the favourable cloud cover conditions and the low dew point temperature characterising the hot-arid regions, largely maximise the radiation heat loss from the horizontal surfaces on the ground, denoting the potential of harnessing the radiative cooling successfully. Yet, the prevailing wind speed indicates that convective gain from the ambient air is likely to reduce the system efficiency.

5.3.2 System description

The proposed radiative cooling system consists of a flat-plate galvanised steel radiator installed above the original roof of the building by a certain height. The radiator surface facing the sky has a glossy white paint to enhance the emissivity. Longitudinal steel purlins are installed beneath the radiator for air flow regulation and structural support of the radiator. A fan is used at the end of the air channels to suck the cooled air into the building interior. The configuration of the radiative cooling system is demonstrated in Figure 5.12. Details of a base case system design along with suggested operating conditions based on Khartoum climate are presented in Table 5.4.

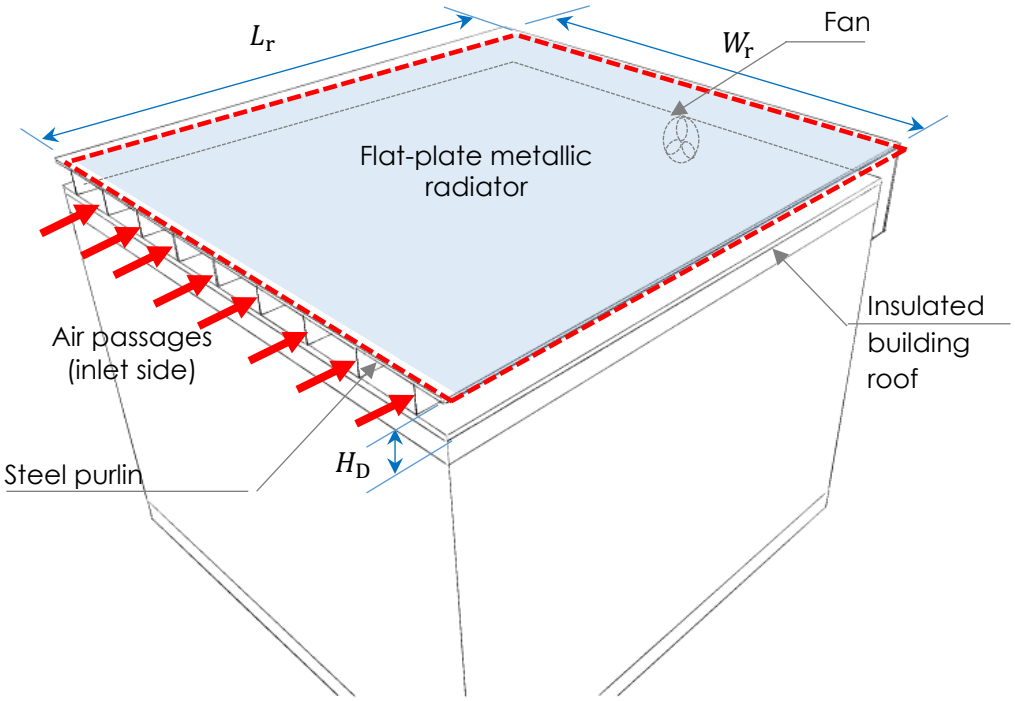


Figure 5.12: Geometrical configuration of the radiative cooling system.

Table 5.4: Details of the radiative cooling system design and operating conditions.

Base case model specifications		
Length of the radiator (L_r)	4.0 m	
Width of the radiator (W_r)	4.0 m	
Emissivity of the radiator (ε_r)	0.95 (Moss, 2002: p.70)	
Thickness of the radiator (d_r)	0.001 m	
Height of the duct (H_D)	0.04 m	
Air volumetric flow rate ($\dot{V}$)	50 L/s	
Climate parameters (Khartoum airport meteorological station)	**Hot summer**	**Moderate summer**
Ambient air temperature (T_{amb})	27 °C	22 °C
Wind speed at roof height (v)	3.0 m/s	3.8 m/s
Cloudiness index (0-10) (n)	2.1	1.3
Dew point temperature (T_{dp})	6 °C	2 °C

5.3.3 Modelling of the radiative cooling system

Detailed calculations for the nocturnal radiative cooling system is conducted. The proposed system is based on a roof integrated flat-plate metallic radiator and using the air as the HTF. The computation of the energy yielded by radiative cooling systems in any climate involves the following steps (Givoni, 1994);

- Assessing the nocturnal radiative cooling potential in the specific location by identifying the net long-wave radiation.
- Computing the stagnation temperature of the radiator surface, using energy balance analysis.
- Calculating the outlet air temperature from the system and determining the potential cooling transferred into the building interior.

The overall energy balance of an uncovered horizontal radiator involves both the radiation heat exchange with the sky and the convective heat exchange with the ambient air. When transferring the cooling produced by the radiative cooling to the building interior, convective gain to the radiator from the air flowing through the channels beneath the plate is taken into account. A schematic showing the heat transfer balance of the proposed radiative cooling system is presented in Figure 5.13.

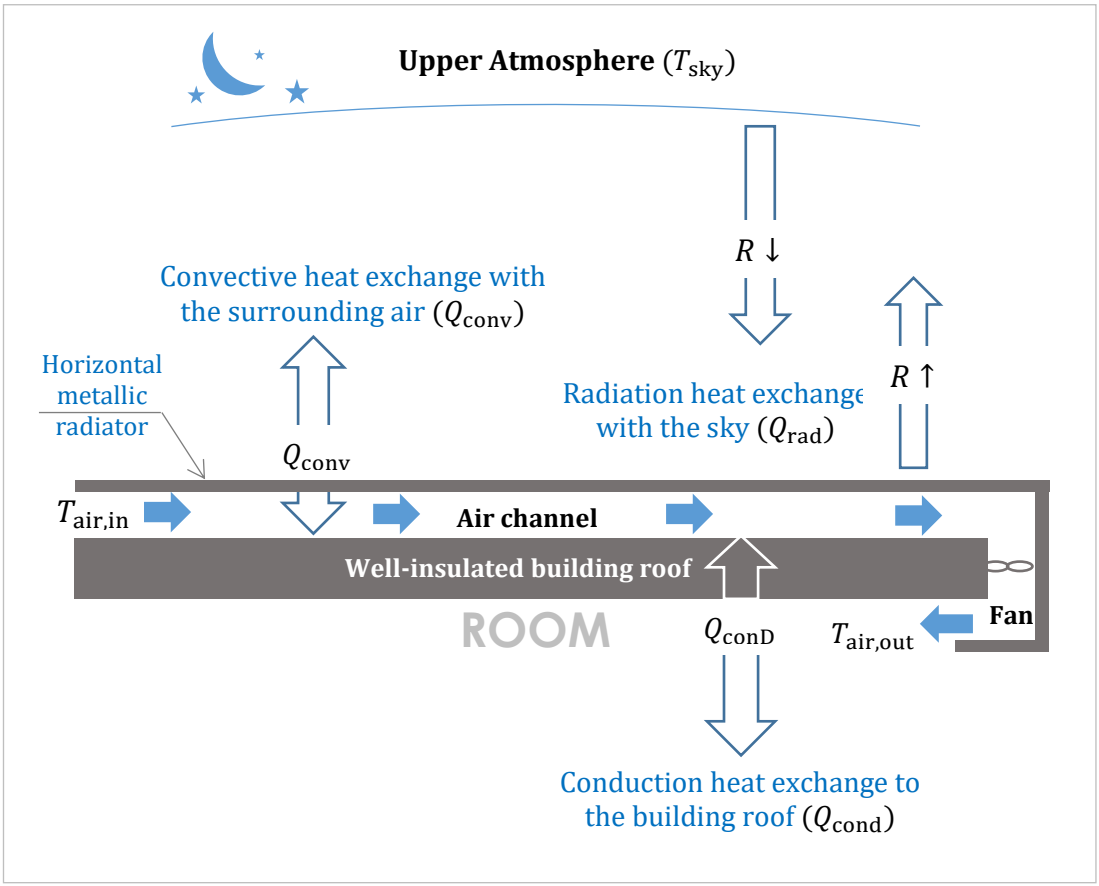


Figure 5.13: Heat transfer balance of the radiative cooling system.

The total cooling rate of a nocturnal radiator (Q_{total}) is estimated by balancing the net long-wave radiation heat exchange (Q_{rad}), the convective heat exchange (Q_{conv}), and the conduction heat exchange (Q_{cond}) using equation (5.2) (Incropera, 2011);

$$Q_{total} = Q_{rad} + Q_{conv} + Q_{cond} \quad (5.2)$$

The Q_{cond} could be neglected due to the thermal insulation of the roof. The roof should be well insulated to minimise cooling loss during the day time.

5.3.3.1 Radiation heat transfer

The correlation between the total radiation emitted by a black body and its absolute temperature is given by Stefan-Boltzmann law (Beckman and Duffie, 1980);

$$R° = \sigma T^4 \tag{5.3}$$

where; $R°$ is the total radiation energy in W/m², T is the absolute surface temperature in K, and σ is the Stefan-Boltzmann constant (5.67×10^{-8} W/m² K^4).

i. Outgoing long-wave radiation from the radiator surface ($R\uparrow$)

The intensity of long-wave radiation emitted toward the atmosphere ($R\uparrow$) is characterised by its emissivity (ε_r) as follows (Hanif et al., 2014);

$$R\uparrow = \varepsilon_r \sigma T_r^4 \tag{5.4}$$

where; T_r is the absolute temperature of the radiator surface.

ii. Incoming long-wave radiation from the atmosphere ($R\downarrow$)

The atmospheric input radiation ($R\downarrow$) can be expressed either based on the apparent sky temperature (T_{sky}) at a particular location and time, which is equivalent to a temperature of a black body that emits a similar amount of radiation to that emitted by the sky and received by an unobstructed horizontal surface on the ground, or, as a function of the effective sky emissivity (ε_{sky}) by assuming the sky having a temperature equals to the absolute dry bulb temperature near the ground (T_{amb}). Consequently, the formula of $R\downarrow$ can be written as follows (Clark and Allen, 1978, Santamouris, 2007:p.265-266);

$$R\downarrow = \sigma T_{sky}^4 = \sigma \varepsilon_{sky} T_{amb}^4 \tag{5.5}$$

In previous studies, the emissivity of the sky (ε_{sky}) was computed using different expressions based on the dew point temperature or dry bulb temperature, and these formulae are reported in (Panchabikesan et al., 2017b). In this model, the equation

(5.6) developed by Berdahl and Martin (1984) to express the emissivity of a clear sky ($\varepsilon_{\mathrm{c.sky}}$) as a function of dew point temperature (T_{dp}) is used.

$$\varepsilon_{\mathrm{c.sky}} = 0.711 + \left[0.56\left(\frac{T_{\mathrm{dp}}}{100}\right)\right] + \left[0.73\left(\frac{T_{\mathrm{dp}}}{100}\right)^{2}\right] \quad (5.6)$$

To account for the clouds effect, a cloudiness factor C_{n} was introduced by Clark (1981) based on the total opaque cloud amount (n) using equation (5.7). The value of n ranges between 0 for a clear sky and 10 for a fully overcast sky.

$$C_{\mathrm{n}} = 1 + (0.0224\, n) - (0.0035\, n^{2}) + (0.00028\, n^{3}) \quad (5.7)$$

Based on equations (5.5)-(5.7), the sky emissivity ($\varepsilon_{\mathrm{sky}}$) and sky temperature ($T_{\mathrm{sky}}$) can be written as follows (Beckman and Duffie, 1980, Clark and Allen, 1978);

$$\varepsilon_{\mathrm{sky}} = C_{\mathrm{n}}\, \varepsilon_{\mathrm{c.sky}} \quad (5.8)$$

$$T_{\mathrm{sky}} = (C_{\mathrm{n}} \varepsilon_{\mathrm{c.sky}})^{0.25} \times T_{\mathrm{amb}} \quad (5.9)$$

iii. **Net long-wave radiation heat transfer**

For an exposed radiator of an area A_{r} positioned horizontally on the ground facing the sky, the net long-wave radiation heat flux (Q_{rad}) can be expressed as the balance between the outgoing long-wave radiation from the radiator towards the atmosphere ($R\uparrow$), and the incoming long-wave radiation from the atmosphere ($R\downarrow$) as follows (Incropera, 2011);

$$Q_{\mathrm{rad}} = R\uparrow - R\downarrow = A_{\mathrm{r}}\, \varepsilon_{\mathrm{r}}\, \sigma\, (T_{\mathrm{r}}^{4} - T_{\mathrm{sky}}^{4}) \quad (5.10)$$

In the case of wind-screened radiators, equation (5.10) can be written as a function of windscreen infrared transmittance(τ) as follows;

$$Q_{\text{rad}} = A_{\text{r}}\, \varepsilon_{\text{r}} \tau\, \sigma\, (T_{\text{r}}^4 - T_{\text{sky}}^4) \quad (5.11)$$

where; τ is equal to 1 for an exposed radiator.

5.3.3.2 Convective heat transfer

i. Convective heat transfer coefficient of the external surface

The convective heat transfer (Q_{conv}) between a nocturnal radiator of a surface temperature T_{r} and the ambient air of a temperature T_{amb} is given by equation (5.12) (Kothandaraman, 2006:p.337, Incropera, 2011);

$$Q_{\text{conv}} = A_{\text{r}}\, h_{\text{A}} * (T_{\text{r}} - T_{\text{amb}}) \quad (5.12)$$

where; h_{A} is the convective heat transfer coefficient due to the wind. It is proportional to wind speed at a height similar to that of the radiator surface (v). According to Panchabikesan et al. (2017b), the formula of h_{A} has a general form of $h_{\text{A}} = a + b(v)$, or $h_{\text{A}} = a(v^b)$, where values of a and b are varied, as many formulations have been developed. In this study, a more general equation is used to estimate the value of h_{A} for a radiator without a windscreen as follows (Mostrel and Givoni, 1982, Givoni, 1994:p.92).

Exposed radiator $$h_{\text{A}} = 0.6 + 3.5 * (v)^{0.5} \quad (5.13)$$

To determine the convective heat transfer coefficient (h_{A}) for a radiator covered by a windscreen, equations (5.14) and (5.15) introduced by Mostrel and Givoni (1982) are used. These are based on extensive experimental studies for a single and a double layer of a polyethene windscreen, respectively.

Single layer $$h_{\text{A,sw}} = 0.5 + 1.2\, (v)^{0.5} \quad (5.14)$$

Double layer $$h_{\text{A,dw}} = 0.3 + 0.8\, (v)^{0.5} \quad (5.15)$$

ii. Convective heat transfer coefficient of the internal surface

The internal surface heat transfer coefficient depends mainly on the design details of the ducting system and the characteristics of the air flow. As a fan is used to draw the air, the forced convection is correlated to the Reynolds number (Re), where laminar and turbulent flow regimes depend upon its magnitude. The Reynolds number (Re) is calculated using equation (5.16) (Schlichting and Gersten, 2016);

$$Re = \frac{u\,D}{\gamma} \tag{5.16}$$

where; u is the velocity of fluid calculated using equation (5.17) based on the volume air flow rate ($\dot{V}$), D is the characteristic linear dimension of the duct, and γ is the kinematic viscosity of the fluid. For a forced convection, the flow regime is considered laminar if $Re < 2100$, transitional if $2100 < Re < 4000$, and turbulent if $Re > 4000$ (Schlichting and Gersten, 2016). According to Fox et al. (1985), for a fluid flowing in a wider duct such as in the present case, where its width (W_r) is much greater than its height (H_D) with an aspect ratio ($ar = H_\mathrm{D}/W_\mathrm{r}$) not remain in the range $0.25 < ar < 4.0$, the characteristic dimension (D) is equal to the distance between the two parallel surfaces, i.e. height of the duct (H_D).

$$u = \frac{\dot{V}}{(W_\mathrm{r} \times H_\mathrm{D})} \tag{5.17}$$

In this study, the flow regime is considered laminar as the calculated Reynolds number (Re) for the range of the investigated air flow rates (0-130 L/s) are lower than 2100.

The internal surface heat transfer coefficient (h_ci) is determined based on the Nusselt number (Nu), characteristic length (D), and the thermal conductivity of the HTF (λ_fluid) using equation (5.18) (Moss, 2002):

$$h_\mathrm{Ci} = (Nu) \times \frac{\lambda_\mathrm{fluid}}{D} \tag{5.18}$$

The Nusselt number (Nu) for a laminar flow is given by equation (5.19) (Moss, 2002);

$$(Nu) = 3.66 + \left(\frac{0.065 \times (Re) \times (Pr) \times \frac{H_D}{L_r}}{1 + 0.04 \left((Re) \times (Pr) \times \frac{H_D}{L_r} \right)^{2/3}} \right) \quad (5.19)$$

where; H_D/L_r is the ratio of the duct height to its length, and Pr is the Prandtl number.

5.3.3.3 Analysis of the system performance

The parameters used to assess the thermal performance of the system are:

i. Stagnation temperature of the radiator

The formula for the overall external heat flux (convective and radiative) between a nocturnal radiator and the ambient (air and sky) can be written as a function of the stagnation temperature (T_{st}), that is the minimum stabilised temperature achieved by the radiator after the heat loss and gain reach the equilibrium as follows (Asimakopoulos, 2013: p.437);

$$Q_{rad} = h_{Ce} * (T_{amb} - T_{st}) \quad (5.20)$$

Thus, the formula for stagnation temperature (T_{st}) can be written as;

$$T_{st} = T_{amb} - \left(\frac{Q_{rad}}{h_{Ce}} \right) = T_{amb} - \left(\frac{\varepsilon_r \tau \sigma (T_{amb}^4 - T_{sky}^4)}{h_{Ce}} \right) \quad (5.21)$$

where; h_{Ce} is the effective or the top heat transfer coefficient calculated as a sum of the convective coefficient of the external surface due to wind (h_A) and the radiative heat transfer coefficient (h_R) by equation (5.22) (Santamouris, 2007: p.268, Mihalakakou and Bagiorgas, 2013);

$$h_{Ce} = h_A + h_R = h_A + (4\, \varepsilon_r\, \tau\, \sigma\, T_{amb}^3) \quad (5.22)$$

ii. Outlet air temperature from the system

The resultant outlet air temperature ($T_{\mathrm{air,out}}$) of the air flowing through a one-dimensional path below the nocturnal radiator is solved based on the characteristic length of the radiator (L_{r}) using equation (5.23) that introduced by Beckman and Duffie (1980) and Ito and Miura (1989).

$$T_{\mathrm{air,out}}\,(L_{\mathrm{r}}) = T_{\mathrm{st}} + \left(T_{\mathrm{air,in}} - T_{\mathrm{st}}\right) \times \exp\left\{\frac{-(UL_{\mathrm{r}}W_{\mathrm{r}})}{\dot{m}\,Cp_{\mathrm{air}}}\right\} \qquad (5.23)$$

where; $T_{\mathrm{air,in}}$ is the inlet air temperature equal to T_{amb} in the present case, W_{r} is the width of the radiator, Cp_{air} is the specific heat of the air, $\dot{m}$ is the air mass flow rate, and U is the overall heat transfer coefficient of the air passing below the radiator and the ambient air. Several equations have been developed to calculate the U value. In this computation, a formula used for a flat-plate heat exchanger is used as follows;

$$U = \frac{1}{\frac{1}{h_{\mathrm{Ce}}} + \frac{1}{h_{\mathrm{Ci}}} + \frac{d_{\mathrm{r}}}{\lambda_{\mathrm{r}}}} \qquad (5.24)$$

where; d_{r} and λ_{r} are the thickness and the thermal conductivity of the radiator, respectively, h_{Ci} and h_{Ce} are the internal and the effective heat transfer coefficients computed using equations (5.18) and (5.22), respectively.

iii. Cooling transferred into the building

The instantaneous cooling rate transferred by the air (Q_{air}) to the building interior is proportional to the temperature difference between the inlet air ($T_{\mathrm{air,in}}$) and the outlet air from the channel ($T_{\mathrm{air,out}}$), the air mass flow rate ($\dot{m}$), and the specific heat of the air (Cp_{air}) by the following formula;

$$Q_{\mathrm{air}} = \dot{m}\,Cp_{\mathrm{air}}\left(T_{\mathrm{air,in}} - T_{\mathrm{air,out}}\right) \qquad (5.25)$$

5.3.4 Results and discussion of the radiative cooling system

Using the base case specifications given in Table 5.4 and the described equations, the sensitivity of radiative cooling performance to a variety of affecting parameters is discussed. These parameters are divided into those relevant to the system design and others relevant to the climate conditions. The thermal performance of the system in typical hot and moderate summer conditions of the study location is also discussed.

5.3.4.1 Influence of system design parameters

The most crucial factors that can be controlled in radiative cooling systems design are; radiator emissivity, height of the radiator above the building roof (duct height), and air flow rate. For each of these factors, the potential cooling rate and the outlet air temperature are discussed based on the system specifications presented in Table 5.4.

i. Impact of radiator emissivity (ε_r)

Figure 5.14 shows that the radiative heat transfer depends largely upon the radiator emissivity. High-emissivity surfaces generate high cooling rates while low-emissivity surfaces stay warmer. Under current design and operating conditions, the useful cooling transferred into the building interior by the high emissivity radiators is far lower by almost 90% than the radiation energy produced, due to the convection gain.

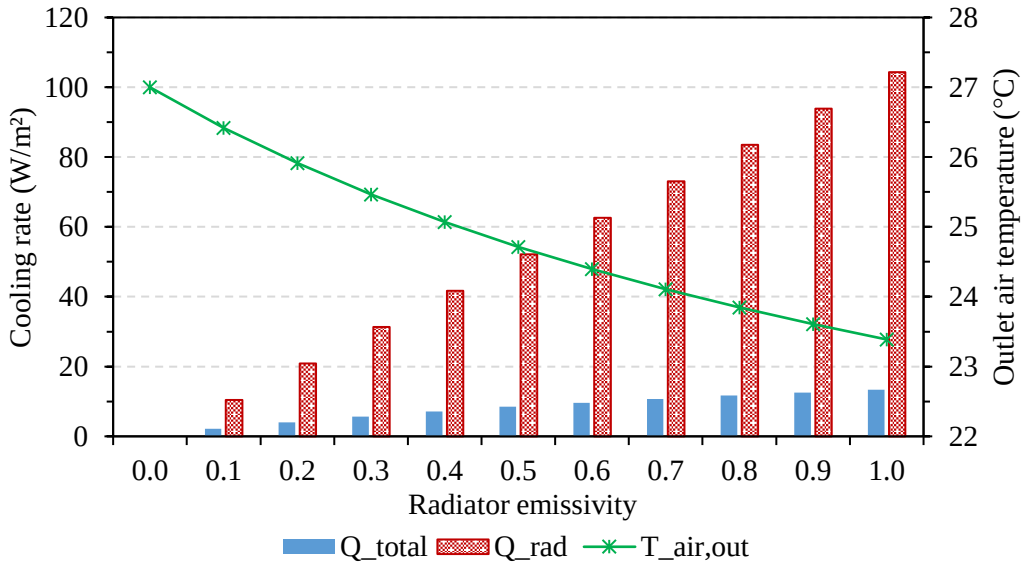


Figure 5.14: Variation of the cooling rate per unit area and the outlet air temperature with the radiator emissivity.

In addition to the high emissivity, radiators with high reflectivity to the shortwave solar radiation should be used in order to lessen the heat gain through the building roof during the daytime. If a radiator is used as a solar collector, the effect of absorptivity must be taken into account, but this may jeopardise the radiative cooling quality. For this study, a metallic radiator painted glossy white is used (emissivity of 0.95) to get the most out of the night radiative cooling, besides reflecting the daytime solar spectrum.

ii. Impact of air flow rate ($\dot{V}$)

The radiative cooling system performance was examined under air flow rates of 10-130 L/s as shown in Figure 5.15. The associated Reynolds numbers for the considered range of air flow rates are between 158 and 2062, which are in the range of a laminar flow. It is clear from Figure 5.15 that the air flow rate has a dominant impact on the cooling rate transfered into the building interior. The cooling rate increases and the outlet air temperature drop decreases with the air flow rate enhancement. The cooling rate increases sharply at low air flow rates up to 50 L/s and nearly stabilises at air flow rates beyond 110 L/s. Therefore, the air flow rate could be appropriately modulated based on the design objectives, whether the cold air is directly used to provide instantaneous cooling with the velocity and temperature of the air set at the thermal comfort level, or to store the cooling for later use, or for both functions at a time.

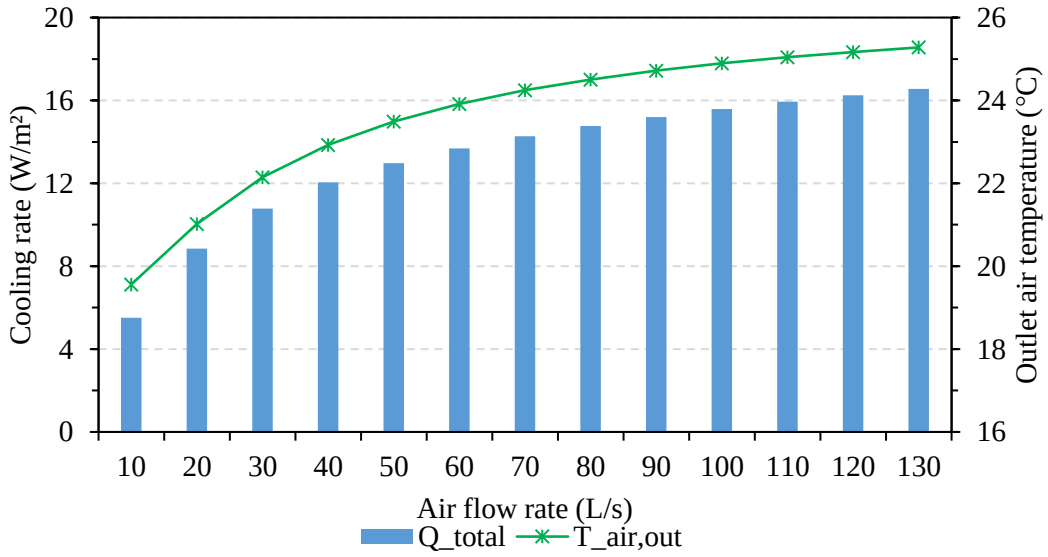


Figure 5.15: Variation of the cooling rate per unit area and the outlet air temperature with the air flow rate.

iii. Impact of air duct height (H_D)

For a duct of a wide width used in this study, the most influential factor is the duct height. Figure 5.16 exemplifies how the height of the air passage between the building roof and the radiator surface influences the radiative cooling rate. It is evident that, the higher the duct height, the lower the cooling rate and vice versa. The cooling rate is highly sensitive to air ducts of small heights in the range of 0.01–0.04 m and the impact is less at duct heights above 0.13 m.

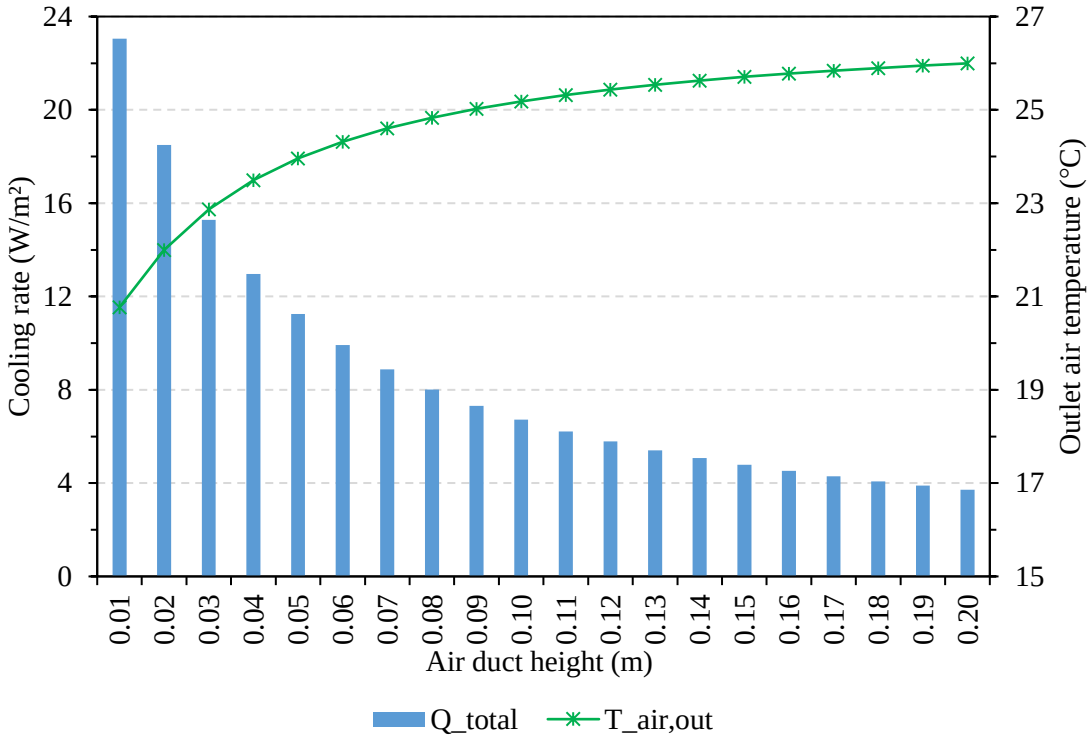


Figure 5.16: Variation of the cooling rate per unit area and the outlet air temperature with the air duct height.

5.3.4.2 Influence of climate conditions parameters

The main climatic parameters affecting the radiative cooling performance considered in the present model are; cloudiness, wind speed, and dew point temperature.

i. Impact of cloudiness

Figure 5.17 shows the radiative cooling performance under a range of cloud coverage from a completely clear sky (0) to a full cloud cover (10). It is clear that the maximum cooling rate is attained in the absence of clouds where the downward radiation is very low. Otherwise, the system performance deteriorates with the clouds accumulation due to the emissivity increase. Under clear sky conditions (cloud cover below 20%), the sky temperature in hot-arid regions could be lower by nearly 16.5-22 K than the ambient air temperature of 27 °C. This indicates that the cooling capacity by heat dissipation to the sky in the considered location is enormous, owing to the clear sky condition for around nine months a year.

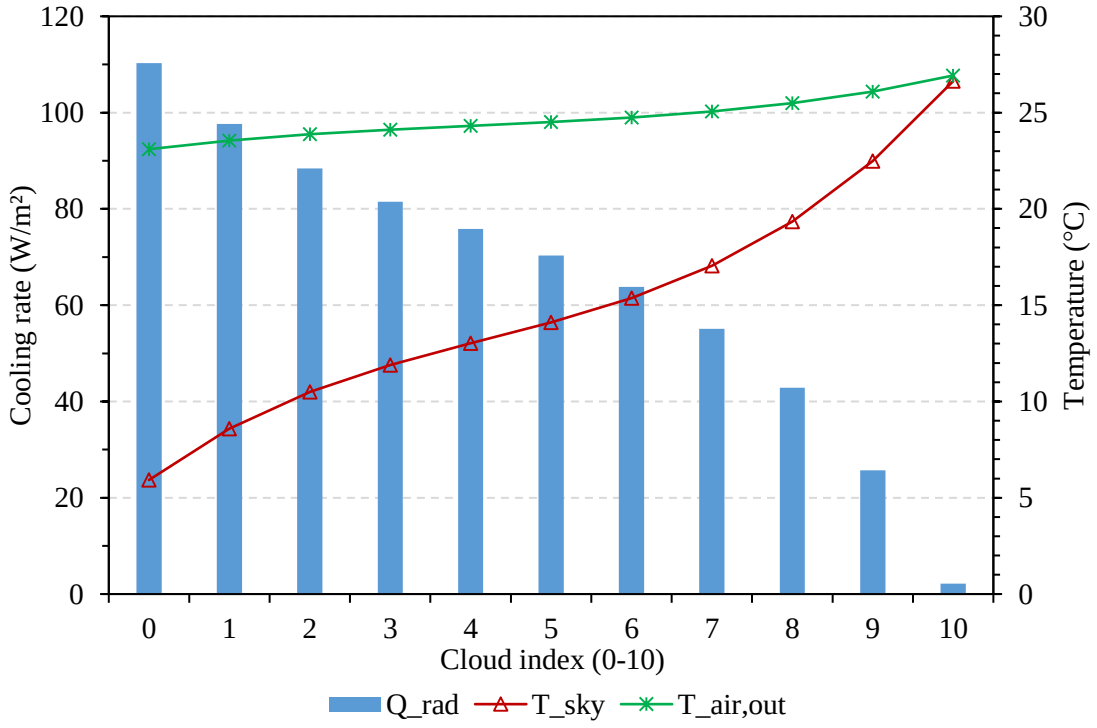


Figure 5.17: Variation of the radiative cooling rate per unit area, the sky temperature, and the outlet air temperature with the cloudiness factor.

ii. Impact of wind speed

An exposed horizontal metallic radiator with a high emissivity surface is always cooler than the ambient air due to the radiation heat exchange with the sky. However, the radiator gains heat by convection from the ambient air, and hence its cooling rate reduces. Figure 5.18 shows that the radiative cooling systems performance is profoundly affected by the wind. The stagnant temperature of the radiator rises with the wind speed as a result of heat transfer coefficient increase, i.e. the cooling rate is higher in the case of the still air or low air speeds. In the current case, the cooling rate is predicted to be independent of wind at velocities approximately beyond 5.5 m/s. An increase in ambient air velocity from 0.5 m/s to 5.0 m/s could lead to a 40% reduction in the cooling rate.

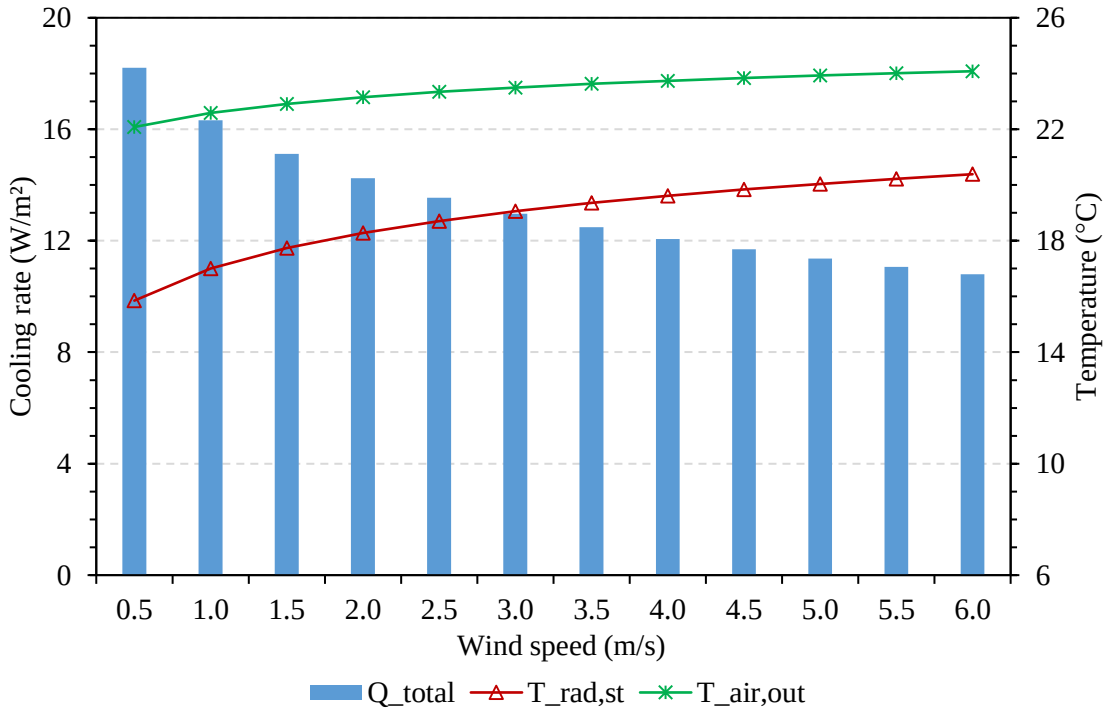


Figure 5.18: Variation of the cooling rate per unit area, the radiator stagnation temperature, and the outlet air temperature with the wind speed.

Moreover, application of a windscreen on the top surface of a radiator is one of the methods used to reduce the convective gain from the ambient without much affecting the radiation heat loss. A polyethylene film, lightweight and inexpensive material, has been widely tested and applied. The radiative properties of polyethylene film have

been measured by Clark and Blanpied (1979) under different climatic conditions, and it was found having a transmissivity of 0.75, a reflectivity of 0.10 and an emissivity of 0.15. Although the windscreen reduces 25% of the long-wave emission, the drop in the convective gain from the ambient air is much greater, leading to a higher temperature drop in the screened radiator compared to an exposed radiator.

Figure 5.19 compares the temperature of an exposed radiator to that of radiators covered with single and double windscreens for a range of wind speeds. It is clear that the application of windscreen to enhance the system cooling rate is greater at high wind speeds compared to low wind speeds. For instance, a single and a double screen radiators have a temperature drop greater by nearly 42% and 52% at high wind speeds (6.0 m/s) and around 15% and 19% only at low wind speeds (0.5 m/s), respectively, than that obtained by an exposed radiator. The performance variation of a single and a double layer windscreen is small, as the higher convective gain obtained by a double layer windscreen overweight the radiation loss. Overall, the usage of windscreens has a positive impact on the system performance, especially in the windy sites. The condensation and dust accumulation are the major obstacles which lessen the radiative cooling system efficiency.

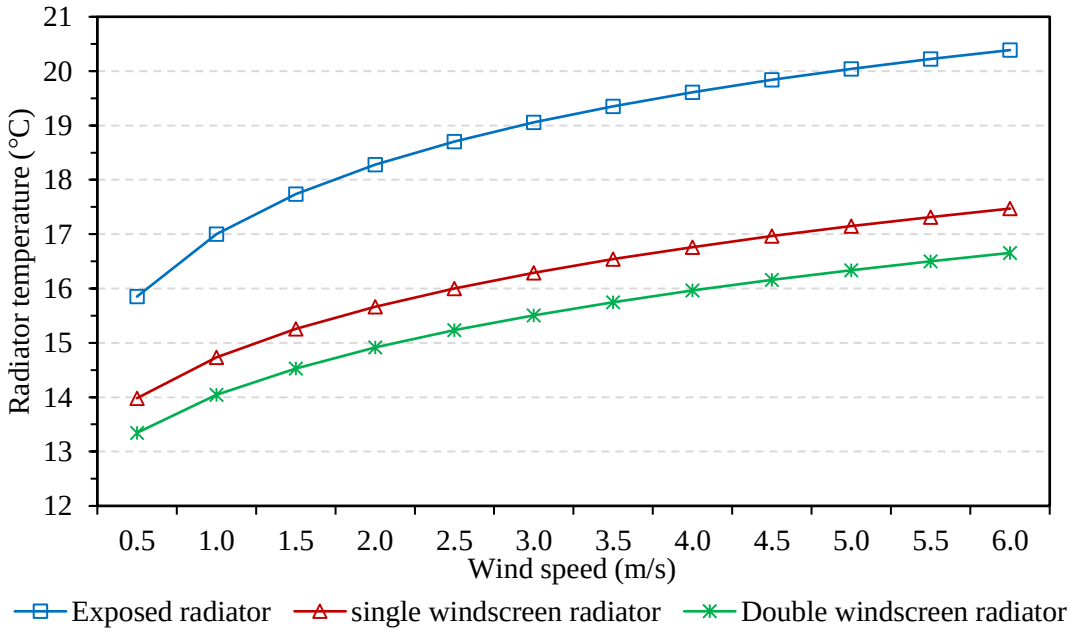


Figure 5.19: Stagnation temperature of the radiator with and without windscreen for different wind speeds.

iii. Impact of dew point temperature

The dew point temperature has a direct impact on the sky emissivity. Figure 5.20 shows how the dew point temperature affects the radiative cooling potential. It is clear that the radiative cooling rate lessens with the dew point temperature rise, as the sky emissivity and temperature rise accordingly. The sky temperature drop below the ambient air temperature reaches the maximum at the lowest dew point temperature. This indicates a great potential to take advantage of radiative cooling in dry locations.

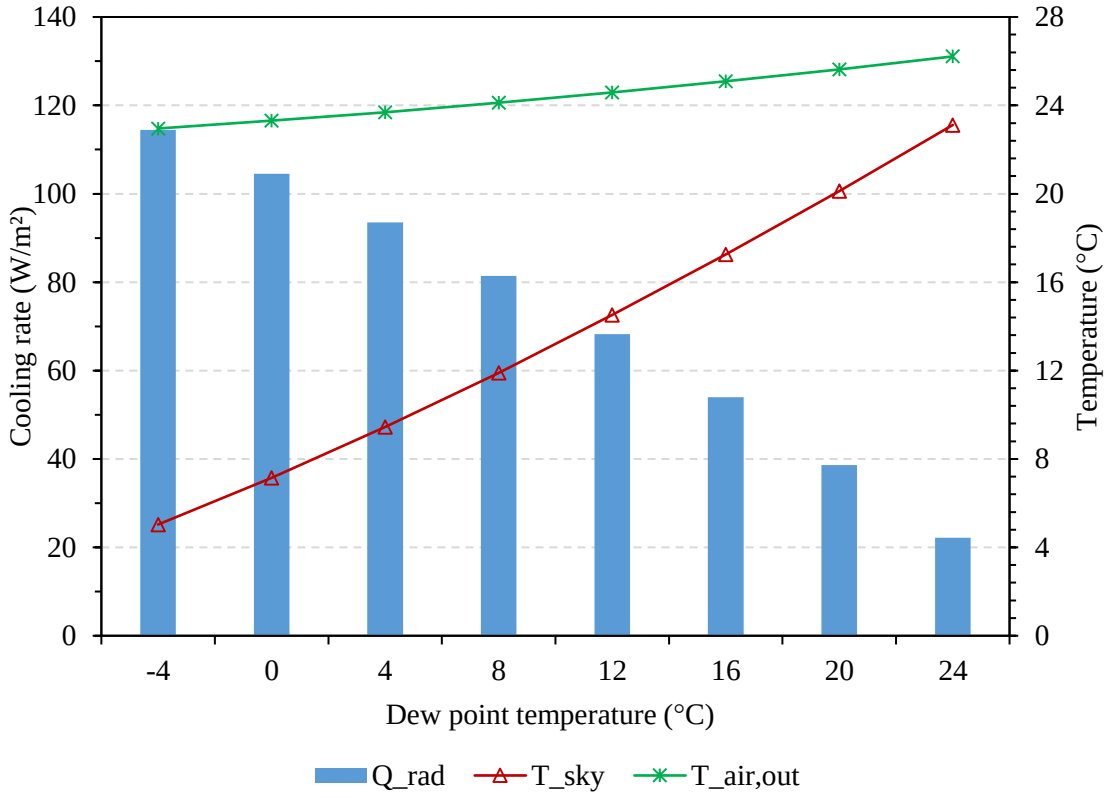


Figure 5.20: Variation of the radiative cooling rate per unit area, the sky temperature, and the outlet air temperature with the dew point temperature.

5.3.4.3 Operational performance under summer conditions

Based on the above discussion of the design and climatic parameters affecting the radiative cooling rate, an optimum system design has been proposed to get the most out of the radiative cooling strategy in hot-arid climates. The optimised system comprises a flat-plate galvanised steel radiator painted glossy white (emissivity 0.95), covered by a single layer polyethylene film windscreen (for convective gain reduction), and placed over the roof creating an air passage 0.04 m height.

The operational performance of the optimised system has been investigated under summer conditions of Khartoum where the night-time extends for around 11 hours. Figure 5.21 demonstrates the potential reduction in ambient air temperature by the radiative cooling operation at air flow rates 30, 50 and 70 L/s. It is evident that a significant temperature drop by around 3.1-5.6 K and 3.4-6.1 K below the ambient air could be realised using a screened radiator in the hot and moderate summer days, respectively, with the lower air flow rate allowing higher temperature drop. For the same air flow rate, more temperature drop could be achieved in the moderate summer months compared to the hot summer months due to the lower dew point temperature.

During the hottest months (May-June), if the air cooled by the radiative cooling system has been passed through the PCM storage before being admitted into the room, it will become warm, and its suitability for instantaneous cooling depends upon the air flow rate. It should also be stressed that low air flow rates are recommended during night periods of high ambient temperatures to obtain low outlet temperatures capable of initiating the PCM charging process at the earliest possible time. On the other hand, maximum air flow rates could be used during night periods of low ambient temperatures to accelerate the PCM charging process. The average temperatures drop, and the daily cooling rates obtained under the investigated conditions are presented in Table 5.5.

Furthermore, in order to explore the potential enhancement in the PCM charging process as a result of the radiative cooling system use, air having variable temperatures as shown in Figure 5.21 has been used to release the heat from the PCM modules in the charging experiments. The experimental results under different operating scenarios have been presented and discussed in Chapter 8.

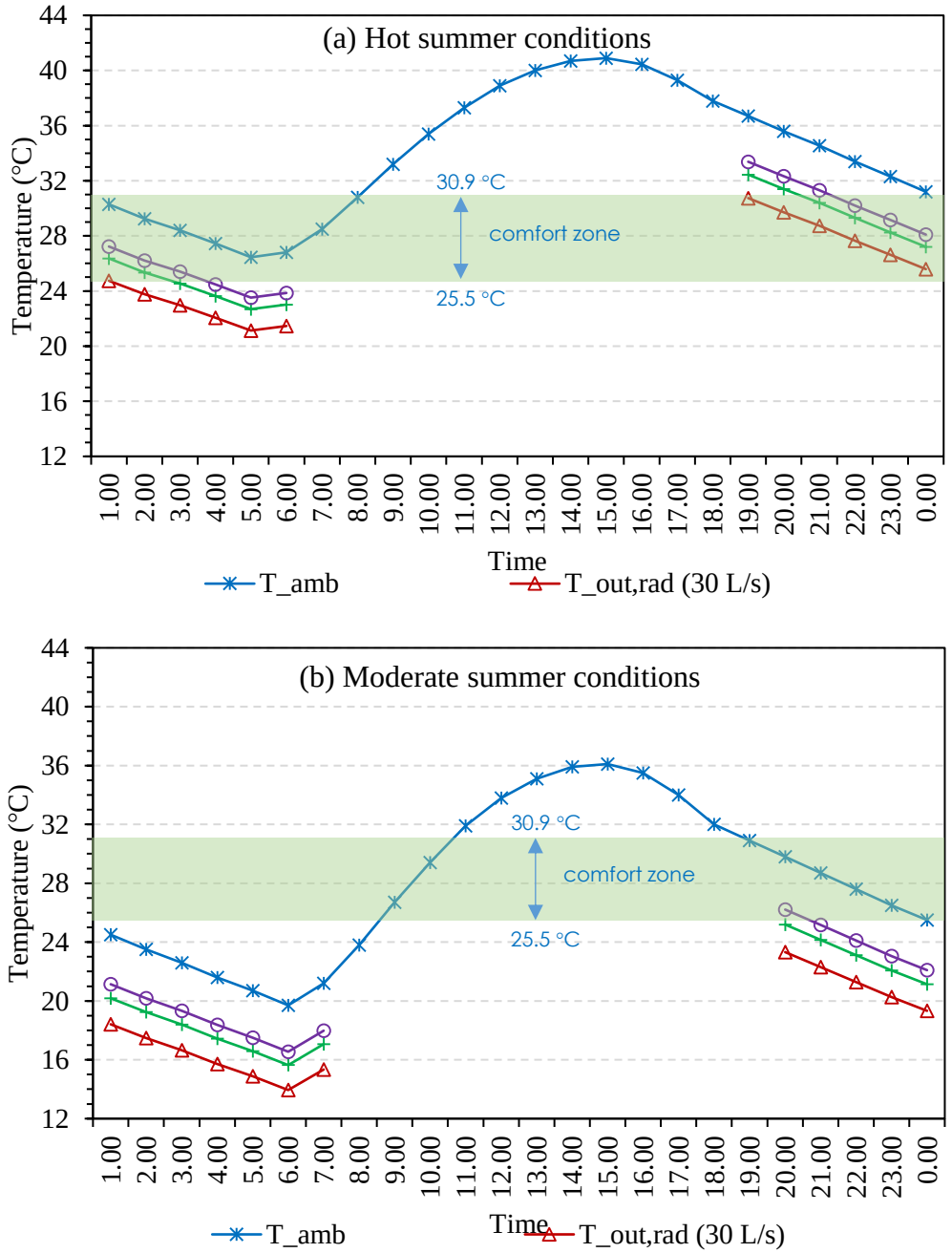


Figure 5.21: The hourly profile of the air temperature drop by the proposed radiative cooling system during summer in Khartoum.

Table 5.5: Air temperature drop and cooling rate obtained by radiative cooling in summer.

	Avg. temperature drop (K)			**Cooling rate (Wh/m² per day)**		
	30 L/s	**50 L/s**	**70 L/s**	**30 L/s**	**50 L/s**	**70 L/s**
Hot summer	5.6	4.0	3.1	135.4	160.4	174.9
Moderate summer	6.1	4.3	3.4	150.3	177.3	193.1

5.4 Summary

Regarding the free cooling, the discussion of the thermal comfort, climate conditions, and building cooling load indicates the possibility of harnessing the free cooling for long duration throughout the overheated period in the considered location of hot-arid climate. Free cooling systems incorporating PCM energy storage are capable of working successfully under moderate summer conditions and less effective during the hot summer conditions as a result of high ambient air temperatures at night.

Regarding the radiative cooling, the favourable climate conditions of clear sky and low dew point temperature most of the year in hot-arid locations such as Khartoum indicates a high potential to get the most out of this cooling strategy. However, the effect of high wind speeds, which may reduce the efficiency of the system, should be carefully addressed. The performance could be improved by considering a high emissivity radiator, low air flow rates, and a narrow air flow channel. Therefore, an optimised system design has been proposed using a metallic radiator painted glossy white (emissivity of 0.95), covered by a single layer polyethylene film to reduce the convective gain from the ambient air, and using a practical duct height of 0.04 m. Under typical summer conditions of Khartoum, an air temperature drop by around 3-6 K below the ambient air temperature could be obtained at air flow rates 30-70 L/s. The radiative cooling potential could be enhanced through the use of selective radiative surfaces.

Chapter 6

CFD Modelling of the PCM-Air Heat Exchanger

6.1 Introduction

This chapter assesses the thermal performance of the proposed PCM-air heat exchanger for cooling of buildings through a transient CFD modelling using ANSYS Fluent. The PCM selection, sizing of the TES unit, and the physical model are initially described, and the computational methodology is detailed. The numerical model was used to carry out a parametric study on the operating conditions and the geometrical configuration of the TES unit. The results have been presented and discussed for both transformation phases.

6.2 PCM selection

The selection of PCMs to meet buildings cooling and heating requirements has been widely considered in the literature (Arkar and Medved, 2007). For building cooling and heating in any location, the desirable PCM should possess certain thermo-physical and chemical properties and economic merits. However, a suitable phase change temperature in the desired operating range and a high enthalpy of fusion are the most significant parameters when selecting a PCM for a particular application (Soares et al., 2013, SOCACIU et al., 2014). However, due to the large seasonal variation predicted in most locations, it is difficult to find a PCM suiting the whole year requirements. It is also difficult to identify a substance that satisfies all the selection criteria to operate as superior thermal storage. In addition to the aforementioned general properties, the PCM for free cooling of buildings in hot-arid climate was selected so;

- The PCM transition temperature suits the diurnal temperature variation of the summer period when the maximum cooling demand exists.
- The outlet air temperature from the system should be within the comfort zone (25.5-30 °C) during the discharging time, and in the same way, allowing rapid PCM solidification during the charging time (Yanbing et al., 2003, Arkar et al., 2007). Thus, a transition temperature close to the upper band of the comfort zone is recommended to expand the charging duration, as hot-arid regions usually feature relatively warm ambient temperatures during summer nights.
- The maximum air temperature should be below the PCM operating temperature. This is usually the case for many kinds of paraffin and salt hydrate PCMs which have a low temperature range between 40 °C and 60 °C. This issue should be considered carefully, specifically during the discharging phase to avoid any unexpected damage to the PCM or inefficient performance.

According to the aforesaid guidelines, several commercial PCM candidates including; RT28HC, SP29Eu (Rubitherm), A28, A29, S27, E27 (EPS), ClimSel C28 (Climator),

TM29T (TEAP), and HC 29 (PLUSS) seem to be the most appropriate for free cooling applications in hot-arid climates, as shown in Table 3.5.

For the present study, a commercial paraffin RT28HC with a transition temperature of 27-29 °C produced by Rubitherm has been selected. It possesses the highest enthalpy of fusion which leads to a minimum usage of PCM mass, besides having the common characteristics of paraffin substances such as congruent melting and non-corrosiveness. Thermo-physical properties of the selected PCM are presented in Table 6.1, and the enthalpy-temperature graph is shown in Figure 6.1.

Table 6.1: Thermo-physical properties of the RT28HC PCM (RUBITHERM).

Property	**Value**
Phase change temperature	27-29 °C
Heat storage capacity (latent+sensible heat between 21 °C and 36 °C)	250 kJ/kg ± 7.5%
Specific heat (both phases)	2 kJ/kg K
Thermal conductivity (both phases)	0.2 W/m K
Density (solid at 15 °C)	880 kg/m³
Density (liquid at 40 °C)	770 kg/m³
Maximum operating temperature	50 °C

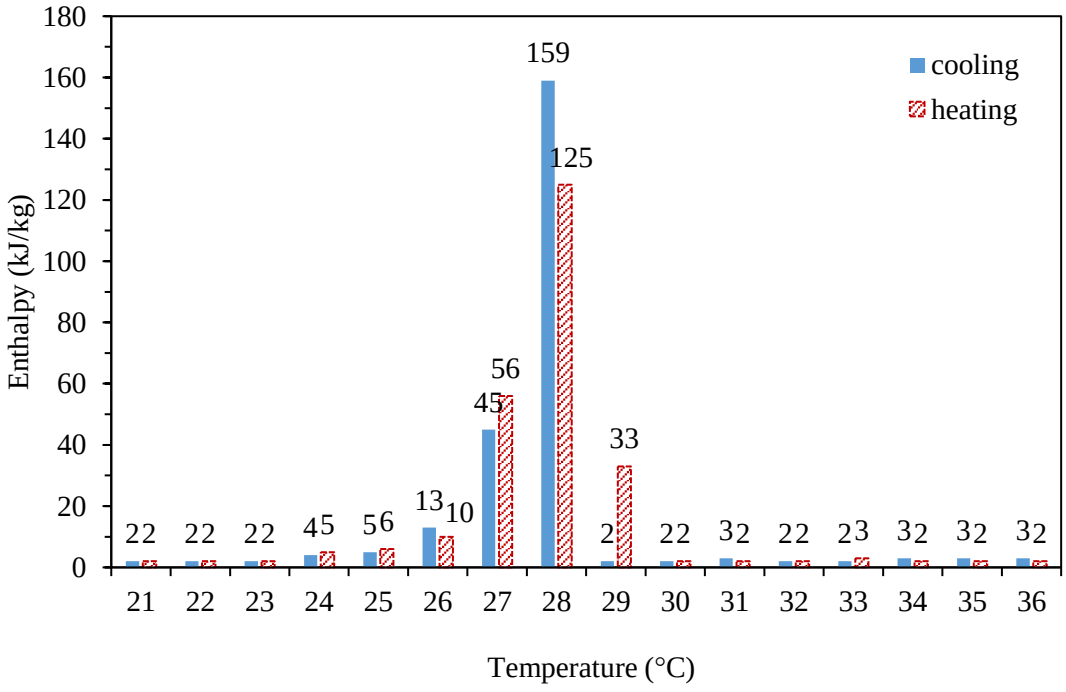


Figure 6.1: Enthalpy-Temperature curve of the RT28HC PCM (RUBITHERM).

6.3 Sizing of the TES unit

Sizing of the TES configuration was based on the PCM specifications and the building cooling load. The system was designed to serve a thermally enhanced single room (16 m²) with insulated roof and walls in domestic buildings in hot-arid climate. The room (south-west) with an average cooling load among the other rooms on the first floor of the investigated building was selected (Figure 5.9). The capacity of the TES system was estimated to meet the overall cooling load of an average day of the peak summer months in Khartoum (May and June).

Figure 6.2a and Figure 6.2b demonstrate the indoor air temperature variation and the hourly cooling load of the adopted room on a typical summer day, respectively. It is evident that the ambient air temperature is below the PCM liquidus temperature for around five hours (3:00-8:00 am), which is the available time for the PCM charging (Figure 6.2a). According to Figure 6.2b, a TES unit with a cooling capacity of 286 W/m² is required to meet the daily cooling demand of the room. The required weight of the PCM was obtained using equation (6.1), and around 4.1 kg/m² was found sufficient.

$$\text{Required PCM weight (kg)} = \frac{\text{Total cooling load of the discharging hours (Wh)}}{\text{PCM heat storage capacity (Wh/kg)}} \qquad (6.1)$$

Since air is the heat transfer fluid, the surface convective heat transfer coefficient will be very low. Thus, enlarging the surface area per unit volume of the PCM heat exchanger is beneficial to enhance the convective heat flux. Therefore, the flat-plate module configuration was selected. A container module with overall dimensions 1.80 m (L) × 0.60 m (W) × 0.01 m (H) has been suggested, so it suits the installation at the walls and ceiling space of a standard room. About 8 PCM modules were found sufficient to accommodate the required PCM weight and are capable to fulfil a cooling rate of 4.6 kWh based on equation (6.2). Aluminium could be used for the encapsulation due to its high thermal conductivity (202.4 W/m K).

$$\text{TES cooling capacity (kWh)} = \text{PCM weight (kg)} \times \text{PCM enthalpy (kWh/kg)} \qquad (6.2)$$

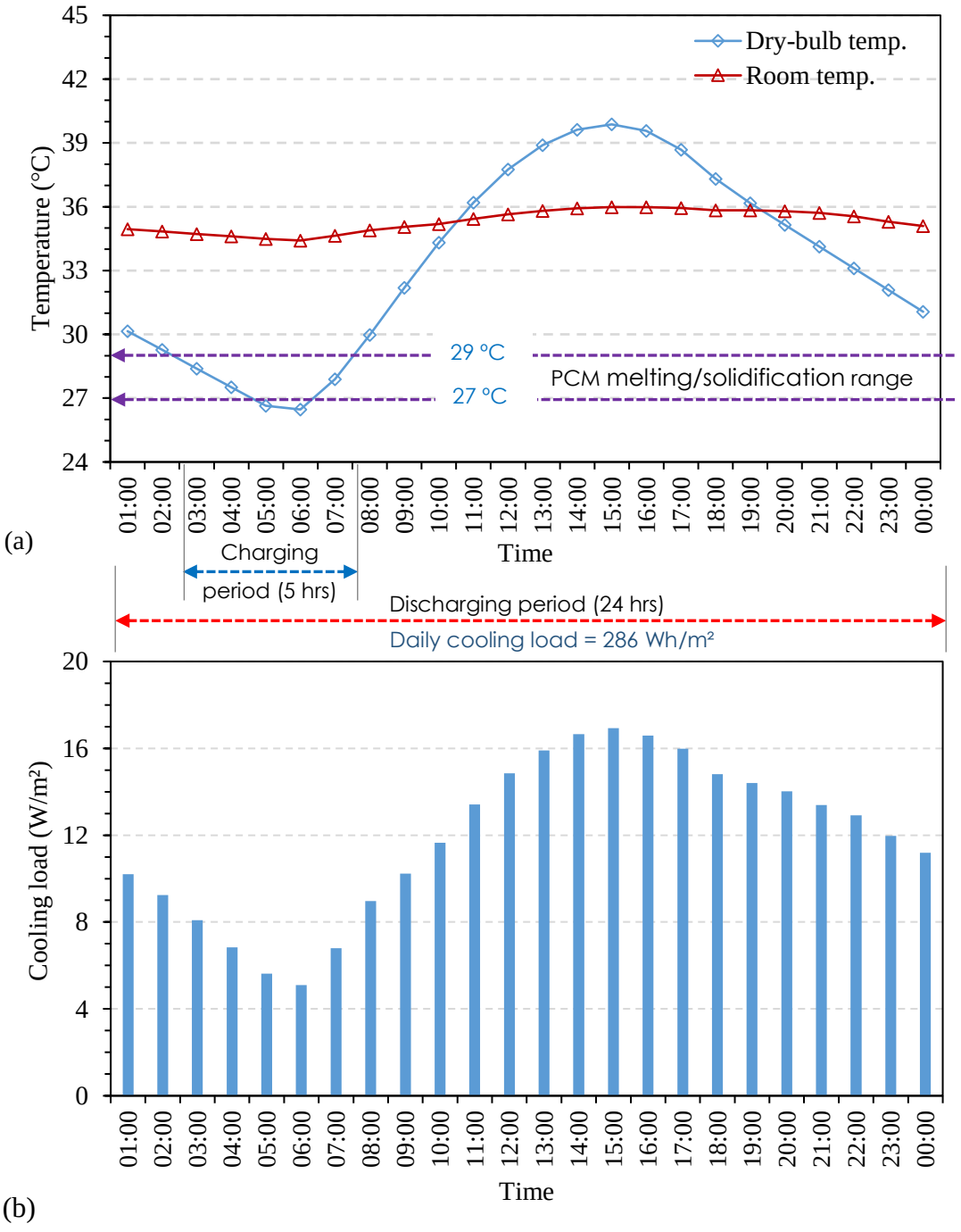


Figure 6.2: (a) Indoor air temperature and (b) cooling load of the room on a typical summer day.

6.4 Geometry description and modelling assumptions

The basic configuration of the modular PCM-air heat exchanger is shown in Figure 6.3. It consists of 8 rectangular aluminium containers filled with RT28HC PCM. The PCM modules are stacked over each other with an air gap 15 mm in between, and each module has a 10 mm thickness as initial assumptions. The thickness of the PCM and height of the air channels are varied to optimise the system design. A well-insulated metallic channel with inlet and outlet apertures was proposed to accommodate the PCM modules and to allow the air flow.

The thermal performance of the proposed cooling system was assessed using CFD modelling (ANSYS software). As the inlet and outlet apertures have nearly the full width of the channel (Figure 6.3), the behaviour would be approximately identical in any longitudinal section through the duct. Therefore, a 2D model has been investigated in the CFD modelling to save the computational time. A schematic of the 2D initial geometry created in ANSYS DesignModeler is depicted in Figure 6.4, and the boundary conditions are labelled.

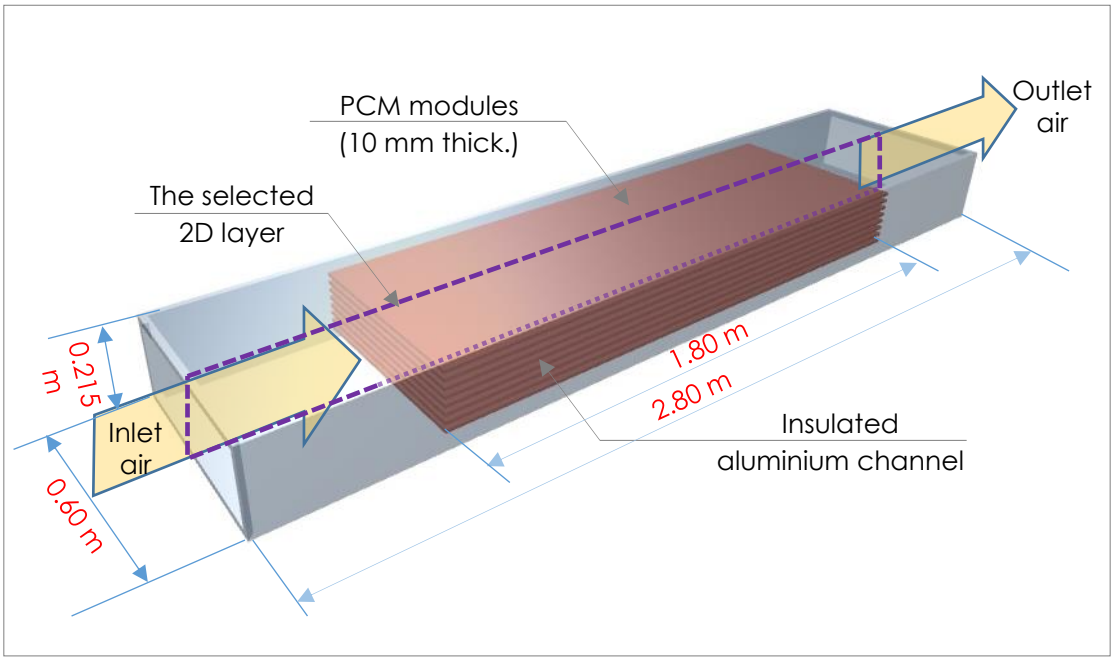


Figure 6.3: Configuration of the modular PCM heat exchanger.

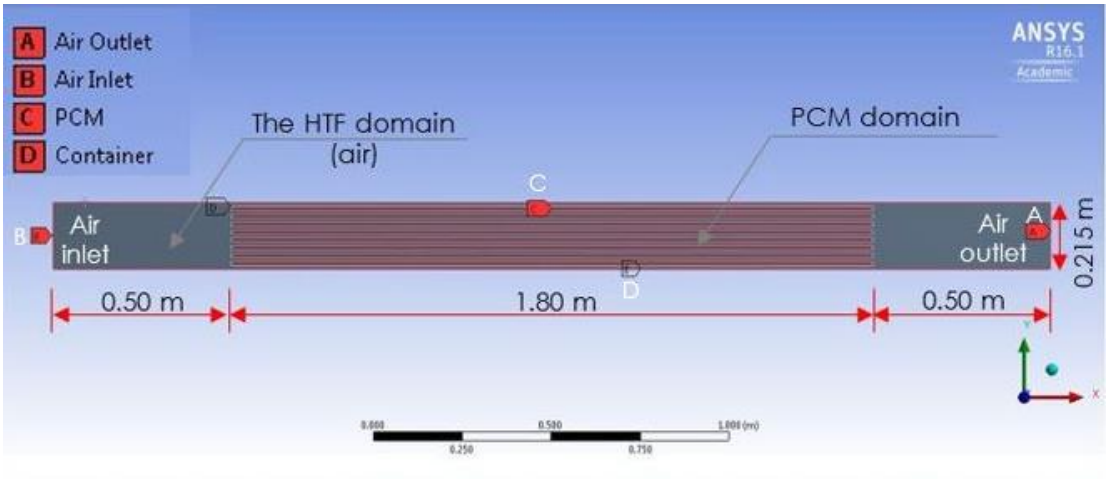


Figure 6.4: Details and boundary conditions of the 2D model created in the ANSYS DesignModeler.

The following assumptions were made to streamline the simulation process and hence shorten the computation period;

- Both fluid domains (air and PCM) are considered incompressible. The reason is that the solidification/melting model in ANSYS Fluent software cannot be used for compressible flows.
- The modelling is transient and two-dimensional (2D).
- The thermo-physical properties of the heat transfer fluid (air) are constant and considered individually for each inlet temperature.
- The specific heat, dynamic viscosity and heat conductivity of the PCM are constant and similar for both transition phases. Whereas, natural convection in the liquid PCM caused by density variation with temperature is considered using the piecewise-linear method available in Fluent.
- The heat exchange with the surroundings was neglected.
- The volume alteration and PCM movement due to the phase change was neglected as the velocity in the completely melted PCM region is only around 2.6×10^{-7} m/s. Consequently, all wall boundaries were set to a non-slip.

6.5 Computational methodology

The modelled and meshed geometry was exported to ANSYS Fluent for setting and solving the fluid flow and the heat transfer problem including the phase change. The Pressure-Based flow equations solver was selected as the HTF is incompressible. The assigned models, materials, boundary conditions, and solution settings utilised in the computation are discussed as follows:

6.5.1 Models and governing equations

The continuity and momentum equations are solved for the viscous air flow. The energy conservation equation is solved for the air flow along with that for the PCM zone using the solidification/melting model.

6.5.1.1 Flow and Energy models for the HTF

For the proposed channel and the range of tested air flow velocities, the flow regime was assumed turbulent for the whole cases according to the computed Reynolds numbers using equation (6.3);

$$Re = \frac{u\, D_h}{\gamma} \tag{6.3}$$

where; u is the velocity of the HTF, D_h is the hydraulic diameter calculated using equation (6.4), and γ is the kinematic viscosity of the HTF. The flow regime is considered laminar if $Re < 2100$, transitional if $2100 < Re < 4000$, and turbulent if $Re > 4000$.

$$D_h = \frac{2 \times W_D \times H_D}{(W_D + H_D)} \tag{6.4}$$

where; W_D and H_D are the width and the height of the duct, respectively.

Since the air flow in the present application is turbulent, the turbulence model which in principle described by the Navier-Stokes equations is used. The most widely applied Reynolds-Averaged Navier-Stokes (RANS) equations are solved. A proper selection of a turbulence model is very important to ensure the quality of the simulation of a given application. The *k-ε* models are one of the RANS models which are commonly used for fully turbulent air flow modelling in industrial CFD. The realizable *k-ε* proposed by Shih (1995) was accepted as being highly recommended and appropriate for modelling flows such as that in this computation. Initial studies have demonstrated that the realizable *k-ε* model possesses substantial enhancements over the k-*ε* family (standard and RNG models) for several validations of a wide range of flows (Kim et al., 1999, Shih, 1995). The enhanced wall treatment effect was activated to calculate the flow near wall surfaces (wall-neighbouring cells).

Based on the utilised models and assumptions, the conservation equations solved for continuity, momentum and energy can be simplified as follows (FLUENT, 2013, Henningson and Berggren, 2005);

Continuity
$$\frac{\partial u_i}{\partial x_i} = 0 \tag{6.5}$$

Momentum
$$\frac{\partial u_i}{\partial t} + \frac{\partial u_i u_j}{\partial x_j} = -\frac{1}{\rho}\frac{\partial p}{\partial x_i} + \nu\frac{\partial^2 u_i}{\partial x_j \partial x_j} - \frac{\partial \overline{\acute{u}_\iota \acute{u}_j}}{\partial x_j} \tag{6.6}$$

Energy
$$\rho C_p\left(\frac{\partial T}{\partial t} + \frac{\partial u_i T}{\partial x_i}\right) = \frac{\partial}{\partial x_i}\left(\lambda_{eff}\frac{\partial T}{\partial x_i}\right) + S_h \tag{6.7}$$

$$(i = 1,2), (j = 1,2)$$

where; ρ is the density, u is the flow velocity, p is the pressure, ν is the kinematic viscosity, C_p is the heat capacity, T is the temperature, λ_{eff} is the effective thermal conductivity, S_h is the heat source term, and $\overline{\acute{u}_\iota \acute{u}_j}$ is the Reynolds stresses modelled by the selected turbulence model in order to close equation (6.6).

6.5.1.2 Solidification/melting model

The solidification/melting model which uses an enthalpy-porosity formulation method is used by ANSYS Fluent to solve the solidification and melting processes of the PCM (Voller, 1987, Voller et al., 1988, Voller and Prakash, 1987). In this technique, the solid-liquid front is not computed explicitly. Instead, a magnitude called liquid fraction associated with each cell in the domain is utilised. The liquid fraction denotes the fraction of the cell volume that is in liquid form, and it is calculated at each iteration based on an enthalpy balance using equations (6.8)-(6.12). The liquid-solid mushy zone is regarded as a porous region with porosity equivalent to the liquid fraction, which ranges from 1 for full melting to zero for complete solidification in a cell.

The enthalpy (H) of the substance is calculated as a sum of the sensible heat (h) and the latent heat (Δh).

$$H = h + \Delta h \tag{6.8}$$

The sensible heat (h) is calculated as a function of the reference enthalpy (h_{ref}), the reference temperature (T_{ref}), and the specific heat at constant pressure (c_p) using equation (6.9);

$$h = h_{\text{ref}} + \int_{T_{\text{ref}}}^{T} c_p dt \tag{6.9}$$

The liquid fraction (β) can be expressed as;

$$\begin{aligned} \beta &= 0 && \text{if } T < T_{\text{solidus}} \\ \beta &= 1 && \text{if } T > T_{\text{liquidus}} \\ \beta &= \frac{T - T_{\text{solidus}}}{T_{\text{liquidus}} - T_{\text{solidus}}} && \text{if } T_{\text{solidus}} < T < T_{\text{liquidus}} \end{aligned} \tag{6.10}$$

The latent heat content (Δh) can vary between 0 for a solid and the latent heat of the material (L) for a liquid. Thus, it can be written based on the liquid fraction (β) as follows;

$$\Delta h = \beta L \tag{6.11}$$

The governing energy equation solved for the solidification/melting model is simplified as follows;

$$\rho \frac{\partial H_i}{\partial t} = \lambda \frac{\partial T_i}{\partial x_i} + S \tag{6.12}$$

where; is the enthalpy computed from equation (6.8), ρ is the substance density, λ is the substance thermal conductivity, T is the temperature, and S is the source term.

6.5.2 Boundary conditions

The assigned boundary conditions are described in Figure 6.4. The inlet boundary condition was specified as velocity inlet with a constant velocity and temperature. The outlet boundary condition was set to a pressure outlet with zero gauge pressure. The interface between the PCM region and the air domain was set to a coupled wall to allow heat exchange. The main channel walls were given a non-slip boundary condition and considered adiabatic.

6.5.3 Solution methods

The coupled algorithm has been applied for the pressure-velocity coupling in all cases. Under spatial discretisation, the second-order upwind scheme was utilised for solving momentum, energy, and transient formulation. PRESTO scheme was used for the pressure correction equation. The under-relaxation factors for density, body forces, turbulent kinetic energy, turbulent dissipation rate, turbulent viscosity, liquid fraction, and energy were set to 1.0, 1.0, 0.8, 0.8, 1.0, 0.9 and 1.0, respectively (default values). The hybrid initialisation method was applied. The maximum iteration per time-step

was set to 20, which is found adequate for fulfilling the convergence criteria of the default residual tolerances of 10^{-3} for continuity, x and y velocities, and turbulence k-ε equations, and 10^{-6} for energy equation.

6.5.4 Initial settings and base case conditions

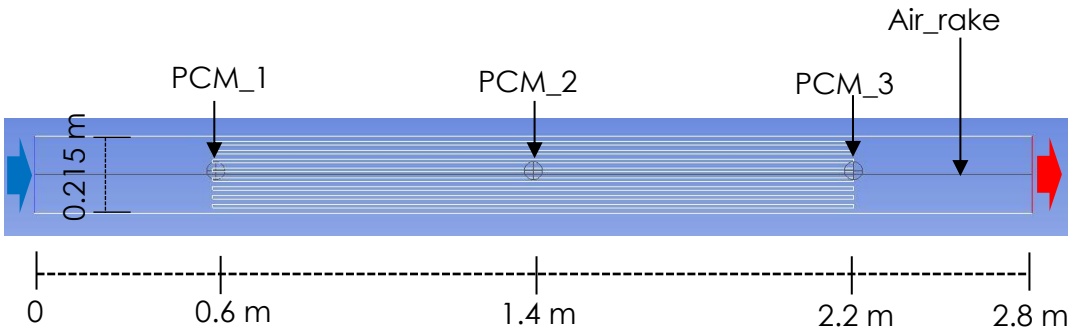
In the charging simulation, the initial state of the PCM (RT28HC) was considered fully liquid with a temperature set to 32 °C above its liquidus temperature by a 3-K. The charging air enters the PCM storage at a certain temperature and flow rate allowing for heat removal from the PCM, which begins to solidify gradually. The reason for using a constant inlet air temperature during the entire charging process is that the charging periods are very short, and the temperatures are close (Figure 5.4a). Thus, the average temperature of that period is a suitable assumption.

In the case of the discharging simulation, the PCM was initially assumed to be completely solid with a temperature set to 24 °C below its solidus temperature by a 3-K. The discharging air of a constant temperature and flow rate adds heat to the PCM, and hence, it starts melting. In this analysis, the inlet air temperature was kept constant during the discharging simulation, as buildings with high thermal mass usually feature slight indoor temperature swing (Figure 6.2a), attributed to many factors including the microclimate conditions, building construction, internal loads, etc.

The base case geometry considered in this study has a 10 mm thickness of the PCM module and a 15 mm height of air channels. The simulations were run under inlet air temperatures of 23 °C and 36 °C and the air flow rate of 213 L/s and 27 L/s for the charging and discharging processes, respectively.

The presented results involve liquid fraction and temperature of the PCM which are computed as an average of the entire PCM domain. The outlet air temperature is calculated as an average of the outlet. As shown in Table 6.2, the temperature was also monitored at several locations within the PCM and air zones. PCM_1, PCM_2, and PCM_3 are the considered positions at the beginning, middle, and end of the 4th PCM module, respectively, and Air-rake for measuring the temperature along the central air channel.

Table 6.2: Coordinates of the monitored points and rakes.



Point	X	Y	Rake/Line	X	Y
PCM_1	0.6	0.12	Air-rake	0	0.1075
PCM_2	1.4	0.12		2.8	0.1075
PCM_3	2.2	0.12			

6.6 Independence tests

For an unsteady-state simulation, independence tests were initially carried out for a preliminary case in order to ensure that the solution is independent of time and mesh size before commencing the main study. This study is beneficial for enhancing the accuracy of the solution and reducing the calculation time.

6.6.1 Time independence study

In this study, three different time-steps were tested; 0.05, 0.1, and 0.2 s. The variation in the PCM liquid fraction under considered time-steps is shown in Figure 6.5a and Figure 6.5b for both charging and discharging phases, respectively.

From Figure 6.5a, it can be seen that the PCM liquid fraction computed using time-steps of 0.05 s and 0.1 s is nearly identical throughout the entire charging process. While a variation is observed in the case of 0.2 s time-step led to a delay in the PCM solidification by around 3.5% of the time compared to 0.05 s. On the other hand, in the case of discharging process, Figure 6.5b shows that the simulation was independent of time for the initial 3 hours. After which, a variation in the PCM liquid fraction computed at 0.2 s time-step is noticed until the end of the simulation, where the PCM full melting occurred quicker by around 3.7% of the time required when using 0.05 s time-step.

As reported in the literature (FLUENT, 2013), for a transient state simulation, the accuracy of the results increases at the smaller time-step. Therefore, for high accuracy with a reasonable computational cost, a 0.1 s time-step was adopted for all charging and discharging simulation of the basic model. It worth mentioning that the smallest time-step of 0.05 s has been used when the geometry is changed.

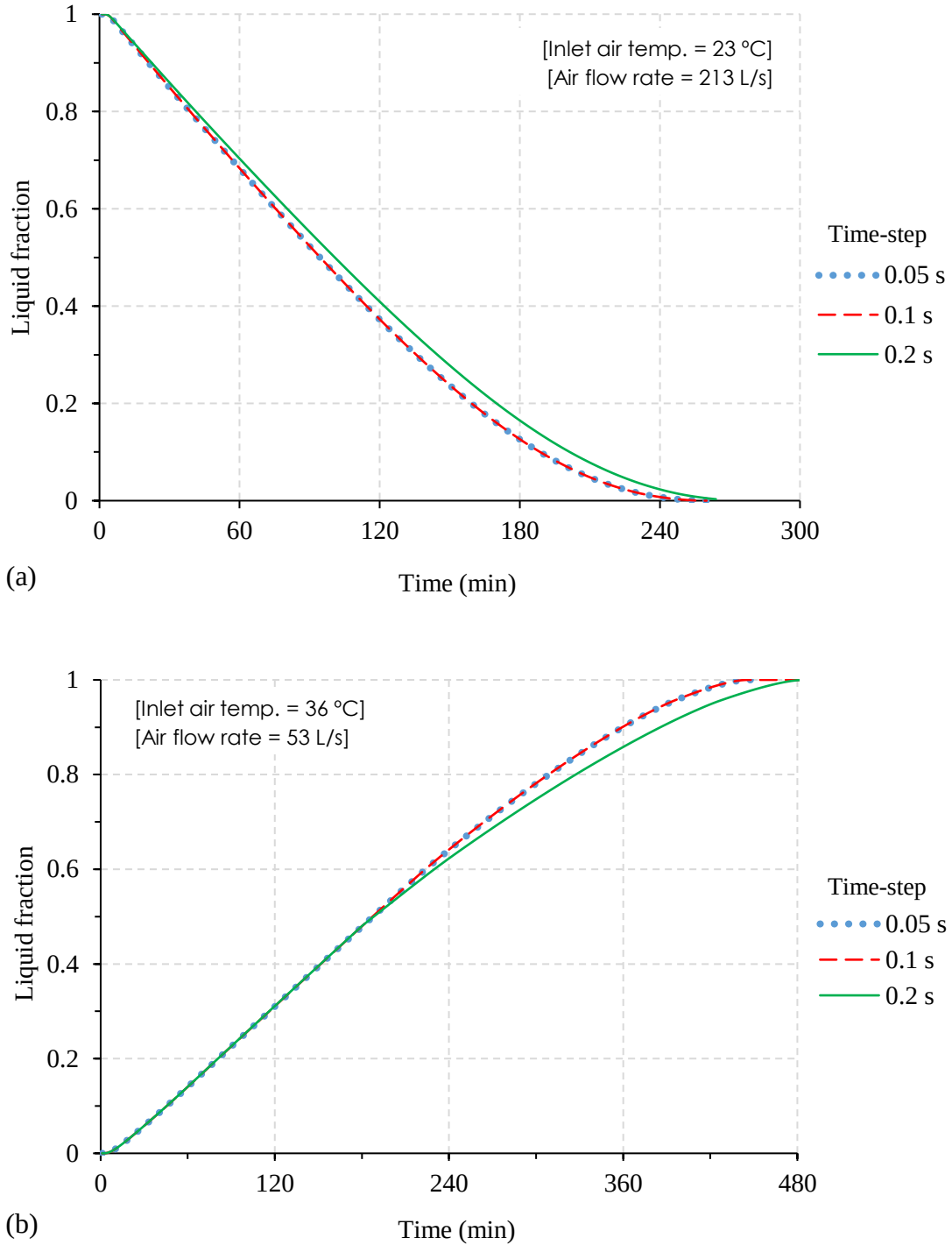


Figure 6.5: PCM mean liquid fraction at different time-steps during the (a) charging and (b) discharging process.

6.6.2 Grid independence study

The simulation quality depends significantly on the mesh size applied to the geometry. An independence test was carried out for a preliminary case under three different grid densities as detailed in Table 6.3 in order to select the optimum grid. The tested sizes of the mesh edge are in the range recommended for natural ventilation applications (Xiang and Gan, 2015). Figure 6.6 compares the PCM mean liquid fraction during full charging process for the three tested grids. It is clear that the PCM liquid fraction in all cases follows a similar trend throughout the whole simulation and the variations are generally small with a maximum of 1.9%. Therefore, an adequate mesh of 2.5 mm edge size (Grid B) was adopted for the entire simulation cases in this study.

Table 6.3: Mesh information.

	Edge size	Total number of cells
Grid A	1.0 mm	192788
Grid B	2.5 mm	70078
Grid C	3.0 mm	48197

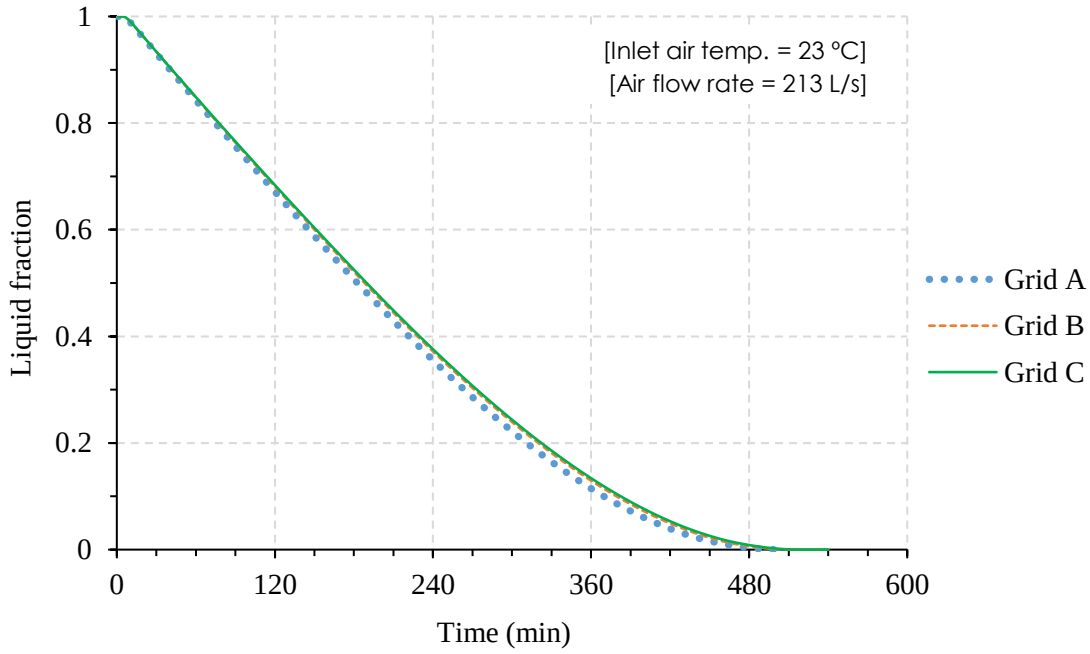


Figure 6.6: Mean liquid fraction of the PCM during a charging phase for different grid sizes.

6.7 Results and discussion

A transient CFD simulation was carried out to investigate the solidification and melting characteristics of the proposed PCM energy storage system for free cooling of buildings application. A parametric study has been performed to optimise the TES geometrical configuration and the operating conditions, and the results have been presented and discussed as follows;

6.7.1 Temperature variation in the PCM-air heat exchanger

This section discusses the temperature variation in the PCM and the air domains. The coordinates of the investigated locations were revealed in Table 6.2.

6.7.1.1 PCM charging

Figure 6.7 shows the temperature decrease with the time at three locations in the PCM region; PCM_1, PCM_2, and PCM_3; during a complete charging phase. The PCM was initially at a liquid state with a temperature of 32 °C, higher than its liquidus point by a 3.0-K. The cold air enters through the inlet aperture and lowers the temperature of the aluminium plates which have direct contact with the PCM. The PCM starts losing its heat to the cooler aluminium container by convection and cools rapidly reaching the liquidus temperature of 28 °C (sensible cooling of the PCM). Then, the phase transition phase starts, where the PCM commence solidifying while its temperature gradually drops at different times according to the PCM location. The solid part of the PCM increases with the time, and therefore, heat is transferred by conduction as well between the PCM and the container. When the PCM reaches the solidus temperature (27 °C), a sensible cooling takes place until the PCM temperature equalises the inlet air temperature. This process continues until reaching the steady-state conditions. The temperature data in Figure 6.7 indicates that the PCM in the front of the module (PCM_1) solidifies substantially faster than the PCM in the rear of the module (PCM_2 and PCM_3). The solidification occurs gradually along the PCM module, due to the temperature gradient of the air passing through the duct, as shown in Figure 6.8.

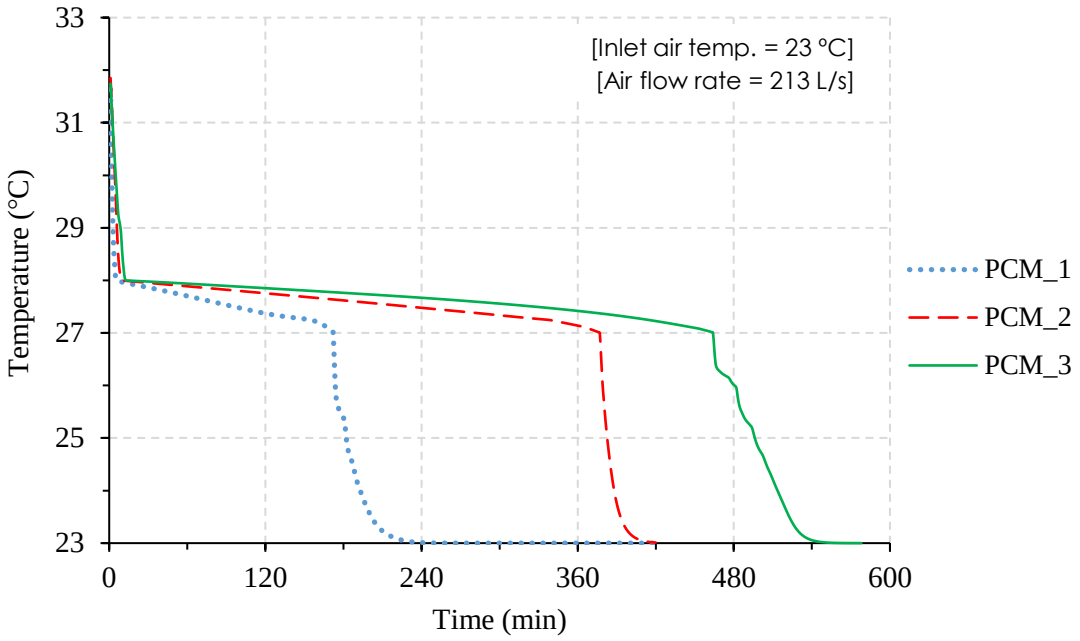


Figure 6.7: Temperature variation at three PCM locations during the charging process.

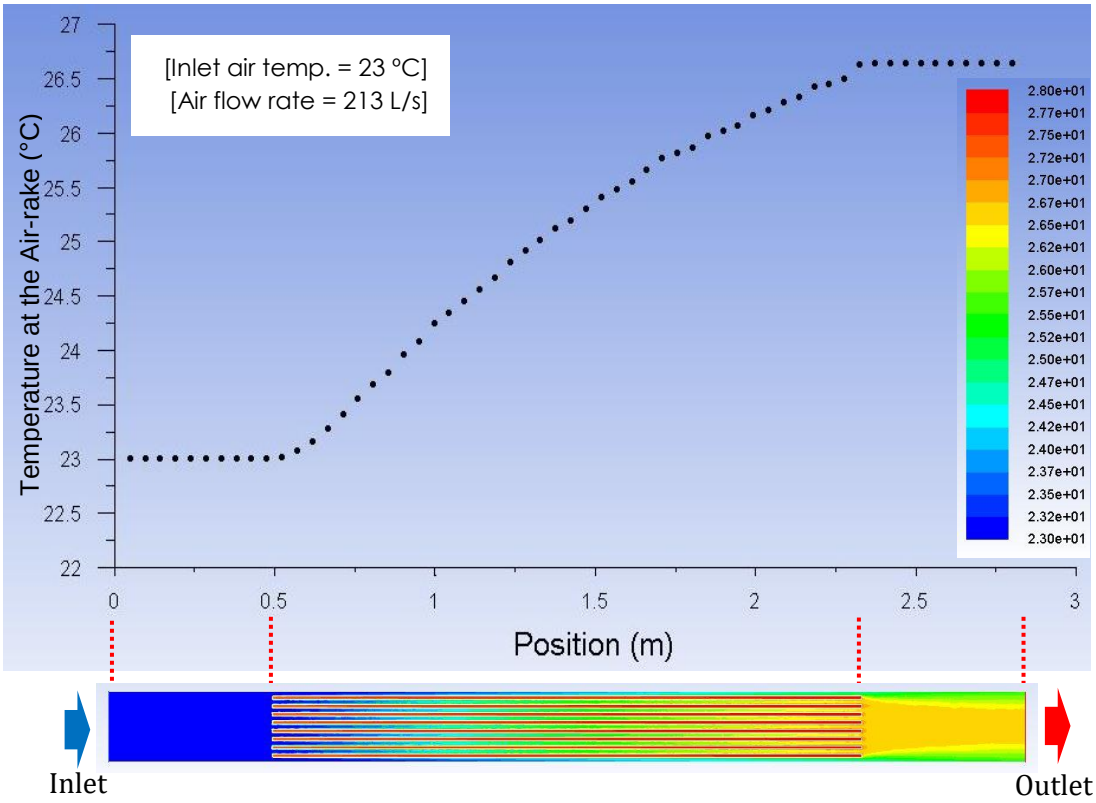


Figure 6.8: Temperature variation after 2 hours of the charging process.

6.7.1.2 PCM discharging

Figure 6.9 demonstrates the temperature increase with the time at the three considered locations in the PCM region during a complete discharging phase. Initially, the PCM was entirely solid at a temperature of 24 °C, lower than its freezing point by a 3.0-K. The inlet air heats the aluminium container plates, which in turn, transfer heat by conduction to the solidified PCM, resulting in a rapid PCM temperature drop to the freezing point (sensible heating of the PCM). Afterwards, the PCM starts melting gradually until it reaches the liquidus temperature of 29 °C at different periods depending on the PCM relative location. Then, sensible heating occurs, where the PCM temperature drops speedily to the inlet air temperature. This process occurs continuously until the steady-state conditions reached. Moreover, it is observed from Figure 6.9 that the PCM melting takes place earlier in the front of the module (PCM_1) and prolong gradually at the rear of the module (PCM_2 and PCM_3) owing to the air temperature drop progressively along the duct, as shown in Figure 6.10.

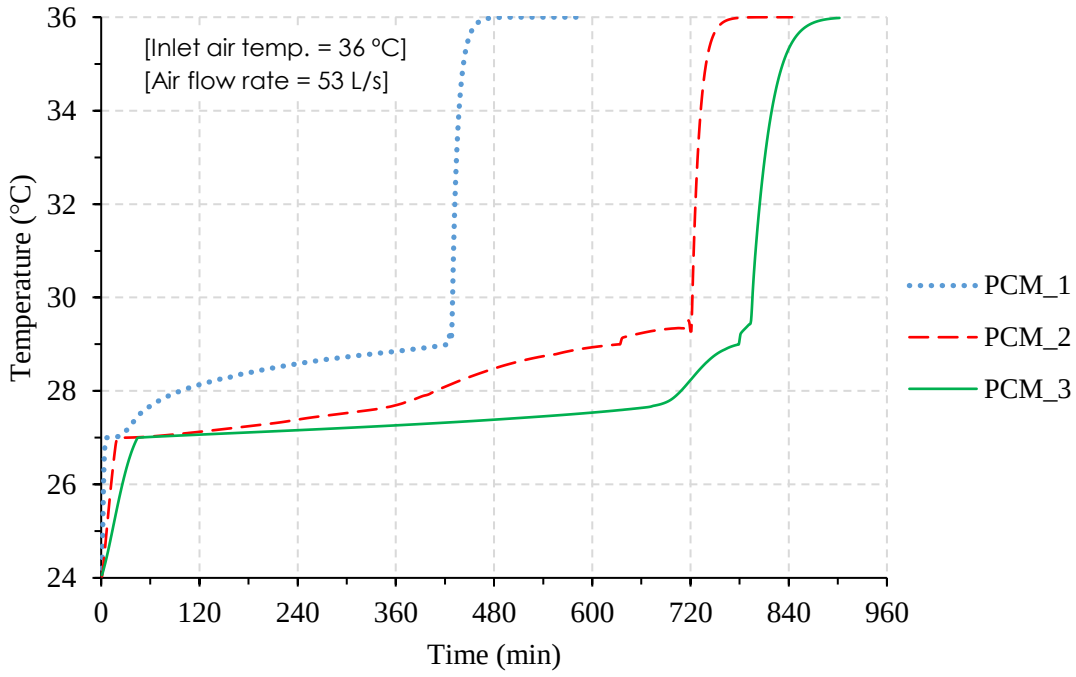


Figure 6.9: Temperature variation at three PCM locations during the discharging process.

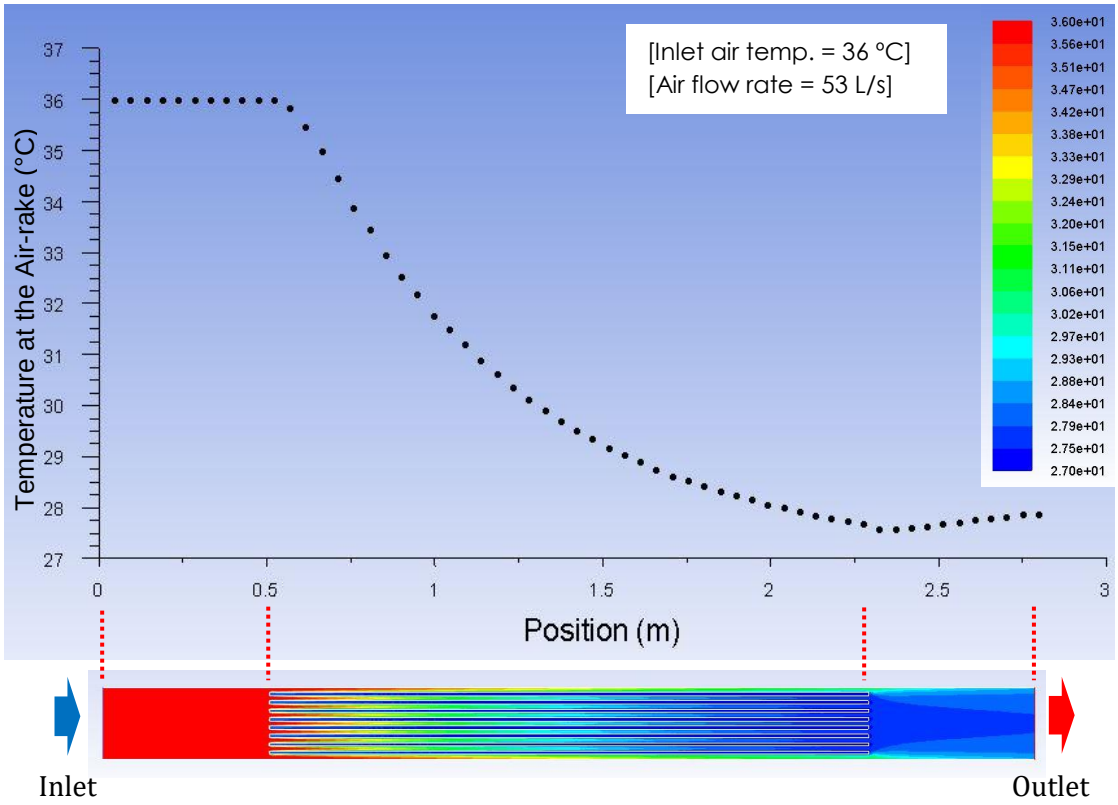


Figure 6.10: Temperature variation after 2 hours of the discharging process.

6.7.2 Influence of inlet air temperature

6.7.2.1 PCM charging

In this study, the charging air temperatures were selected based on the prevailing ambient conditions during the summer and transitional months in Khartoum. Five inlet air temperatures were tested 21 and 23 °C to simulate the charging under moderate summer conditions, and 25, 26, and 27 °C for the charging under hot summer conditions. The tests were carried out using an air flow rate of 213 L/s.

Figure 6.11a and Figure 6.11b show the variation in the PCM liquid fraction and the outlet air temperature, respectively, during full charging process for the tested inlet air temperatures at air flow rate 213 L/s. As shown in Figure 6.11a, in the current PCM arrangement and the suggested air flow rate, complete PCM solidification can be realised as early as 5.75 hours when the inlet air is at a temperature 21 °C and may last for up to 21.95 hours at a charging temperature of 26 °C. The full solidification was difficult to be obtained when the inlet temperature was 27 °C, even after 24 hours of charging process where the solid PCM fraction reached 59%, due to the small temperature difference between the PCM and the air. Based on these figures, optimising the geometrical configuration of the TES system and the air flow rate is recommended to improve the charging performance. Furthermore, it is observed from Figure 6.11b that the outlet air temperature from the system remained within the comfort range, i.e. below 30°C, all the time in all cases, except for the first 10-30 minutes of sensible heat removal. The lower the inlet temperature, the lower the outlet temperature would be. Yet, the air flow rate may be very high to be directly admitted into an occupied space.

Table 6.4 summarises the required time for obtaining full PCM solidification under proposed operating conditions. It is inferred that the change in solidification time with the inlet air temperature has a nonlinear relation. As an example, the solidification time prolongs by around 45% with a 2 K inlet temperature rise from 21 °C to 23 °C and by around 65% with the temperature rise from 25 °C to 26 °C. Figure 6.12 depicts contours of temperature and liquid fraction in the PCM domain after 4 hours of the charging for the tested inlet air temperatures.

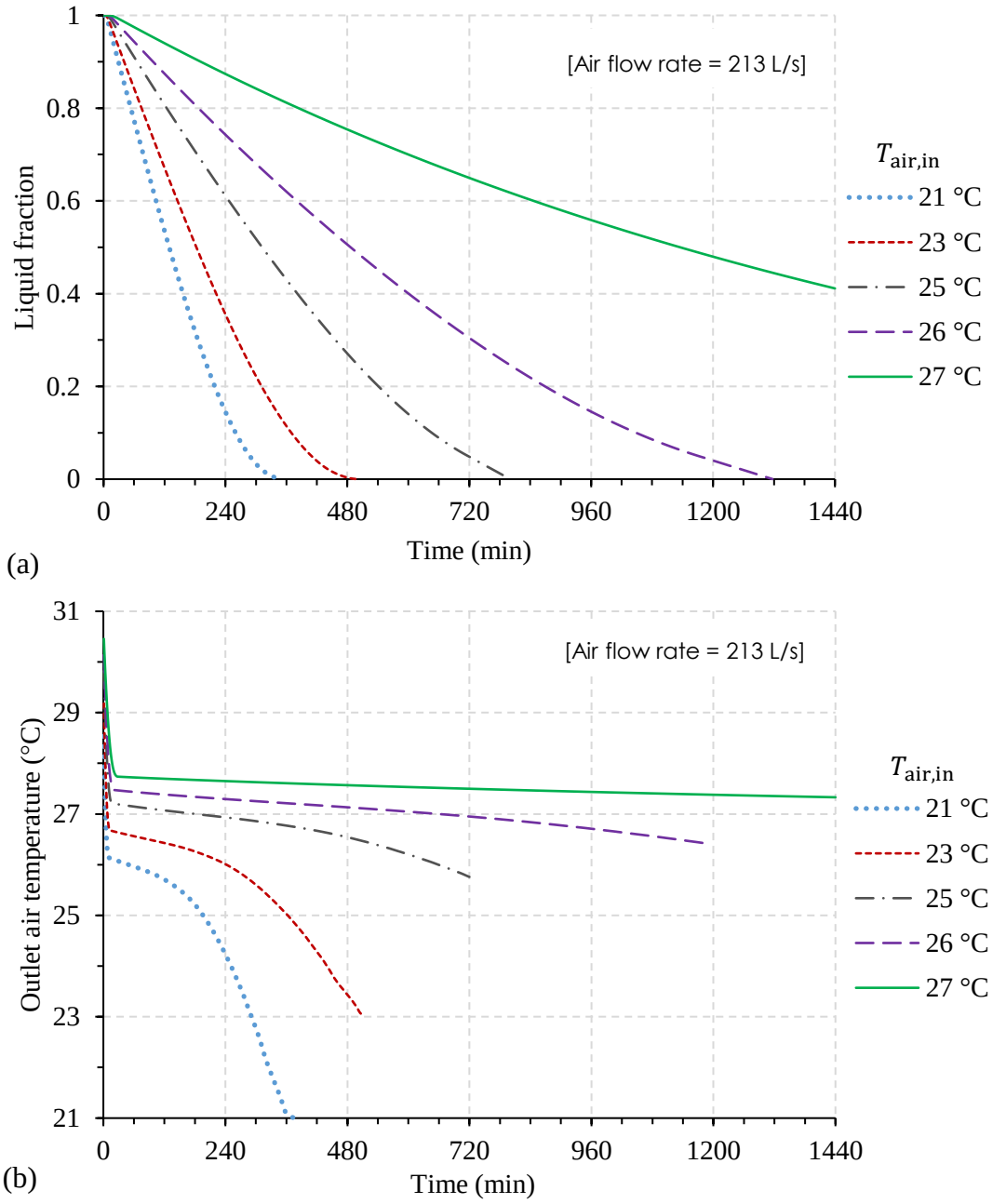


Figure 6.11: Variation of (a) PCM liquid fraction and (b) outlet air temperature for different inlet air temperatures during the charging process.

Table 6.4: Solidification time under tested inlet temperatures at an air flow rate of 213 L/s.

	Inlet air temperature				
	21 °C	**23 °C**	**25 °C**	**26 °C**	**27 °C**
Solidification time (hours)	5.75	8.33	13.33	21.95	N.A

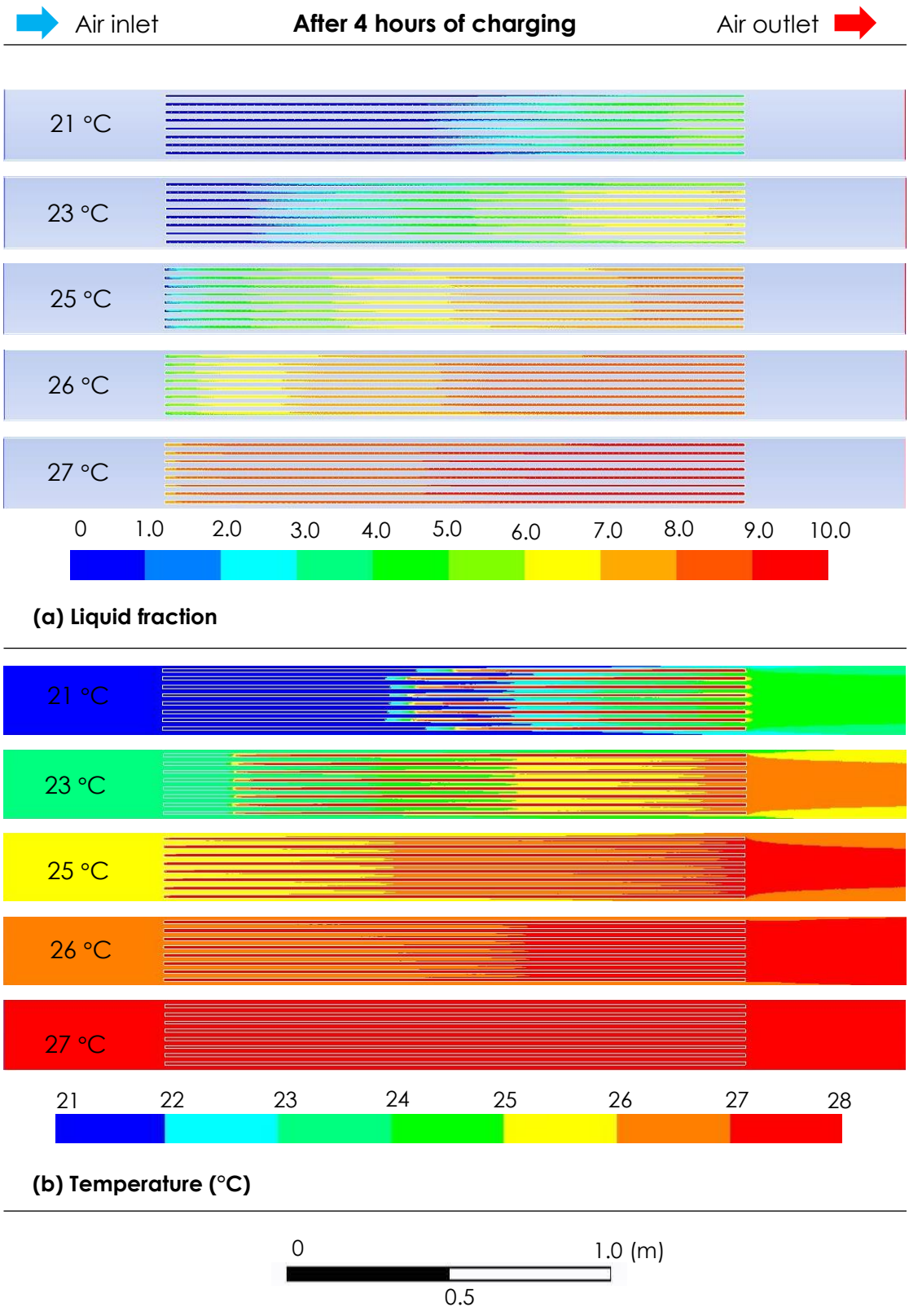


Figure 6.12: Contours of (a) PCM liquid fraction (b) temperature after 4 hours of charging for inlet air temperatures 21, 23, 25, 26, and 27 °C and at air flow rate of 213 L/s.

6.7.2.2 PCM discharging

The indoor air could be circulated through the PCM storage for the cooling discharging during the daytime instead of the hotter ambient air. In real applications, a certain ration of ambient air may be occasionally admitted into the building indoors for air quality improvement. In this test, three inlet air temperatures were investigated for the discharging process; 34 and 36 °C which could represent the indoor air temperatures of a well-insulated room during summer of hot-arid climates, and 38 °C for a room with a high indoor temperature or could be the ambient temperature. An air flow rate of 53 L/s which compatible with the comfort ventilation in residential buildings was used.

Figure 6.13a and Figure 6.13b demonstrate the variation in the PCM liquid fraction and the outlet air temperature, respectively, throughout the discharging process for the adopted inlet air temperatures, at air flow rate 53 L/s. It is evident from Figure 6.13a that the full PCM melting took approximately around 10.87, 13.15, and 16.76 hours, when the operating air temperatures were 38, 36 and 34 °C, respectively. As shown in Figure 6.13b, the outlet air temperature was well within the thermal comfort limit for around 7.54, 10.19, 14.46 hours, when the discharging temperatures were 38, 36, 34 °C, respectively. These results indicate that the small difference between the PCM temperature and the HTF temperature reduces the heat transfer rate, which results in a slower PCM melting and a longer comfort duration. The increase of the melting time and the comfort duration with the temperature decrease is not linear. For instance, an air temperature decrease by 2 K from 38 °C to 36 °C resulted in comfort duration extension by 35%, while another decrease from 36 °C to 34 °C allowed 42% increase.

The PCM melting time and the thermal comfort period provided by the system under tested inlet temperatures are given in Table 6.5. The contours of PCM liquid fraction and temperature distribution in the PCM-air heat exchanger after 4 hours of the discharging process are shown in Figure 6.14. It is inferred that the outlet air temperature exceeds the upper limit of the comfort zone prior to the full melting incidence. In all cases, the comfort level is maintained until melting of 70-86% of the PCM. This partial melting is advantageous in boosting the next solidification cycle by

14-30%, which reduces the fan power consumption and shorten the charging period. However, the continuation of the discharging process to obtain full PCM melting can lower the room temperature, and therefore, reduces the cooling load of the operated conventional systems.

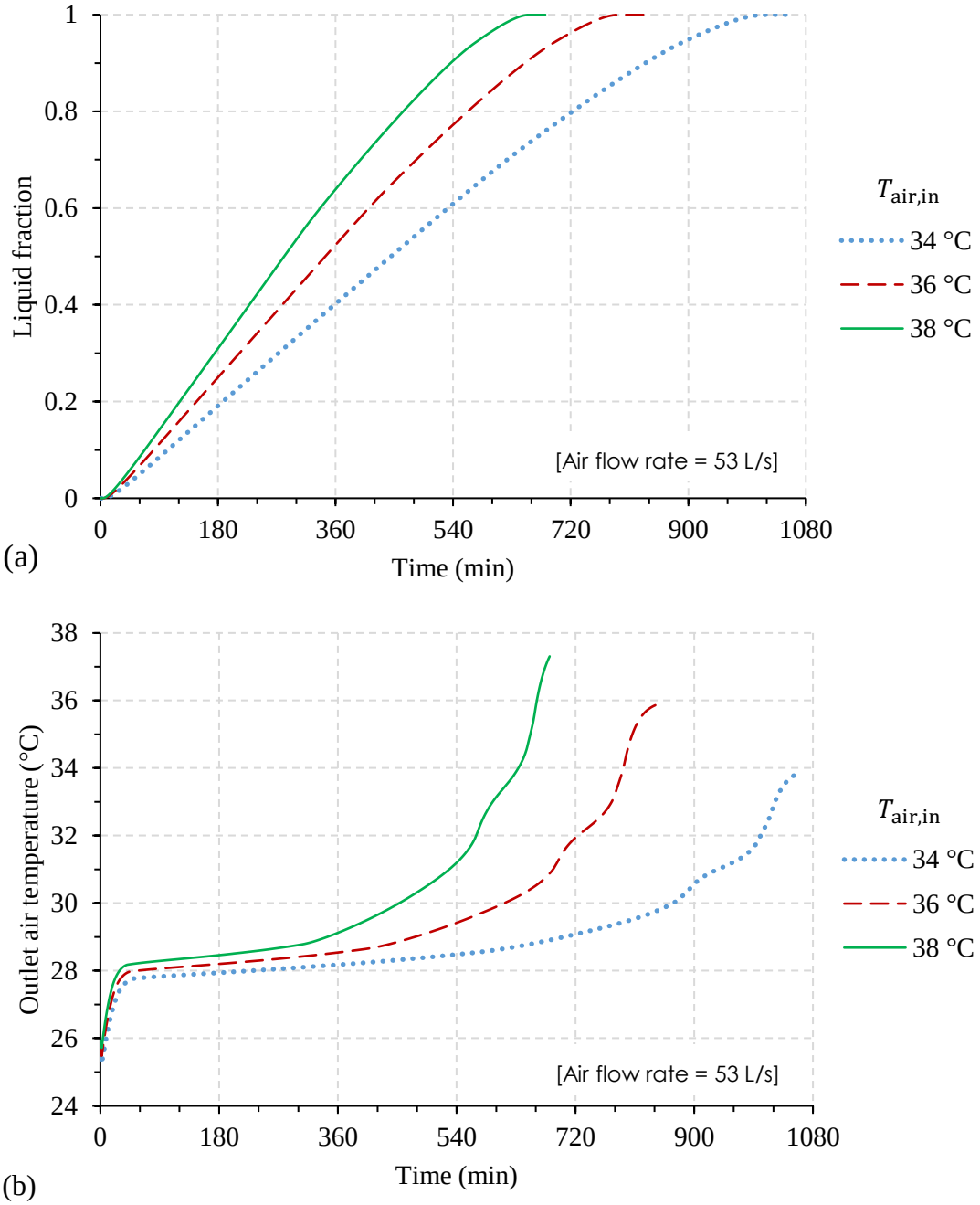
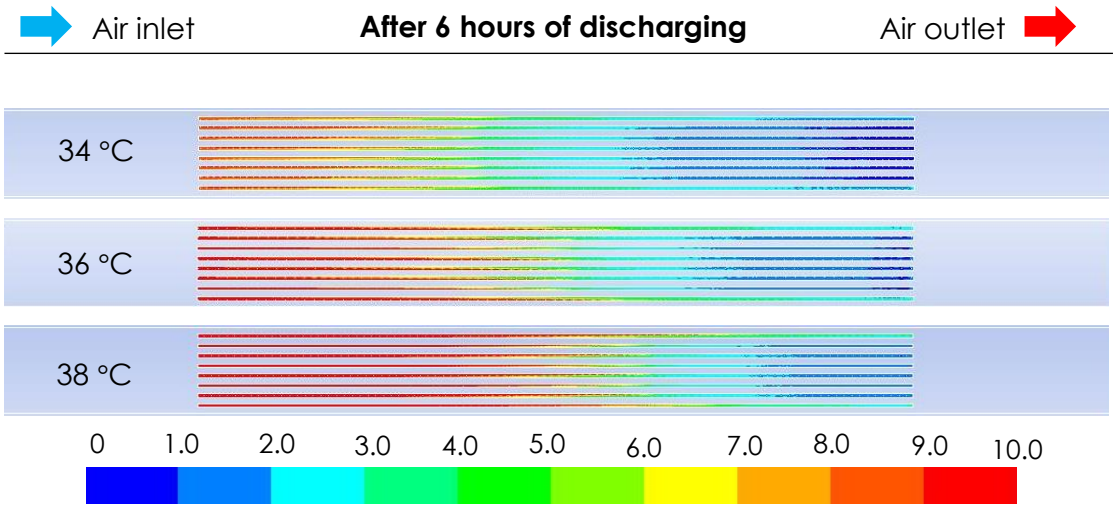


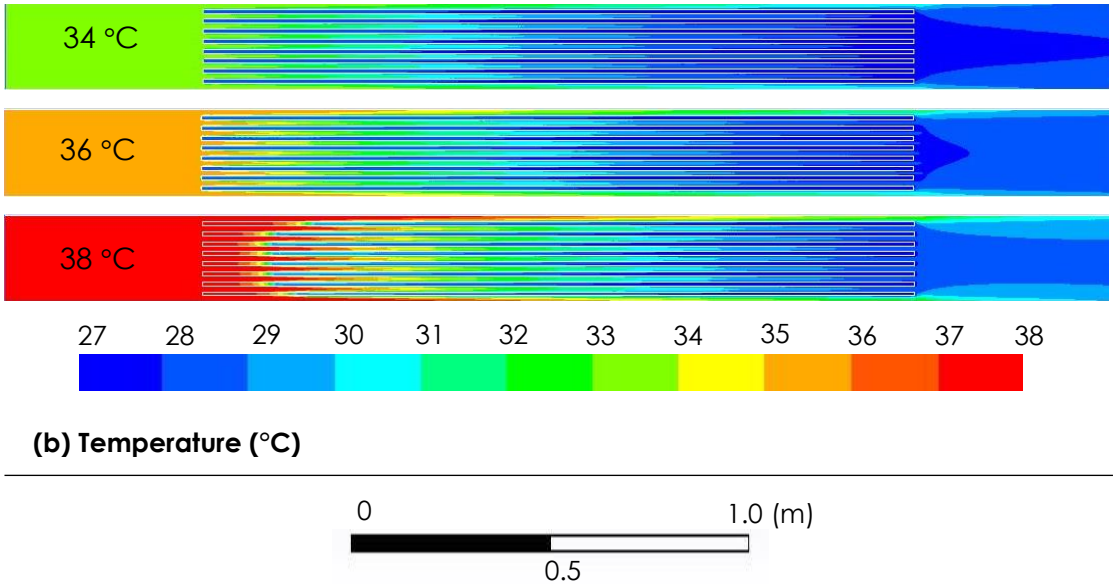
Figure 6.13: Variation of (a) PCM liquid fraction and (b) outlet air temperature for different inlet air temperatures during the discharging process.

Table 6.5: Melting time and comfort period maintained under tested inlet air temperatures at an air flow rate of 53 L/s.

	Inlet air temperature		
	34 °C	**36 °C**	**38 °C**
Melting time (hours)	16.76	13.15	10.87
Comfort duration (hours)	14.46	10.19	7.54



(a) Liquid fraction



(b) Temperature (°C)

Figure 6.14: Contours of (a) PCM liquid fraction (b) temperature after 6 hours of discharging for inlet air temperatures 34, 36, and 38 °C and at air flow rate of 53 L/s.

6.7.3 Influence of air flow rate

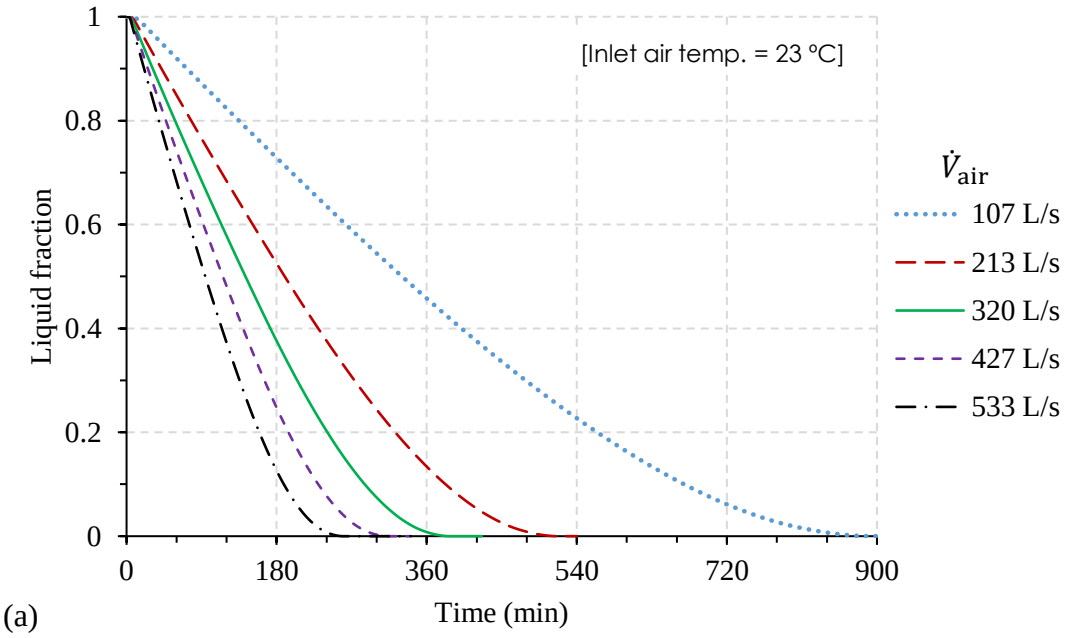
The optimisation of air flow rate based on the cooling availability and requirements is a crucial factor in the TES systems operation. Thus, the objective of this test was to investigate the impact of the air flow rate on the charging and discharging performance of the PCM. Five air flow rates for both transition phases were tested as tabulated in Table 6.6. The air flow rates adopted for the discharging process (13-107 L/s) are equivalent to 0.5-8 ACH in a typical room of an air volume 48 m³.

Table 6.6: Tested air flow rates.

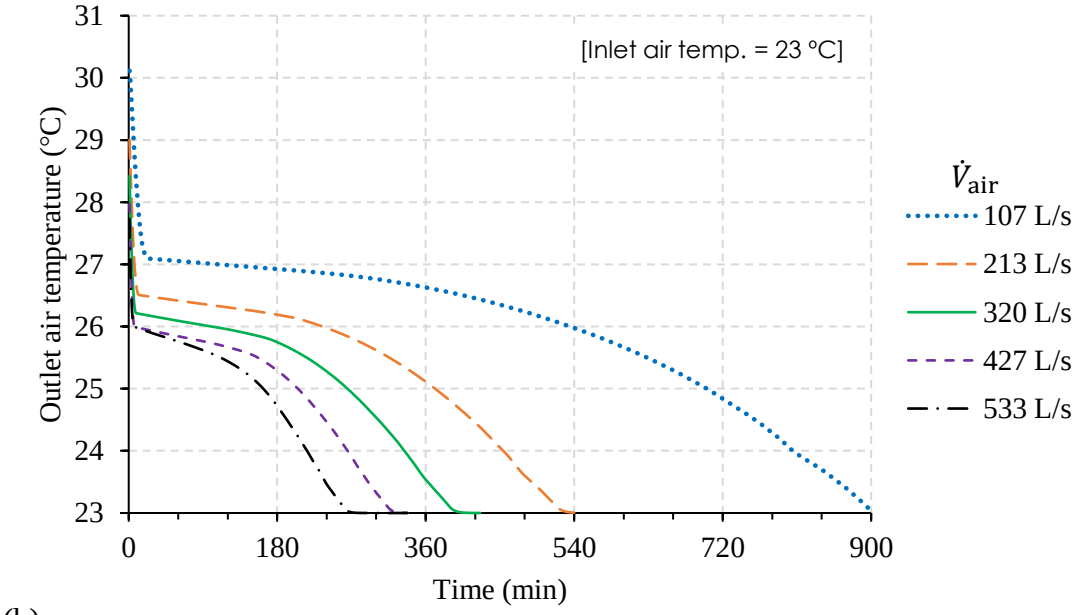
	Inlet air temp. (°C)	Air flow rate (L/s)
Charging test	23	107, 213, 320, 427, and 533
Discharging test	36	13, 27, 53, 80, and 107

6.7.3.1 PCM charging

Figure 6.15a and Figure 6.15b show the variation in the PCM liquid fraction and outlet air temperature, respectively, for several air flow rates in the range of 107-533 L/s during the charging process. It is clear that the rate of heat removal from the PCM was greater at high air flow rates and hence, the solidification was more rapidly, owing to the high convective heat transfer coefficient. The full solidification occurred in 4.2-14.3 hours, for the air flow rates 533-107 L/s, respectively (Table 6.7). Increasing the air flow rate by a double from 107 L/s to 213 L/s lessened the solidification time by 40%, whereas, an increase by 4-fold to 533 L/s led to a 70.6% solidification time reduction. This denotes that the increase/decrease in the solidification time is significant at the low air flow rates (107-320 L/s) and gradual at high air flow rates, nearly above 320 L/s (Figure 6.15a). The outlet air temperature data for the tested cases in Figure 6.15b revealed that the higher the air flow rate, the lower the outlet air temperature would be. Overall, high air flow rates are recommended during the charging process to enhance the PCM solidification in a short period and to provide acceptable comfort temperature during night-time.



(a)



(b)

Figure 6.15: Variation of (a) PCM liquid fraction and (b) outlet air temperature for different air flow rates during the charging process.

Table 6.7: Solidification time under tested air flow rates at an inlet temperature of 23 °C.

	Air flow rate				
	107 L/s	**213 L/s**	**320 L/s**	**427 L/s**	**533 L/s**
Solidification time (hours)	14.3	8.4	6.3	5.1	4.2

6.7.3.2 PCM discharging

During the discharging period, the air flow rate can be adjusted to fulfil various cooling demands, taking into account appropriateness of the flow rate to the occupants and activity inside the space.

Figure 6.16a and Figure 6.16b illustrate the variation of the PCM liquid fraction and outlet air temperature, respectively, for several air flow rates between 13 L/s and 107 L/s during the discharging process. It is evident that the greater the air flow rate, the shorter the melting time and hence, the comfort duration, as a result of the high convective heat transfer coefficient (Figure 6.16a). The outlet air temperature in all cases was within the comfort zone with varying durations, with the lower air flow rate maintains a longer comfort period (Figure 6.16b).

The melting time and the thermal comfort durations for the adopted air flow rates are presented in Table 6.8. It is evident that the variation in the melting time and the comfort duration with the air flow rate is not linear. Boosting the air flow rate from 13 L/s to 27 L/s reduced the melting and comfort time by approximately 40%, while a 7-fold enhancement to 107 L/s resulted in melting and comfort time reductions by 70.6%. This implies that the effect of the air flow rate on the melting and comfort durations is considerable in the case of low flow rates (13-53 L/s) and lower at high flow rates, possibly higher than 53 L/s. It can be stated that air flow rate in the range 27-53 L/s (2-4 ACH) can be appropriate for ventilative cooling in domestic building allowing for thermal comfort durations between 19.6-10.2 hours, respectively.

Significantly, the air flow rate plays a prime role in the heat transfer rate between the flowing air and the PCM. Low air flow rates are advantageous during the discharging process for a provision of air at a lower and a steady temperature than the high air flow rates.

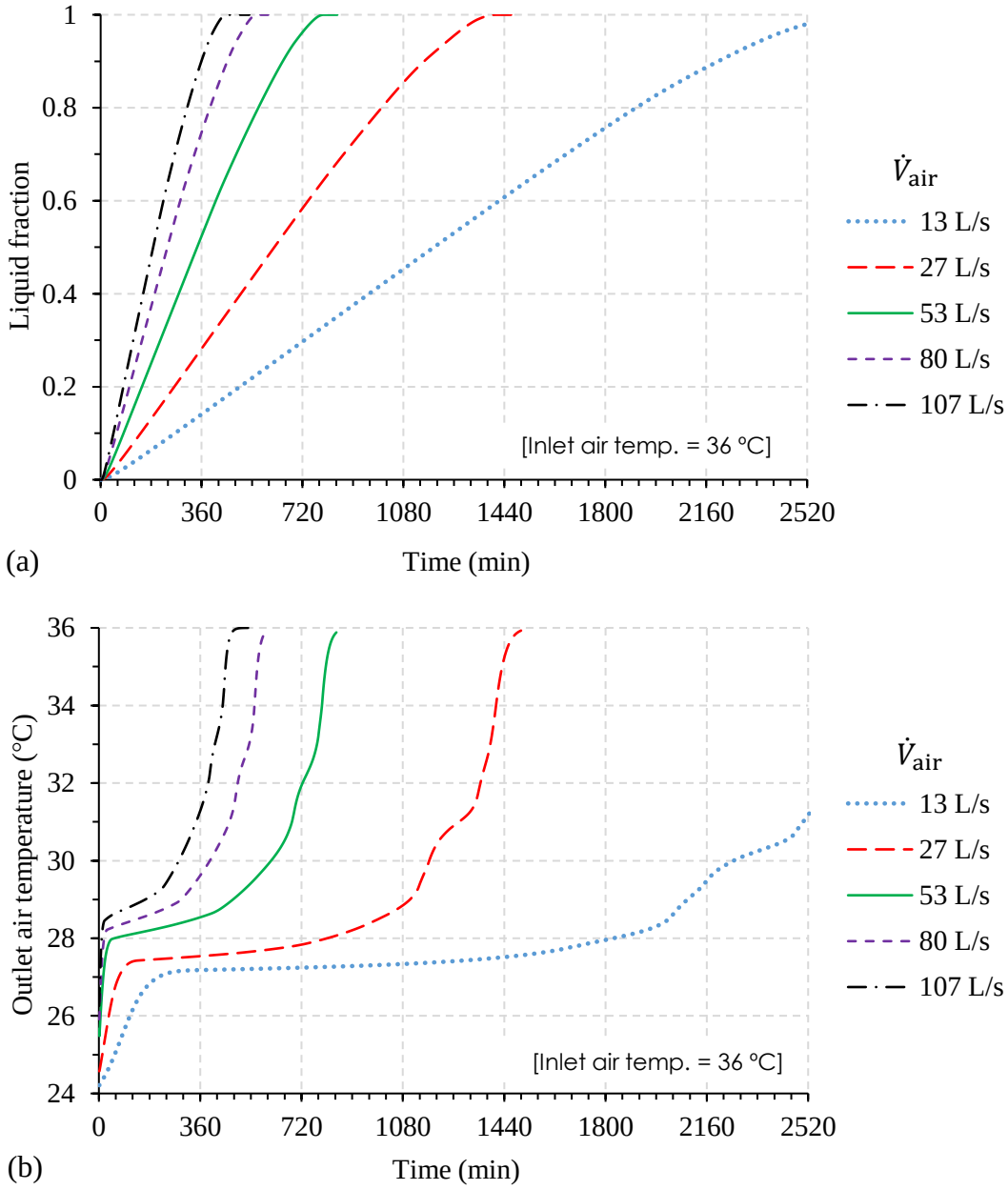


Figure 6.16: Variation of (a) PCM liquid fraction and (b) outlet air temperature for different air flow rates during the discharging process.

Table 6.8: Melting time and comfort durations under tested air flow rates at inlet air temperature of 36 °C.

	Air flow rate				
	13 L/s	**27 L/s**	**53 L/s**	**80 L/s**	**107 L/s**
Melting time (hours)	42.5	23.4	13.2	8.8	7.0
Comfort duration (hours)	37.5	19.6	10.2	6.6	4.7

6.7.4 Influence of TES geometrical configuration

The primary objective of this test was to optimise the geometrical configuration of the TES system that is appropriate for both charging and discharging processes of the free cooling systems. Therefore, six TES configurations have been investigated with similar energy storage capacities at varying PCM thicknesses and air channels height. Details of these cases are presented in Table 6.9. Results are discussed for an inlet air temperature of 23 °C and air flow rate of 213 L/s during the charging process, and for an inlet air temperature of 36 °C and air flow rate of 53 L/s during the discharging process.

Table 6.9: Geometrical details of the tested cases.

Case	PCM thickness (mm)	Air channel height (mm)	Number of PCM modules	Main duct height (m)
Case 1		5		0.165
Case 2	5	10	16	0.25
Case 3		15		0.335
Case 4		10		0.17
Case 5	10	15	8	0.215
Case 6		25		0.305

6.7.4.1 PCM charging

The variation of the PCM liquid fraction and the outlet air temperature for all tested cases during a complete charging phase is shown in Figure 6.17a and Figure 6.17b, respectively. As illustrated in Figure 6.17a, the solidification rate varied depending on the PCM thickness and the air channels height. The fastest solidification took place in case 1 (5.5 hours) when the PCM thickness and the air channels height were at the lowest level (5 mm). While around 10.1 hours are required to achieve the full solidification in case 6, where wider air channels (25 mm) and thicker PCM modules (10 mm) exist. Figure 6.17b demonstrates that the TES system configuration has a considerable impact on the outlet air temperature during the charging phase. During the transition phase, the outlet temperature was in the range 26-28 °C, higher than the inlet temperature by 3-5 K for cases 1-6, respectively. The outlet air temperature was

higher in the case of narrow air channels and thinner PCM modules, due to the enhanced heat transfer rate. This could be attributed to the higher air velocity in the narrow channels than in wide channels. Following the phase change period, the outlet temperature drops reaching the inlet temperature at varying periods depending on the heat transfer rate.

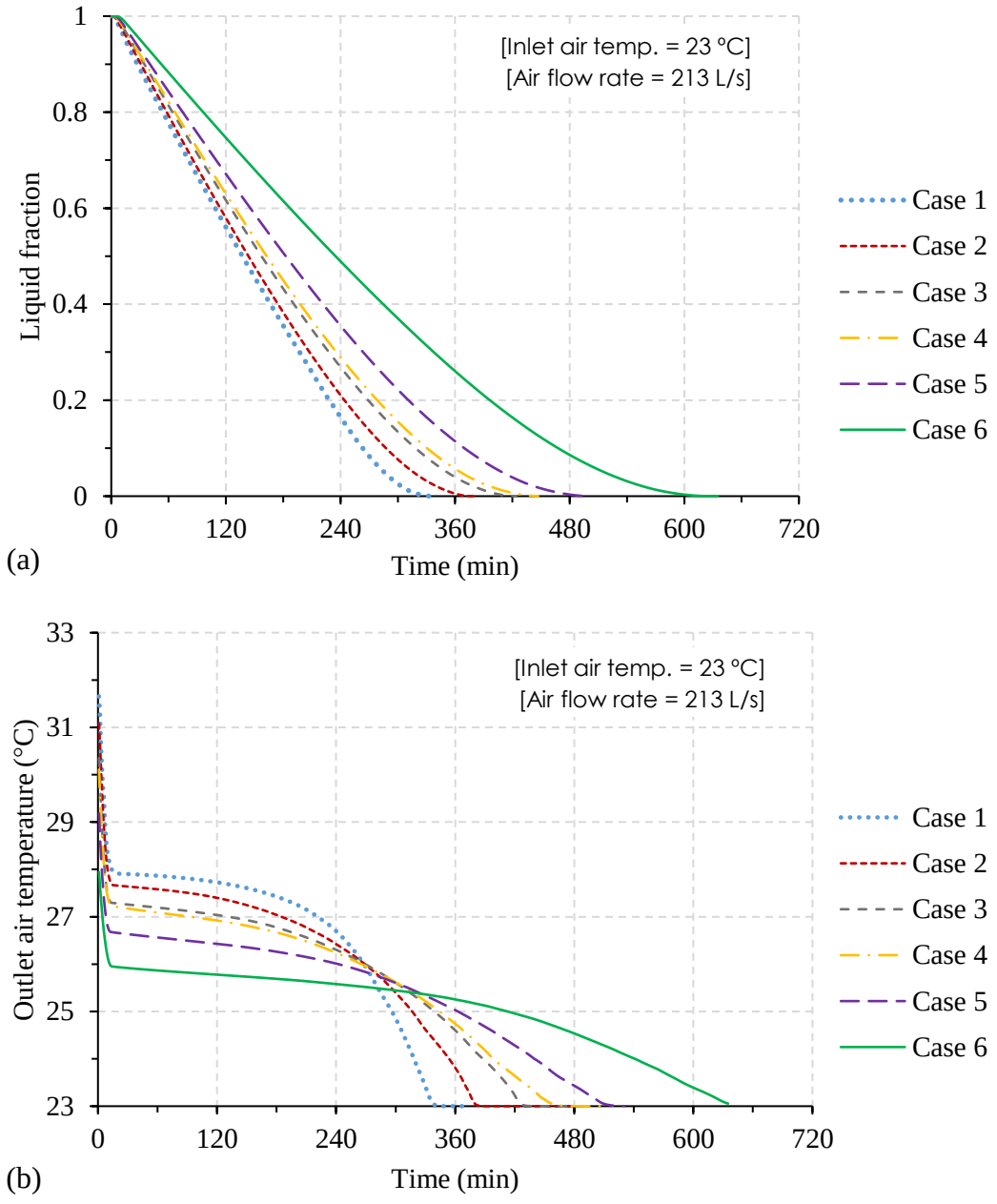


Figure 6.17: Variation of (a) PCM liquid fraction and (b) outlet air temperature during the charging process for different TES configurations.

The solidification periods for all test cases are compared in Figure 6.18. For the same PCM thickness, increasing the air channel by 5 mm leads to about 11-12% increase in the solidification time. This denotes that the rate of heat removal from the PCM is higher in the case of narrow air channels than the wide channels. For cases with the same air channels height but different PCM thicknesses (cases 2 and 4 or cases 3 and 5), the solidification period was shorter by around 16-17% in the cases with thinner PCM modules, i.e. cases 2 and 3.

It is observed from Figure 6.18 that despite the ratio of the PCM thickness to the air channel height in cases 1 and 4 is 1:1, where the main duct heights are varied slightly by 5 mm (Table 6.9), the solidification period was 24% shorter in case 1 with thin PCM modules and narrow air flow channels. Also, it can be noticed that the difference in solidification time for cases 3 and 4 was only 4%, although the main duct height in case 3 was double of that for case 4. Overall, these results prove the substantial impact of both PCM thickness and air channels height on the heat transfer rate, with a greater impact for the PCM thickness.

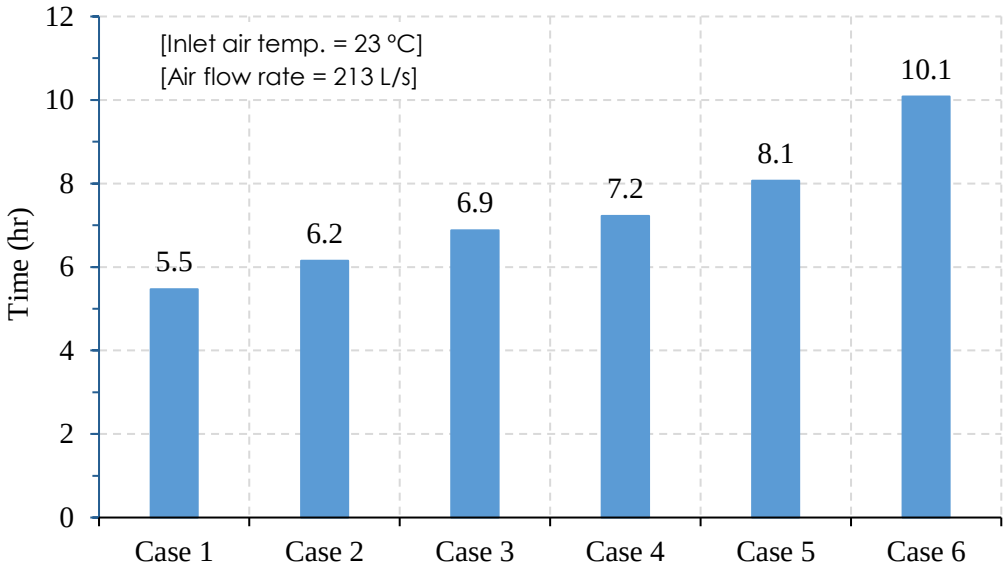


Figure 6.18: PCM solidification time for different TES configurations.

Figure 6.19 depicts temperature contours in the PCM and air domains after 4 hours of the charging process. It is obvious that the front part of the PCM modules reached the steady-state temperature at 23 °C in all cases with the highest percentage in case 1.

The temperatures at the top and bottom PCM modules were lower than in the other modules, owing to the higher rate of heat removal from the PCM caused by the cooler air flowing at the upper and lower channels compared to the air passing through the middle of the duct.

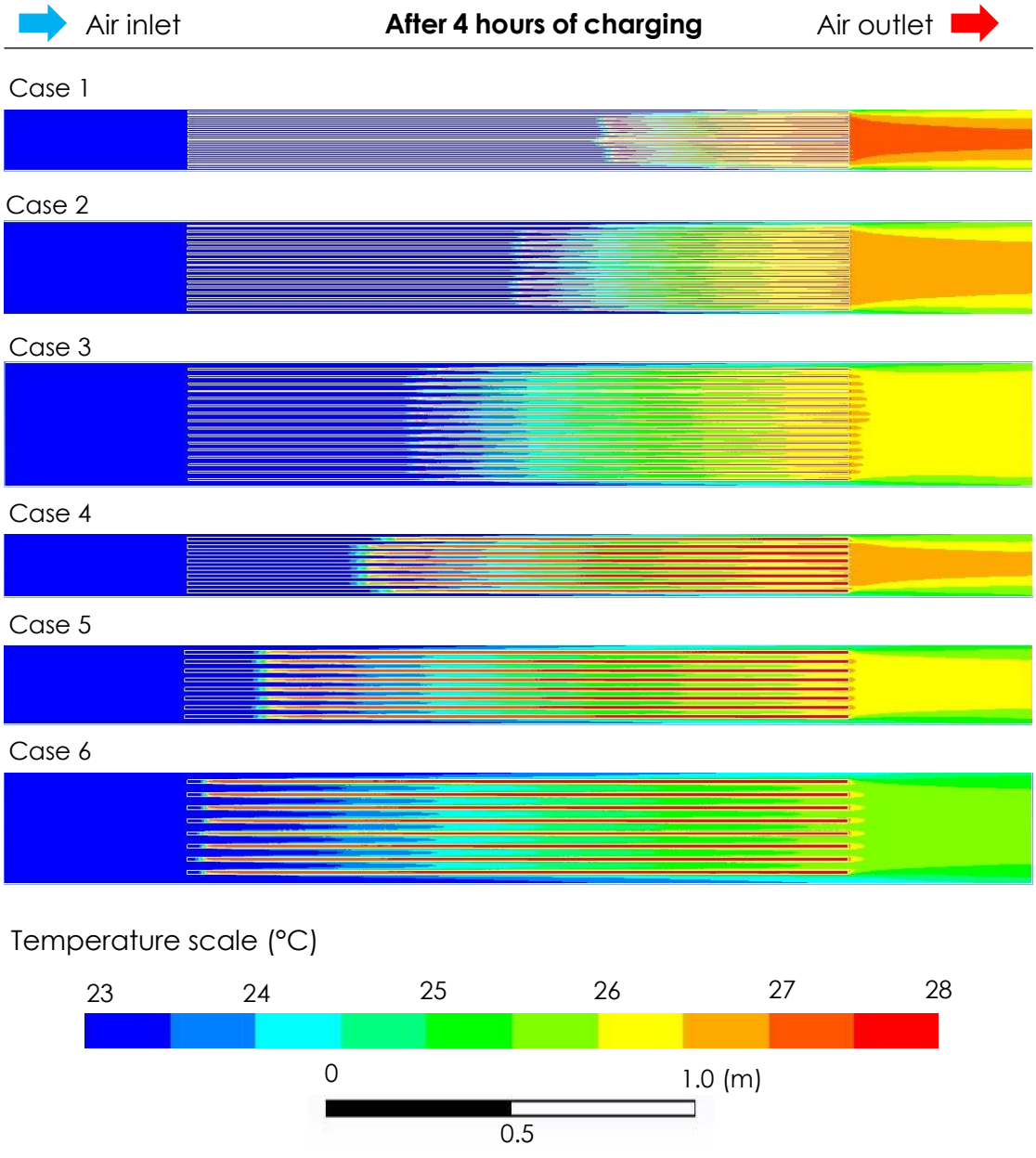


Figure 6.19: Contours of temperature distribution in the tested TES configurations after 4 hours of charging at inlet air temperature 23 °C and air flow rate 213 L/s.

6.7.4.2 PCM discharging

The variation of the PCM liquid fraction and the outlet air temperature during the discharging process are demonstrated in Figure 6.20a and Figure 6.20b, respectively, for the tested cases with different configurations.

It is clear from Figure 6.20a that the melting time varies according to the TES configuration. The quickest melting was achieved after 10.7 hours in case 1, due to the high thermal absorption rate by the PCM, as a result of the compact design with a 5 mm height for both the PCM module and the air channel. On the other hand, it took almost 15.2 hours for the full melting process to complete in case 6, where the PCM thickness and the air channels height were 10 mm and 25 mm, respectively.

As shown in Figure 6.20b, the outlet air temperatures were within the comfort zone for around 10 hours. During the transition phase, the temperatures were between 27 °C and 29 °C (PCM melting range) for cases 1-5 and higher than 29 °C for case 6. This was due to the large PCM thickness coupled with the high ratio of channel height to the PCM thickness (2.5:1) in case 6 compared to the other cases, which resulted in a poor heat transfer rate between the PCM and the HTF.

Since the variations in the comfort duration were relatively small, especially in the case of thin PCM modules, the aim during the discharging phase was to achieve the largest drop in the outlet air temperature below the inlet temperature. Configurations with thinner PCM modules coupled with small air channel height permitted a larger outlet air temperature drop. For instance, the maximum temperature drop obtained was around 10 K in case 1, when the outlet temperature was maintained at 26 °C for around 7 hours. While a lower temperature drop was achieved in case 6, where the outlet temperature fluctuated between 29 °C and 30 °C.

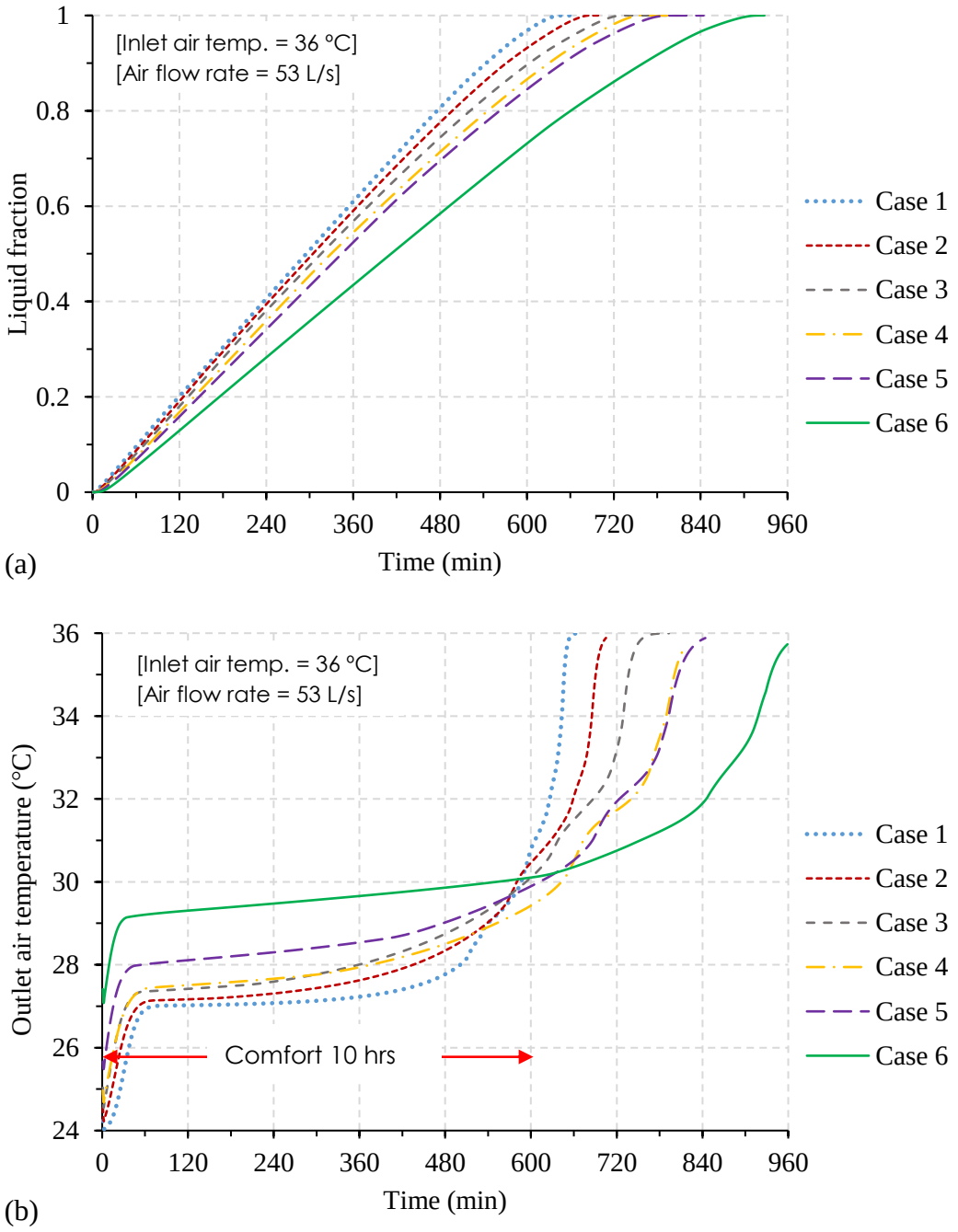


Figure 6.20: Variation of (a) PCM liquid fraction and (b) outlet air temperature during the discharging process for different TES configurations.

In most cases, it can be stated that the full melting was not the major concern during the discharging phase, rather, the main target was to cool the air to the comfort level for the longest possible period.

The required time for full PCM melting along with the thermal comfort durations for all tested cases are presented in Figure 6.21. It is obvious that the melting rate and thermal comfort durations varied slightly according to the TES configuration. For similar PCM thickness, when the air channels are increased by 5 mm, the thermal comfort period reduced by around 1%-4.5%, with lower variations in the case of thinner PCM (cases 1-3). This implies that the impact of the channel height on the thermal comfort duration is intangible in the case of thin PCM (5 mm) compared to thick PCM (10 mm). For cases with the same air channels height but different PCM thicknesses (cases 2 and 4 or cases 3 and 5), the comfort period was longer in the case of thick PCM than the thin due to the thermal resistance, as indicated earlier. However, the impact of the PCM thickness was less with increasing the air channels height. For example, the enhancement in the comfort period was 9% from case 2 to 4, and 5% from case 3 to 5. These results demonstrate that the PCM thickness is more influential on the discharging performance than the air channels height.

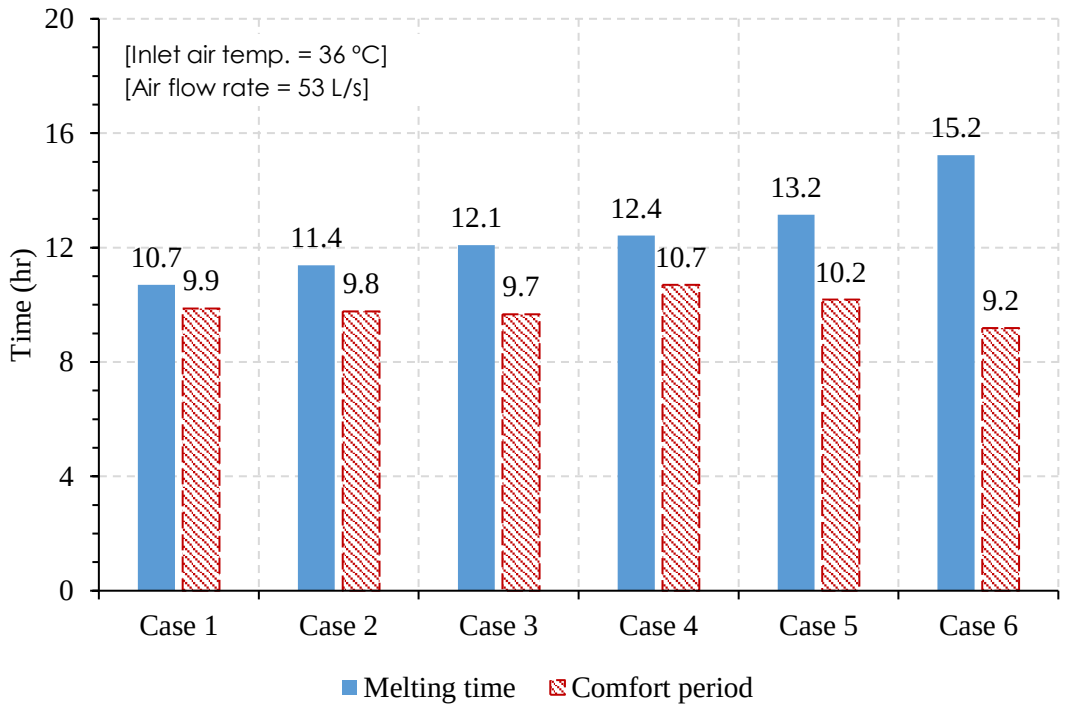


Figure 6.21: PCM melting time and comfort duration for different TES configurations.

The contours of temperature distribution in the PCM and air domains in all investigated configurations after 4 hours of the discharging process are depicted in Figure 6.22. It is evident that the melting fraction of the PCM was the highest in case 1, where the heat transfer rate was at the highest. The front section of the PCM modules melted quicker than the back modules, as a result of the gradual drop in the temperature difference between the PCM and the air towards the outlet.

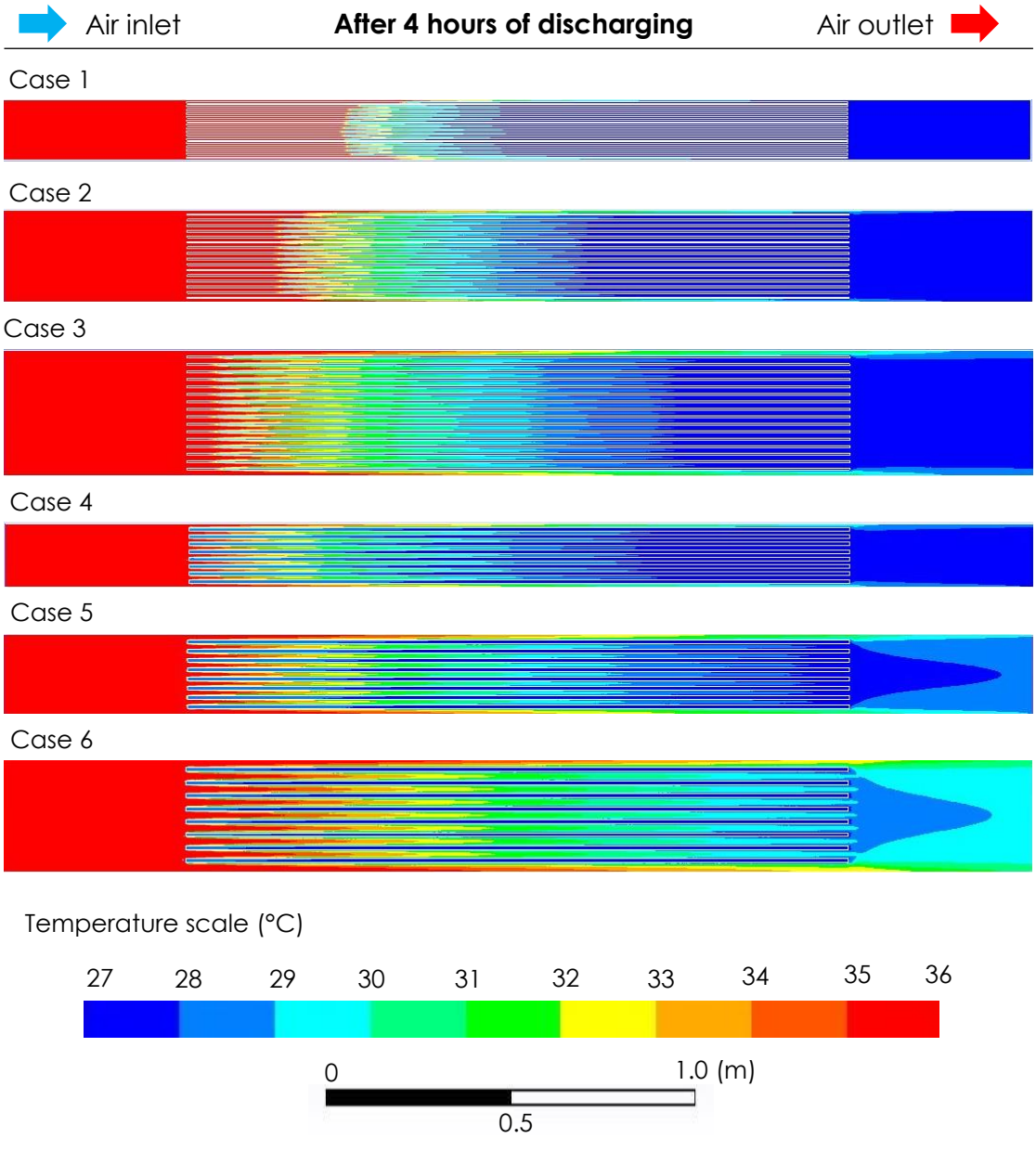


Figure 6.22: Contours of temperature distribution in the tested TES configurations after 4 hours of discharging at inlet air temperature 36 °C and air flow rate 53 L/s.

Since the variations in the comfort durations were relatively small among all test cases, besides taking into account enhancement of the charging performance, an optimised TES system comprising thin PCM modules coupled with narrow air flow channels could be considered for both charging and discharging processes. Through such a system, the charging process could be accelerated. The daytime thermal comfort could be maintained at a temperature lower than that supplied by a system with thicker PCM and wider air flow channels. In addition to the enhanced thermal performance, the compact TES arrangement requires smaller space for the system installation.

6.8 Summary

This chapter presented and discussed the results of a numerical CFD investigation of a proposed TES system for free cooling of buildings. The system was used to fulfil a cooling demand of a typical domestic room on a typical summer day in hot-arid regions. The CFD analysis indicates that there is a great potential to maintain the thermal comfort day and night under certain conditions, and hence, reducing the building cooling load. The following observations have been derived from the parametric study on the TES configuration and the operating conditions;

- The impact of inlet air temperature and flow rate on the solidification and melting of the PCM is significant. Larger temperature differences between the PCM and the inlet air are contributory to a faster PCM charging and vice versa. On the other hand, small variations are preferred during the discharging phase to maintain the thermal comfort for a long time. In the case of air flow rate, it can be adjusted based on the charging and discharging requirements. High air flow rates are recommended to complete the PCM solidification in a short time, while low air flow rates are required for gradually extracting the coolness during the discharging phase.
- A compact TES system with thin PCM modules and narrow air flow channels is the best for the acceleration of PCM solidification process during the charging phase than a system with thick PCM and wide channels. However, this would result in a faster melting and a shorter comfort period during the discharging phase. As the variations in the comfort durations are almost insignificant, particularly in the case of thin PCM, a compact TES configuration could be appropriate for both transition phases. However, higher energy consumption by the fan is predicted.
- The effect of TES geometrical configuration on the thermal performance was more obvious in the charging process than the discharging. This may be attributed to the higher air flow rates that used to accelerate the charging process than that allocated for gradual extraction of cooling from the PCM.

Chapter 7

Experimental Investigation of the PCM-Air Heat Exchanger under Steady-state Inlet Air Conditions

7.1 Introduction

This chapter investigates the charging and discharging performance of the proposed TES system experimentally under various inlet operating conditions for different arrangements of PCM modules with varying air flow channels. The chapter provides a detailed geometrical description of the TES system; demonstrates the experiment setup; system operation; test procedure; and description of the measuring instruments. The equations used to evaluate the system performance are demonstrated. The analysis and discussions of the PCM charging and discharging results under varied conditions are also presented.

7.2 Description of the system

The laboratory system for free cooling of buildings consists of an arrangement of macro-encapsulated PCM modules placed inside an aluminium enclosure; an air circulating fan coupled with a variable speed controller; and ducting system components such as circular ducts, divergent, convergent and regulating dampers. The perspective demonstrated in Figure 7.1 describes the main parts of the cooling system. Detailed specifications of all the device components and the fabrication procedure are discussed in this section.

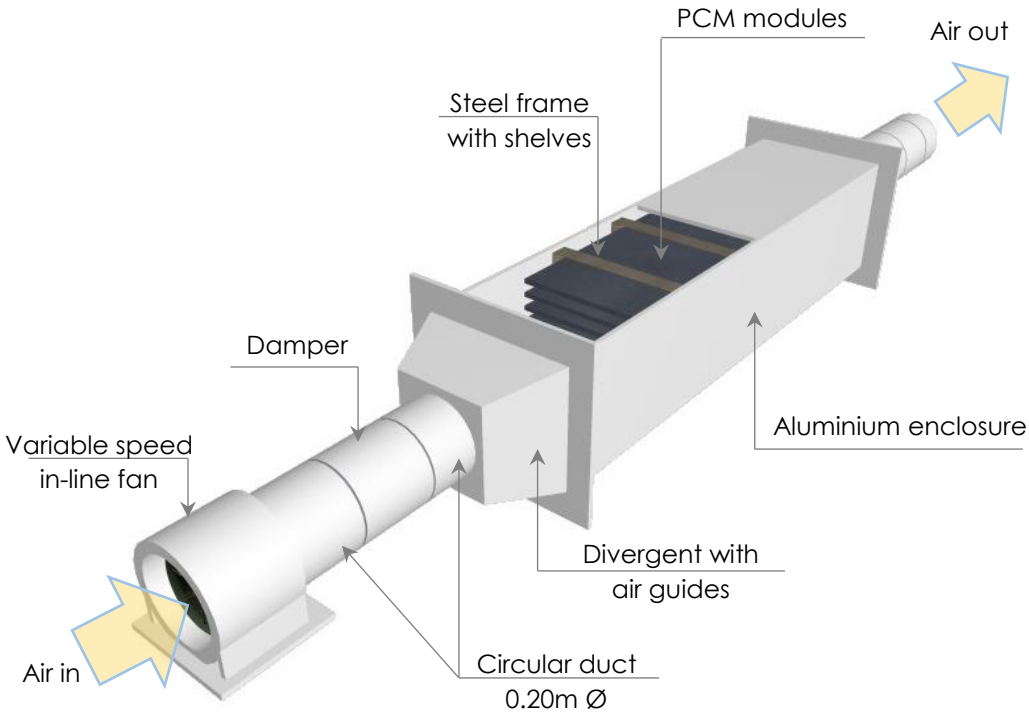


Figure 7.1: A 3D view of the experimental PCM cooling storage system.

7.2.1 TES unit

The TES unit has been designed and fabricated based on a rectangular flat module configuration. This configuration has been selected as it provides a flexible surface area to volume ratio, allows simple control of air passages through PCM modules to vary the air volume flow rate, and offers very low pressure drop compared to some other arrangements such as packed bed (Zalba et al., 2004). Furthermore, according to Zivkovic and Fujii (2001), flat PCM modules can provide a shorter solidification

period by up to 50% compared to cylinder-shaped modules of an equivalent volume and heat transfer area between the HTF and the container wall, as a result of heat transfer resistance. Regarding PCM encapsulation, aluminium has been selected due to its compatibility with paraffin, its capability to enhance the heat transfer rate as paraffin PCMs usually possess low thermal conductivity, in addition to other obvious advantages such as strength, low weight, and low corrosiveness rate (Zeinelabdein et al., 2018).

The compact storage modules (CSM) filled with RT28-HC PCM which produced by Rubitherm were used in the TES unit. The selected module comprises two particularly shaped aluminium plates sticked together at their edges and jointed at two-centred points as shown in Figure 7.2. The inner and outer sides of the module container have been coated with an anticorrosive layer. The percentage by volume of PCM filling to the air inside the container is 87.5% to 12.5% in order to contain the resultant volume expansion as a result of the phase transformation from solid to liquid.

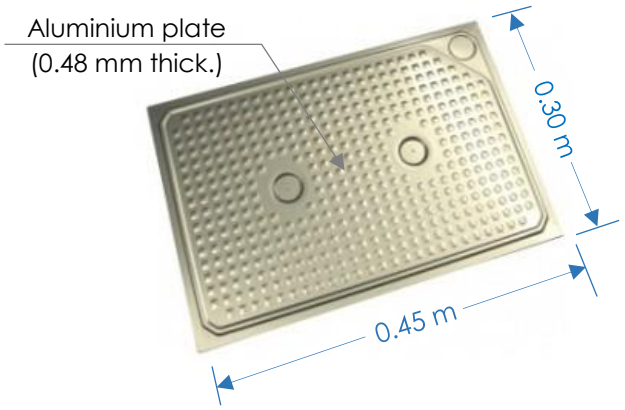
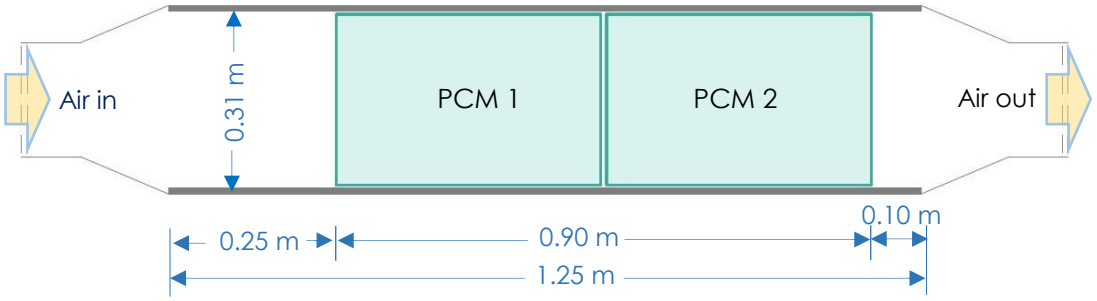
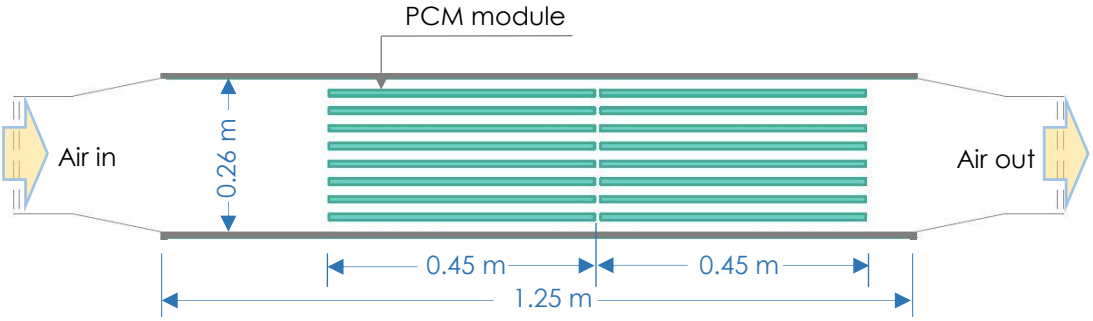


Figure 7.2: The CSM unit produced by Rubitherm GmbH (RUBITHERM).

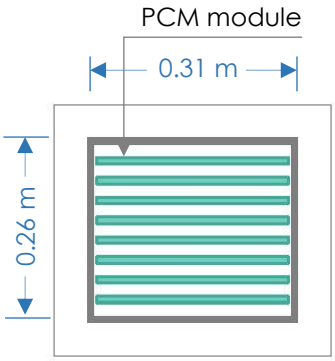
The proposed TES unit comprises 16 modules, filled with RT28-HC PCM, stacked horizontally over each other in eight parallel rows with two modules in each row. The total mass of the PCM is 8.8 kg, which is sufficient to fulfil a cooling storage capacity of 0.616 kWh. A rectangular aluminium enclosure was fabricated to accommodate the entire arrangement of the PCM energy storage modules. Details and arrangement of the PCM modules inside the main container are illustrated in Figure 7.3. The geometrical parameters of the TES system are presented in Table 7.1.



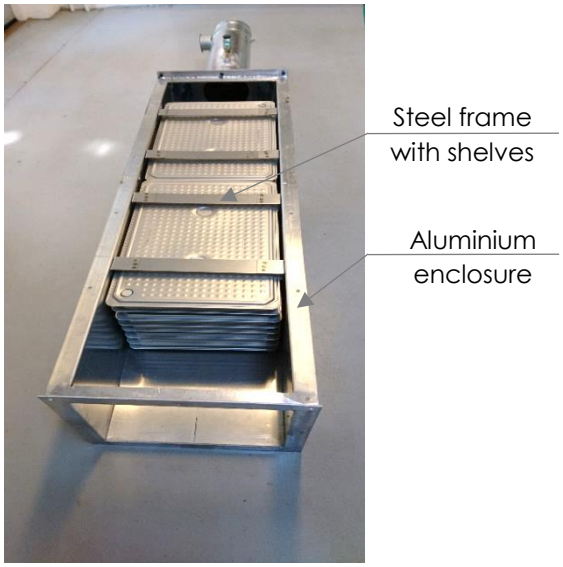
(a) Top view



(b) Side view



(c) Front/back view



(d) PCM modules arrangement

Figure 7.3: Details of the proposed TES unit.

Table 7.1: Geometrical parameters of the TES system

Parameter	**Value**
Dimensions of the PCM module	0.45 m (L) x 0.30 m (W) x 0.01 m (H)
Thickness of the module plates	0.48 mm
Tare weight of the module	0.317 kg
Weight of PCM inside a single module	0.549 kg
Dimensions of the TES enclosure	1.25 m (L) × 0.31 m (W) × 0.26 m (H)
Wall thickness of the TES enclosure	6.0 mm
Total weight of the PCM in the TES unit	8.8 kg
Number of PCM modules in the TES unit	16 modules

In the present study, both mass and thickness of the PCM were kept constant in all case studies, while the height of air passages between the PCM modules was varied in order to understand the impact of the TES compactness on the system thermal performance. Three different air channels heights 10, 15, and 20 mm were considered, and thus, three stainless steel supporting frames with shelves were constructed (Figure 7.4). In the structures with air channels height 10 and 15 mm, the PCM modules were placed in the middle of the duct, and rigid insulation boards of 22.5 mm and 45.0 mm thickness, respectively. The insulation has been used at the top and bottom sides of the main duct in order to fill the remaining interior space, as demonstrated in Figure 7.5.

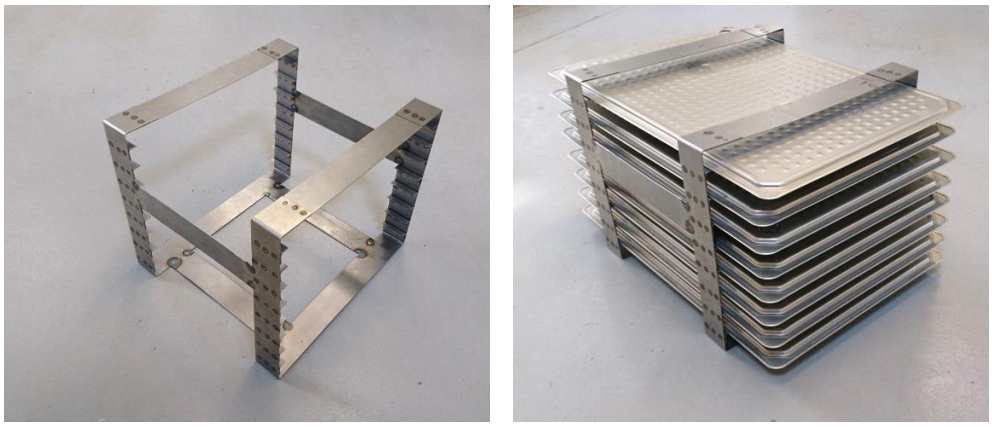


Figure 7.4: Photographs of the stainless steel supporting frame with PCM shelves.

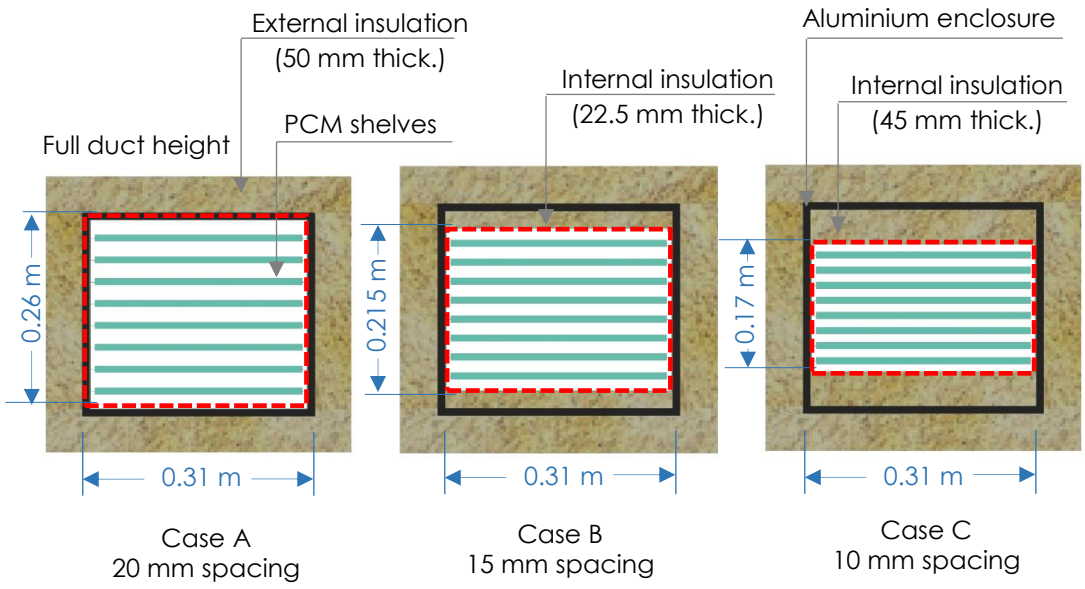


Figure 7.5: Details of the three tested PCM modules arrangements.

7.2.2 Air circulating fan

An in-line axial fan of a 150 mm diameter manufactured by Vent-Axia has been placed in the duct upstream to blow the air from an environmental chamber through the PCM modules. The fan operates with a maximum electrical power of 48 W and allows a maximum air volume flow rate of 0.16 m³/s at zero static pressure. The required volume of air is obtained by adjusting the variable speed controller coupled with the fan. Photographs of the fan and the speed controller are shown in Figure 7.6, and their main specifications are given in Appendix A (Vent-Axia).

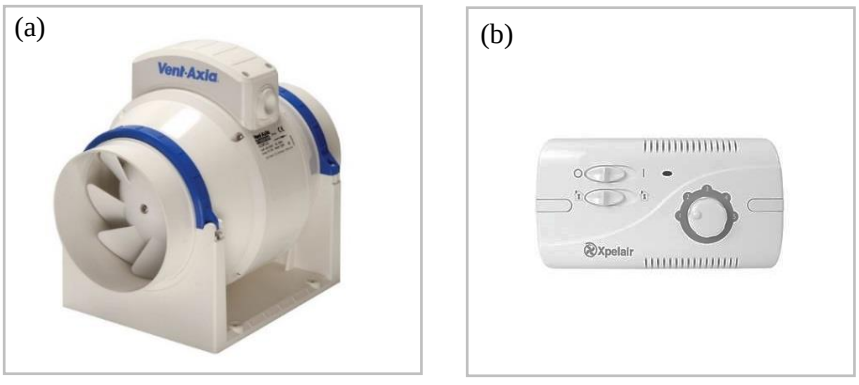


Figure 7.6: Photographs of the (a) axial flow fan and (b) the fan speed controller.

7.2.3 Air ducting system

Two single blade regulating dampers made of 0.8 mm mild steel casing and 1.2 mm blade thickness have been fitted at the inlet and the outlet of the PCM energy storage for air flow control (Figure 7.7a).

Air guides made of 0.9 mm thick aluminium sheets were used at the inlet divergent to allow a uniform air flow distribution among all channels between the PCM modules. The divergent with the attached air guides are depicted in Figure 7.7b.

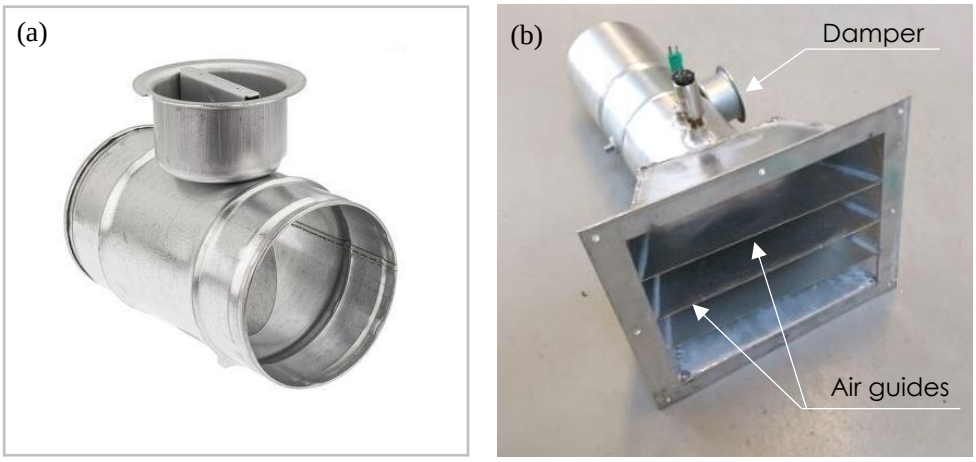


Figure 7.7: Photographs of (a) the regulating damper and (b) the divergent duct with air guides.

The entire rig was thermally insulated to reduce the heat exchange with the surrounding environment. A 50 mm thick rigid polyisocyanurate foam insulation of a thermal conductivity 0.022 W/m K coupled with low emissivity aluminium foil facings on both sides was used all around the TES unit as depicted in Figure 7.8. The aluminium foil facings have the advantage of substantially reducing the radiative heat exchange with the surrounding. Moreover, silicone pastes and rubber sheets have been used on the joints for air tightness.

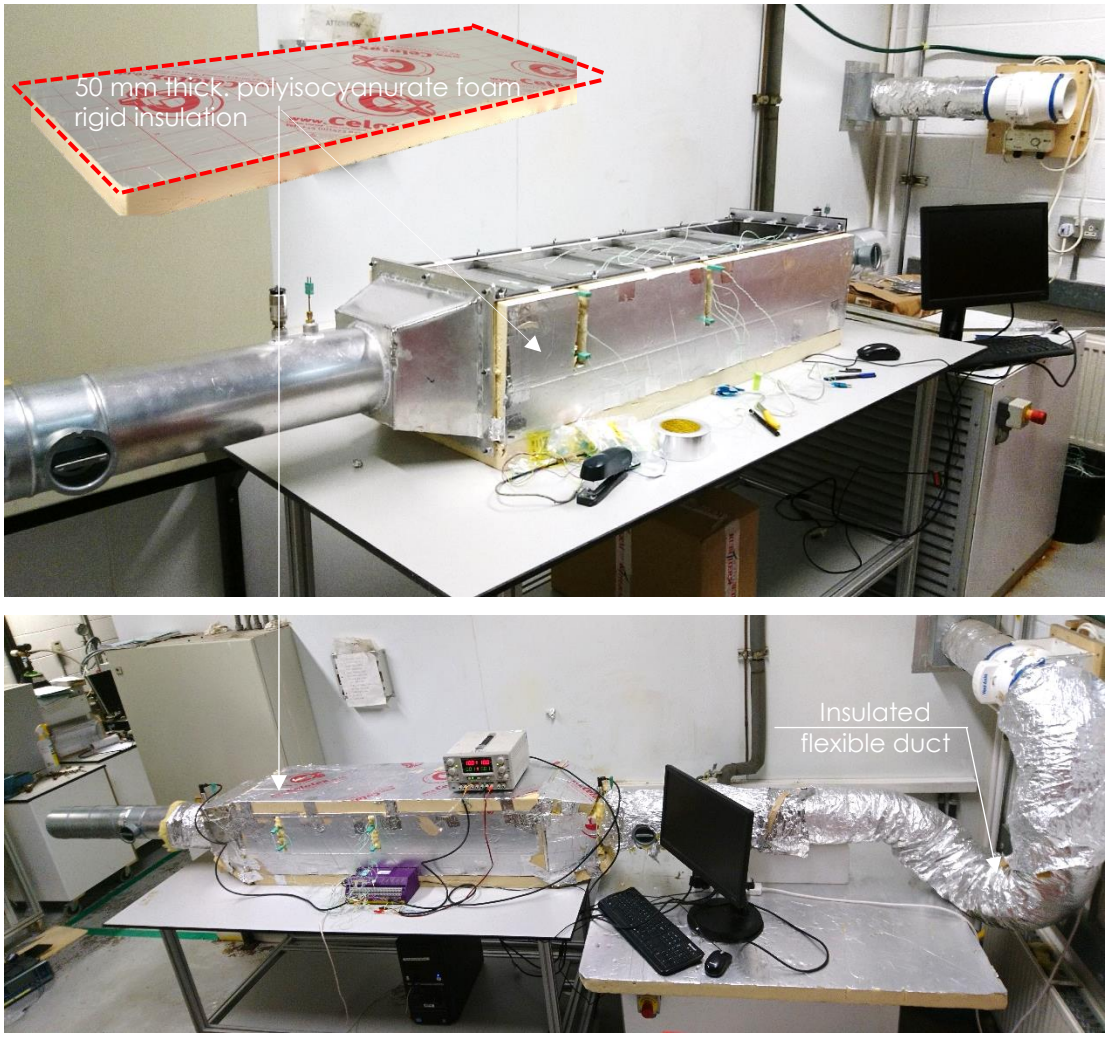


Figure 7.8: Insulation of the TES system.

7.3 Experiment setup and operation

The experiments have been carried out in a laboratory environment where an environmental chamber was used to simulate the climate conditions of the hot-arid regions. The cooling system is used as an open air circuit. The rig was installed outside the environmental chamber which used to supply air into the cooling system via a duct system, while the outlet air is discharged into the laboratory space as illustrated in Figure 7.9.

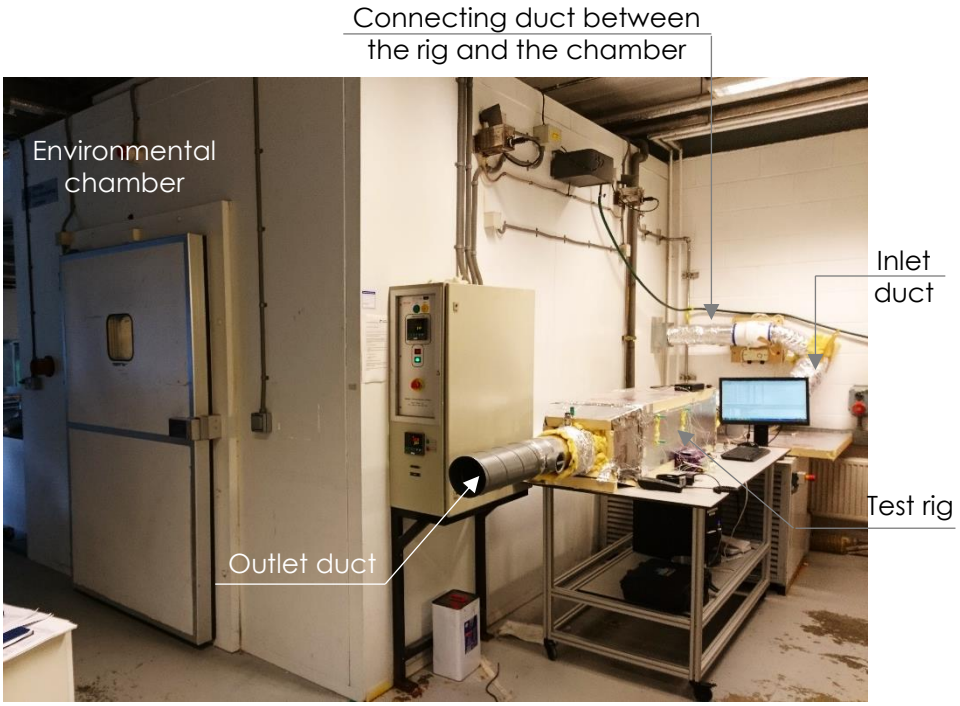
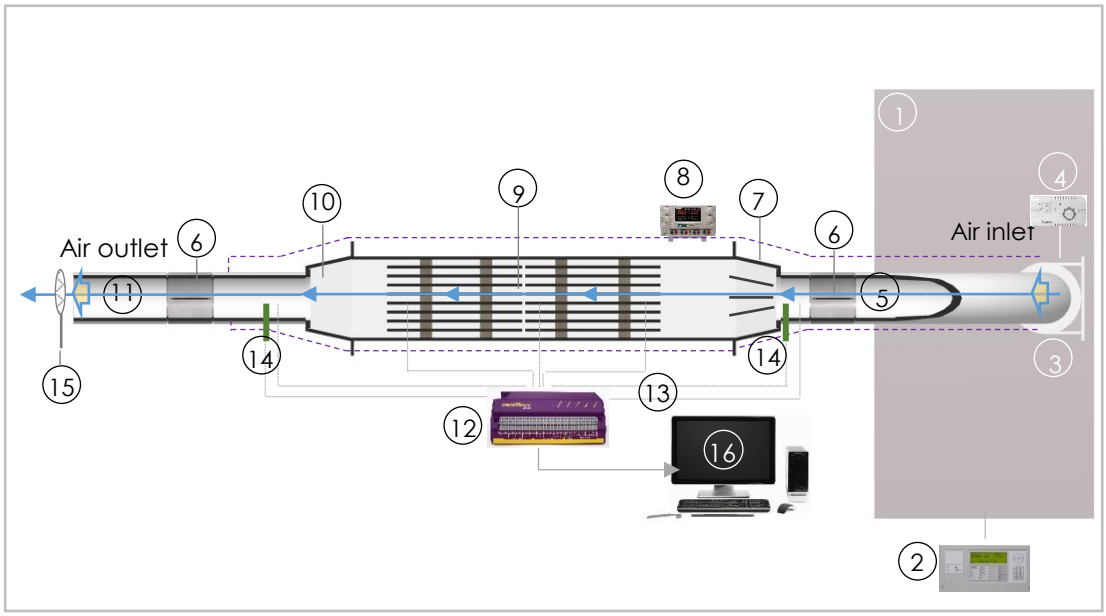
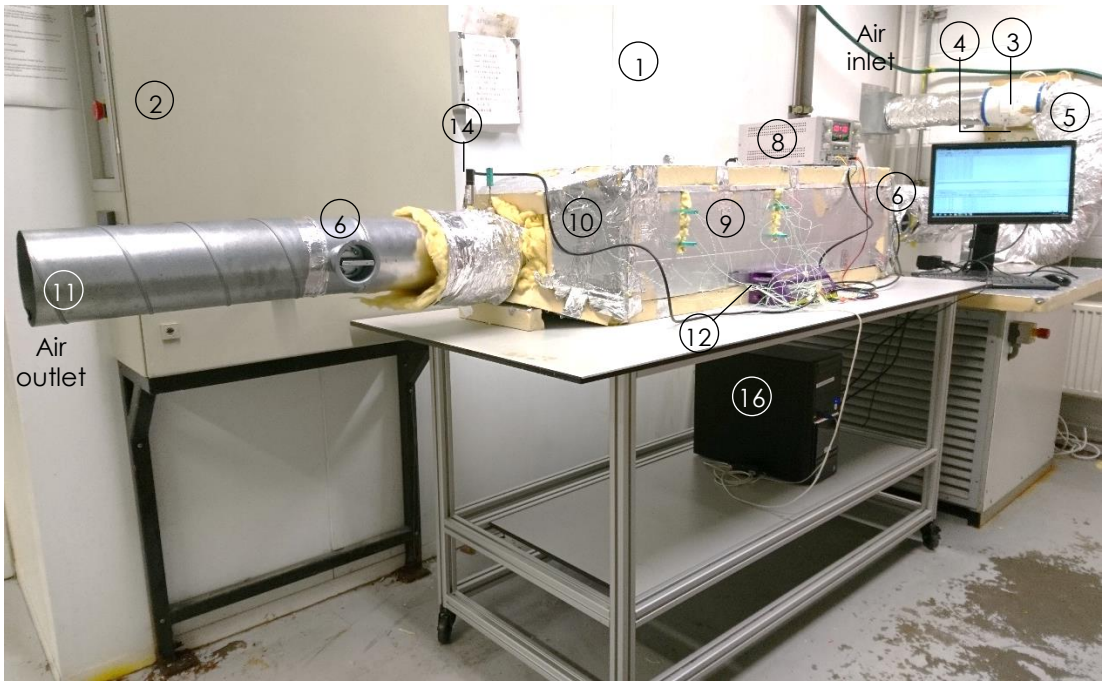


Figure 7.9: Rig connection with the environmental chamber.

A schematic diagram and a photograph of the experimental setup are illustrated in Figure 7.10. The air was the only flowing fluid in the experiments. When air temperature and humidity inside the environmental chamber (1) reach the required values set using the chamber control panel (2), the axial fan (3) is used to blow the controlled air from the chamber at a given flow rate regulated by the fan speed controller (4) through the connected insulated duct. The air circulates through an insulated flexible duct (5) and a connected divergent with air guides (7) to the main duct which contains the PCM modules (9). The air extracts or adds heat to the PCM based on the operating mode (charging or discharging) before exiting the system through the outlet aperture (11) to the surrounding space. A data-taker (12) was used to acquire data from thermocouples (13) and transducers sensors (14) and records these for analysis.





1	Environmental Chamber	2	Chamber control panel
3	Axial fan	4	Fan controller
5	Insulated flexible duct	6	Damper
7	Divergent	8	Power supply unit
9	PCM energy storage unit	10	Convergent
11	Outlet aperture	12	Data Logger
13	Thermocouples	14	Pressure transducer
15	Anemometer	16	Personal PC

Figure 7.10: A schematic and a photograph of the experiment setup.

7.4 Instrumentation setup and measurements

The measuring instruments used in the experiments included thermocouples for temperature measurement, anemometers for air flow, and a data taker for data acquisition and recording.

For temperature measurements, two types of thermocouples have been used; one to measure the temperature on the PCM container surface, and one for measuring the temperature of the air passing along the system as follows:

- The temperature on the top surfaces of the PCM containers was measured using type K thermocouples of a copper probe of a diameter 6.35 mm as depicted in Figure 7.11a. These thermocouples have an accuracy of ± 0.4% and are suitable for temperature measurements in the range 0° to + 200°C. As illustrated in Figure 7.12, eight thermocouples have been used; 1, 2, 3, and 4 along the top surface of the 8^{th} (top) row modules and 5, 6, 7, and 8 along the 4^{th} (middle) row modules.
- The air temperature at various locations in the rig was measured using type K thermocouples of a stick probe shown in Figure 7.11b. These thermocouples have probe diameter and length of 3 mm and 150 mm, respectively, the accuracy of ± 0.4%, and are suitable for temperature measurements in the range 0° to +1100°C. As shown in Figure 7.12, seven thermocouples have been used for air temperature measurement; two at the inlet (9) and the outlet (10); four distributed along the air channels (11 and 12 in the central air passage and 13 and 14 in the spacing between the top PCM modules and upper surface of the main duct); and number 15 installed out of the TES unit to measure the surrounding air temperature.

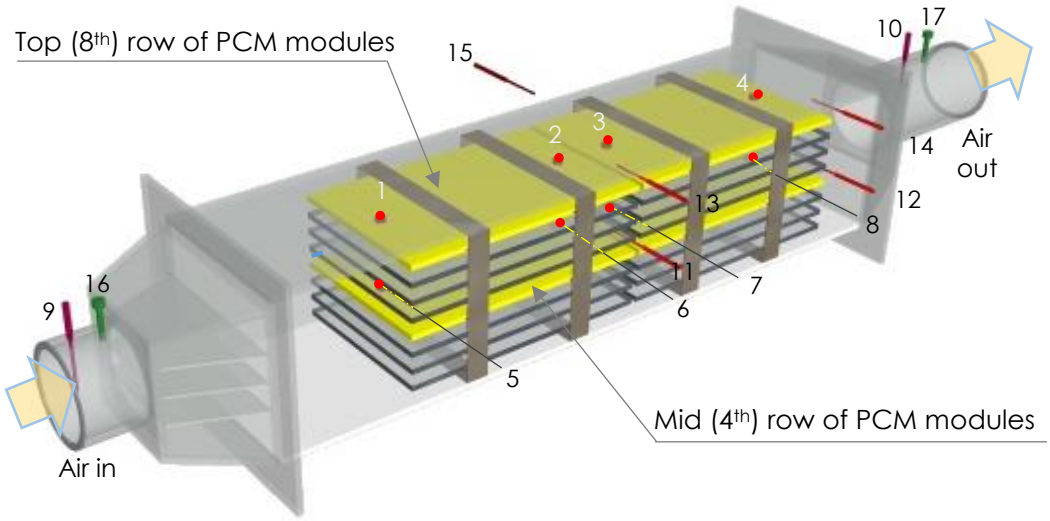
For air pressure measurements, two pre-calibrated pressure transducers (Figure 7.11c) measuring a gauge pressure in the range 0-1 bar were used at inlet position (16), and outlet position (17) of the air streams, as illustrated in Figure 7.12. These pressure transducers have an accuracy of less than ± 0.25% within the operating pressure range.

A data-Taker DT800 (Figure 7.11d) was employed to acquire data from the connected thermocouples and pressure transducers. The time interval used for data collection is 1 minute throughout the experiment, which was found appropriate to capture the temperature variation.

For air flow measurements, a handheld digital van anemometer (TSI, model LC501 as depicted in Figure 7.11e) has been used. It measures air velocities in the range 0.25-30 m/s with an accuracy of ± 1%. The air flow measurements have been taken at five locations across the outlet duct, and an average value was adopted.



Figure 7.11: Photographs showing the measurement tools; (a) Type K a stick probe thermocouple, (b) Type K a copper probe thermocouple, (c) Gauge pressure transducer, (d) DT 800 Data tacker, (e) a handheld van anemometer.



1	PCM_top1	5	PCM_mid1	9	Air inlet	13	Air_up1
2	PCM_top2	6	PCM_mid2	10	Air outlet	14	Air_up2
3	PCM_top3	7	PCM_mid3	11	Air_cent1	15	Air surrounding
4	PCM_top4	8	PCM_mid4	12	Air_cent2	16	Pressure in
						17	Pressure out

Figure 7.12: A drawing showing the positions of thermocouples and pressure sensors.

The uncertainty (U_x) of the measured parameters in the experiment was estimated utilising the method proposed by (Moffat, 1988) depending on the sensitivity of the measuring instruments ($\Delta x_1, \Delta x_2, \ldots \Delta x_n$) and the minimum value measured of each independent variable considered ($x_1, x_2, \ldots x_n$) by the following expression;

$$U_x = \sqrt{\left(\frac{\Delta x_1}{x_1}\right)^2 + \left(\frac{\Delta x_2}{x_2}\right)^2 + \cdots + \left(\frac{\Delta x_n}{x_n}\right)^2} \times 100\% \qquad (7.1)$$

For the present experiments, the uncertainty can be attributed to the inaccuracy of temperature, air velocity, and PCM mass measurements. These parameters are given as ±0.4%, ±1%, and ±0.32%, respectively. Based on equation (7.1), the overall uncertainty of the experiment was approximated at ±1.12%.

7.5 Experiments procedure and setup

The performance of the experimented unit has been investigated under both steady-state and transient inlet operating conditions as explained below;

7.5.1 Steady-state inlet operating conditions

In these experiments, a range of inlet air temperatures and air flow rates have been investigated for both charging and discharging phases. Each test was performed considering steady inlet temperature and air flow rate throughout the entire test period. The tests plan is detailed in the schematic shown in Figure 7.13. The results of these experiments are discussed in sections 7.7 and 7.8.

7.5.1.1 Charging operation Mode

In the charging experiments, the PCM was initially fully melted at a temperature 34 °C, approximately higher than its liquidus point by around 5 K. Air temperature inside the chamber was set to a constant value lower than the PCM solidus point, and air humidity was set constant at 25%. The selected air temperature and humidity were based on the ambient conditions observed during nights of summer and transitional months in Khartoum city, a hot-arid region. The rig was tested at three inlet temperatures 21, 23, and 25 °C and air flow rates 30, 50, and 70 L/s. When the fan is operated, the PCM releases its heat to the passing cold air from the chamber causing a gradual PCM solidification.

7.5.1.2 Discharging operation mode

In the discharging experiments, the PCM was initially fully solidified at a temperature approximately 22 °C, lower than its solidus point by 5 K. Air temperature inside the chamber was higher than the PCM liquidus point, and air humidity was kept unchanged at 25%, reflecting a daytime humidity in summer in Khartoum. Three inlet temperatures 32, 36, and 40 °C and air flow rates 7, 17, and 27 L/s were considered. When the fan is operated, the PCM absorbs heat from the passing air leading to a gradual melting of the PCM.

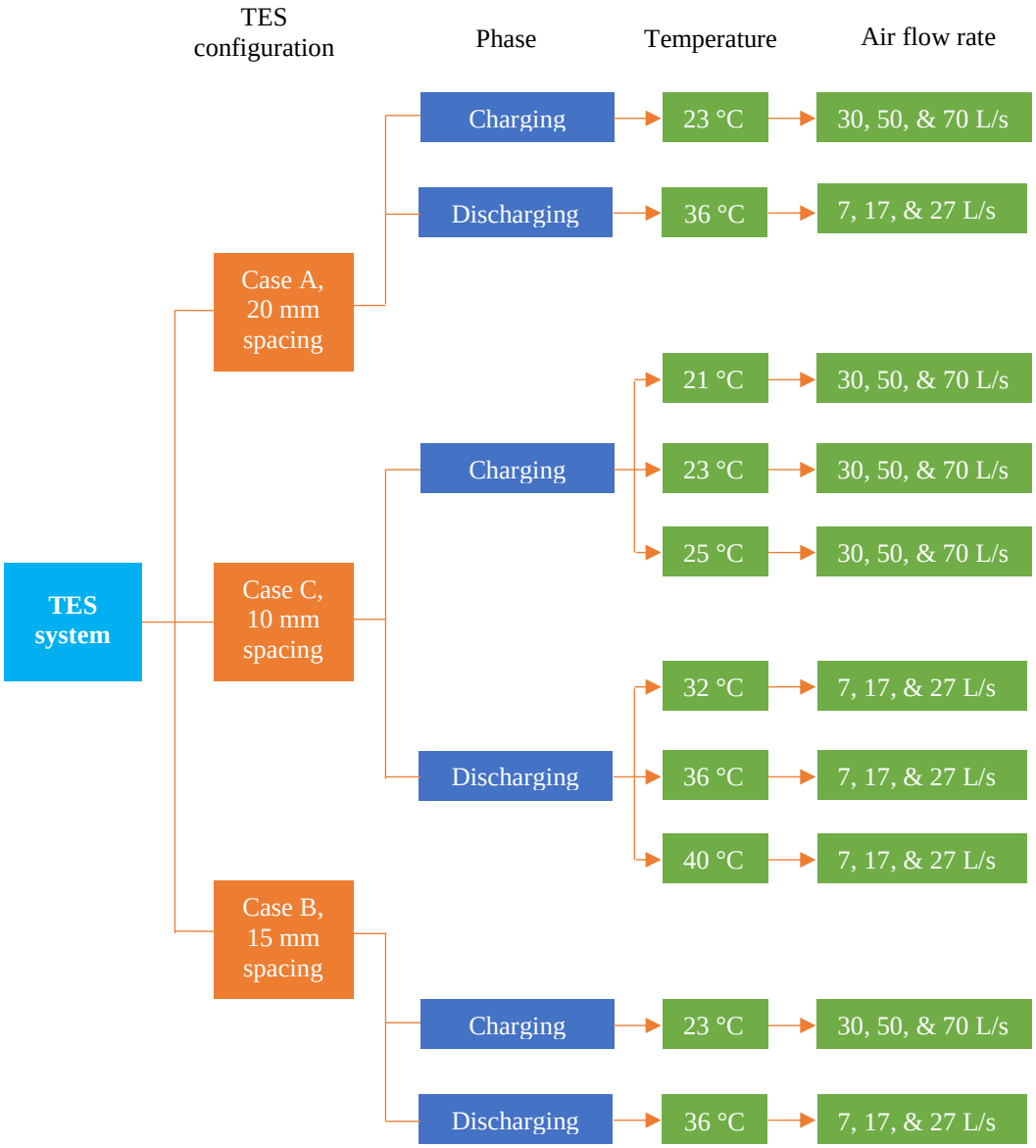


Figure 7.13: Plan of the experiments under steady-state inlet operating conditions.

7.5.2 Transient inlet operating conditions

In these experiments, the charging performance was assessed considering unsteady inlet air temperatures, simulating real profiles in summer and transitional months in Khartoum. In addition, the temperature profiles predicted by the application of the radiative cooling in Chapter 5 were used to evaluate the PCM charging when incorporating the radiative cooling system. The results of these experiments are discussed in Chapter 8.

7.6 Assessment of the PCM charging and discharging process

The thermal performance of the PCM-air heat exchanger has been assessed experimentally using the thermal energy absorbed/released by the PCM during the charging/discharging processes. Figure 7.14 shows a sketch describing the heat transfer balance of the TES unit.

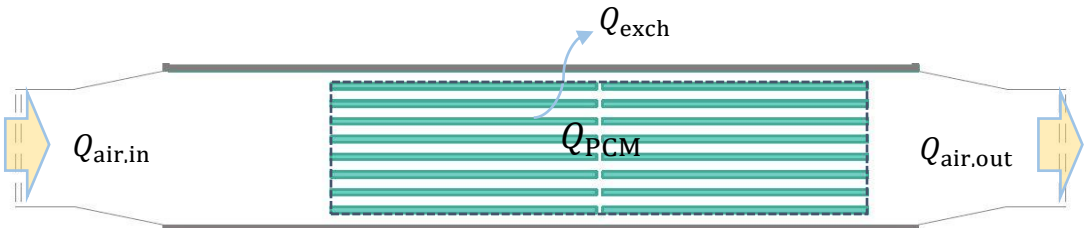


Figure 7.14: Heat transfer balance of the PCM-air heat exchanger.

Using heat balance analysis, the heat absorbed/released by the PCM (Q_{PCM}), and the heat gained/given up by the flowing air ($\Delta Q_{air} = Q_{air,in} - Q_{air,out}$) and the surrounding environment (Q_{exch}) can be expressed as follows (7.2);

$$Q_{PCM} = \Delta Q_{air} - Q_{exch} \tag{7.2}$$

Assuming constant thermal properties of the air, the heat exchange rate of the air (ΔQ_{air}) at a time-step i can be estimated knowing the temperature difference between the inlet air ($T_{air,in}$) and the outlet air ($T_{air,out}$) through the duct, the air mass flow rate ($\dot{m}_{air}$), and the specific heat capacity of air (Cp_{air}) using the following equation (7.3);

$$\Delta Q_{air} = \int_{t=0}^{i} \dot{m}_{air}\, Cp_{air}\, (T_{air,out} - T_{air,in})\; dt \tag{7.3}$$

The heat exchange rate between the TES unit and the surrounding environment (Q_{exch}) is mainly by convection from the internal flowing air to the duct, conduction through the duct wall, and natural convection to the surrounding air, and can be estimated by the relation (7.4);

$$Q_{\text{exch}} = UA\,(T_{\text{surround}} - T_{\text{TES}}) \tag{7.4}$$

where; A is the surface area of the TES enclosure, T_{surround} is the surrounding air temperature measured around the test rig in the lab space, T_{TES} is the temperature of the TES unit assumed as an average temperature of the inlet and outlet air, and U is the overall heat transfer coefficient estimated using equation (7.5);

$$U = \frac{1}{\left(\frac{1}{h_{\text{si}}}\right) + \left(\frac{\lambda_{wall}}{d_{wall}} + \frac{\lambda_{ins}}{d_{ins}}\right) + \left(\frac{1}{h_{\text{so}}}\right)} \tag{7.5}$$

where; h_{si} and h_{so} are convective heat transfer coefficients at the inside and outside surfaces of the TES unit, λ_{wall} and d_{wall} are thermal conductivity and thickness of the duct wall material, λ_{ins} and d_{ins} are thermal conductivity and thickness of the insulation used around the TES unit, respectively.

7.7 Results and discussion of PCM charging

This section analyses and discusses the results of the charging process of the TES system for free cooling of buildings. It initially describes the charging process and then assesses the impact of operating conditions, air channels height, and PCM supercooling on the charging performance of the TES system.

7.7.1 Charging process

During the charging mode, the cold air was drawn from the environmental chamber with constant temperature and flow rate over the PCM modules via a fan connected between them. The flowing air allowed heat removal from the liquid PCM which changed its state gradually to solid. The charging tests were carried out until the complete PCM solidification is achieved. The occurrence of full PCM solidification was determined at a time corresponding to the flexure point at which the outlet air temperature began to stabilise at a level equal or close to that of inlet air temperature. The measured PCM and air temperatures during full charging process are discussed for a case under the following conditions: a 10 mm distance between PCM modules; a steady inlet air temperature 23 °C; a constant air flow rate of 70 L/s; and an initial temperature of the entire system 34 °C. Furthermore, the heat exchange with the surrounding environment is discussed for the three proposed TES configurations to understand its impact on the charging process.

7.7.1.1 Temperature variation in the PCM-air heat exchanger

Figure 7.15 shows the variation in the measured temperatures during charging process along the PCM modules as detailed in Figure 7.12. PCM_mid1 to PCM_mid4 are the four points located on the top surface of the 4th (middle) row modules, whereas PCM_top1 to PCM_top4 are those at similar positions along the 8th (top) row modules. It is clear that the large temperature variation at the beginning of the charging operation allowed a high rate of heat transfer between the PCM and the HTF. This sensible cooling process takes place quickly so that the PCM temperature dropped steeply reaching its liquidus point in less than 25 minutes for the tested case. The PCM temperature continued decreasing beyond its liquidus point indicating a supercooling

of about 1.0 K for a maximum duration of 20 minutes without any phase change. Then, the temperature rose up again to the liquidus point, at which the PCM commenced the solidification process showing a gradual temperature drop with the progression of time until the full solidification has achieved. The continuation of the cold air flow through the TES device afterwards triggered a sensible heat removal from the PCM until the system reached the steady state, whereby the outlet air temperature was almost equal to the inlet air temperature.

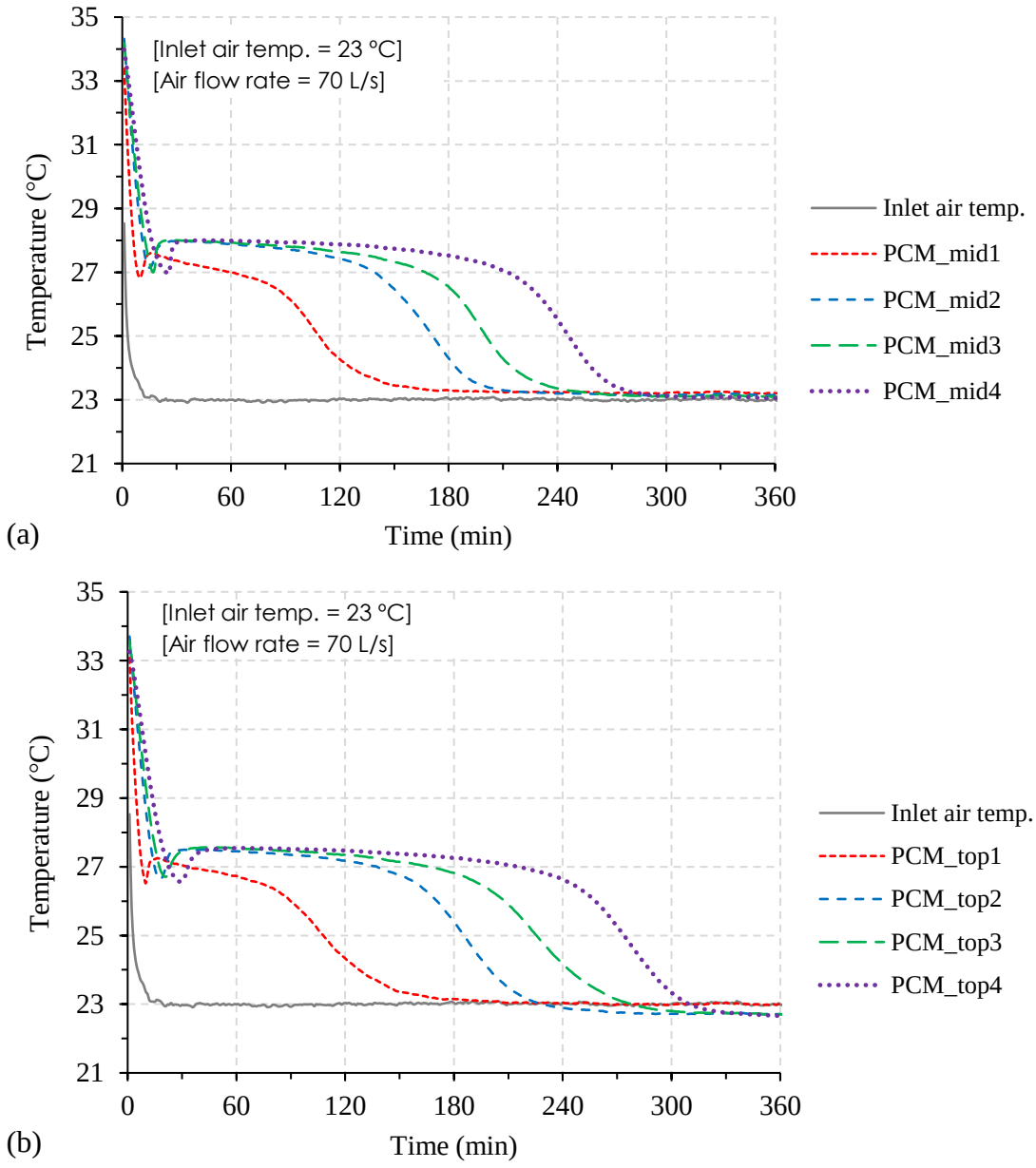


Figure 7.15: Variation of the PCM modules temperatures during the charging process at four locations along (a) the 4th-row modules "middle" (b) the 8th-row modules "top".

There was a variation in the period and the rate of solidification for the different PCM modules based on their relative locations. The solidification periods of the middle row modules PCM_mid1 to PCM_mid4 were 2.6, 3.5, 4.1, and 4.8 hours, respectively (Figure 7.15a), while the solidification periods along the top row modules PCM_top1 to PCM_top4 were 2.7, 3.7, 4.4, and 5.1 hours, respectively (Figure 7.15b). These results denote that the solidification occurs faster in the forefront modules and prolongs gradually towards the outlet, owing to the air temperature gradient along the duct. On the other hand, when comparing temperatures of the middle row modules in Figure 7.15a with their counterparts at the top in Figure 7.15b, it could be observed that PCMs in the middle of the duct solidified faster than those at the top. The variation in solidification time was small for the modules adjacent to the inlet (5 minutes between PCM_mid1 and PCM_top1), and it increased progressively with the distance augment towards the outlet (20 minutes between PCM_mid4 and PCM_top4). This variation is attributable to the higher heat transfer rate at the middle side of the duct where air velocity is relatively higher than at the upper and lower air channels. This indicates the importance of geometrical design to allow uniform and constant air flow through the PCM-air heat exchanger.

Figure 7.16 shows the variation of the measured air temperatures over the charging phase at various locations in the test rig. It is noticeable that the inlet air reached the target temperature of 23 °C in around 10 minutes and remained stable until the end of the charging period. Air temperature in the mid-region of the duct (Air_cent1 and Air_up1) was lower than that in the end region (Air_cent2 and Air_up2, respectively). This was due to a predicted drop in the heat removal factor from the PCM over the air duct as reflected in the air temperature gradient. Moreover, air temperatures at the central channels (Air_cent1 and Air_cent2) and in the upper channel (Air_up1 and Air_up2, respectively) followed a similar trend. However, the central channel air exhibited a slightly higher temperature profile by around 0.2 K during the phase change period due to the high heat transfer rate that usually attributed to the increase in air velocity in the middle region of the duct compared to the top region. Afterwards, the situation reversed so that air temperature in the central channel dropped below that at the upper channel for the rest of the charging period, owing to the solidification of the PCM in the middle modules more than the top modules.

Additionally, it is worth mentioning that the convergence between the inlet and the outlet air temperatures shown in Figure 7.16 after completion of the PCM charging denotes that the convective gain from surrounding was significantly low, i.e. the test rig was well-insulated.

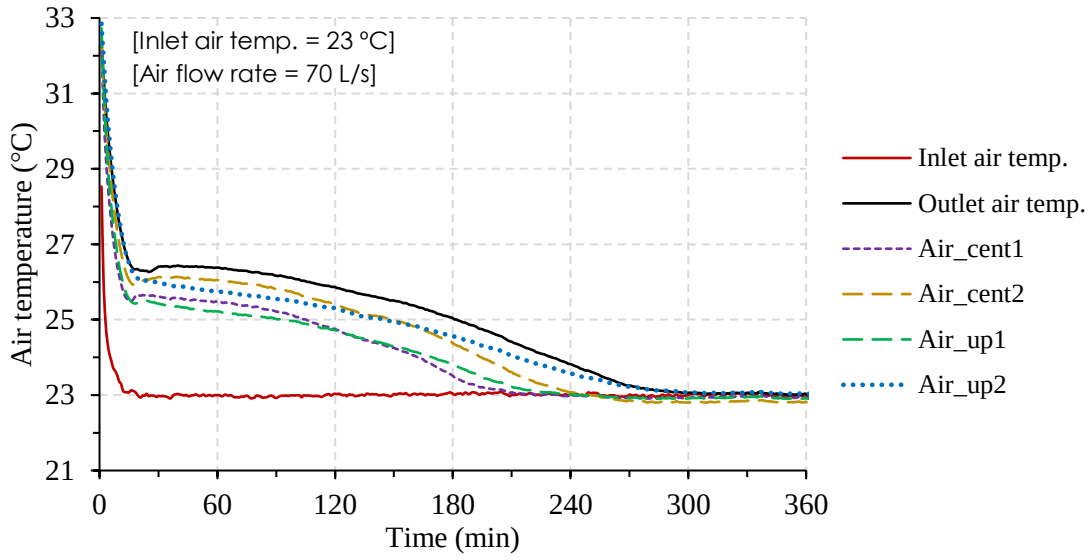


Figure 7.16: Air temperature variation in the test rig during the charging phase.

7.7.1.2 Impact of the surrounding air

The rate of heat exchange between the TES system and the surrounding has varied in the current experiments. This is mainly due to the surrounding air temperature variation throughout the tests period, besides the dissimilarity in thermal resistance of the investigated three TES configurations of the different air channels heights. Therefore, the heat exchange rate was estimated for the three tested configurations under all adopted operating conditions to find out its impact on the thermal performance of the PCM energy storage. Selected data are presented in Figure 7.17 and Figure 7.18, when the inlet air temperature was 23 °C and the air flow rate was at 70 L/s.

Figure 7.17 illustrates the measured air temperature around the test rig during charging experiments of the three tested cases. It is clear that the surrounding air temperature has varied showing an incessant rising with the time during each test. In the working environment of the laboratory, the surrounding air temperature was difficult to be

maintained at a constant level due to continuous heat generation by the environmental chamber drivers located inside the laboratory space. It should be noted that the trend of air temperature around the test rig nearly resembles the room temperature during summer nights in hot-arid regions (28-31 °C) if only night ventilation is allowed.

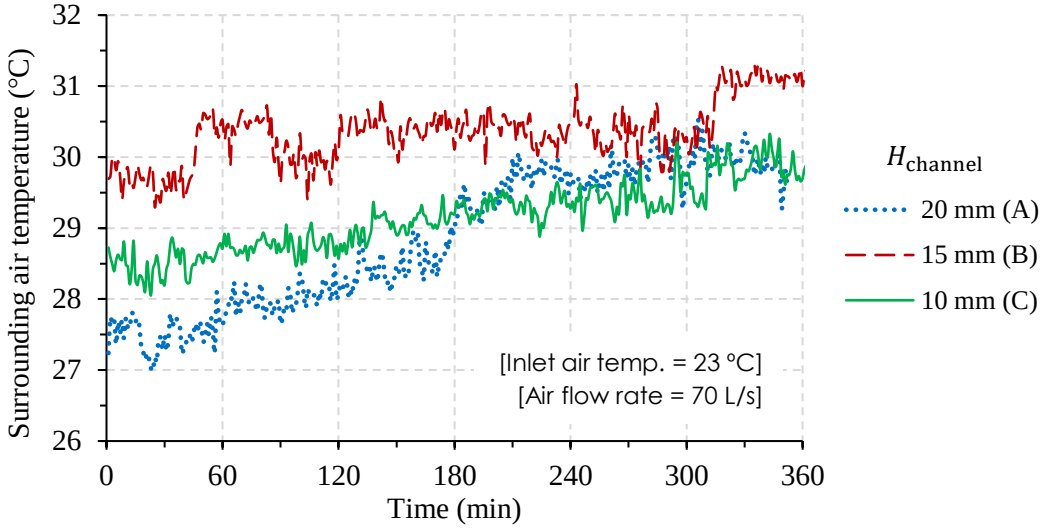


Figure 7.17: Surrounding air temperature during charging experiments of the three tested TES configurations.

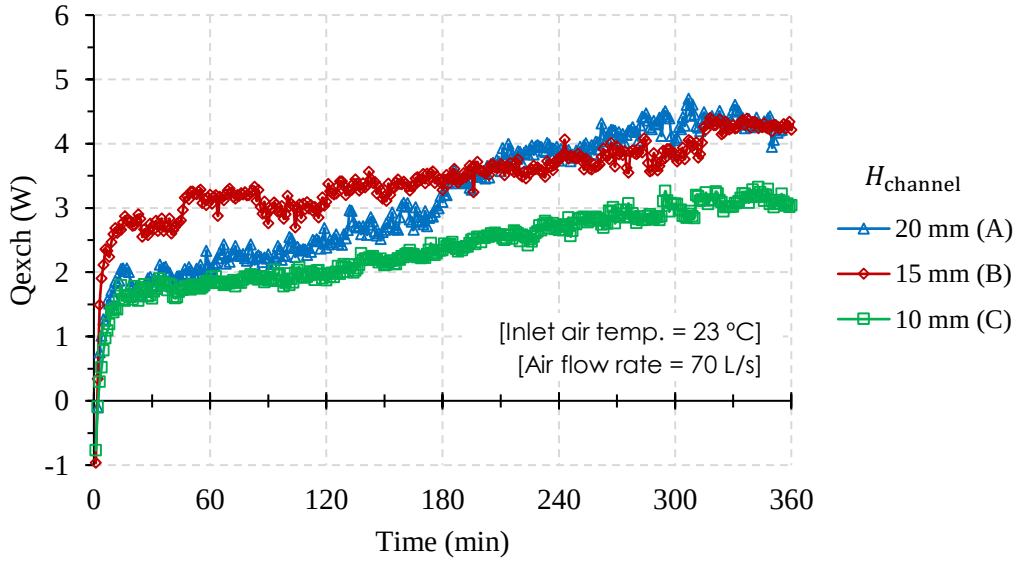


Figure 7.18: Heat exchange rate with the surrounding during charging experiments of the three tested TES configurations.

As presented in Figure 7.18, heat gain by the system was present due to the lower temperature of the TES unit than the surrounding air except for the initial 15 minutes. The heat gain has increased with the time as the surrounding air temperature rose and the PCM temperature cooled down simultaneously. The heat gain is varied between 2.0-4.5, 3.0-4.5, and 2.0-3.0 W for the arrangements A, B, and C, respectively. The highest rate of heat gain was achieved in case B of a higher thermal resistance than case A due to the higher surrounding air temperature experienced during the test as shown in Figure 7.17.

Significantly, under all tested conditions, the rate of heat gain was relatively small in the range of 1-4% of the average PCM cooling rate during the transition period. The heat loss range in the current experiments indicates that the utilised insulation is vastly sufficient and heat gain from the surrounding appeared to be having a negligible impact on the charging results.

7.7.2 Influence of inlet operating conditions

This section discusses the impact of both inlet air temperature and air flow rate on the thermal performance of the PCM-air heat exchanger during the charging process based on the tests conditions shown in Table 7.2. Moreover, the PCM solidification time was discussed under all combinations of the adopted charging air temperatures and flow rates.

Table 7.2: Inlet air conditions for the charging process.

	PCM initial temp.	**Inlet air temp.**	**Air flow rate**
Inlet air temp. test	34 °C	21, 23, and 25 °C	70 L/s
Air flow rate test	34 °C	23 °C	30, 50, and 70 L/s

The impact of inlet air temperature on the PCM charging is shown in Figure 7.19, which compares the outlet air temperatures and the cooling rate of the PCM for the three adopted inlet air temperatures, during the charging phase. It is evident that the higher the inlet air temperature, the lower the rate of heat removal from the PCM. Decreasing the inlet air temperature by 2 K from 23 to 21 °C reduced the solidification time by almost 25% from 4.8 to 3.6 hours, while increasing the inlet air temperature

by 2 K from 23 to 25 °C extended the solidification time to almost double (7.2 hours). These findings demonstrate that the charging performance is largely subject to the temperature difference between the inlet air and the PCM liquidus point, the larger the variation, the faster the solidification and vice versa.

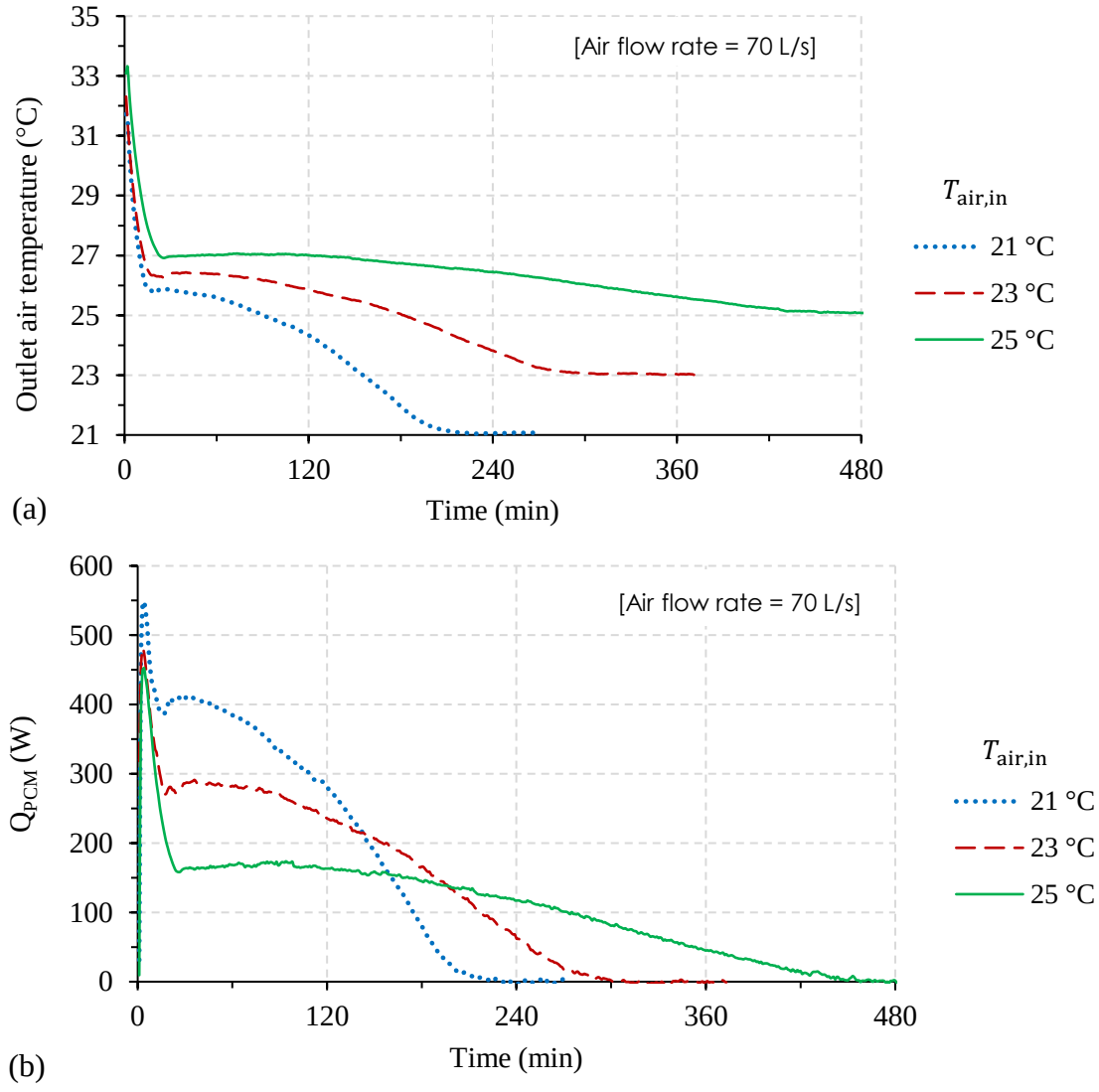


Figure 7.19: Impact of inlet air temperature on PCM charging; variation in (a) the outlet air temperature, and (b) the PCM cooling rate.

The impact of air flow rate on the PCM charging is presented in Figure 7.20, which shows the variation of the outlet air temperatures and the PCM cooling rate for the examined air flow rates over the charging period. It is evident that the higher the air flow rate, the higher the cooling rate during the phase change period, hence, the

quicker the PCM solidification rate and vice versa. The rate of heat removal from the PCM was higher at the beginning of the charging process and declined gradually as the temperature difference between the PCM and the HTF decreased. Increasing the air flow rate by 40% from 50 to 70 L/s reduced the solidification time by nearly 24% from 6.3 hours to 4.8 hours, while reducing the flow rate by a similar percentage from 50 to 30 L/s increased the solidification time by 50% to about 9.4 hours. Thus, it is noted that the air flow rate has a significant influence on the PCM charging time, and therefore higher air flow rates are highly recommended to effectively exploit the available natural cooling and accelerate the solidification process.

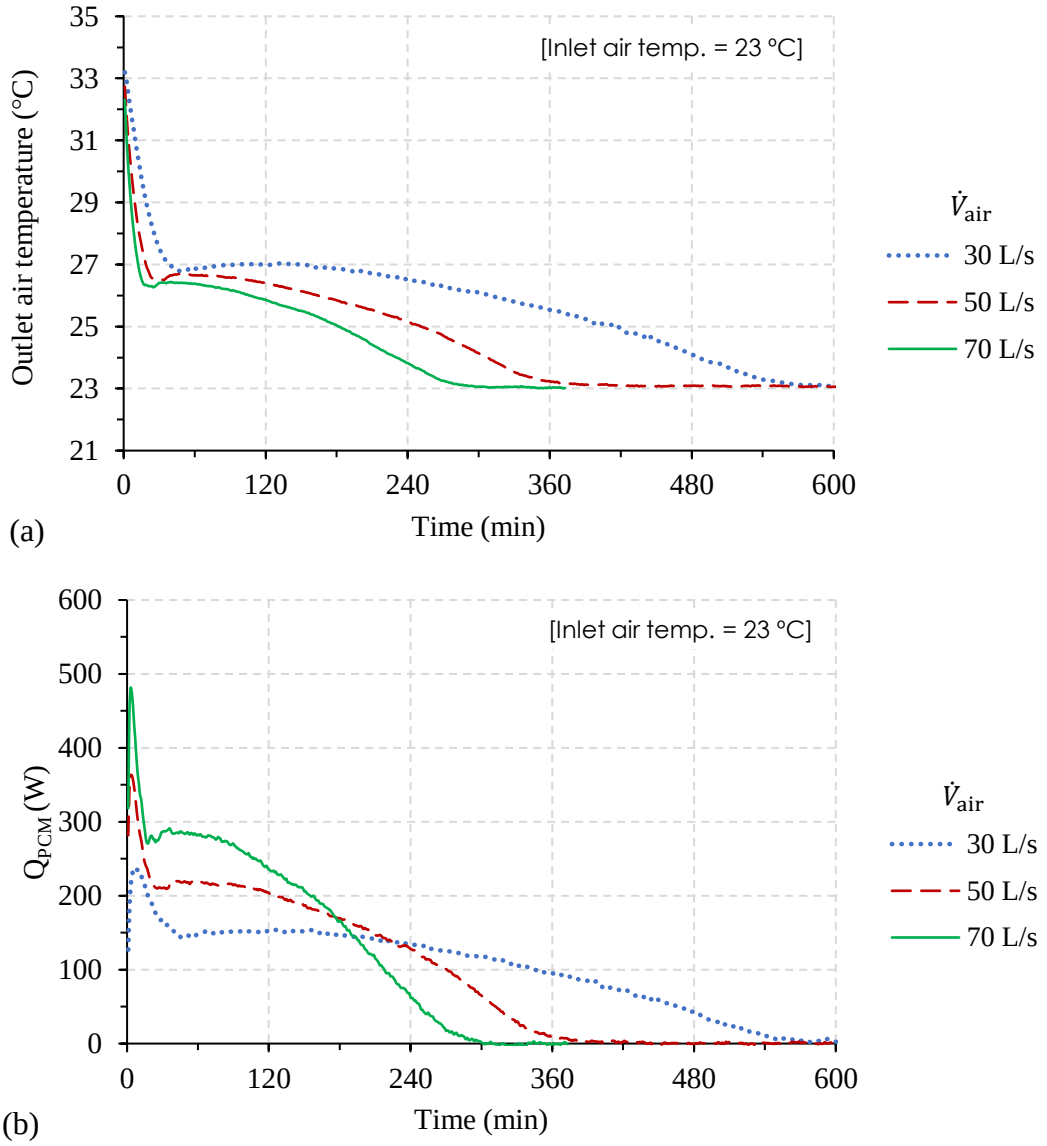


Figure 7.20: Impact of air flow rate on PCM charging; variation in (a) the outlet air temperature, and (b) the PCM cooling rate.

The combined influence of both inlet air temperature and air volume flow rate on PCM charging time is examined in order to find out the best time required for attaining a complete PCM solidification. As illustrated in Figure 7.21, each inlet air temperature has been tested under the three adopted air flow rates. It is observed that, at any air flow rate, an inlet air temperature rise from 21 to 23 °C increased the solidification time by around 33%. An additional rise in temperature by 2 K to 25 °C enhanced the solidification time by 50%, which represents doubles the time compared to the lower charging temperature of 21 °C. That means the increase of solidification time with inlet air temperature rise is not linear. It illustrated a gradual rise at low inlet air temperature range, which changed to a sharp rise at the inlet air temperature range close to the PCM solidus point. On the other hand, for any charging air temperature, the solidification time alteration with air flow rate has a nonlinear relation. It illustrated a significant drop by about 33% at low air flow rates from 30 to 50 L/s and a gradual drop by around 24% at high air flow rates from 50 to 70 L/s.

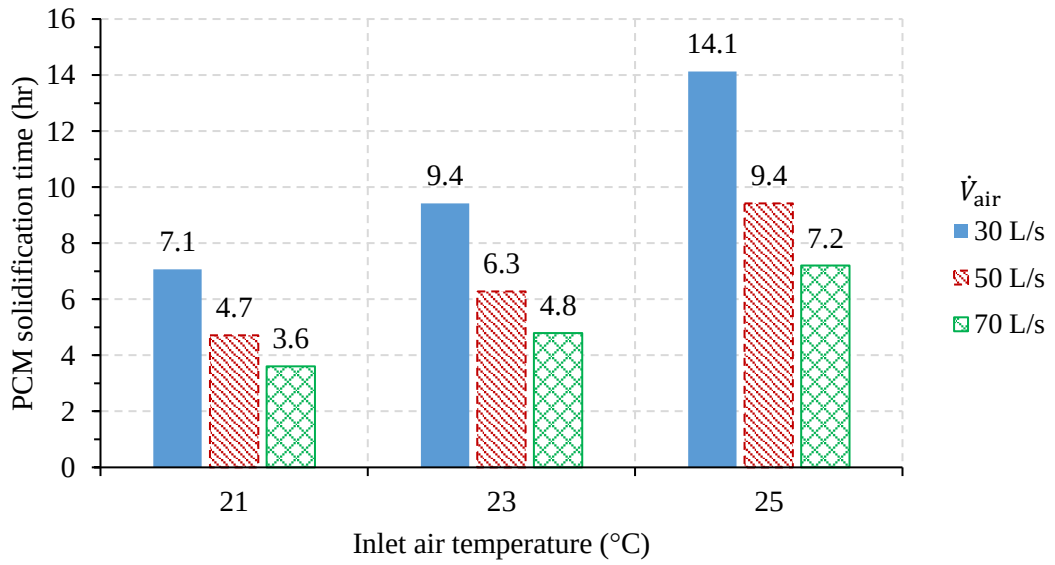


Figure 7.21: PCM solidification period under operating conditions of the charging process.

Additionally, observation of Figure 7.21 demonstrates that combining a high inlet air temperature with a high air flow rate in many cases may trigger a solidification time almost similar to one reached by a lower charging temperature at a lower air flow rate. For instance, the solidification periods obtained with inlet air temperature 25 °C at air flow rate 70 L/s and with inlet air temperature 21 °C at 30 L/s were 7.2 hours and 7.1

hours, respectively with a discrepancy less than 2% (8 minutes). Thus, the air flow rate should be carefully considered based on the charging ambient air temperature to harness the most out of free cooling in the required time using a low input power to the fan.

7.7.3 Influence of air channels height

In order to maximise the amount of cooling stored in the PCM, the impact of the TES compactness was investigated. The number of PCM modules was kept constant, and only the distance between the modules was varied. Three cases were tested A, B, and C with air channels heights of 20, 15, and 10 mm, respectively. The test was carried out under operating conditions shown in Table 7.2 above.

Figure 7.22 compares the outlet air temperature and the heat transfer rate for the three tested cases at the inlet air temperature of 23 °C and the air flow rate of 70 L/s. It is noticed that the outlet air temperature in the case of the smaller channels height arrangement was higher during the initial half of the charging period and lower during the latter period than the larger channels height arrangement (Figure 7.22a). The TES system with a smaller channels height exhibited a higher cooling rate during the phase change period compared to that of larger channels height (Figure 7.22b). This is attributed to the enhanced heat transfer rate yielded by air velocity increase inside the narrow channels, leading to a faster solidification time. Moreover, it is clear that a longer solidification time is required with larger air flow channels. At inlet air temperature 23 °C and air flow rate 70 L/s, the chrging periods were 5.6, 5.2, and 4.8 hours for cases A, B, and C, respectively, with the narrow channels achieving faster solidification.

The required time for achieving a complete PCM solidification can be used to assess the compactness of the TES design by minimising or optimising the height of the air channel. The charging time for the three TES arrangements under adopted operating conditions is presented in Figure 7.23. It can be clearly seen that the increase of PCM charging time with the air channels height is varied according to charging inlet air temperature. For the considered range of inlet temperatures (32-40 °C), minimising the air channels height from 20 to 10 mm accelerated the melting time by 11-14%,

when the air flow rate was 70 L/s (Figure 7.23a). On the other hand, the delay in the PCM charging with the air channels height increase is also varied depending on the air flow rate. However, the variations were generally small. For the considered range of air flow rates (30-70 L/s), the reduction in the PCM charging period was in the range 10-14% when lessening the air channels height from 20 to 10 mm, at the inlet air temperature 23 °C (Figure 7.23b).

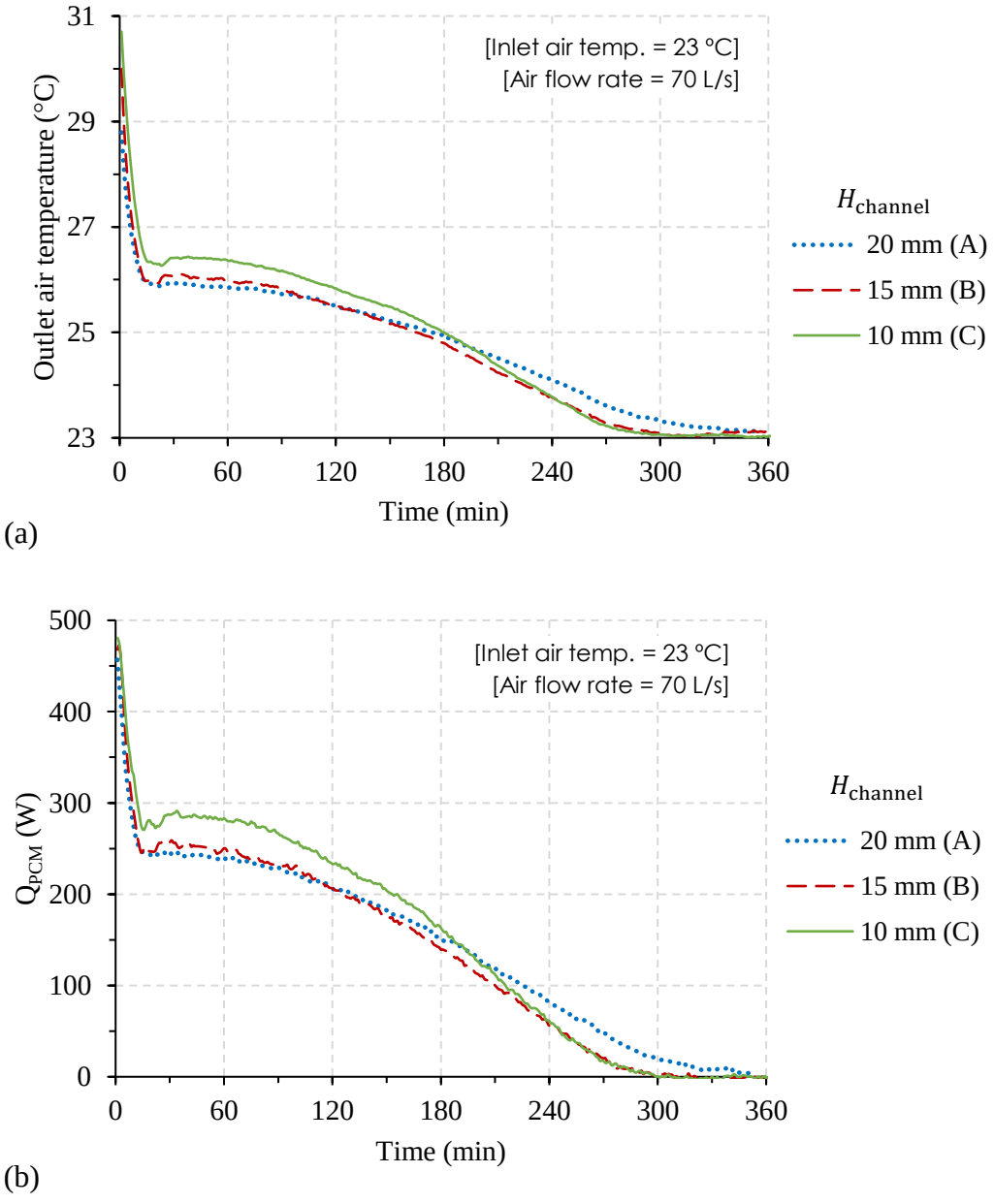
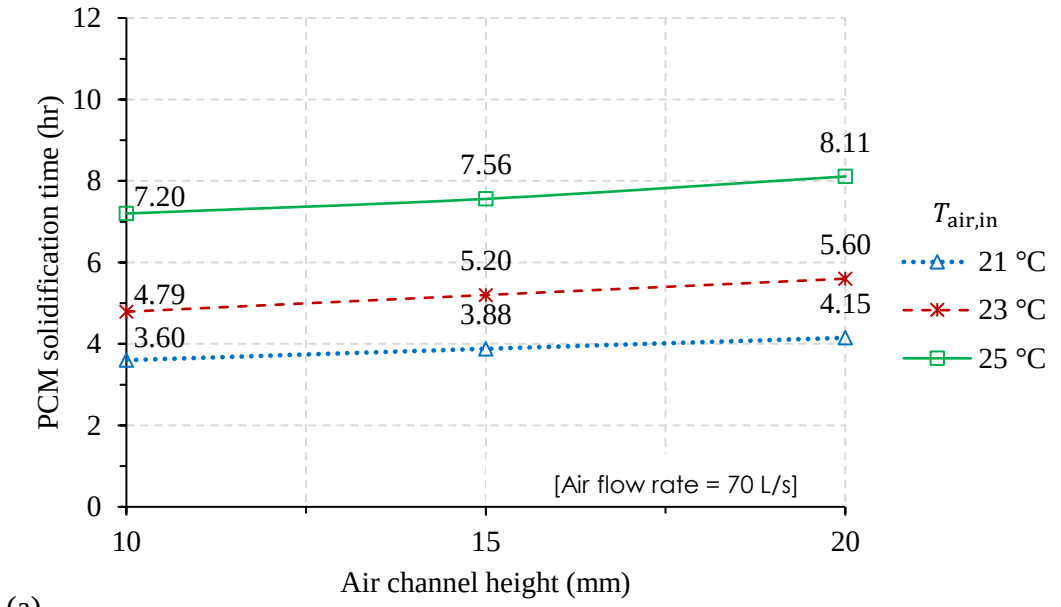
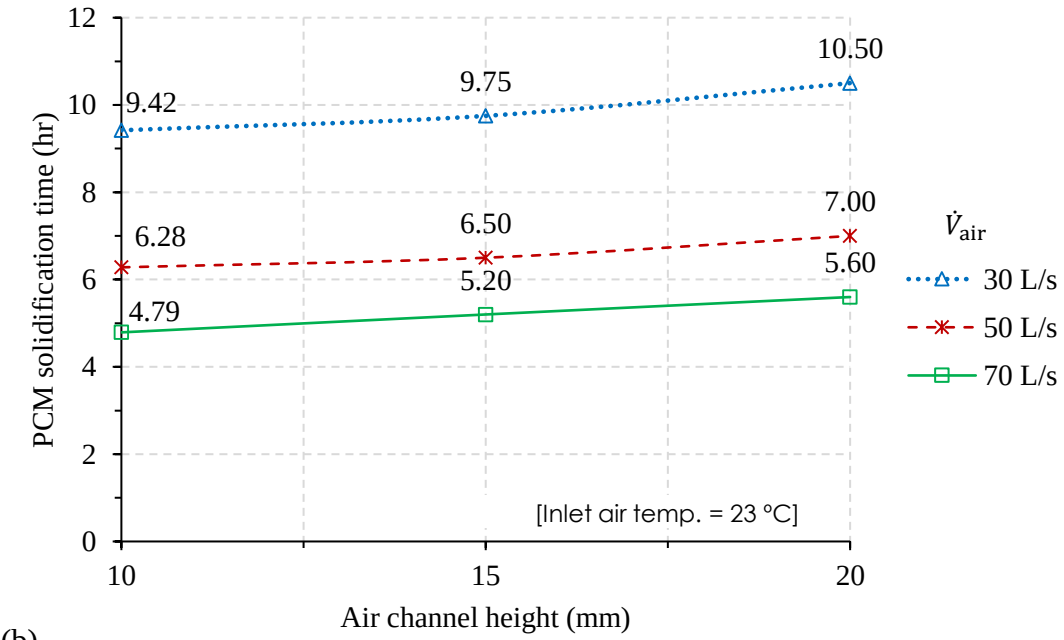


Figure 7.22: Impact of air channels height on PCM charging; variation in (a) the outlet air temperature, and (b) the PCM cooling rate.



(a)



(b)

Figure 7.23: Sensitivity of PCM solidification time to the air channels height under various (a) inlet air temperatures, and (b) air flow rates.

In brief, narrow air flow channels are highly desirable for achieving quicker PCM solidification during the charging phase. The negative impact is that narrow channels may induce high-pressure drop and hence, higher fan power requirements. Overall, a compact PCM-air heat exchanger is more efficient during the charging process.

7.7.4 Influence of PCM supercooling

Supercooling of the liquid phase at the beginning of the charging process is one of the common drawbacks that limit the PCM usage for building cooling and heating owing to the associated heat transfer problem. The supercooling nearly occurred at a similar temperature drop in all PCM zones. However, its duration varies in accordance with the PCM cooling behaviour. The supercooling duration was shorter in the forefront modules and longer in the rear PCM modules towards the outlet. This conclusion was deduced from Figure 7.15 that presents the measured temperatures at eight different PCM locations in the TES device.

To find out in what manner the supercooling is being affected by the operating conditions, the temperature-time relation was plotted for the PCM-mid3 during the initial 70 minutes of the charging process in Figure 7.24a for varied charging air temperatures, and in Figure 7.24b for varied air flow rates. It has been noticed that the PCM exhibited a steady supercooling of around 1 K in all conditions. The inlet air temperature has a small influence on the supercooling duration. The supercooling remains longer whenever the charging temperature is closer to the PCM transition temperature. In the present case, the supercooling durations observed were 7, 9, and 16 minutes at inlet air temperatures 21, 23, and 25 °C, respectively (Figure 7.24a). Moreover, PCM supercooling is also affected by air flow rate. Boosting the air flow rate decreased the supercooling period slightly at high flow rates 50 and 70 L/s taking between 7 and 10 minutes, respectively, and significantly at low air flow rate of 30 L/s when the supercooling time prolonged to around 30 minutes (Figure 7.24b).

In short, the supercooling observed under all tested operating conditions in the current charging experiments was relatively small and had no obvious impact on the outlet air temperature. To reduce the impact of supercooling, the temperature difference between the PCM and air should be sufficient and make use of high air flow rates. If the charging air temperature was higher than the supercooling temperature of the PCM (27 °C in this case), the solidification would not be initiated. However, it is worth indicating that the low supercooling seems an advantageous characteristic of the organic PCM (RT28HC) utilised in the present experiments.

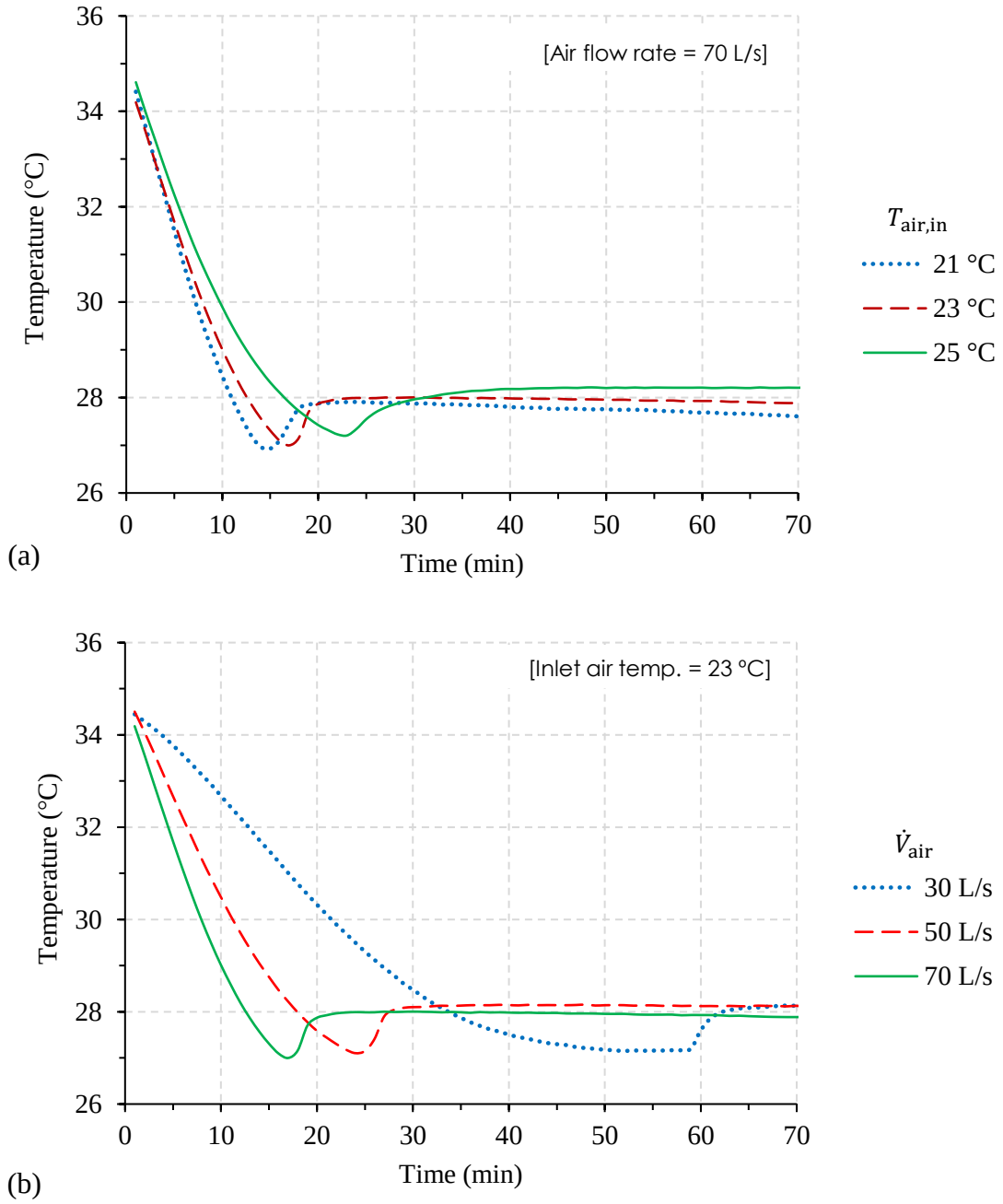


Figure 7.24: The supercooling at PCM-mid3 under adopted (a) inlet air temperatures, and (b) air flow rates.

7.8 Results and discussion of PCM discharging

This section analyses and discusses the results of the discharging process of the TES system for free cooling of buildings. It explains the discharging process and assesses the impact of inlet operating conditions and air channels height on the PCM discharging. The discharging performance was evaluated based on the time required to achieve complete melting of the PCM. The period in which the system can provide thermal comfort in buildings under hot-arid regions was also assessed. In the present study, the selected thermal comfort boundary was based on the previous studies conducted by Merghani (2001) and Nicol and Humphreys (2002) who pointed out that an indoor air temperature up to 30 °C is acceptable for human thermal comfort in hot-arid regions based on the adaptive thermal comfort principles.

7.8.1 Discharging process

During the discharging mode, a fan was used to draw the hot air from the environmental chamber with a constant temperature and flow rate over the PCM modules. The flowing air added heat to the solid PCM which changed its state gradually to liquid. The discharging tests were carried out until the whole PCM turned into liquid. The melting time was determined at the time the exit air temperature from the system started to stabilise around the inlet air temperature.

The discharging behaviour is discussed for a case under the conditions: a 10 mm distance between the PCM modules; a steady inlet air temperature 36 °C; a constant air flow rate 17 L/s; and an initial PCM temperature 22 °C. In addition, the heat exchange between the TES system and the surrounding is discussed for the three tested configurations.

7.8.1.1 Temperature variation in the PCM-air heat exchanger

Figure 7.25 presents the measured temperatures during the discharging process at eight PCM locations as shown in Figure 7.12. The PCM temperature increased sharply at the beginning of the discharging process due to the sensible heat release until reaching the PCM solidus temperature of about 27 °C. Afterwards, the phase transition from solid to liquid was activated, and consequently, the PCM temperature gradually

increased with the time until attaining the liquidus temperature of about 29 °C. After which, the PCM modules went through sensible heat exchange of the PCM, where the PCM temperature rose sharply and reaches the steady state conditions around the inlet air temperature.

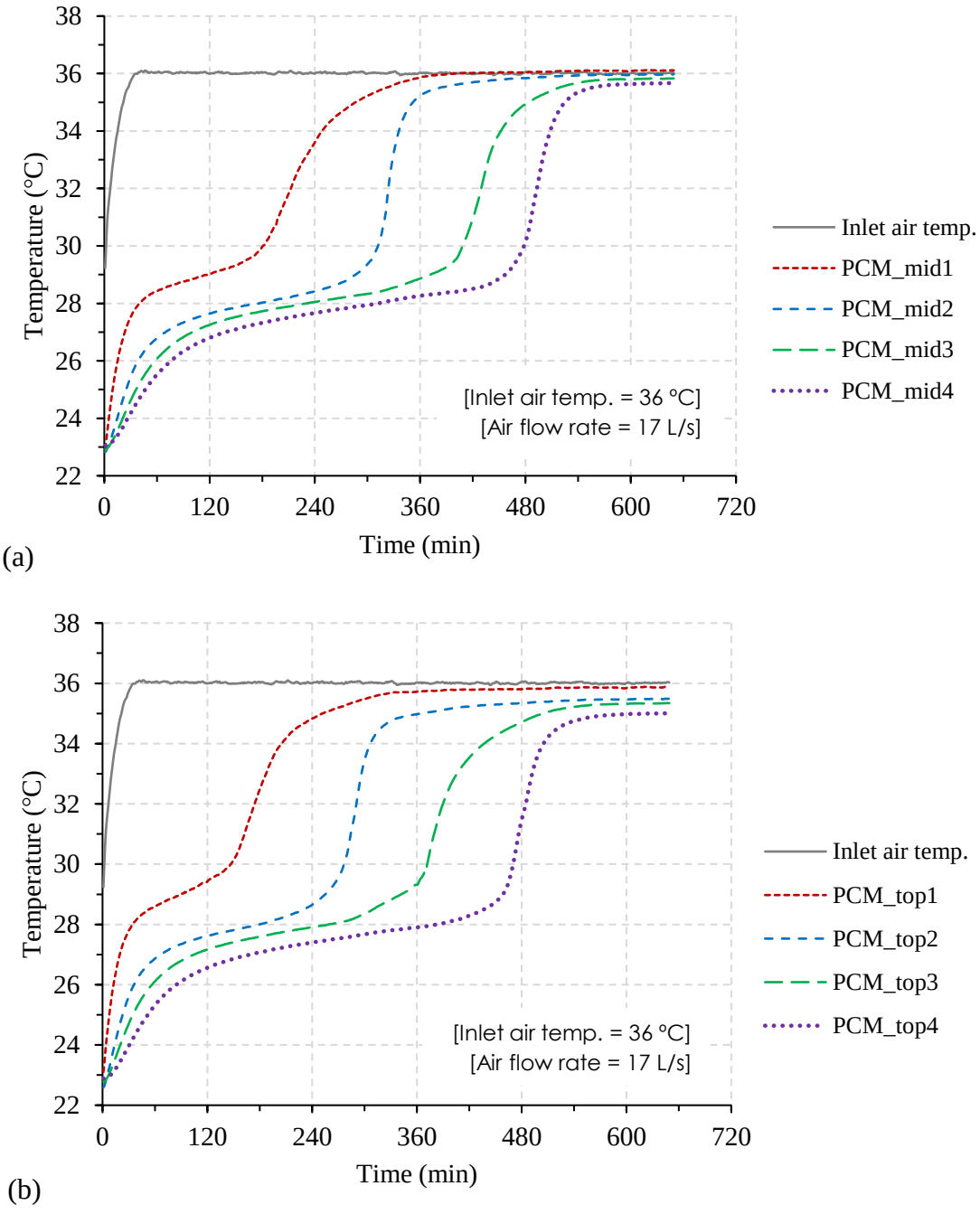


Figure 7.25: Variation of the PCM modules temperatures during the discharging process at four locations along (a) the 4th-row modules "middle" (b) the 8th-row modules "top".

The melting periods varied based on the PCM locations. Along the middle row modules PCM_mid1 to PCM_mid4 the melting periods were 5.3, 6.5, 8.7, and 8.8 hours, respectively (Figure 7.25a), and for those along the top row PCM_top1 to PCM_top4 were 5.0, 5.8, 8.2, and 8.7 hours, respectively (Figure 7.25b). These results revealed that the melting occurred quicker in the forefront modules and was slower in the rear PCM modules as a result of gradual air temperature drop towards the outlet. Another observation is that the top PCM modules melted faster than those in the middle, contrary to what occurred during the charging process. That means the heat transfer rate was higher at the upper and lower regions of the duct compared to the middle. The reason behind that was the damper placement by an angle of 110° to obtain the required air volume flow rate of 17 L/s. That placement enhanced the air flow through the top and bottom channels.

Figure 7.26 exemplifies the variation of the measured air temperatures in the discharging process at various locations in the test rig. It is observed that the inlet air reached the targeted temperature of 36 °C in almost 25 minutes and remained constant until the end of the discharging period. The PCM full melting occurred after 8.9 hours, and the outlet temperature was within the thermal comfort zone (below 30 °C) for around 6 hours. It can be clearly seen that air temperature in the middle of the duct (Air_cent1 and Air_up1) was higher than at the end (Air_cent2 and Air_up2, respectively), owing to the convective heat transfer rate drop along the air channels caused by the gradual drop in the temperature difference between the PCM and the HTF. Moreover, the upper channel positions (Air_up1 and Air_up2) demonstrated higher temperatures than their counterpart in the middle channel (Air_cent1 and Air_cent2, respectively) by around 0.9 K throughout the transition phase. This was due to higher heat flux as a result of enhanced air velocity caused by the damper's positioning as previously stated.

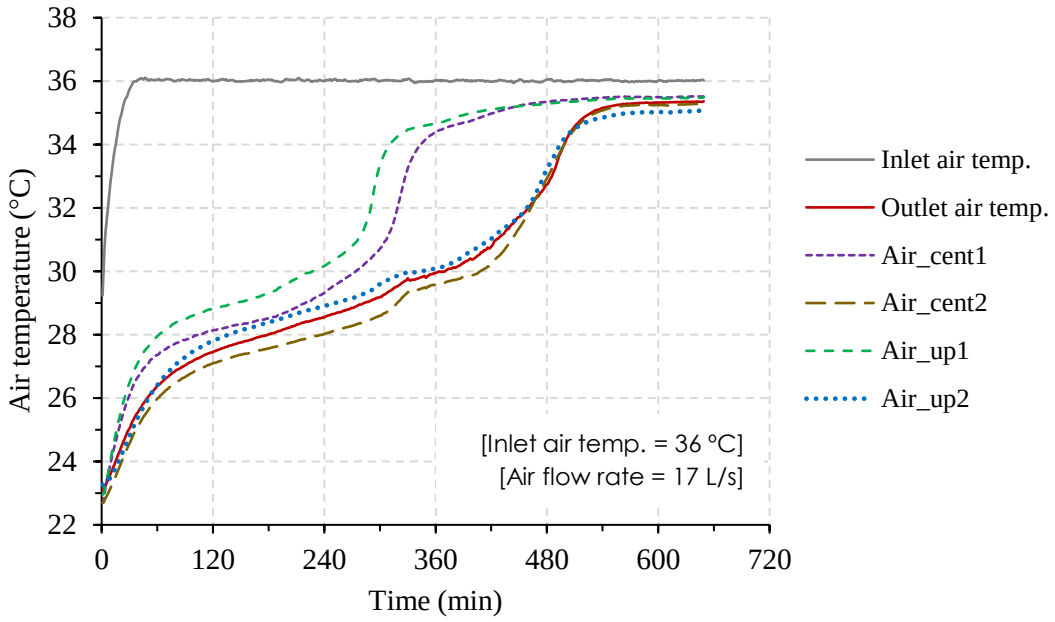


Figure 7.26: Air temperature variation in the test rig during the discharging phase.

7.8.1.2 Impact of the surrounding air

Figure 7.27 illustrates the surrounding air temperature during selected discharging experiments of the three tested PCM module configurations when the inlet air temperature was 36 °C and the air flow rate was at 17 L/s. It is clear that the surrounding air temperatures gradually increased throughout the test period and values were lower than the system temperature most of the time. Thus, heat loss from the system was present except for the initial few minutes when the PCM was at a lower temperature as reflected in Figure 7.28. It is noticeable from Figure 7.28 that the highest rate of heat loss was around 4.5 W which took place in configuration A of the smallest thermal resistance as a result of the lower surrounding temperature compared to cases B and C. It is noted that the sudden increase in the heat loss rate by configuration A after 6 hours to around 7 W was a direct reflection to the sudden drop in surrounding temperature caused by opening of a laboratory door for an hour. Heat losses from cases B and C were very low around 2-3 W representing approximately less than 3% of the average cooling extracted from the PCM during the transition phase.

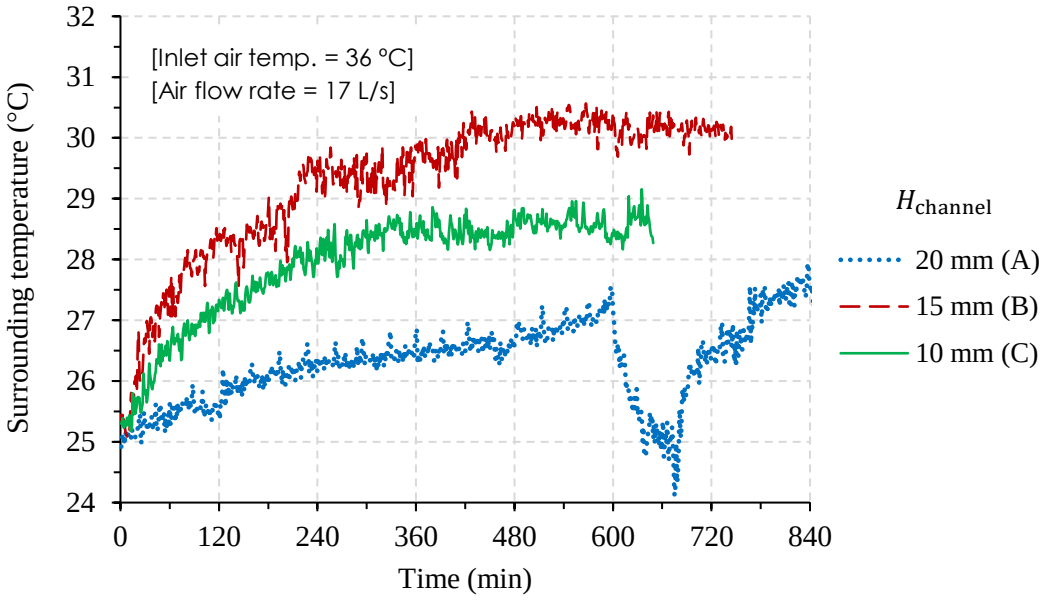


Figure 7.27: Surrounding air temperature during discharging experiments of the three tested TES configurations.

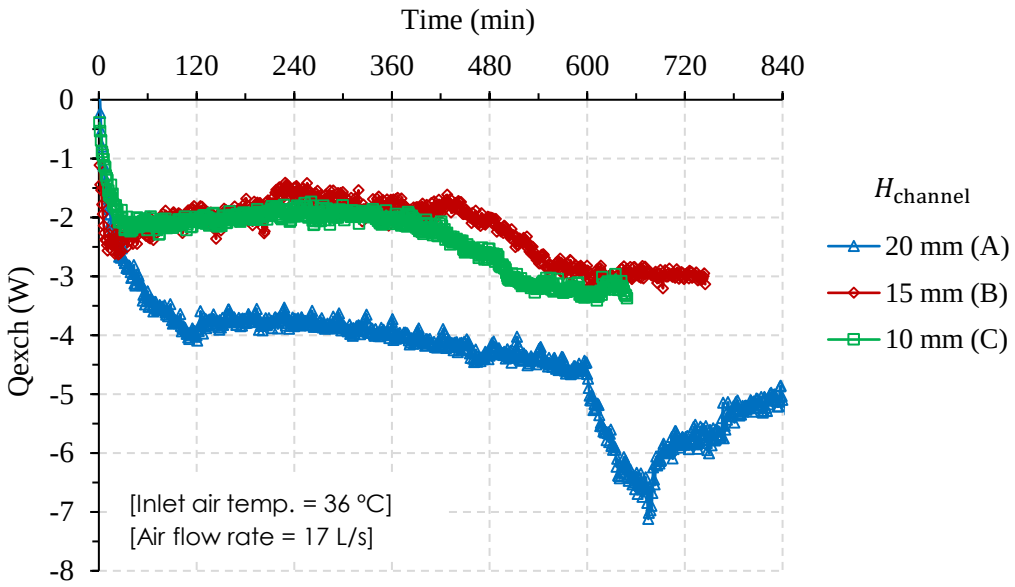


Figure 7.28: Heat exchange rate with the surrounding during discharging experiments of the three tested TES configurations.

7.8.2 Influence of inlet operating conditions

This section discusses the impact of both inlet air temperature and air flow rate on the thermal performance of the TES system during the discharging process. The air inlet conditions are presented in Table 7.3. In addition, the PCM melting time and the thermal comfort duration were discussed under all combinations of the adopted discharging air temperatures and flow rates.

Table 7.3: Inlet air conditions for the discharging process.

	PCM initial temp.	**Inlet air temp.**	**Air flow rate**
Inlet air temp. test	22 °C	32, 36, and 40 °C	17 L/s
Air flow rate test	22 °C	36 °C	7, 17, and 27 L/s

The impact of inlet air temperature on the PCM discharging is illustrated in Figure 7.29, which compares the outlet air temperature and the heating rate of the PCM for the three adopted inlet air temperatures, during the discharging phase. It is observed that the higher the discharging air temperature, the higher the rate of the cooling extraction from the PCM, leading to a faster PCM melting and a shorter thermal comfort period. Decreasing the inlet air temperature by 4 K from 36 to 32 °C boosted the melting time by around 80% from 8.8 to 15.8 hours and extended the comfort period from 6.2 hours to 14.1 hours. Whereas, an increase in inlet air temperature by 4 K from 36 to 40 °C reduced the melting time by 26% to around 6.5 hours and decreased the comfort period to 3.7 hours. These findings indicate that the discharging performance depends largely on the temperature difference between the discharging air and the PCM solidus temperature, and small differences are desirable to prolong the thermal comfort period.

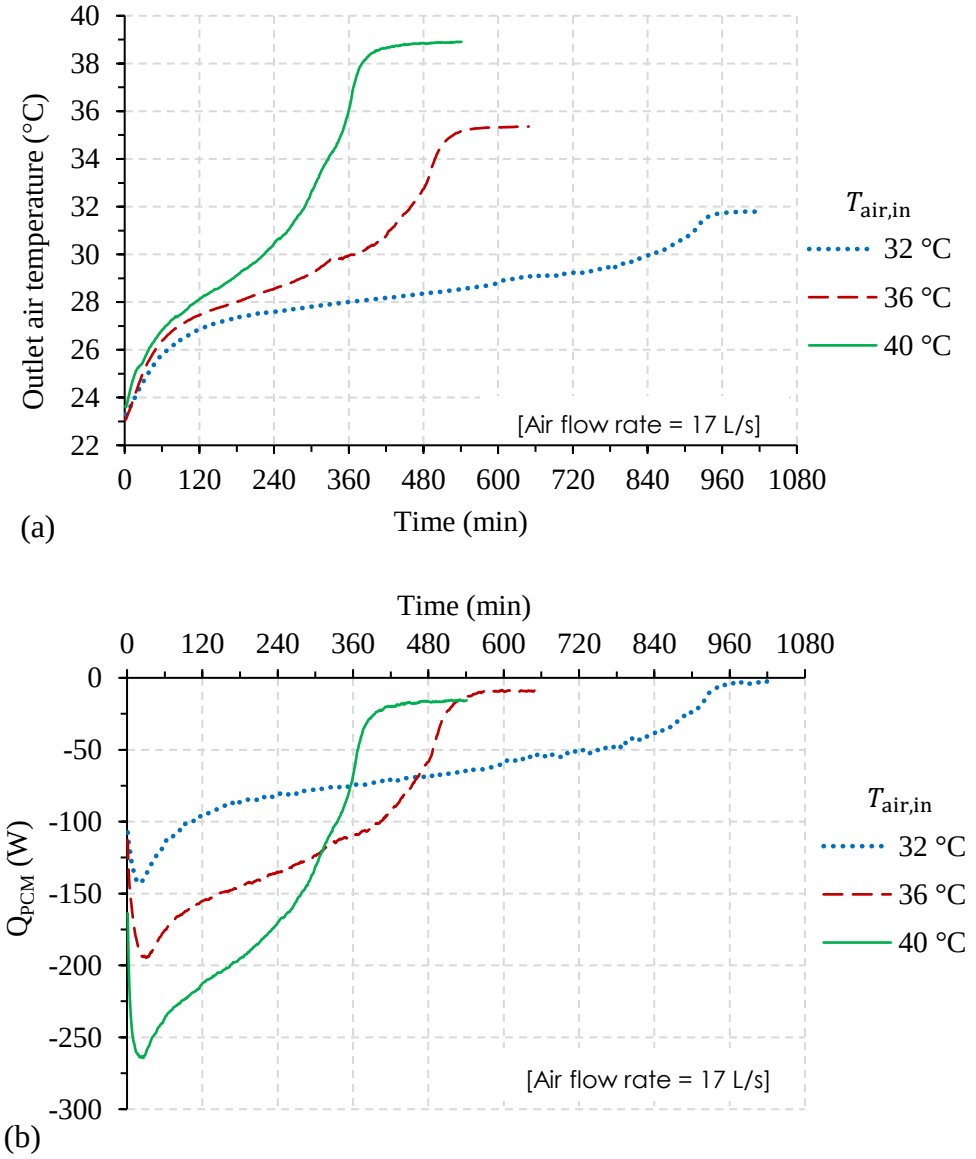


Figure 7.29: Impact of inlet air temperature on PCM discharging; variation in (a) the outlet air temperature, and (b) the PCM heating rate.

The impact of air flow rate on the PCM discharging is shown in Figure 7.30, which shows the variation of the outlet air temperature and the rate of cooling extracted from the PCM for the adopted air flow rates over the discharging period. It is observed that the higher the air flow rate, the larger the heat absorption rate by the PCM during the transition phase, and therefore, the quicker the PCM melting rate and vice versa. The higher the air flow rate, the sharper the increase in outlet air temperature leading to a shorter comfort duration. Boosting the air flow rate by around 59% from 17 to 27 L/s shortened the melting time by around 23% from 8.8 to 6.7 hours, and thus, curtailed

the comfort period from 6.2 to 3.3 hours. Whilst decreasing the flow rate by a similar ratio from 17 to 7 L/s delayed the melting time by 77% to about 15.5 hours and prolonged the comfort time to 13.5 hours. These results denote that lower air flow rates are required during the discharging operation to maintain longer comfort duration. However, the supplied air velocity should be within the limit provides comfort cooling.

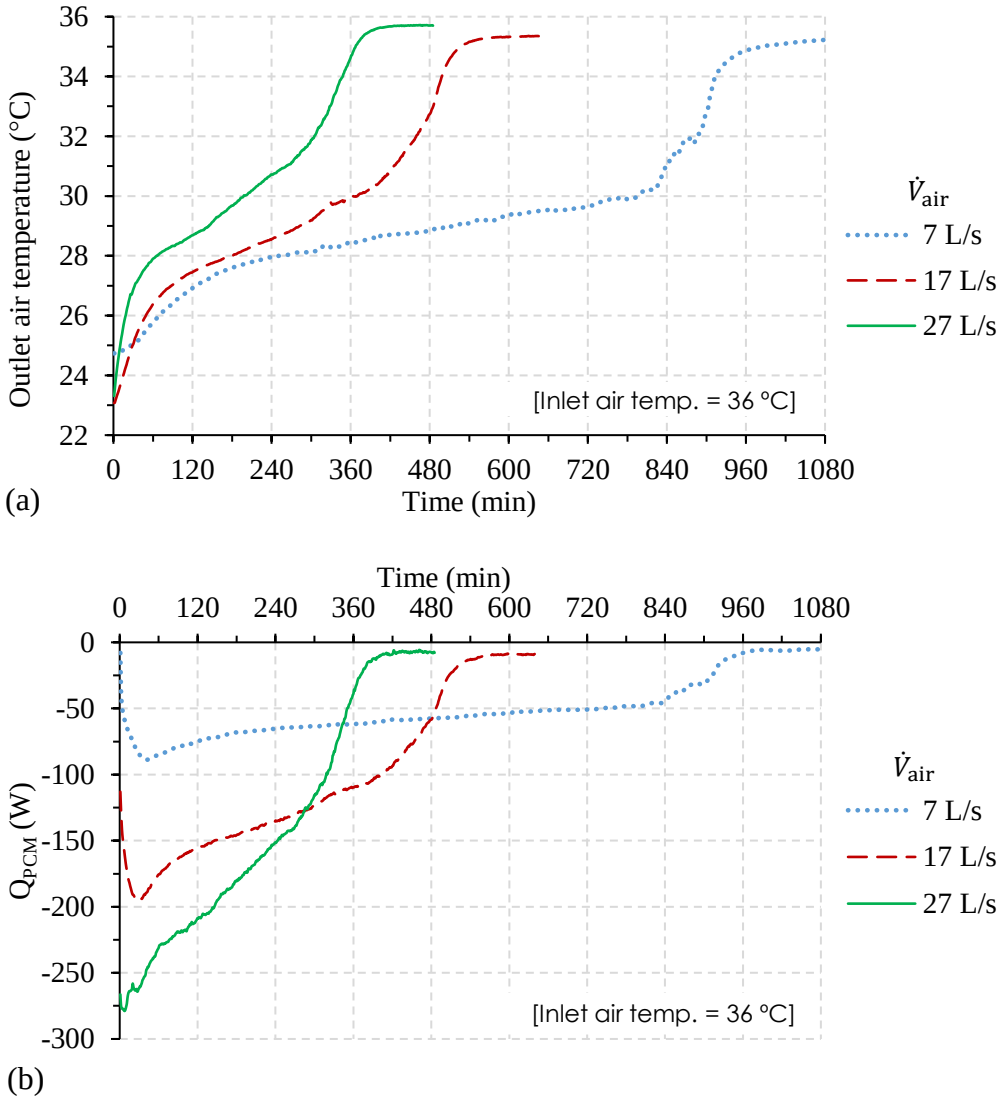


Figure 7.30: Impact of air flow rate on PCM discharging; variation in (a) the outlet air temperature (b) the PCM heating rate.

The time required for attaining full PCM melting under all combination of the adopted inlet temperatures and air flow rates is presented in Figure 7.31. It is evident that the melting time at different inlet temperatures is independent of the air flow rate. The

melting time shortened by 44% with the inlet air temperature rise from 32 to 36 °C and by 26% with the further rise from 36 to 38 °C under all air flow rates. On the other hand, the melting time varied with the air flow rate by the same rate of 45% when the air flow rate enhanced from 7 to 17 L/s, and by nearly 23% for a similar enhancement from 17 to 27 L/s. Therefore, regardless of air temperature, the melting time could be adjusted by adopting the right air flow rate regardless of the inlet air temperature.

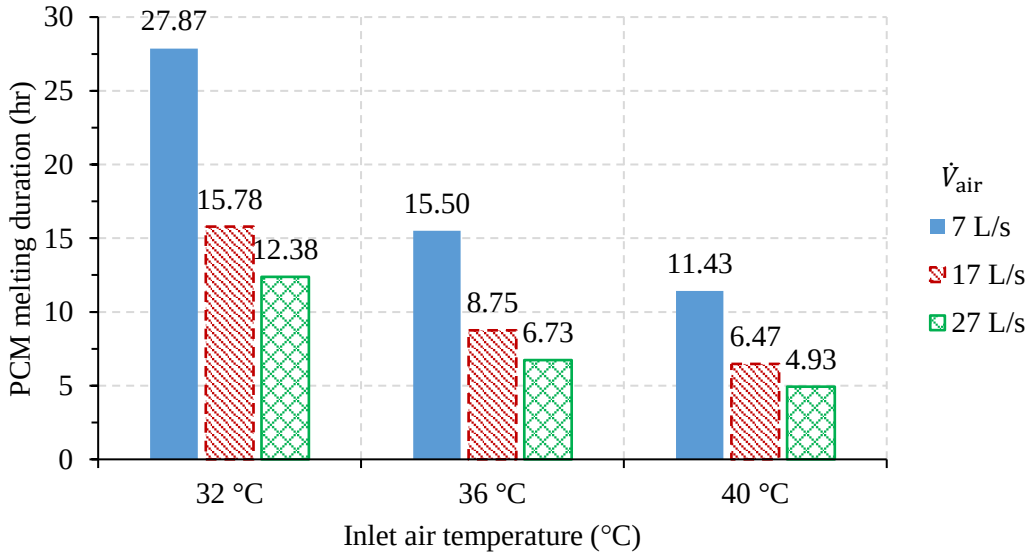


Figure 7.31: PCM melting period under operating conditions of the discharging process.

During the discharging phase, the comfort level time is of main interest more than the time required for the full PCM melting. The comfort period was determined at a time the outlet air temperature equalises the upper temperature of the comfort zone (30 °C in the considered climate). Once the supply air temperature exceeds the comfort temperature, the continuation of free cooling system operation allows coolness extraction at a higher temperature not suitable for comfort ventilation. However, this could assist in the conventional air conditioning system operation at lower power consumption. Alternatively, the system can be switched off to allow a charging cycle start with partially solid PCM, which can be beneficial in the case of insufficient cooling availability during the night-time.

The thermal comfort period achieved under all investigated operating conditions is illustrated in Figure 7.32. The increase of inlet air temperature from 32 to 36 °C reduced the comfort period by 50-67% for the flow rates 7-27 L/s, respectively. An

additional rise in temperature by 4 K to 40 °C has a limited impact on the comfort period by 31-39% for the air flow rates 7-27 L/s, respectively. The reduction of comfort period with the air flow rise from 7 to 17 L/s ranged from 47-60% for the inlet temperature range of 32-40 °C, respectively, and with the air flow rise from 17 to 27 L/s the comfort time shortened by 29-46% based on the inlet temperature range 32-40 °C, respectively.

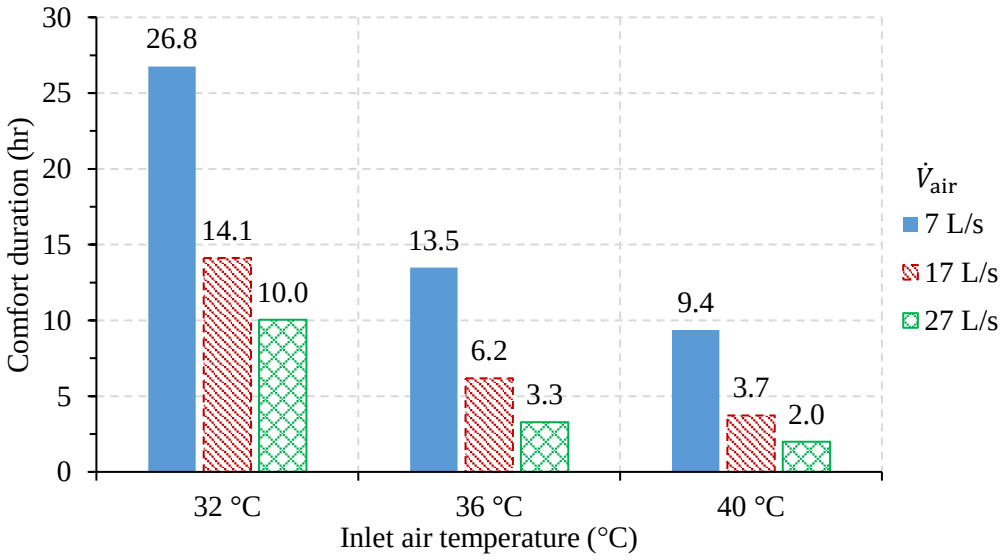


Figure 7.32: Comfort duration under operating conditions of the discharging process.

7.8.3 Influence of air channels height

Figure 7.33 compares the outlet air temperature and the heating rate for the three tested cases, when the inlet air temperature was 36 °C and the air flow rate was 17 L/s. It is observed that the smaller the air channels height, the lower the outlet air temperature will be during the initial half of the discharging period. This was due to the higher heat transfer rate caused by the enhanced air velocity inside the narrower channels compared to the wider ones. The situation reverses after a certain period, so the cooling extraction from the PCM was lower in the case of the smaller channels height design, and hence, the outlet temperature increases more sharply resulting in a faster PCM melting. This occurred because the temperature difference between the PCM and the discharging air has gradually dropped with the time.

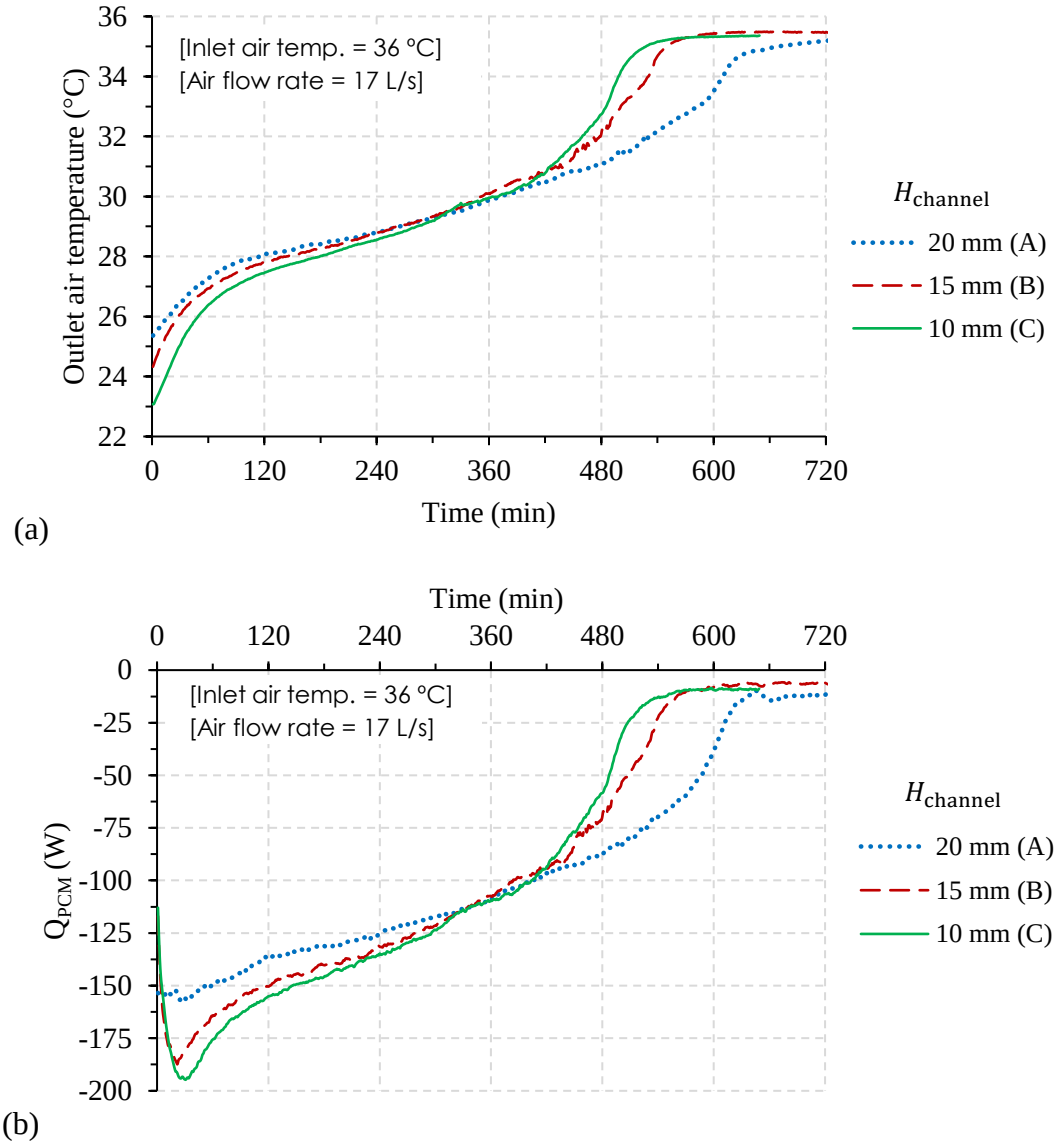


Figure 7.33: Impact of air channels height on PCM discharging; variation in (a) the outlet air temperature, and (b) the PCM heating rate.

The melting time and the corresponding comfort level duration achieved are illustrated in Figure 7.34 and Figure 7.35, respectively, for the three cases under tested conditions. It is obvious that the time required for the complete PCM melting and hence the comfort period prolonged with the air channels height. As shown in Figure 7.34a, the increase in the melting time with the air channels height rise varies based on the discharging air temperature. It was higher at the low inlet air temperatures compared to the high temperatures. For instance, increasing the height of the air channels from 10 to 20 mm prolonged the melting time by 26-20% at inlet air

temperatures 32-40 °C, respectively, when the air flow rate was 17 L/s. On the other hand, as shown in Figure 7.34b, the melting time varied with the augment of air channels height depending on the air flow rate. The melting time increase was higher at low air flow rates compared to the high flow rates. As an illustration, with air channels height increase from 10 to 20 mm, the melting time extended by approximately 28-25% for the air flow rates 7-27 L/s, respectively, when the inlet air temperature was 36 °C.

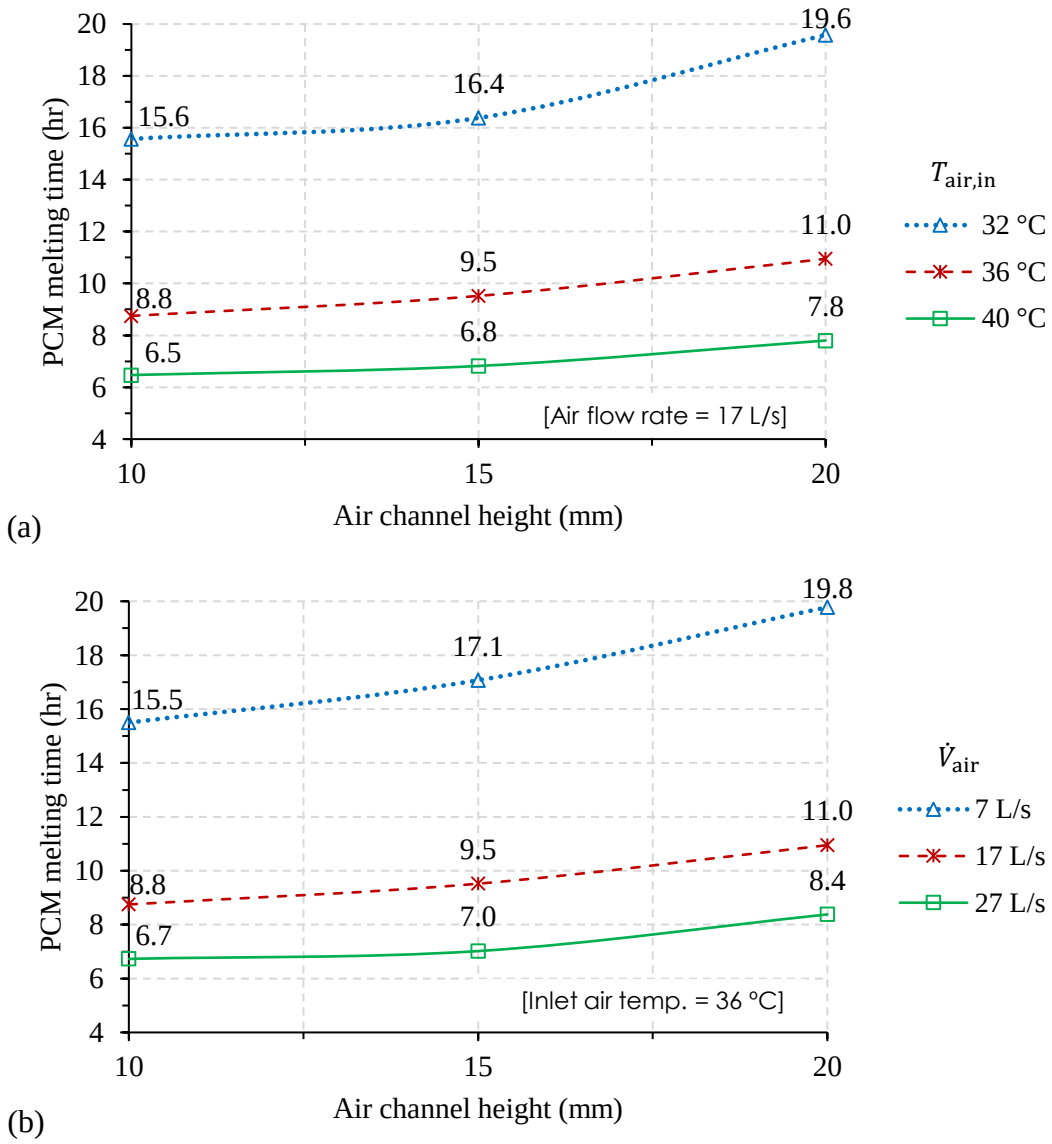


Figure 7.34: Sensitivity of PCM melting time to the air channels height under various (a) inlet air temperatures, and (b) air flow rates.

Figure 7.35 indicates that the variation in the comfort period for the three tested PCM modules arrangements was very slight under all tested conditions. This is evident in Figure 7.33, where the outlet air temperature curves met at the maximum comfort temperature of 30 °C. At the given temperature, the variation in the comfort time was less than 7% in all cases, however, except for the case when the air flow rate was 27 L/s (Figure 7.35b), at which configuration C exhibited a longer comfort time by nearly 20% compared to the other arrangements. This is because the initial temperature of the PCM was lower by almost a 2-K in case C at the beginning of the discharging process.

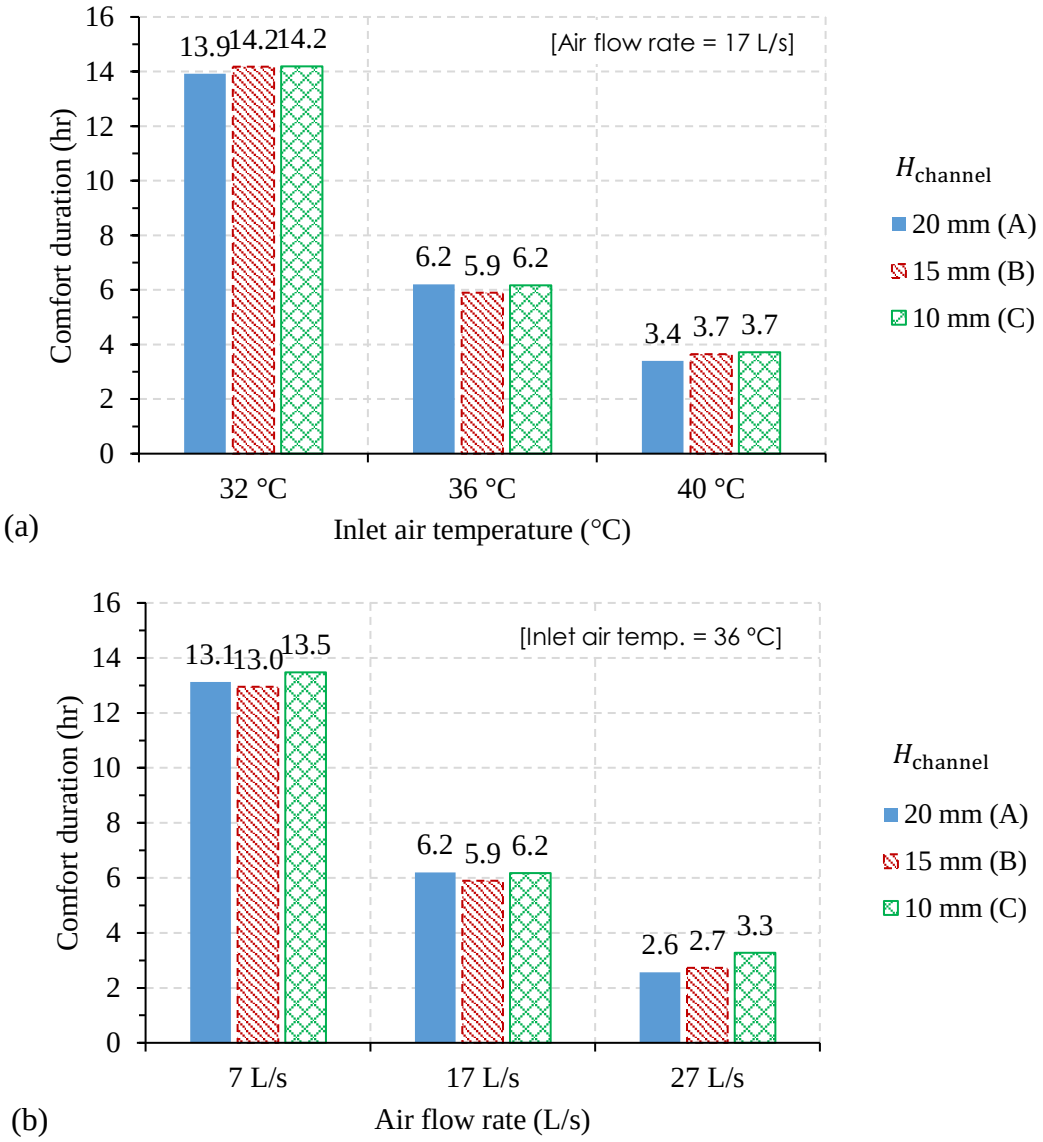


Figure 7.35: Influence of air channels height on the comfort level period under various (a) inlet air temperatures, and (b) air flow rates.

7.9 A comparison of the experimental and modelling results

A comparison between the predicted results using CFD simulation and the experimental results for the TES system has been carried out to validate the CFD model. A 2D geometrical model (Figure 7.36), comparable to the experimental apparatus (Figure 7.10), was created, meshed, and tested in ANSYS Fluent for thermal performance analysis. The boundary conditions were set similar to the experimental setup. The assumptions and settings of the calculation models, governing equations, and solutions methods were similar to those described in Chapter 6. The validation was performed for both transition phases; a charging phase at inlet air temperature of 25 °C and air flow rate of 70 L/s, and a discharging phase at inlet air temperature of 36 °C and air flow rate of 16 L/s. The temperature was measured at the outlet and on the surface of the PCM container which nearly follows the same behaviour of the PCM inside. The PCM average temperature was estimated at two locations along the channel; PCM_A and PCM_B for the front and the rear sets of PCM modules, respectively (Figure 7.36). The adopted measurements locations in the model were in correspondence with that in the experiments. Details of the investigated CFD geometrical model, boundary conditions, and monitored temperature locations are presented in Figure 7.36.

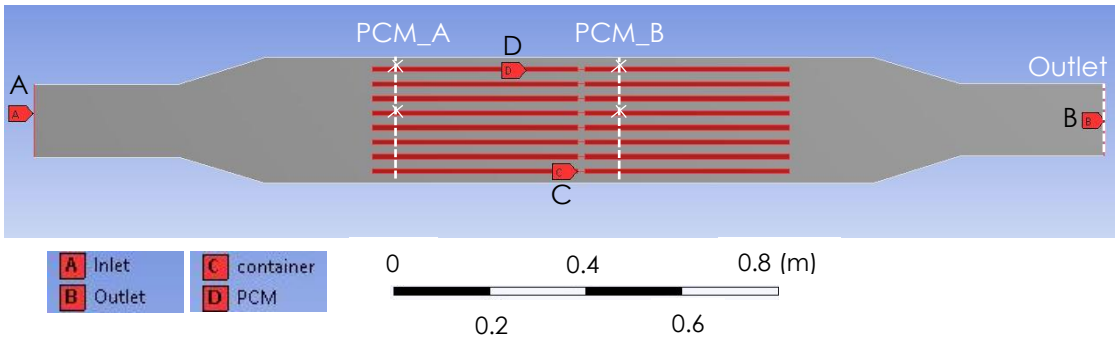


Figure 7.36: Details, boundary conditions, and measurement locations of the tested geometry in ANSYS software.

7.9.1 Results of the PCM charging

For the charging process, the numerical and experimental results of the PCM temperature at the considered locations along with the outlet air temperature are compared in Figure 7.37, for inlet air temperature of 25 °C and air flow rate of 70 L/s.

From Figure 7.37a and Figure 7.37b, it can be clearly seen the three successive phases that the PCM passes through during the charging process (the sensible cooling, the phase change, and the latter sensible cooling) in both modelling and experimental results. During the initial sensible cooling phase, the drop in the PCM temperature was very sharp from the initial temperature (34 ºC) to the liquidus temperature (28 ºC), with a lower severity in the case of the experiment than the simulation. One of the reasons could be the inlet air temperature variation at the beginning of the charging process. Unlike the numerical analysis where the inlet temperature has been considered constant all the time, the air drawn from the environmental chamber possessed a slightly higher temperature, which required few minutes to stabilise at the target temperature. Moreover, the variation at some point prior to the phase change process was due to the supercooling of the experimentally tested PCM, owing to the nature of the paraffin. During the transition phase, where the PCM temperature declined gradually from 28 ºC to 27 ºC, it can be observed that the measured and predicted temperatures at the considered locations have shown a good agreement throughout the entire phase, with a maximum difference of 1.55%. Subsequently, the sensible cooling was quite rapid in the simulation and gradual in the experiment. This is likely to be due to the presence of some latent heat in the experimentally investigated PCM (18 kJ/kg in the range 25-27 ºC), which can be noticed from the enthalpy-temperature graph in Figure 6.1.

As exemplified in Figure 7.37c, the outlet air temperatures obtained through the simulation and the experiment have shown an identical trend, except at the commencing of the charging process (initial 30 minutes) where the sensible cooling was slower in the case of the experiment. This can be attributed to the lower temperature difference between the air and the PCM initially, prior to reaching the target temperature for the inlet air. During the phase transition, the modelling predicted a slightly lower temperature by a maximum of 1.46% than the measured temperature, before converging during the latter sensible cooling stage. This may be as a result of the heat gain from the surrounding since the air temperature was between 28.6 and 31.5. However, this aspect was ignored in the CFD modelling, assuming the duct walls as adiabatic.

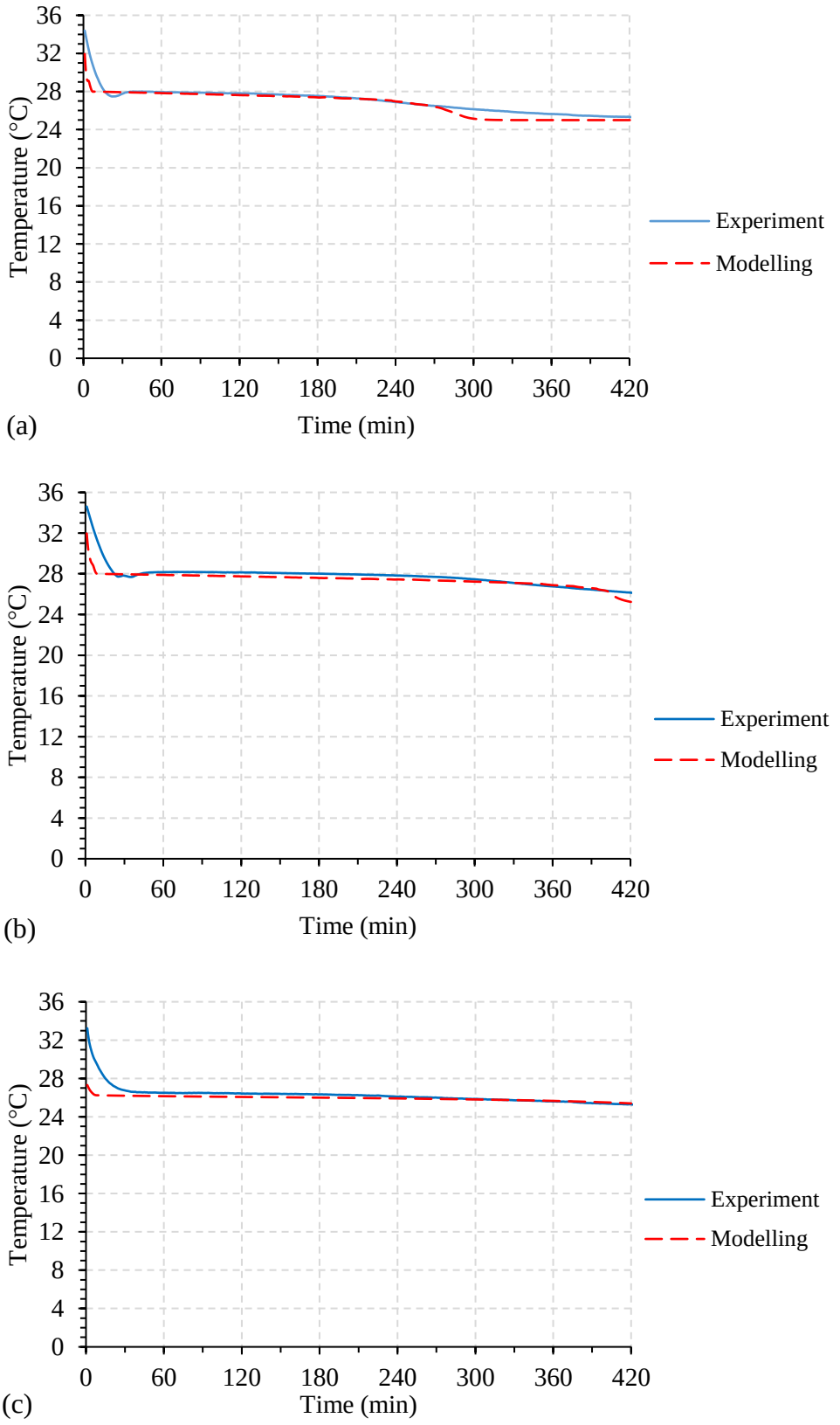


Figure 7.37: Charging process; (a) PCM temperature at PCM_A, (b) PCM temperature at PCM_B, and (c) Outlet air temperature.

7.9.2 Results of the PCM discharging

For the discharging process, the modelling and experimental results of the PCM temperature and outlet air temperature are compared in Figure 7.38, for the inlet air temperature of 36 °C and the air flow rate of 16 L/s.

It is evident from Figure 7.38a and Figure 7.38b that the PCM in all cases passes through initial sensible heating phase, followed by a phase change stage, and later sensible heating ahead of reaching the steady-state conditions. The initial sensible heating took longer time in the case of the experiment than in the simulation, owing to the slightly lower inlet air temperature than the required temperature initially. This was caused by heat losses from the air in the way from the environmental chamber to the inlet before reaching the target temperature at a time depending on the air flow rate. During the phase change, the PCM temperature obtained through the numerical and experimental analysis were in a good agreement most of the time. Following the phase change process, the increase in PCM temperature was sharp in the case of numerical analysis where the melting range was only in the range of 27-28 °C, However, this is not the case for experiments where the temperature increase was gradual and smooth due to the presence of some latent heat at temperatures higher and lower than the dominant range (Figure 6.1).

Moreover, it is observed from Figure 7.38c that the outlet air temperature followed a similar trend throughout the discharging process, but with a lower temperature predicted by the modelling than that obtained via the experiment. The deviation was estimated in the range 2.2%-4.19% which can be justified as the surrounding temperature was much lower than the system temperature, led to heat loss to the surrounding. This can be understood from stabilisation of the outlet air temperature at a level lower than the inlet temperature in the case of the experiment, while it was equal to the inlet temperature in the modelling case (36 ºC).

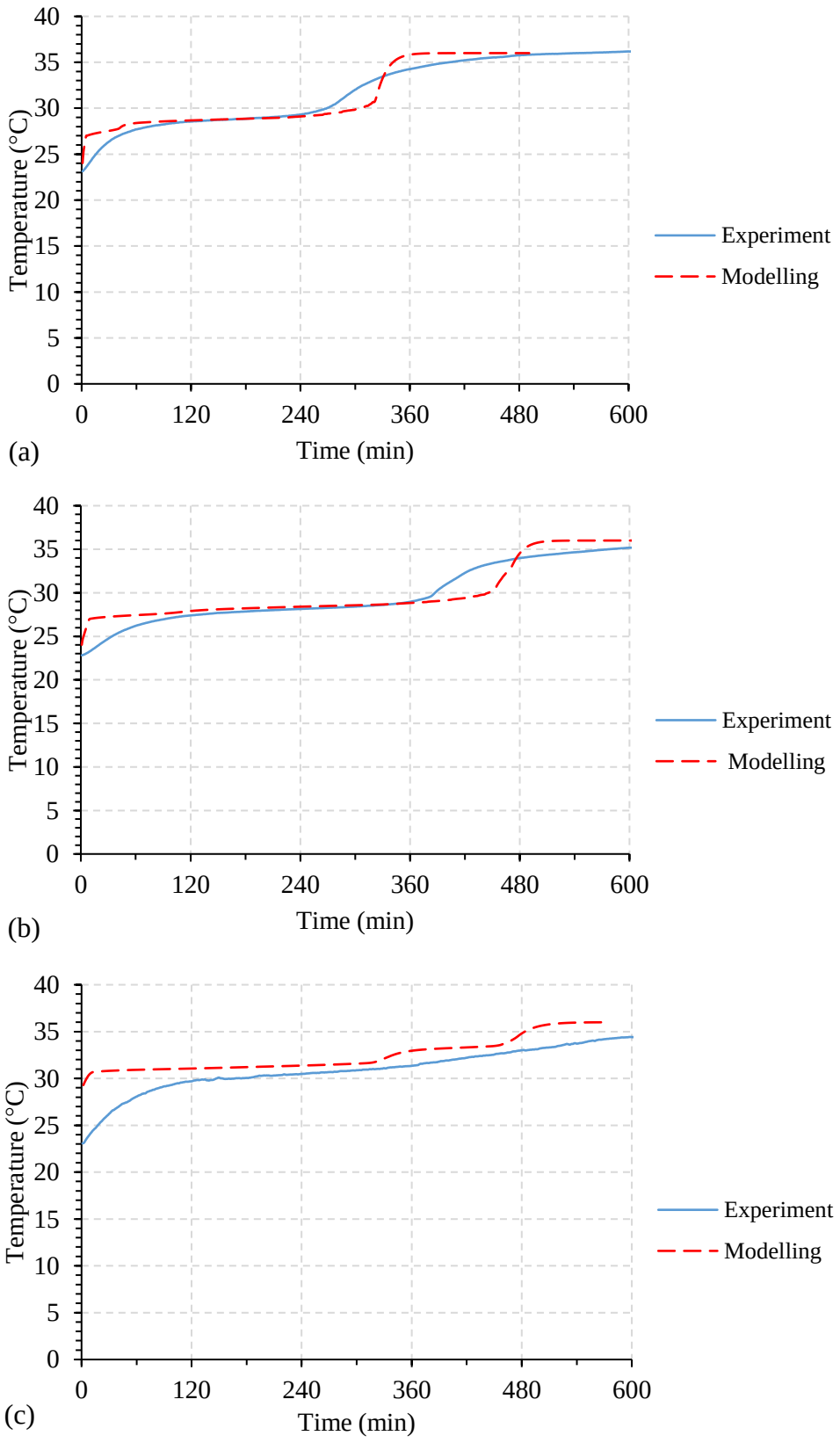


Figure 7.38: Discharging process; (a) PCM temperature at PCM_A, (b) PCM temperature at PCM_B, and (c) Outlet air temperature.

Furthermore, other reasons for the discrepancies in all data could likely be (I) the variation in PCM thermo-physical properties with the temperature in the case of the experiment, contrary to the modelling where these were assumed constant, except for the density. The density variation was estimated using the piecewise-linear method available in Fluent, which means consideration of natural convection inside the melted PCM in the current computation. (II) the inaccuracy of the experimental measurements, taking into account that the overall uncertainty of the current experiments was estimated at ±1.12%.

In summary, a successful experimental validation for the considered CFD modelling was accomplished for both charging and discharging processes. The temperature obtained numerically and experimentally have followed a similar trend and were in a good agreement in all cases. The temperature profile was very smooth in the case of real conditions (experiment) and linearly in the modelling results, as a result of natural variation of thermo-physical properties with the temperature, which met by constant values assumed in the computational modelling. Overall, it can be stated that the CFD modelling considered in the present study is well verified and can be appropriately utilised for the phase change simulation.

7.10 Summary

This chapter presented the fabrication, experimental setup, and operating procedure of the proposed TES system for building cooling applications. The thermal performance results of both PCM charging and discharging processes were discussed for various inlet operating conditions and air channels heights. The PCM supercooling during the charging phase was also investigated. A comparison between the modelling and experimental results has been carried out, which has shown a good agreement.

Based on the charging and discharging experimental results, the following observations have been drawn;

- Inlet air temperature has a significant impact on PCM charging/discharging duration depending on the variation from the PCM liquidus/solidus temperature. Larger variations are advantageous for a quicker charging process, while small variations are desirable to prolong the thermal comfort period throughout the discharging phase.

- Air flow rate has a significant impact on the charging process. Higher air flow rates are recommended to accelerate the PCM solidification. However, the flow rate should be carefully adjusted based on the available charging temperature to harness the most out of the night cooling in the required time with low input power to the fan. In contrast, lower air flow rates may be necessary for gradual cooling extraction from the PCM during the discharging period to maintain longer thermal comfort duration, considering air supply at an adequate velocity to meet the occupant's comfort.

- Optimising the distance between the PCM panels is an important aspect to enhance the system performance. Narrow air channels result in higher cooling storage and hence, shorter solidification time during the charging process. On the other hand, a system with wider air channels provides a slower melting rate during the discharging process, whereas, comfort durations are not affected by the height of the air channel.

- The supercooling rate in the selected PCM is relatively small around 1 K. Its duration is affected by the air flow rate, showing longer time at lower flow rates. The supercooling is also affected by the charging air temperature, with longer durations at inlet temperatures close to the PCM solidus temperature. The results pointed out that the supercooling has delayed the charging process and had no noticeable impact on the outlet air temperature.

In short, it has been demonstrated that the proposed TES system is capable of meeting building cooling requirements, and thus, has a potential to minimise the operation hours and energy use of the conventional air conditioning systems.

Chapter 8

Experimental Investigation of the PCM-Air Heat Exchanger under transient Inlet Air Conditions

8.1 Introduction

This chapter presents the results of experiments investigating the charging performance of the proposed TES system under transient inlet air conditions. In Chapter 7, it was found that a TES system with 10 mm air channels height is the configuration with the best performance, and this configuration has been used in this analysis. The system thermal performance was evaluated during hot and moderate summer conditions of the hot-arid climate under both nocturnal ventilative and radiative cooling strategies.

8.2 Experiments procedure and operation setup

The current experimental investigation was performed utilising the TES rig of 10 mm air flow channels between the PCM modules and the same equipment setup described in Chapter 7. However, the test procedure and operating conditions are different. The charging process, in this case, was performed using transient inlet air conditions, simulating that of the hot-arid climate of the case study.

The system was investigated under hot and the moderate summer conditions, as there is no need for cooling in winter months (November–February) of the case study. A reference day with hourly average temperatures during the extreme summer months (May-June) was used for the hot conditions study, and a reference day with hourly average temperatures during March was used for the moderate conditions study as shown in Figure 8.1.

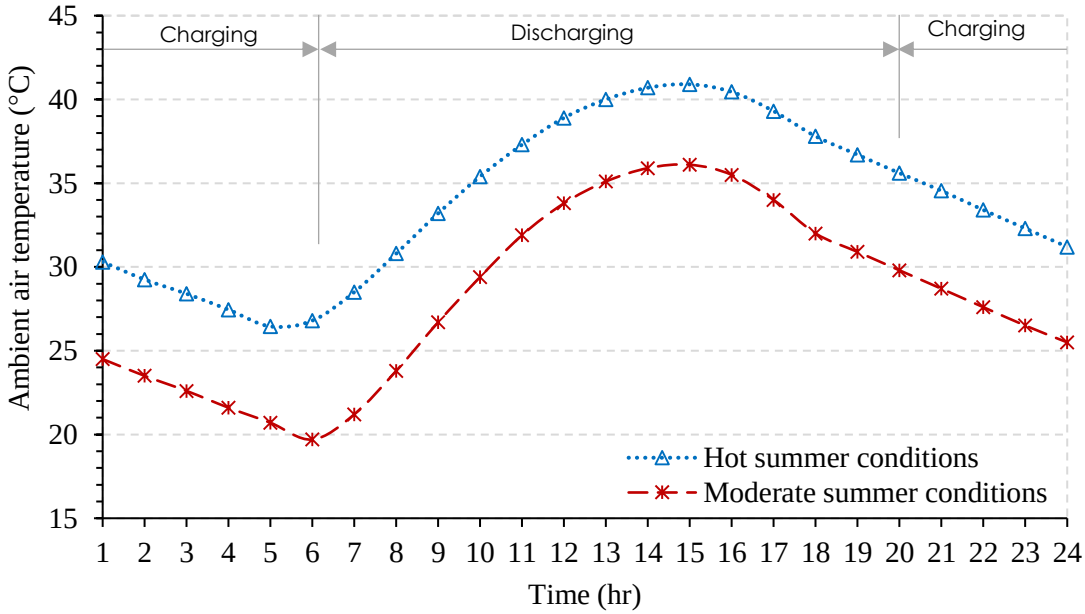


Figure 8.1: Ambient temperature profiles of typical days in peak summer and transitional months (case study for Khartoum).

The system was examined under two modes of operations; firstly, a free cooling mode by storing the natural cooling of the ambient air in the TES unit, and secondly, a radiative cooling mode by storing the cooling produced by the ambient air flowing through the proposed radiative cooling system.

The free cooling mode was run using the ambient air temperature available at the location and the maximum air flow rate of 70 L/s of the fan employed in order to achieve the fastest PCM charging time. While for the system operation under radiative cooling mode, the cold air temperature obtained by the system with the optimum design was used as discussed in Chapter 5. The charging air temperatures were obtained as an average of each hour throughout the cooling mode. The tests were carried out at three air flow rates 30, 50, and 70 L/s. A schematic of the experiments plan is shown in Figure 8.2. The temperature profiles for the night ambient air and the outlet air from the nocturnal radiative cooling system under various air flow rates are illustrated in Figure 8.3 for both hot and moderate summer conditions.

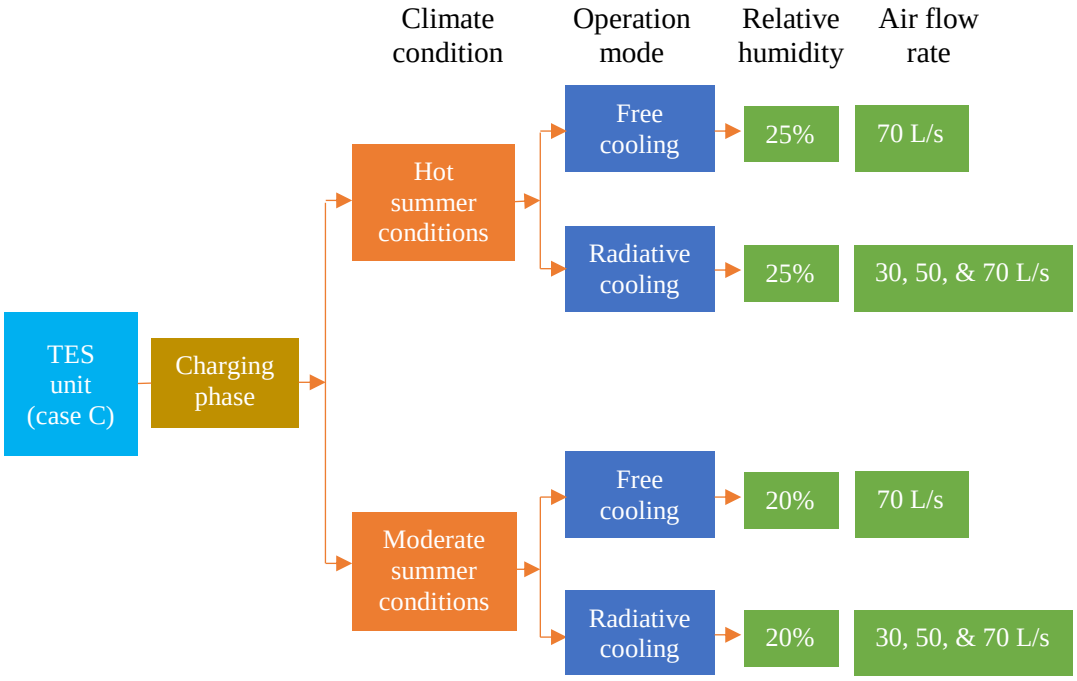


Figure 8.2: Plan of the experiments under transient inlet operating conditions.

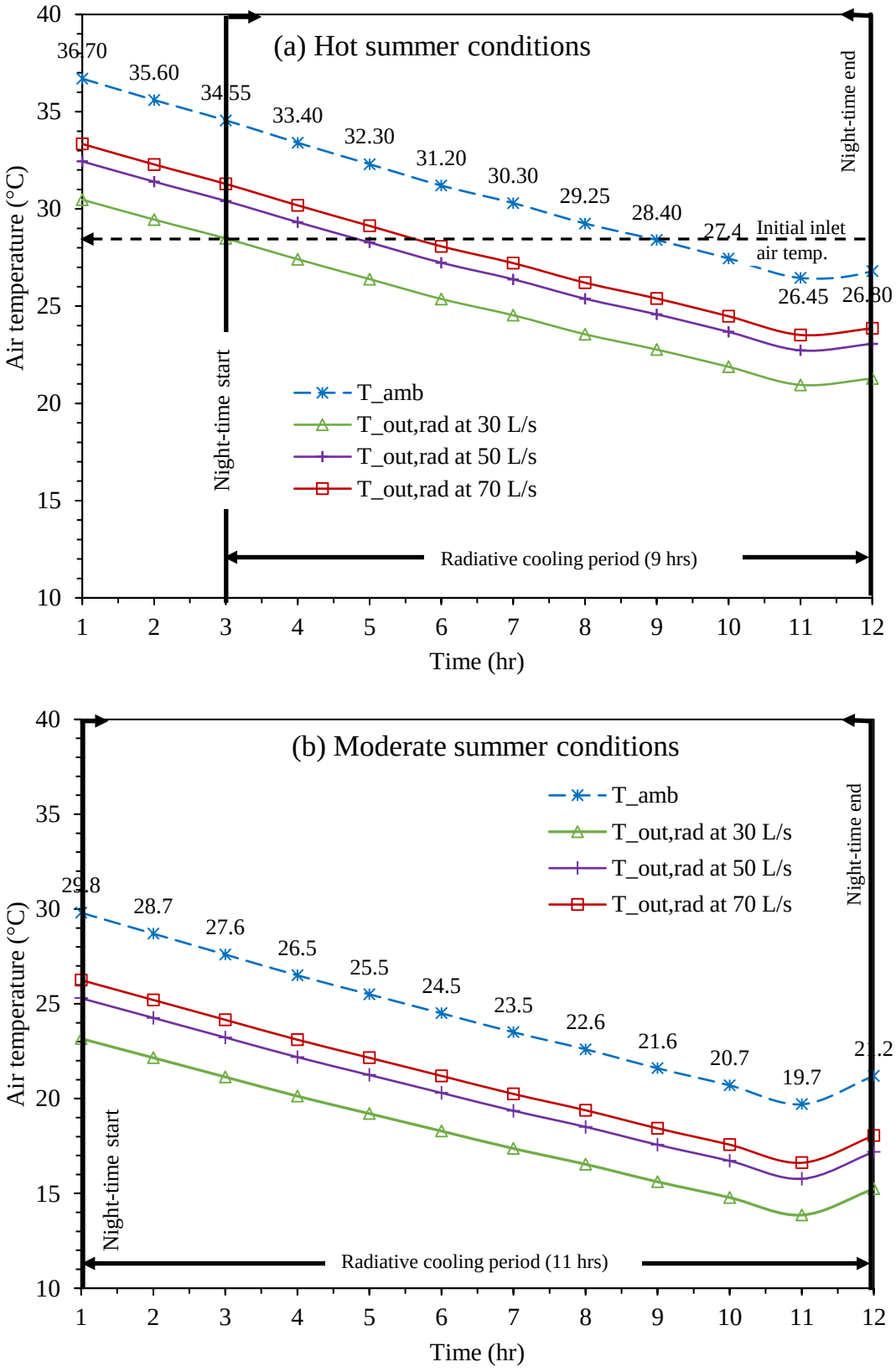


Figure 8.3: Hourly profile of the air temperature reduction obtained by the radiative cooling system.

Prior to the charging experiment, the entire PCM was initially fully melted at 32 °C in all cases. The humidity inside the chamber was kept constant throughout the test period at 25% and 20% for the hot and moderate conditions, respectively, according to weather data of Khartoum. The initial air temperature used for the PCM charging under hot conditions was 28.5 °C, as any temperature above this value would not be able to alter the PCM phase and only allows sensible reduction of PCM temperature.

During the experiment, the axial fan was used to circulate the air with a steady flow rate from the environmental chamber through the PCM modules. The air temperature was gradually adjusted (increased or decreased) between any two temperature values based on the given profile using the chamber control panel until the end of the charging period. Full charging is expected to occur once the system reaches the steady-state, whereby the outlet air temperature starts stabilising in the vicinity of the inlet air temperature.

8.3 Assessment of the PCM charging process

The thermal performance of the PCM-air heat exchanger was assessed based on the PCM cooling rate during the charging process using equations (7.2)-(7.4) described in Chapter 7.

In this analysis, the effectiveness of PCM charging ($\bar{f}$) at a given time was determined as a ratio of the instantaneous energy transfer rate and the maximum (initial) energy transfer rate from the air to the PCM using equation (8.1) (Darzi et al., 2013);

$$\bar{f} = \frac{T_{\text{air,out}} - T_{\text{air,in}}}{T_{\text{air,out-initial}} - T_{\text{air,in}}} \tag{8.1}$$

where; $T_{\text{air,out}}$ and $T_{\text{air,in}}$ are the outlet and the inlet air temperature, respectively, and $T_{\text{air,out-initial}}$ is the initial outlet air temperature from the system.

8.4 Impact of the surrounding air on the PCM charging

At the beginning of the investigation, the impact of the surrounding environment on the PCM charging process was studied. The rate of heat exchange between the PCM and the surrounding air is presented in Figure 8.4a and Figure 8.4b for the experiments conducted under hot and moderate summer conditions, respectively. Figure 8.4a exemplifies that there was a heat loss by system throughout the whole period of the free cooling test, due to the lower surrounding air temperature (24 °C). The heat loss rate was in the range between 1.0 and 2.2 W, which indicates that about 1.7% of the free cooling rate was from the surrounding air. During the radiative cooling experiments, there was heat gained from the surrounding air and has reached a maximum of 3.2 W for the entire rig.

On the other hand, for the experiments under moderate conditions, Figure 8.4b shows that the variation of the heat gain rate from the surrounding air was as high as 4.5 W for the whole rig, representing approximately less than 3% of the heat released by the PCM. Overall, it appears that the surrounding air has some impact on the charging process, but this could be considered as minor.

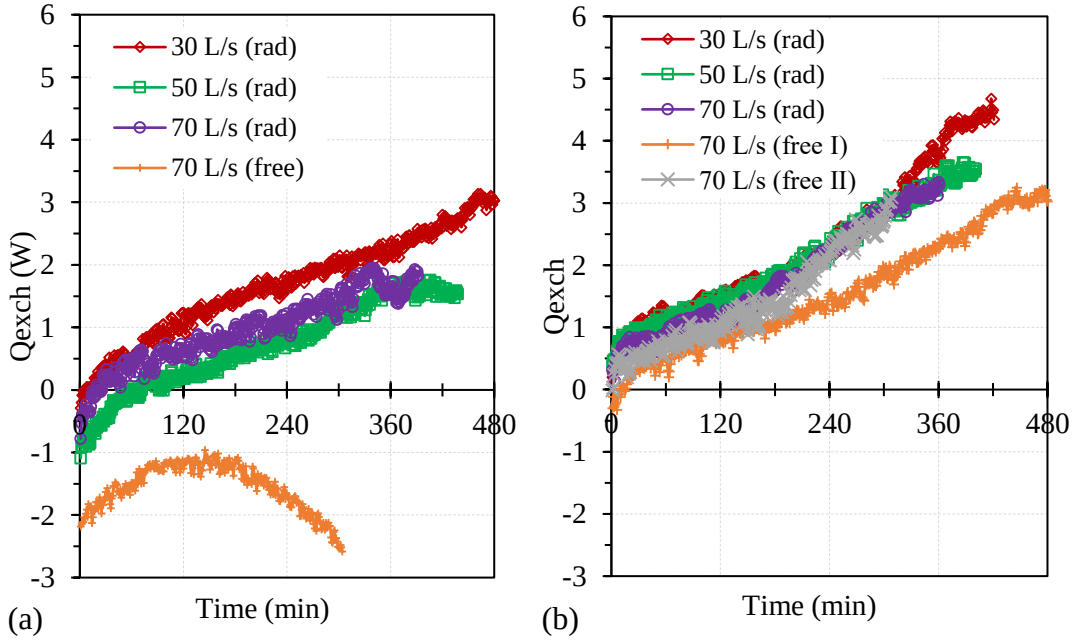


Figure 8.4: Variation of heat exchange rate with the surrounding during the charging experiments under (a) hot and (b) moderate summer conditions.

8.5 Results and discussion of PCM charging under hot conditions

8.5.1 Operation under free cooling mode

The temperature variation of the outlet air and the PCM modules at various locations across the test rig under hot summer conditions using free cooling mode with an air flow rate 70 L/s is illustrated in Figure 8.5. The variation of charging effectiveness and PCM cooling rate with the time is shown in Figure 8.6.

As shown in Figure 8.5, the potential night-time charging period is only three hours during which the ambient air temperature has gradually dropped from 28.3 °C to 26.2 °C, before the temperature starts increasing owing to the daytime solar heating.

During the initial charging period, the PCM dissipated its sensible heat to the passing cold air and reached the liquidus temperature in around 30-40 minutes as a result of the high heat transfer rate caused by the vast temperature difference between the PCM and the air. Then, the PCM supercooled without any phase change for about an hour, where the outlet air temperature was nearly equal to the inlet air temperature (Figure 8.5), i.e. the heat transfer rate and charging effectiveness were zero as shown in Figure 8.6. The PCM temperature then gradually returned to the liquidus point at varying periods based on the relative location of the PCM module. At which the phase transition initiated and continued until the inlet temperature exceeded the outlet temperature in approximately 2.3 hours, denoting ending of the charging period. The continuous air flow through the system afterwards resulted in a cooling discharge from the PCM owing to the inlet air temperature rise after the sunrise (Figure 8.5).

At the end of the charging period (minute 230), Figure 8.5 shows that the temperatures at all PCM modules were in the range 27.6-28.2 °C, and there is no gradual temperature drop noticed. The maximum difference between the inlet and the outlet air temperature during the phase transition period (minute 90-230) was 1 K. This indicates that the heat transfer rate between the PCM and the air was very low. The total cooling rate of the PCM was about 195.9 Wh during 3.8 hours of charging process.

The continuation of the charging process after the night hours elapsed was based on the fact that the free cooling can sometimes be harnessed during the early morning hours until the ambient air temperature reaches the PCM temperature. In the present experiment, the charging process continued for around 50 minutes after the sunrise, in which, the charging effectiveness has decreased rapidly from 0.3 to 0.03 (Figure 8.6a), and the cooling rate was 39.2 Wh representing around 20% of the total.

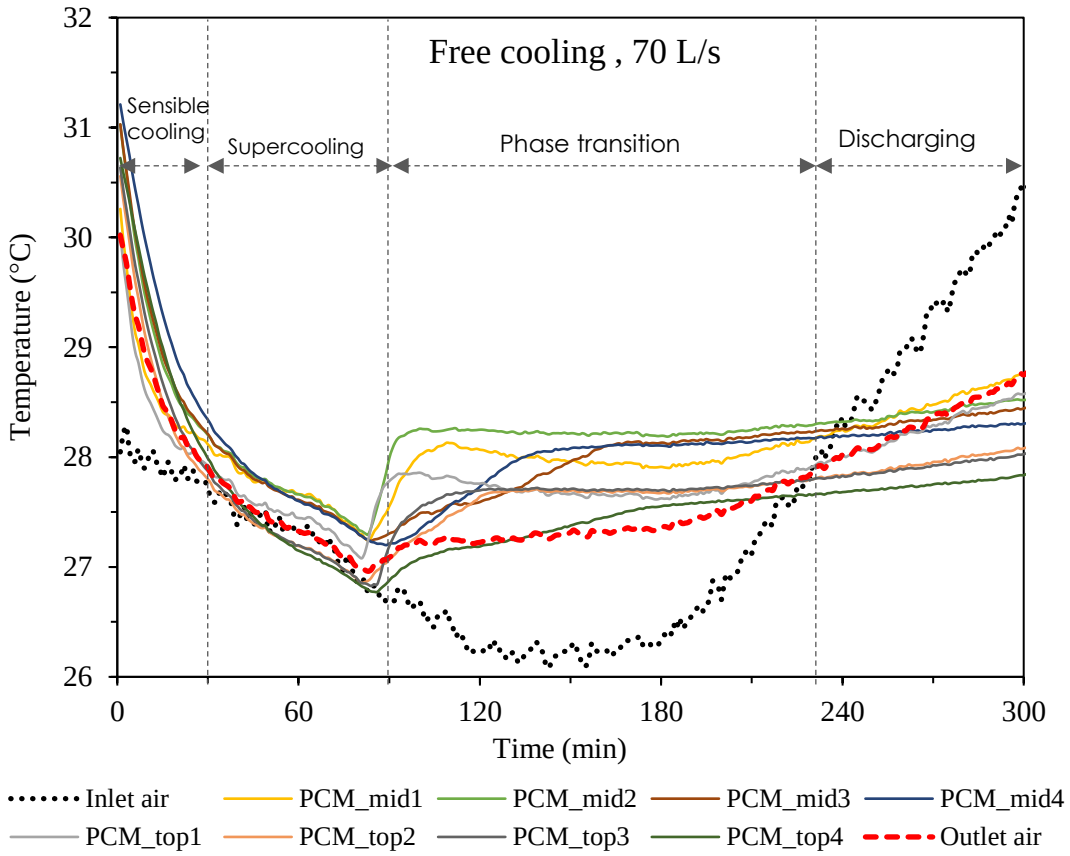


Figure 8.5: Temperatures variation with the time under hot summer conditions (free cooling mode).

It is established that the higher the air flow rate, the quicker the PCM charging process and vice versa. This gives an insight that, if an air flow rate lower than 70 L/s has been used in this case, the entire PCM may remain in the liquid phase as there is a limited time available for charging in the case of extreme summer period in Khartoum city.

According to previous studies (Takeda et al., 2004, Raj and Velraj, 2010), the free cooling strategy is site and climate dependent and operates efficiently in locations

possess diurnal temperature difference between 12 K and 15 K. In the present case, during peak summer months, the daily average maximum and minimum ambient air temperature are 40.9 °C and 26.5 °C, respectively as shown in Figure 8.1. Although the diurnal variation is around 14.5 K, the charging effectiveness was very low, and the solidification rate was also slow. Thus, it should be stressed that the diurnal temperature variation by its own is not enough to evaluate the free cooling potential in any location, and the prevailing charging air temperature and the charging time should be taken into consideration as significant parameters.

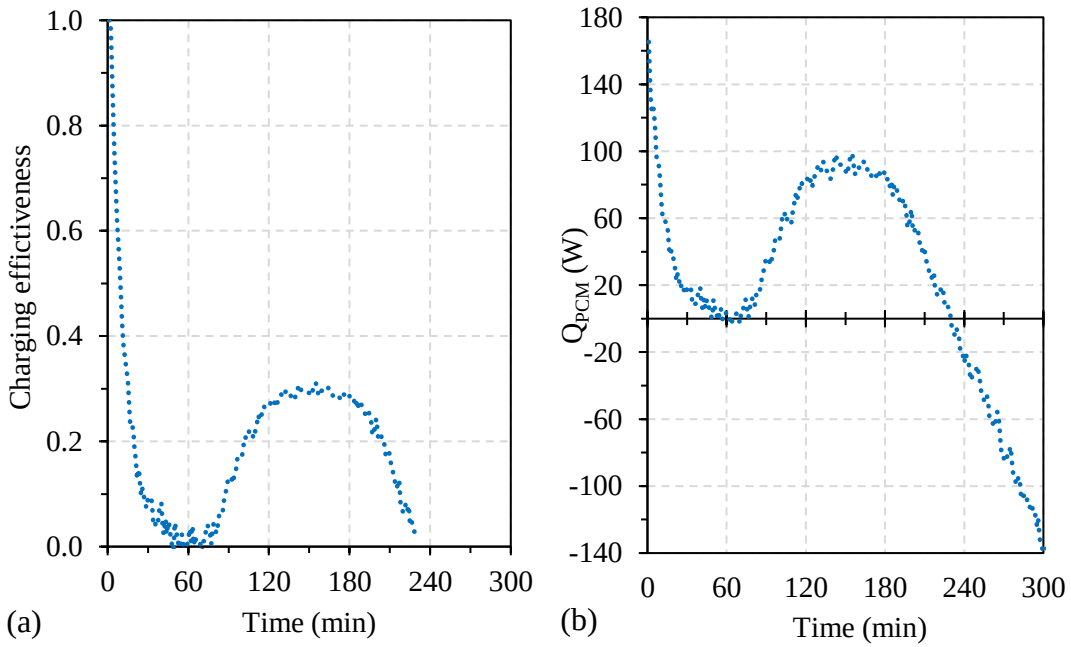


Figure 8.6: Variation of (a) charging effectiveness, and (b) PCM cooling rate under hot summer conditions (free cooling mode).

It could be concluded that the free cooling systems are not very effective under hot summer conditions in hot-arid regions. The solidified PCM portion was small, and most of the PCM region remained in the liquid state due to the insufficient charging attributed to the short period when the temperature difference between the PCM and the HTF is sufficient. Therefore, the radiative cooling has been suggested in the present study to enhance the charging performance of the free cooling system.

8.5.2 Operation under radiative cooling mode

In the case of system operation under hot summer conditions using radiative cooling mode, the temperature of the outlet air from the radiative cooling system is varied depending on the air flow rate. Accordingly, both the duration and start time of the charging process also differed. As previously shown in Figure 8.3, at air flow rates 30, 50, and 70 L/s the charging periods were 9.0, 7.5, and 6.5 hours, respectively, showing that low air flow rates allowing longer charging time, this is because the higher the air flow rate, the lower the energy transferred from the air to the exchanging medium.

8.5.2.1 Temperature variation with the time

Figure 8.7 shows the temperature variation of the outlet air and the PCM modules with the time at air flow rates of 30, 50, and 70 L/s under hot summer conditions using radiative cooling mode. The initial inlet air temperature in all experiments was kept constant at 28.5 °C. The PCM solidification was identified based on the measured temperature along the top surfaces of the PCM containers, which gives a general indication of the phase prevailed in the region around the measured point. The PCM solidifies when its temperature reaches 27 °C, and any temperature drop afterwards is attributed to sensible heat.

It is evident from Figure 8.7 that the temperature of the entire PCM modules dropped quickly to the liquidus point at the beginning of the charging process and continued decreasing showing a supercooling by about 1.0 K in all cases. However, the supercooling duration varied according to the PCM relative location and the air flow rate. The supercooling occurs faster in the front PCM modules and slowly at the rear modules, based on the air temperature gradient. The supercooling duration increases at low air flow rates compared to high flow rates. After going under supercooling, the PCM has gone under gradual phase transformation until reaching the solidification temperature of 27 °C, and then sensibly cooled.

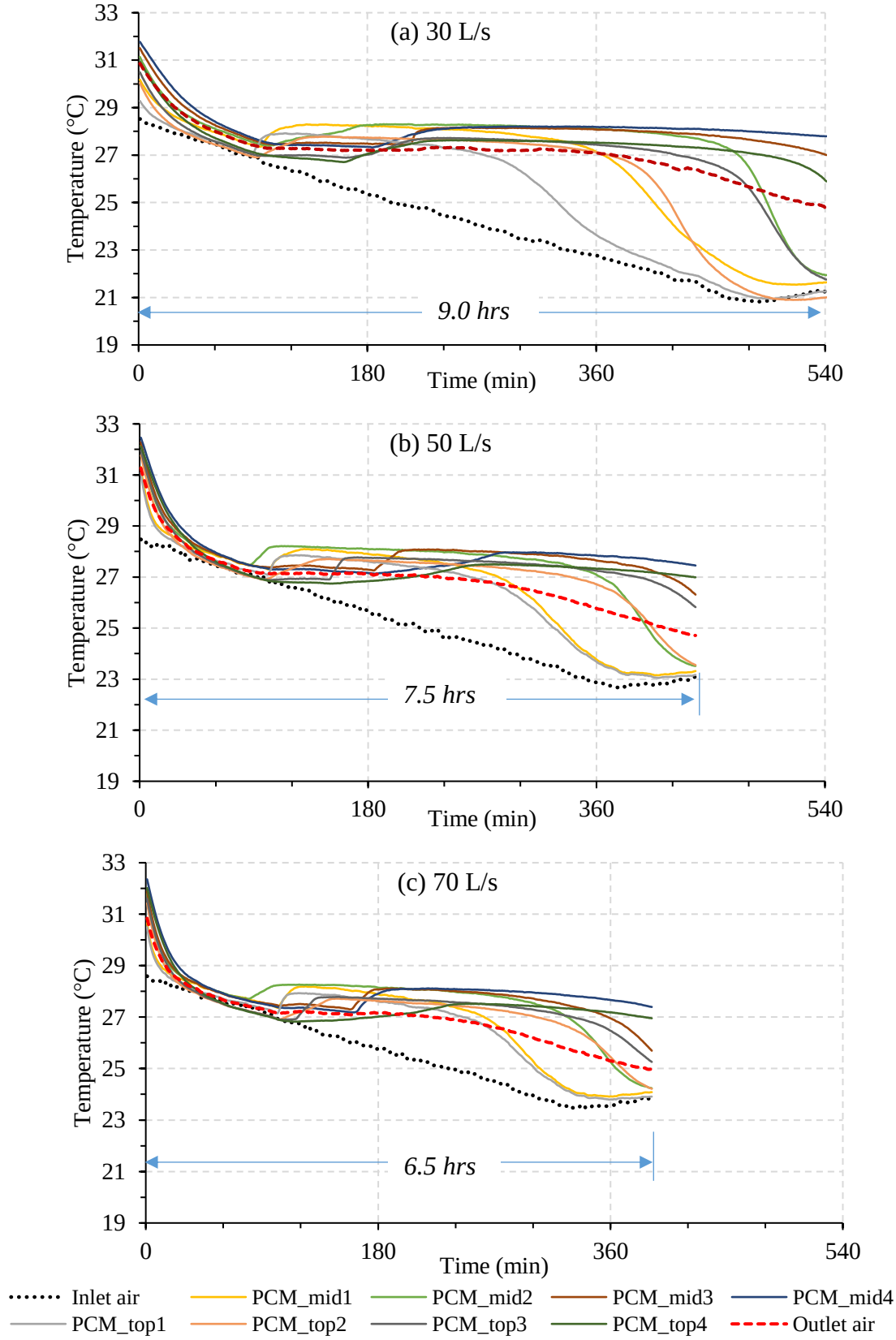


Figure 8.7: Temperatures variation with the time under hot summer conditions (radiative cooling mode).

It could be noticed from Figure 8.7 that, the PCM has gone through a phase change under all tested air flow rates. It is confirmed that the PCM turned into solid in all locations except at the last region of the second modules. The temperature of PCM mid4 locations did not reach the solidus temperature 27 °C by the end of the charging period. Thus, it can be stated that only the first set of PCM modules has completely solidified. Moreover, it seems that if the charging process is continued in order to get the advantage of free cooling during early morning hours when the radiative cooling ceased, the PCM may gain heat from the ambient air.

8.5.2.2 PCM charging performance

The PCM charging performance under hot summer conditions for the system operation using radiative cooling is assessed by the charging effectiveness and the cooling absorbed by the PCM in the given charging time.

The effectiveness of PCM charging has been estimated at air flow rates 30, 50, and 70 L/s as shown in Figure 8.8. It is clear that the charging effectiveness is largely affected by the temperature difference between the PCM and the flowing air, the larger the difference, the higher the effectiveness and vice versa. The charging effectiveness was higher in the case of lower air flow rates as these allow higher heat transfer rates. During the supercooling period, the effectiveness was minimum in all cases. Accordingly, it is recommended to initiate the charging process with a lower air flow rate which could be enhanced after the supercooling period, especially in the case of short charging periods.

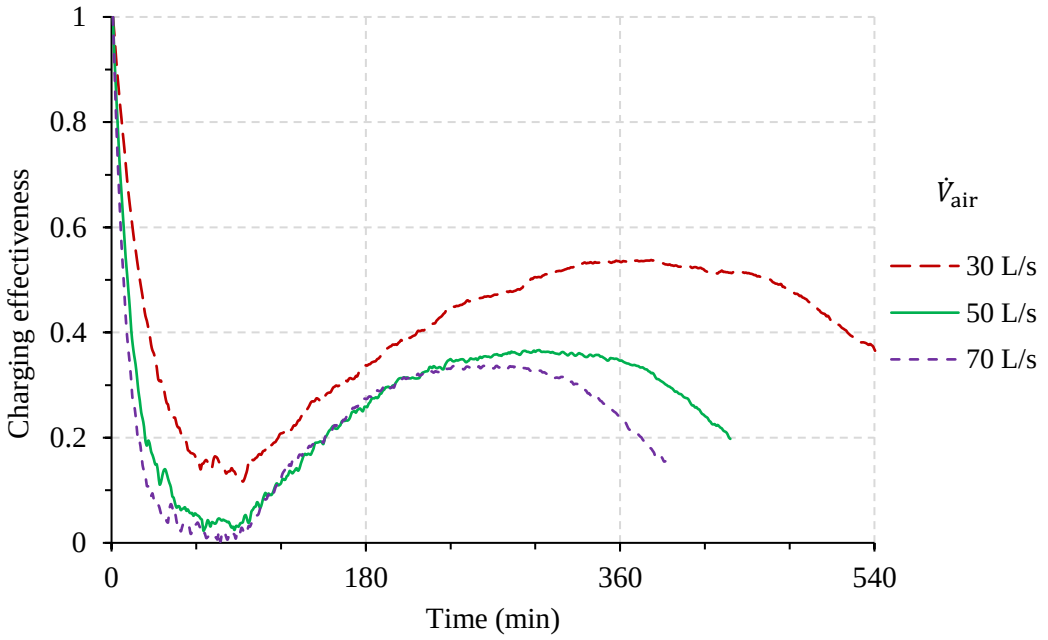


Figure 8.8: Variation of charging effectiveness at different air flow rates under hot summer conditions (radiative cooling mode).

Figure 8.9 compares the PCM cooling rate during the charging phase for the experiments incorporating radiative cooling at air flow rates 30, 50, and 70 L/s and free cooling at air flow rate 70 L/s. It is evident that the heat transfer rate was high during the initial 30 minutes of the charging, due to the large temperature difference. This has dropped to reach the minimum value during the supercooling period with better performance at lower air flow rates. During the transition phase, the cooling rate has enhanced gradually at low air flow rates and sharply at higher air flow rates. The drop in heat transfer rate during the final hour was owing to the lower temperature difference between the PCM and the HTF, as a result of inlet air temperature rise. Summary of the overall cooling rates of the PCM during the possible charging periods under free and radiative cooling modes are presented in Table 8.1.

It can be concluded from Table 8.1 that, for a system operated at low air flow rates, longer charging period is needed and vice versa. Compared to the cooling rate of free cooling only mode, the variation was substantial. The total cooling rate of the PCM by free cooling accounted for about 23.5%, 26.8%, and 28.6% of that achieved by radiative cooling under air flow rates 30, 50, and 70 L/s, respectively.

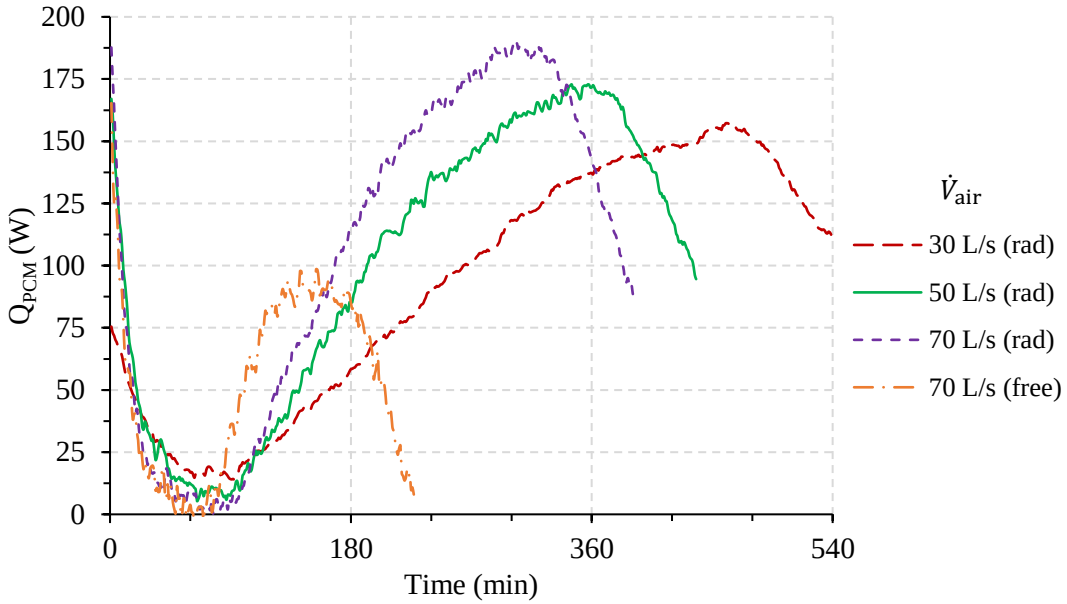


Figure 8.9: Variation of the PCM cooling rate at different air flow rates under hot summer conditions.

Table 8.1: Total PCM cooling rate and the corresponding charging period under hot summer conditions.

	Air flow rate (L/s)	**Charging period (hour)**	**Total cooling rate of the PCM (Wh)**
Free cooling	70	3.8	195.9
Radiative cooling	30	9.0	834.1
	50	7.5	730.9
	70	6.5	684.7

It is crucial to underline that the usage of radiative cooling to enhance the performance of free cooling systems under hot summer conditions in hot-arid climate is highly effective. An additional cooling rate up to 4.3 times (depending on the air flow rate) of that obtained by free cooling using the maximum air flow could be achieved. A mixed charging mode can be used for more enhancement, bearing in mind that more electrical energy is required for the fan operation. However, in order to overcome the effect of supercooling taking place at higher charging air temperatures, the free cooling mode should be only activated if the ambient air temperature is lower than the PCM average melting temperature.

8.6 Results and discussion of PCM charging under moderate conditions

8.6.1 Operation under free cooling mode

In the case of the system operation under moderate summer conditions using free cooling mode, the ambient air temperature shown in Figure 8.3b indicates that there is a considerable cooling potential throughout the night and early morning hours, extending to more than 10 hours. Therefore, the PCM charging process has been carried out considering two scenarios; (I) charging during the initial night hours, and (II) charging during the last night hours. In both scenarios, the maximum air flow rate given by the operated fan (70 L/s) was used in order to get the most out of the free cooling.

Figure 8.10a and Figure 8.10b exemplify the temperature variation of the outlet air and the PCM modules with the time when the inlet air temperature dropped from 28.4 to 21.2 °C, and from 25 to 20.3 °C for scenario I and scenario II, respectively. It is clear from Figure 8.10 that, the system reached the steady-state conditions and full PCM solidification was achieved for both scenarios after 7.6 hours (I) and 5.0 hours (II). The reason that the charging was slower in scenario I is the higher charging air temperature, which also resulted in a higher supercooling compared to scenario II. Due to the supercooling, the heat transfer rate and hence the charging effectiveness in scenario I were very low between minutes 30 and 90 as shown in Figure 8.11, where the outlet air temperature reached the inlet air temperature. In the case of scenario II, the supercooling ended quickly in about 20 minutes in most of the PCM modules, where a large temperature difference between the inlet air and the supercooling temperature was existing (Figure 8.10b).

The night-time thermal comfort in buildings in the hot-arid climate could be obtained via direct night ventilation during the transitional months. However, as shown in Figure 8.3b, the night-time ambient temperature in Khartoum is lower than the comfort temperature of 28.8 °C determined by Merghani (2001) for buildings in hot-arid climate during the spring months. Thus, the air supplied by the TES system at a higher temperature than the ambient air could be used for thermal comfort provision during night hours (Figure 8.10).

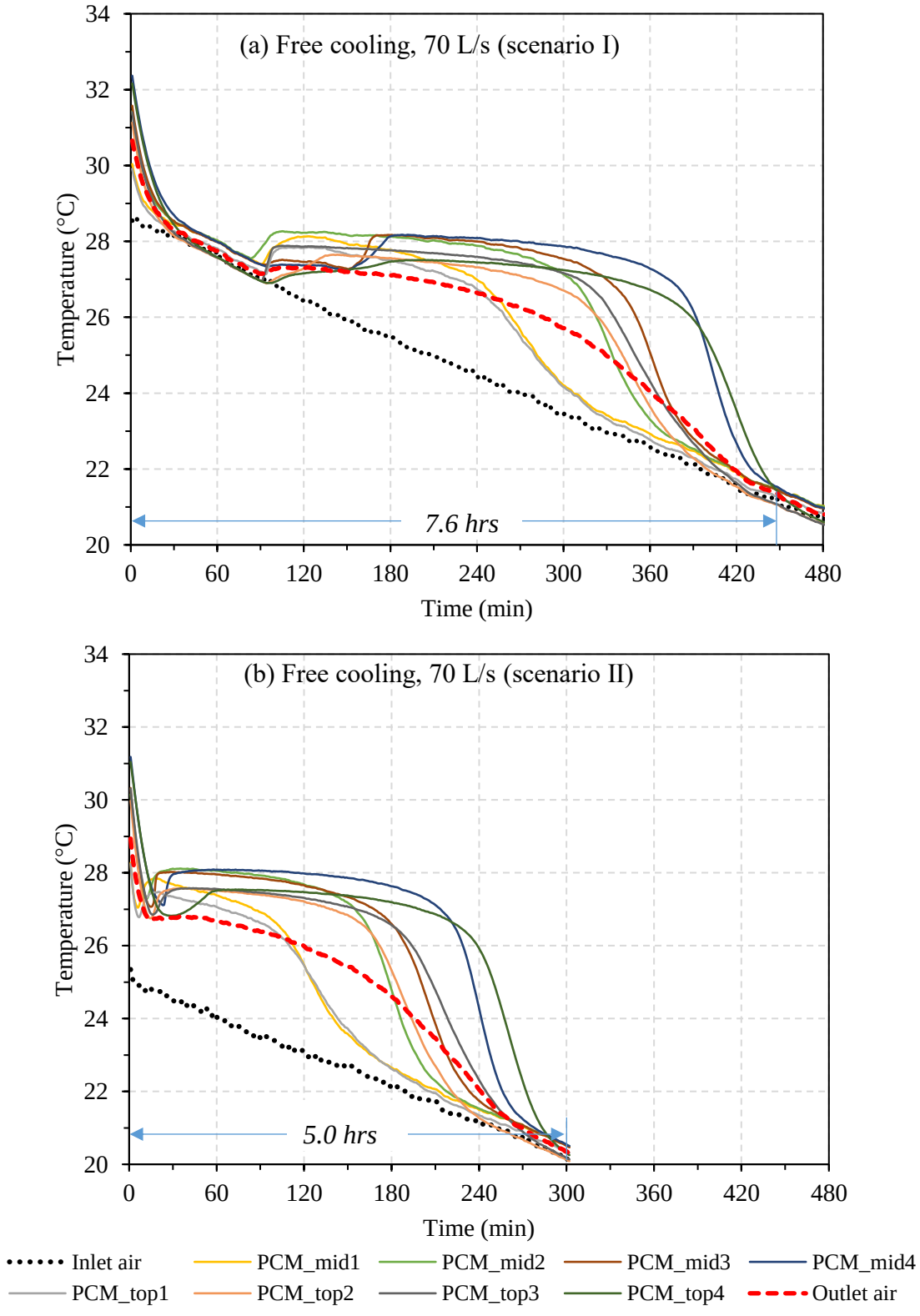


Figure 8.10: Temperatures variation with the time under moderate summer conditions; (a) charging during first night hours, and (b) charging during last hours (free cooling mode).

As shown in Figure 8.11a and Figure 8.11b, the charging effectiveness and the PCM cooling rate were higher for the system operation during the late hours of the night than the early hours, owing to the considerable temperature variation of the PCM and the air. The charging effectiveness during the transition phase was around 0.54 and 0.35, and the total cooling rate of the PCM was about 762.8 and 841.4 for scenario I and II, respectively. The charging duration was 52% longer in the case of scenario I.

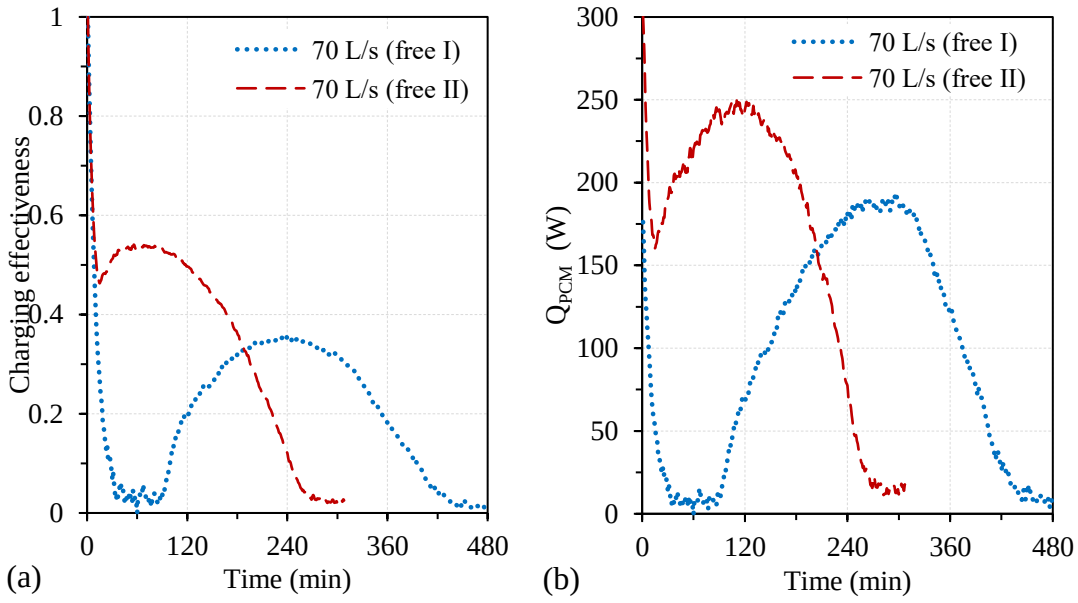


Figure 8.11: Variation of (a) charging effectiveness, and (b) PCM cooling rate under moderate summer conditions (free cooling mode).

Based on the above results, the charging of PCM using night-time free cooling under moderate summer conditions in hot-arid climates has a high potential. In the present case study, the available free cooling was higher than the capacity of the proposed TES system. The modular design of the proposed TES system allows addition of more PCM modules to harness the excess energy at night if needed. According to the results, charging the PCM during the latest part of the night has the advantage of minimising the effect of supercooling. Besides, the air flow rate can be adjusted based on the free cooling potential and the daytime cooling requirements to ensure a minimum power consumption by the fan.

8.6.2 Operation under radiative cooling mode

Under moderate summer conditions using radiative cooling, the charging process initiates directly at the commencing of the night-time due to the suitable charging temperatures. According to Figure 8.3b, the temperature of the outlet air from the radiative cooling system is varied depending on the air flow rate. Hence, the initial charging temperature also differs. Results in section 8.5.1 have indicated that full PCM solidification can be achieved using the free cooling. Therefore, it will be possible to achieve this using the radiative cooling. In this section, the potential of radiative cooling performance in comparison to the free cooling mode is evaluated.

8.6.2.1 Temperature variation with the time

Figure 8.12 exemplifies the variation of the outlet air temperature and the PCM modules with the time at air flow rates of 30, 50, and 70 L/s. It is evident that the PCM has gone through a sensible cooling phase at the beginning of the charging process, then the phase transition, followed by a sensible cooling until reaching the steady-state conditions. It can also be observed that the supercooling was generally small and has no obvious impact on the charging effectiveness in all test cases, due to the low charging air temperature. The system has reached the steady-state conditions after 7.0, 6.3, and 5.5 hours at air flow rates 30, 50, and 70 L/s, respectively.

It is also noticeable from Figure 8.12 that the supplied air temperature of the system during the later hours of the charging process was far lower than the comfort temperature during the transitional months. Thus, the conventional night ventilation through the building's fenestrations may be more practical for the instantaneous thermal comfort during the charging period. However, this would not be the case if a large TES system has been utilised (depending on the cooling demand during the daytime), as the charging time prolongs and the outlet air temperature slightly swings around the PCM transition temperature for a longer period.

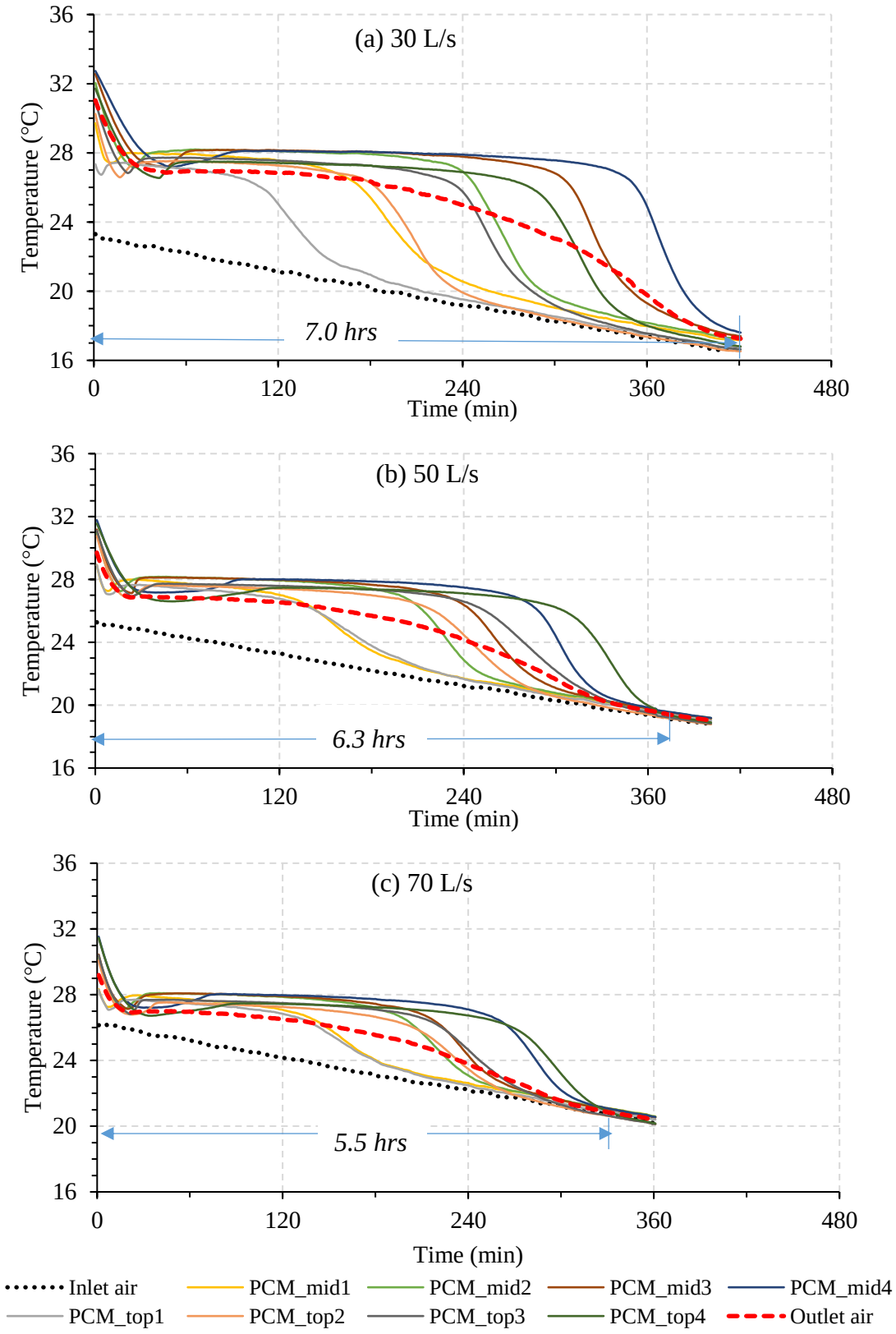


Figure 8.12: Temperatures variation with the time under moderate summer conditions (radiative cooling mode).

8.6.2.2 PCM charging performance

The charging performance of the TES system under moderate summer conditions when coupled with the radiative cooling system was assessed by determining the charging effectiveness and the PCM cooling rate.

The variation in PCM charging effectiveness with the time is presented in Figure 8.13 for the system operation using radiative cooling mode at different air flow rates. It can be seen that the charging effectiveness followed a similar trend under all air flow rates, with a lower air flow rate exhibiting higher charging effectiveness. Generally, the charging effectiveness was high initially due to the large temperature difference between the PCM and the HTF. Then, it became nearly steady around 0.58, 0.51, and 0.47 at the air flow rates 30, 50, and 70 L/s, respectively during the transition phase, and gradually dropped to nearly zero at the end of the charging process.

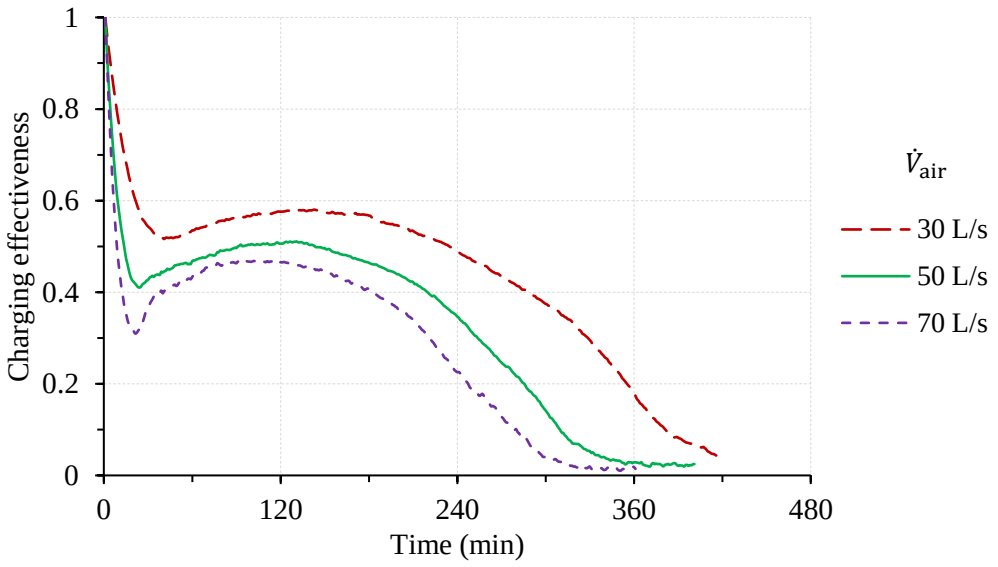


Figure 8.13: Variation of charging effectiveness at different air flow rates under moderate summer conditions (radiative cooling mode).

The variation in the PCM cooling rate with the time when using radiative cooling at various air flow rates compared to the free cooling at an air flow rate of 70 L/s is shown in Figure 8.14. A comparison of the total PCM cooling rate and the required charging durations are presented in Table 8.2. It is evident from the results that the cooling rate was high initially and then dropped rapidly due to supercooling effect in

all test cases. During the period of latent heat exchange, the higher the air flow rate, the higher the cooling rate under radiative cooling mode. However, the variation was small. The charging of PCM using free cooling during the last part of the night at air flow rate 70 L/s has shown the highest heat transfer rate between the PCM and the HTF throughout the phase transition period, as a result of the initial lower inlet air temperatures.

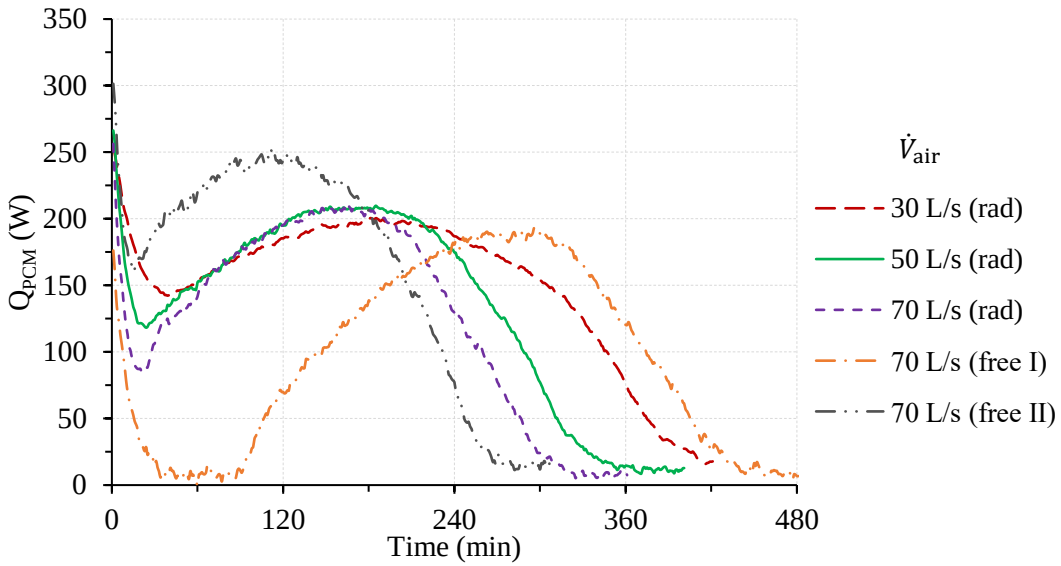


Figure 8.14: Variation of the PCM cooling rate at different air flow rates under moderate summer conditions (free and radiative cooling modes comparison).

According to Table 8.2 which summarises the system performance, the total cooling rate of the PCM through the free cooling scenario I represented about 72.3%, 85.7%, and 99.8% of that obtained via the radiative cooling at air flow rates 30, 50, and 70 L/s, respectively. This denotes that the use of radiative cooling to enhance the charging performance of the free cooling systems depends largely on the air flow rate. Therefore, the optimisation of air flow rate is crucial to balance between the cooling requirements and the charging time.

It is also clear from Table 8.2 that at the same air flow rate of 70 L/s, the system operation using free cooling during later night hours (scenario II) produced a higher cooling rate by about 10% with a shorter charging period of 10% (30 minutes) compared to those obtained via the radiative cooling during the initial night hours.

This shows that in the case of small TES systems, it is better to use the free cooling during the last hours of the night than using radiative cooling. Unlike the case of large TES systems, where the demand exceeds the free cooling capacity and operation of the radiative cooling system from the beginning of the night is more beneficial to support the free cooling performance.

Table 8.2: Total PCM cooling rate and the corresponding charging period under moderate summer conditions.

	Air flow rate (L/s)	**Charging period (hour)**	**Total cooling rate of the PCM (Wh)**
Free cooling, scenario I	70	7.6	762.8
Free cooling, scenario II	70	5.0	841.4
Radiative cooling	30	7.0	1055.4
	50	6.3	889.8
	70	5.5	764.3

8.7 Summary

This chapter presented and discussed the experimental results of a TES system for building cooling under transient inlet air conditions. The PCM charging performance was assessed under hot and moderate summer conditions of hot-arid climates. Two modes of operation have been adopted; a free cooling mode at air flow rate 70 L/s, and a radiative cooling mode exploring three air flow rates 30, 50, and 70 L/s. The major conclusions derived from this investigation are:

- Under hot summer conditions in hot-arid climates, the results confirmed that the performance of free cooling systems is inefficient as only a small amount of cooling can be stored, owing to higher ambient air temperature and limited charging period. Conversely, the use of the radiative cooling system in conjunction with free cooling was substantially effective.

- Under moderate summer conditions, the performance of the free cooling system is effective, due to the large availability of natural cooling for longer durations. However, charging during the later night hours was found beneficial for a faster PCM solidification than during the initial hours.

The results have also shown that the PCM supercooling has a significant impact on the charging effectiveness, and its impact is higher at the low temperature difference between the PCM and the HTF. The effect of supercooling can be significantly minimised by the integration of the radiative cooling system with the free cooling.

In general, the incorporation of radiative cooling strategy in the TES system to enhance the charging performance of free cooling systems is highly promising. The proposed system has shown a high capability to reduce the cooling load or minimise the conventional cooling systems energy requirements. The radiative cooling has a higher potential under hot summer conditions compared to moderate summer conditions in hot-arid climate.

Chapter 9

Energy Saving Potential of the NRV-LHS System

9.1 Introduction

This chapter discusses the potential energy saving of the proposed hybrid NRV-LHS system in comparison with the conventional cooling systems.

9.2 Performance evaluation

The proposed NRV-LHS system is designed to serve a single room in a domestic building under hot-arid climate conditions as discussed in Chapter 5 and Chapter 6. The TES capacity was determined based on the cooling load of a room with well-insulated roof and external walls during an average day of hot summer months (May and June).

Under considered hot-arid climate conditions, there is a considerable cooling potential during the transition months (March and April), with adequate time up to 11 hours for full PCM charging (Table 9.1). Therefore, the entire cooling load could be fulfilled through the use of free cooling only. Moreover, with the assistance of radiative cooling, the cooling storage capacity could be enhanced, and this reduces the fan energy requirements. On the other hand, provision of sufficient cooling during the summer period (May-October) using passive systems is quite challenging in buildings in hot-arid climate, where the ambient temperature is high relative to PCM transient temperature and the available time for charging is limited (3-5 hours only) as shown in Table 9.1. Therefore, the system performance evaluation in this section will base on these six months, where the cooling demand is dominant.

Table 9.1: Suitable conditions for PCM charging in a reference day during summer and transitional months in a hot-arid climate of Khartoum.

	Mar.	**Apr.**	**May**	**Jun.**	**Jul.**	**Aug.**	**Sep.**	**Oct.**
Charging period (hr)	11	7	2	3	3	5	3	3
Avg. ambient temperature (°C)	23	25	27	27	26	26	26	26

The total heat absorbed by the PCM during the discharging time was determined using heat balance analysis (equation (7.2)) based on the outlet air temperatures calculated using CFD simulation in ANSYS Fluent. The building cooling load was estimated using Energy-Plus simulation model in DesignBuilder.

The power consumption in the proposed system is due to the fan. The Bernoulli equation (9.1), which relates the conservation of pressure, kinetic, and potential

energies of a fluid stream, can be applied to estimate the fan power (Munson et al., 2013).

$$\Delta p_{\text{total}} + \frac{1}{2}\rho v^2 + \rho g h = constant \tag{9.1}$$

where; Δp_{total} is the total pressure drop, ρ is the fluid density, v is the fluid velocity, g is the gravitational acceleration, and h is the height.

In the current analysis, the third term related to gravity can be ignored, since there is no difference in height between the inlet and the outlet. Taking into consideration the effect of kinetic energy, the power used by the fan (P_{fan}) can be expressed using equation (9.2);

$$P_{\text{fan}}(W) = \dot{V} \times \left(\Delta p_{\text{total}} + \left(\frac{1}{2}\rho v^2\right)\right) / \eta_{\text{fan}} \tag{9.2}$$

where; $\dot{V}$ is the air volume flow rate, and η_{fan} is the fan efficiency which has been assumed at 0.55 according to Franconi and Bradford (2000).

The total energy consumption (E_{fan}) in the current system involves the fan operation during both charging and discharging time (t), and can be estimated using equation (9.3) (Mosaffa et al., 2013b);

$$E_{\text{fan}}(Wh) = \left(P_{fan} \times t\right)_{\text{charging}} + \left(P_{fan} \times t\right)_{\text{discharging}} \tag{9.3}$$

The coefficient of performance (COP) of the system can be determined (similar to that of heat pump systems) as a ratio of the total useful energy discharged to the building (Q_{useful}) to the total energy consumption by the fan (E_{fan}) as follows (9.4) (Mohamed et al., 2019)

$$COP = \frac{Q_{\text{useful}}}{E_{\text{fan}}} \tag{9.4}$$

9.3 Pressure analysis and fan power consumption

In order to evaluate the system performance, the energy consumption due to the fan operation should be taken into consideration. Therefore, the pressure drop between the inlet and the outlet of the TES system has been investigated. In the proposed TES system, there is a local pressure rise in the region where the inlet air hits the PCM module, owing to the conversion of kinetic energy into pressure energy. This causes a pressure drop after the air passes the PCM modules (outlet). In the current analysis, the pressure drop is mainly proportional to the flow rate of the HTF and the PCM modules arrangement inside the duct. Since the overall PCM thickness/volume is equal in all cases, the influential design parameter will be the height of the air channels. The pressure drop was estimated using CFD simulation. The fan power consumption was calculated using equation (9.3).

The variation of the predicted pressure drop and fan power consumption with the air volume flow rate is presented in Table 9.2 and Figure 9.1, for a base model with a 10 mm PCM module thickness and 15 mm air channel height. The tested range of air flow rates involved the charging and discharging operation. It has been observed that the pressure drop increases with the air flow rate with a polynomial relation. The pressure drop varied between 0.68 Pa and 71.19 Pa, for air flow rates between 27 L/s and 533 L/s, respectively.

Table 9.2: Predicted pressure drop and fan power consumption for different air flow rates.

Air flow rate (L/s)	Pressure drop (Pa)	Fan power (W)*
27	0.68	0.04
53	1.75	0.18
80	3.35	0.52
107	5.23	1.10
213	16.31	6.94
320	29.74	19.41
427	48.14	42.37
533	71.19	78.73

* Calculated assuming fan efficiency of 0.55 and an air temperature of 27 °C.

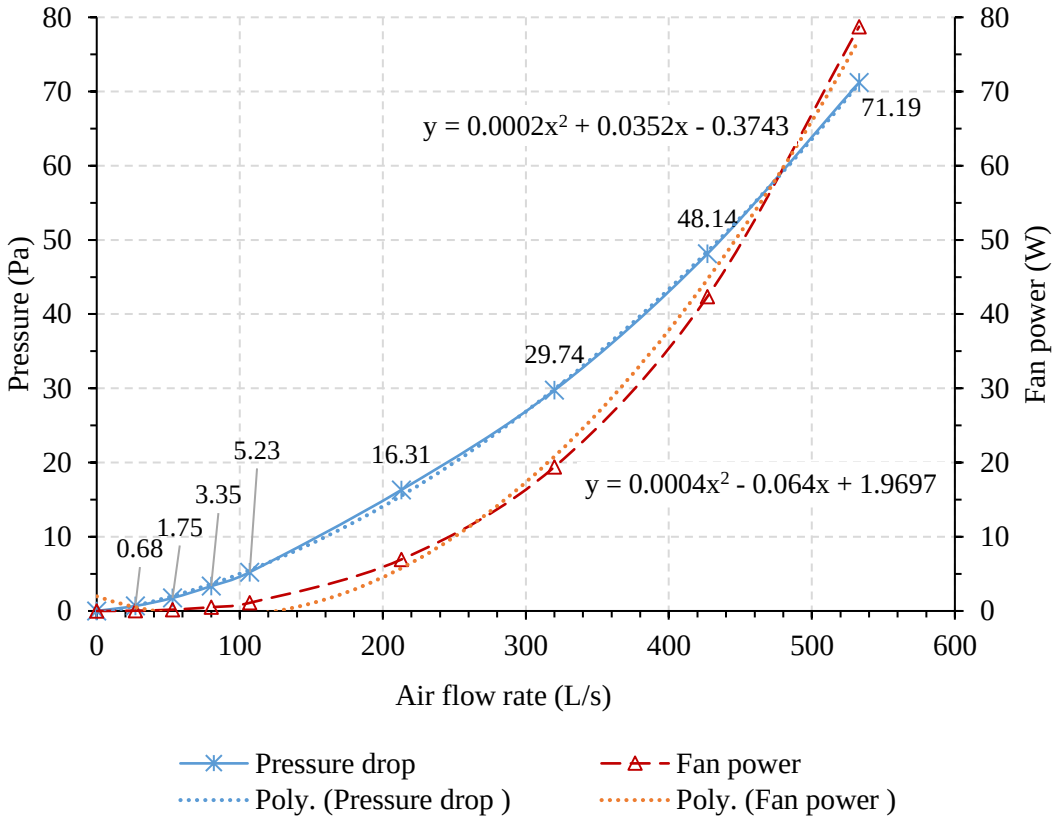


Figure 9.1: Predicted pressure drop and fan power consumption for different air flow rates.

Table 9.3 presents the predicted pressure drop and fan power consumption for various TES configurations (cases 1-6, described in section 6.7.4) at air flow rate 213 L/s (PCM charging). It is inferred from Table 9.3 that the TES geometrical configuration has a significant impact on the fan power consumption. The variation in the fan power consumption was considerable between the systems with narrow air flow channels and wide channels. For instance, the fan power was lower in case 5 (10 mm PCM thickness and 15 mm air channels height) by around 81% than case 1 (5 mm for both PCM thickness and air channels height). On the other hand, during the discharging phase, the required fan power for cooling extraction is generally low. The maximum pressure drop and fan power consumption were estimated at 8.5 Pa and 0.38 W, respectively, at the air flow rate of 27 L/s, which are obtained in the most compacted TES design (case 1).

Though a compact TES unit allows better thermal performance as discussed in Chapter 6, high power use by the fan is predicted during the charging process according to the data given in Table 9.3. Therefore, optimisation of the TES system design should depend on the overall performance evaluation including the fan power use, the cooling load provided, and the potential energy savings to the conventional systems operation.

Table 9.3: Predicted pressure drop and fan power consumption for different TES configurations.

	Charging phase		**Discharging phase**	
	air flow rate 213 L/s		**Air flow rate 27 L/s**	
Case	**Pressure drop (Pa)**	**Fan power* (W)**	**Pressure drop (Pa)**	**Fan power* (W)**
Case 1	123.3	54.39	8.5	0.42
Case 2	18.39	10.01	1.07	0.05
Case 3	5.59	3.77	0.33	0.02
Case 4	47.78	24.74	2.26	0.11
Case 5	16.31	10.21	0.68	0.03
Case 6	3.63	3.34	0.16	0.01

* Calculated assuming fan efficiency of 0.55 and an air temperature of 27 °C.

9.4 Cooling capacity of the proposed system

The operational performance was assessed for two TES system configurations; a compact system with a 5 mm of both PCM thickness and air channels height (case1), and a less compacted system with a 10 mm PCM thickness and 15 mm air channels height (case 5). The assessment of the system charging performance was based on the prevailing ambient climate conditions in hot-arid regions presented in Table 9.1. Air flow rates of 213 L/s and 533 L/s were used for the free cooling operation, whilst 30 L/s and 70 L/s were considered in the radiative cooling operation. In the case of the discharging operation, the evaluation was based on a gradual extraction of the cooling stored in the PCM using an air flow of 27 L/s, which is considered appropriate for thermal comfort conditions in buildings.

Based on the considered two TES systems configurations, modes of operation, and the inlet air conditions mentioned above, an energy performance evaluation was conducted for eleven different conditions (A-K) as presented in Table 9.4, which summarises the total cooling produced, fan's power, and potential percentages of cooling load reduction for the entire summer period from May to October. The total cooling load for the considered summer months was 577.3 kWh, estimated using Energy-Plus model. It is inferred from Table 9.4 that a compact system design may provide a higher cooling capacity, owing to the higher heat transfer rate. However, the required power to operate the fan was much high for the range of optimum air flow rates required for the charging process.

Table 9.4: A comparison of performance for different TES configurations and operating conditions in summer of hot-arid climates (May-June).

TES arrangement	**Case**	**Air flow rate**	**Pressure drop**	**Cooling produced**	**Fan energy use***	**AC energy use****	**Cooling load reduced**
		(L/s)	(Pa)	(kWh)	(kWh)	(kWh)	(%)
	Free cooling system						
Case 5	A	213	16.31	146.9	4.0	73.3	25.4%
	B	533	71.19	243.9	40.2	121.8	42.2%
Case 1	C	213	123.3	194.9	28.3	97.6	33.8%
	D	533	541.6	355.3	234.1	177.5	61.5%
	Radiative cooling system						
Case 5	E	30	0.7	86.5	0.08	43.3	15%
	F	70	2.5	86.5	0.39	43.3	15%
Case 1	G	30	9.81	96.1	1.05	47.9	16.6%
	H	70	27.44	96.1	4.13	47.9	16.6%
	Hybrid cooling system						
Case 5 (A+F)	I	243	18.81	233.4	4.1	116.6	40.4%
Case 5 (B+F)	**J**	**563**	**73.69**	**330.4**	**40.3**	**165.1**	**57.2%**
Case 1 (C+H)	K	243	150.74	291.0	29.3	145.5	50.4%

* Calculated assuming fan efficiency of 0.55. ** Calculated assuming COP of an AC system at 2.0.

Note: Calculations are based on a total cooling load of a room about 577.3 kWh during summer (May-October).

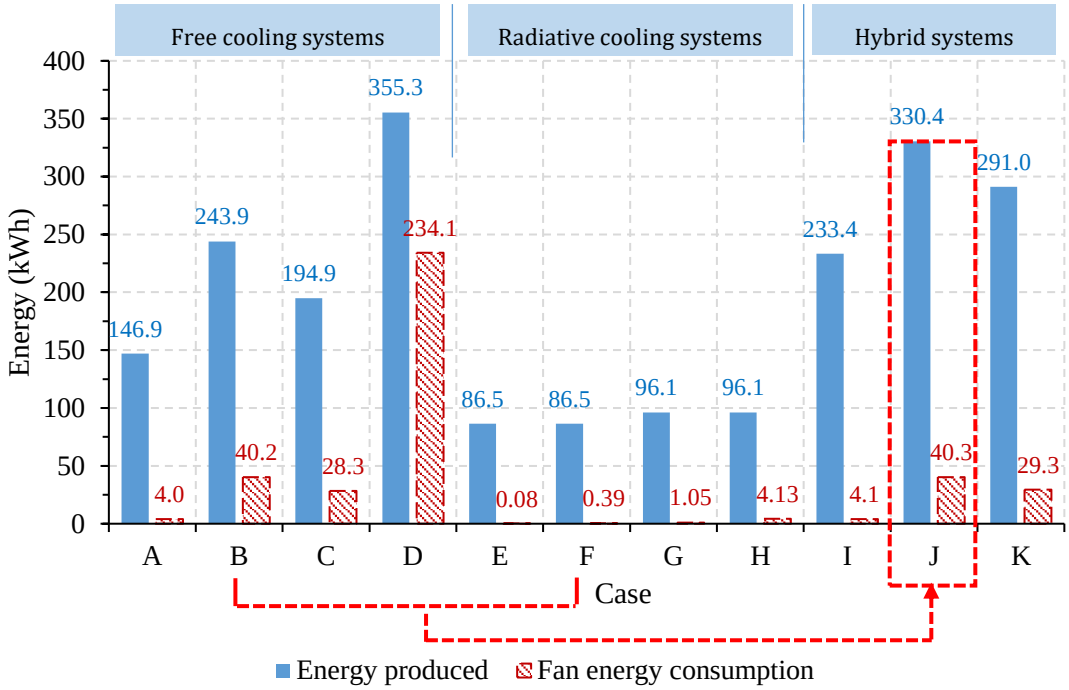


Figure 9.2: A comparison of energy produced and energy consumed by the system for different TES configurations and operating conditions.

Significantly, by comparing the performance of the tested conditions A-K shown in Table 9.4 and Figure 9.2, a hybrid system with less compacted PCM modules arrangement (case J) have shown the best performance, with the highest cooling load drop and a significant potential energy saving.

The monthly performance of the optimised hybrid cooling system is detailed in Table 9.5. It can be observed that the performance is lower during peak summer months (May and June) compared to the rest of the overheated period (July-October). Under peak summer conditions, the estimated COP varied between 5.82 and 6.98, where the system could fulfil around 26%-32% of the cooling load, with nearly half of the cooling obtained via the radiative cooling. The lower performance is attributed to the limited cooling potential, where the ambient air temperature is as high as 27 °C and the charging periods are between 2 and 3 hours. In the period from July to October, a higher cooling capacity could be achieved. The COP was estimated to be around 9.0. Particularly, in August, the use of a lower air flow rate could be sufficient to fulfil the entire cooling demand. Thus, it is essential to vary the air flow rate according to the cooling requirements for efficient performance.

Table 9.5: Performance of the optimum hybrid cooling system during the overheated months.

Month	Available free cooling		Radiative cooling	Daily Avg. cooling load	Cooling load covered	Energy prod-uced	Fan energy use*	COP
	Temp. (°C)	Period (hr)	Period (hr)	(kWh)	%	(kWh)	(kWh)	
May	27	2	9	4.270	26%	1.104	0.158	6.98
Jun.	27	3	9	4.278	32%	1.378	0.237	5.82
Jul.	26	3	8.5	2.893	75%	2.137	0.237	9.01
Aug.	26	3	8.5	2.006	100%	2.121	0.235	8.95
Sep.	26	3	8.5	2.830	76%	2.137	0.237	9.01
Oct.	26	3	8.5	2.965	74%	2.137	0.237	9.01

* Calculated assuming fan efficiency of 0.55.

During the entire summer period, it is difficult to attain the complete solidification of the PCM storage of a total capacity around 4.6 kWh. The solidification percentage could be between 26-76% of the total PCM energy storage. The chart in Figure 9.3 provides a breakdown of contributions of the passive and active cooling systems to the overall cooling load for the summer period (May-October).

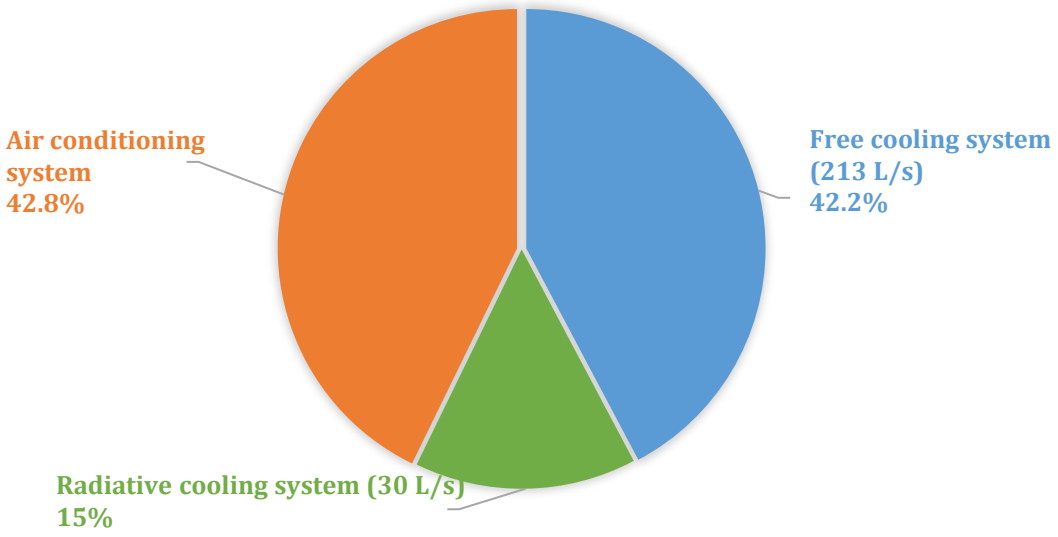


Figure 9.3: Contribution of cooling systems to the building cooling load during summer months (May-October).

9.5 Comparison with conventional air conditioning systems

A comparison between the proposed hybrid NRV-LHS system performance (Case J) and a typical mechanical vapour compression cooling system has been carried out. According to (Duan, 2011), the COP of mechanical AC systems is usually low at an average of 2.0 in the case of operation in hot climates, owing to the high ambient temperature. As shown in Figure 9.4, the total electrical energy savings achievable by the hybrid NRV-LHS system operation during summer (May-October) was estimated at 124.82 kWh, accounting for around 76% of conventional AC systems consumption.

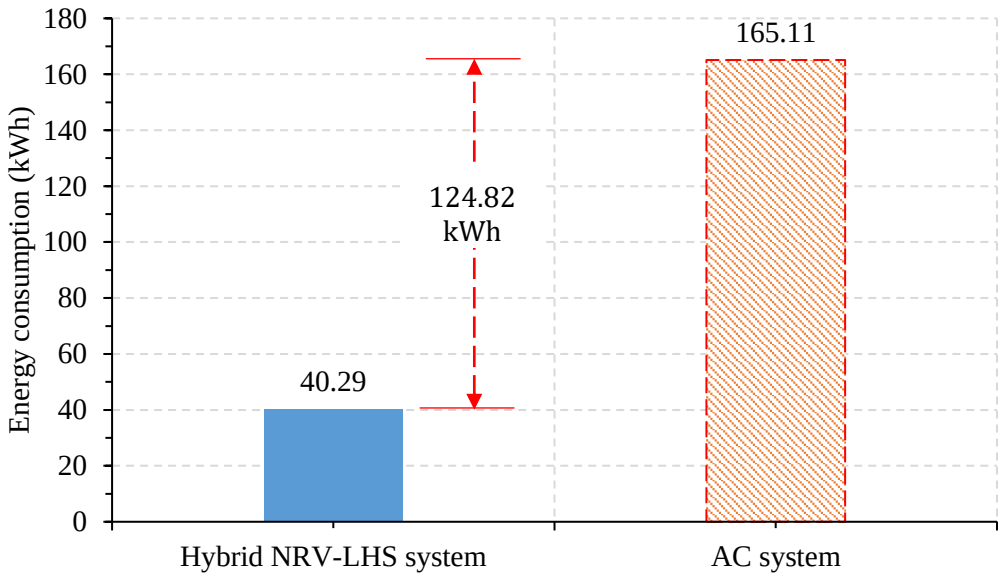


Figure 9.4: A comparison of electrical energy consumption between the hybrid NRV-LHS system and conventional AC systems.

Although the initial cost of the sustainable cooling system can be higher by around 10% than the conventional air conditioning system of an equivalent cooling capacity and the payback period is estimated to be around 3-4 years (Zalba et al., 2004, Kamali, 2014), the operational cost is far lower, based on the significant energy savings obtained (Figure 9.4). In all studies, the PCM usually has the largest share of the system production cost. However, with the ongoing intensive research and the increasing number of PCM manufacturers around the world, the overall cost is predicted to drop in the near future.

Chapter 10

Conclusions and Future Work

10.1 Conclusions

The current study is aimed at enhancing the charging performance of night free cooling systems in buildings through the incorporation of nocturnal radiative cooling strategy. The proposed novel system aims to make use of the natural coolness of radiative exchange with the sky. The system may have a potential application in buildings in hot-arid regions, where the cooling demand is dominant most of the year. CFD simulations and experimental investigation were carried out to study the solidification and melting behaviour of the proposed thermal energy storage under different operating conditions and system configurations. The comparison of modelling and experimental results has shown a good agreement.

The major findings and conclusions drawn from this research are as follows;

- The free cooling potential in the hot-arid climate is very high during the moderate summer and transitional months. This is attributed to the considerable diurnal temperature variation and the low ambient air temperature for long durations in the night-time. However, the PCM charging is more effective during the late hours of the night.
- The free cooling system performance is less efficient during the severe hot summer conditions, owing to the high ambient air temperature and limited available charging time at night. Therefore, it would be better to select a PCM that possesses a transition temperature close to the upper band of the summer comfort zone (25.5-30 °C). The results have shown that the use of the radiative cooling in conjunction with the free cooling system can considerably enhance the charging process.
- The nocturnal radiative cooling in the hot-arid climate has a high potential most of the year, except during the autumn season. This is because of the clear sky conditions and the low humidity levels characterised such regions most of the year. To exploit the available radiative cooling efficiently, a horizontally positioned metallic radiator with a high emissivity coating and a narrow air flow channel underneath the radiator. The use of windscreens in the windy locations to reduce the convective gain is also recommended. A cooling rate in

the range of 135-193 Wh/m² is achievable under typical summer conditions of hot-arid climate through the integration of an optimised radiative cooling system with the free cooling system. The inlet air temperature to the PCM storage could be reduced by up to 6.1 K when the air flow rate as low as 30 L/s, which speeds up the PCM charging.

- Under moderate summer conditions, the utilised PCM has completely solidified under both free cooling and radiative cooling operation modes. The energy transferred from the air via the free cooling system using air flow rate of 70 L/s accounted for about 72.3%-99.8% of that acquired via the radiative system at air flow rates 30-70 L/s. While under hot summer conditions, it was about 23.5%-28.6% of that obtained by the radiative system at the air flow rates 30-70 L/s. The results exhibit that the proposed NRV-LHS system has a higher cooling potential under hot summer conditions than the moderate summer conditions. Although full PCM solidification was not attained under severe summer conditions in the present case study, the amount of cooling stored has been increased four times by the combined system. Yet, boosting the air flow rate may be required for better thermal performance.
- The supercooling is a major obstacle which affects the PCM charging performance. According to the experimental results, the adopted PCM had exhibited a supercooling of 1 K. The impact of the supercooling was greater in the case of the low temperature variation of the PCM and the HTF and when the air flow rate was at a lower level. The supercooling duration varies according to the PCM relative location; it occurs quicker in the PCM zones close to the air inlet as a result of the higher cooling rate and prolongs gradually towards the outlet. The results indicated that the supercooling effect could be minimised through the use of the radiative cooling assistive the free cooling system.

In the free cooling systems using PCM, the primary target during the charging process is to achieve full PCM solidification in a short time, while during the discharging period, the aim is to cool the inlet air to the comfort temperature for a long duration. Achievement of these objectives is subject to many factors including the operating temperature and flow rate of the HTF and the geometrical design of the TES. Based on a parametric study on these influential parameters, the following remarks are drawn;

- Inlet air temperature has a major impact on the PCM charging/discharging duration depending on the PCM transient temperature. Larger variations are contributory to the acceleration of the PCM charging, whilst small variations are preferred during the discharging phase to maintain the thermal comfort for longer durations.
- Air flow rate plays a prime role in the heat transfer rate between the flowing air and the PCM for both transition phases. For the charging process, High air flow rates are recommended to achieve faster PCM solidification. Previous studies (Arkar and Medved, 2007, Medved and Arkar, 2008) have recommended air flow rates 3-4 times of that used in the discharging process. However, it has been demonstrated that such flow rate would not be high enough for the PCM charging process under hot summer conditions of hot arid climates, owing to the limited night cooling availability. Conversely, low air flow rates, appropriate for occupant's comfort, are necessary for a progressive coolness extraction during the discharging phase. The air flow rate could be adjusted to fulfil various cooling demands during the discharging period.
- Optimisation of the TES geometrical design is a determining factor in enhancing thermal performance. A compact TES system comprising thin PCM modules coupled with narrow air flow channels could be appropriate for both charging and discharging processes. Such a configuration could lead to faster PCM solidification and melting. However, the influence on the thermal comfort duration is almost insignificant. A compact TES system has the merits of maintaining all day indoor thermal comfort, provision of lower indoor air temperature during the discharging period, and the need for a small space for

installation compared to a system with thick PCM and wider channels. However, higher energy consumption may be required. Thus, the energy consumption by the fan should be taken into account when selecting the TES geometrical configuration.

Overall, operation of the proposed hybrid system depends on several aspects including available free cooling and duration, size of the TES system, and building cooling load. The modular design of the PCM storage permits large flexibility to modulate the capacity according to the cooling requirements. The key remark from the numerical and the experimental investigation is that the proposed hybrid system is capable of maintaining thermal comfort inside buildings day and night. The system could replace the air conditioning system during the transitional months (March and April). For the summer period (May-October), the combined system is capable of meeting about 57% of the total cooling load. The estimated COP of the system varied between 5.82 and 9.01. Compared to conventional air conditioning systems (COP at an average of 2.0), energy savings up to 76% could be achieved by the combined system.

10.2 Future work

In this section, areas for further research have been suggested to enhance the performance of the free cooling systems and their application as follows;

- Examining the thermal performance of the NRV-LHS system in real weather conditions, as the system has been tested experimentally using an environmental chamber.
- Testing the capability of the hybrid NRV-LHS system for winter space heating provision, in addition to the cooling purposes in locations with a composite climate. This could be via functioning the metallic radiator as a solar collector/absorber during the daytime.
- Investigating the use of a water-based radiative cooling system using unglazed collector radiators to enhance the charging performance of the free cooling systems. The system could also be advantageous for domestic hot water provision during the daytime.

References

ABHAT, A. 1980. Short term thermal energy storage. *Revue de physique appliquee,* 15**,** 477-501.

ABHAT, A. 1983. Low temperature latent heat thermal energy storage: heat storage materials. *Solar energy,* 30**,** 313-332.

ABUELNUOR, A., ALHAG, I. H. I., OMARA, A. A. M., AWAD, M. K. & MOHAMMED, M. H. Buildings cooling: An experimental study of Phase Change Materials storage for low energy buildings. Communication, Control, Computing and Electronics Engineering (ICCCCEE), 2017 International Conference on, 2017. IEEE, 1-5.

AGYENIM, F., HEWITT, N., EAMES, P. & SMYTH, M. 2010. A review of materials, heat transfer and phase change problem formulation for latent heat thermal energy storage systems (LHTESS). *Renewable and Sustainable Energy Reviews,* 14**,** 615-628.

AGYENIM, F. B. 2007. *The development of medium temperature thermal energy storage for cooling applications.* University of Ulster.

AKBARI, H. 2009. Cooling our communities. A guidebook on tree planting and light-colored surfacing.

AKEIBER, H., NEJAT, P., MAJID, M. Z. A., WAHID, M. A., JOMEHZADEH, F., FAMILEH, I. Z., CALAUTIT, J. K., HUGHES, B. R. & ZAKI, S. A. 2016. A review on phase change material (PCM) for sustainable passive cooling in building envelopes. *Renewable and Sustainable Energy Reviews,* 60**,** 1470-1497.

AL-ABIDI, A. A., BIN MAT, S., SOPIAN, K., SULAIMAN, M. Y., LIM, C. H. & TH, A. 2012. Review of thermal energy storage for air conditioning systems. *Renewable and Sustainable Energy Reviews,* 16**,** 5802-5819.

AL-NIMR, M., KODAH, Z. & NASSAR, B. 1998. A theoretical and experimental investigation of a radiative cooling system. *Solar energy,* 63**,** 367-373.

AL-NIMR, M., TAHAT, M. & AL-RASHDAN, M. 1999. A night cold storage system enhanced by radiative cooling—a modified Australian cooling system. *Applied Thermal Engineering,* 19**,** 1013-1026.

AL-OBAIDI, K. M., ISMAIL, M. & RAHMAN, A. M. A. 2014. Passive cooling techniques through reflective and radiative roofs in tropical

houses in Southeast Asia: A literature review. *Frontiers of Architectural Research,* 3**,** 283-297.

AL-SAADI, S. N. & ZHAI, Z. 2013. Modeling phase change materials embedded in building enclosure: A review. *Renewable and Sustainable Energy Reviews,* 21**,** 659-673.

ALAM, M. 2017. A comparative study on the effectiveness of passive and free cooling application methods of phase change materials for energy efficient retrofitting in residential buildings.

ALI, A. H. H. 2013. Desiccant enhanced nocturnal radiative cooling-solar collector system for air comfort application in hot arid areas. *Sustainable Energy Technologies and Assessments,* 1**,** 54-62.

ALI, A. H. H., SAITO, H., TAHA, I. M. S., KISHINAMI, K. & ISMAIL, I. M. 1998. Effect of aging, thickness and color on both the radiative properties of polyethylene films and performance of the nocturnal cooling unit. *Energy Conversion and Management,* 39**,** 87-93.

ALIZADEH, M. & SADRAMELI, S. M. 2016. Development of free cooling based ventilation technology for buildings: Thermal energy storage (TES) unit, performance enhancement techniques and design considerations – A review. *Renewable and Sustainable Energy Reviews,* 58**,** 619-645.

ALVA, G., LIU, L., HUANG, X. & FANG, G. 2017. Thermal energy storage materials and systems for solar energy applications. *Renewable and Sustainable Energy Reviews,* 68, Part 1**,** 693-706.

AMIR, A. & VAN HOUT, R. 2019. A transient model for optimizing a hybrid nocturnal sky radiation cooling system. *Renewable Energy,* 132**,** 370-380.

AMORI, K. E. & MOHAMMED, S. W. 2012. Experimental and numerical studies of solar chimney for natural ventilation in Iraq. *Energy and Buildings,* 47**,** 450-457.

ARKAR, C. & MEDVED, S. 2005. Influence of accuracy of thermal property data of a phase change material on the result of a numerical model of a packed bed latent heat storage with spheres. *Thermochimica Acta,* 438**,** 192-201.

ARKAR, C. & MEDVED, S. 2007. Free cooling of a building using PCM heat storage integrated into the ventilation system. *Solar Energy,* 81**,** 1078-1087.

ARKAR, C., VIDRIH, B. & MEDVED, S. 2007. Efficiency of free cooling using latent heat storage integrated into the ventilation system of a low energy building. *International Journal of Refrigeration,* 30**,** 134-143.

ASCIONE, F., BIANCO, N., DE MASI, R. F., DE' ROSSI, F. & VANOLI, G. P. 2014. Energy refurbishment of existing buildings through the use of phase change materials: Energy savings and indoor comfort in the cooling season. *Applied Energy,* 113**,** 990-1007.

ASIMAKOPOULOS, D. 2013. *Passive cooling of buildings,* Routledge.

AUE 2015. Arab Union of Electricity, Statistical bulletin.

BAETENS, R., JELLE, B. P. & GUSTAVSEN, A. 2010. Phase change materials for building applications: a state-of-the-art review. *Energy and Buildings,* 42**,** 1361-1368.

BAGGS, D. & MORTENSEN, N. 2006. Thermal mass in building design. *Environmental Design Guide*.

BAGIORGAS, H. S. & MIHALAKAKOU, G. 2008. Experimental and theoretical investigation of a nocturnal radiator for space cooling. *Renewable Energy,* 33**,** 1220-1227.

BANU, D., FELDMAN, D. & HAWES, D. 1998. Evaluation of thermal storage as latent heat in phase change material wallboard by differential scanning calorimetry and large scale thermal testing. *Thermochimica Acta,* 317**,** 39-45.

BARKMANN, H. G. & WESSLING, F. Use of buildings structural components for thermal storage. Proceedings of the Workshop on Solar Energy Storage Subsystems for the Heating and Cooling of Buildings, Charlottesville (Virginia, USA), 1975.

BATHGATE, S. N. & BOSI, S. G. 2011. A robust convection cover material for selective radiative cooling applications. *Solar Energy Materials and Solar Cells,* 95**,** 2778-2785.

BAYLIN, F. 1979. Low temperature thermal energy storage: a state-of-the-art survey. Solar Energy Research Inst., Golden, CO (USA).

BECKMAN, W. A. & DUFFIE, J. A. 1980. *Solar engineering of thermal processes,* John Wiley and Sons.

BERDAHL, P. 1984. Radiative cooling with MgO and/or LiF layers. *Appl. Opt,* 23**,** 370-372.

BERDAHL, P. & MARTIN, M. 1984. Emissivity of clear skies. *Solar Energy,* 32**,** 663-664.

BLONDEAU, P., SPÉRANDIO, M. & ALLARD, F. 1997. Night ventilation for building cooling in summer. *Solar energy,* 61**,** 327-335.

BORDERON, J., VIRGONE, J. & CANTIN, R. 2015. Modeling and simulation of a phase change material system for improving summer comfort in domestic residence. *Applied Energy,* 140**,** 288-296.

BOSI, S. G., BATHGATE, S. N. & MILLS, D. R. 2014. At last! A durable convection cover for atmospheric window radiative cooling applications. *Energy Procedia,* 57**,** 1997-2004.

BOYLE, G. 2004. *Renewable energy*, OXFORD university press.

BRAUN, J. E. 1990. Reducing energy costs and peak electrical demand through optimal control of building thermal storage. *ASHRAE transactions,* 96**,** 876-888.

BRUN, A., WURTZ, E., HOLLMULLER, P. & QUENARD, D. 2013. Summer comfort in a low-inertia building with a new free-cooling system. *Applied energy,* 112**,** 338-349.

BULUT, H. & AKTACIR, M. A. 2011. Determination of free cooling potential: A case study for Istanbul, Turkey. *Applied Energy,* 88**,** 680-689.

BUTALA, V. & STRITIH, U. 2009. Experimental investigation of PCM cold storage. *Energy and Buildings,* 41**,** 354-359.

CABEZA, L., CASTELL, A., BARRENECHE, C., DE GRACIA, A. & FERNÁNDEZ, A. 2011. Materials used as PCM in thermal energy storage in buildings: a review. *Renewable and Sustainable Energy Reviews,* 15**,** 1675-1695.

CÁRDENAS, B. & LEÓN, N. 2013. High temperature latent heat thermal energy storage: Phase change materials, design considerations and performance enhancement techniques. *Renewable and Sustainable Energy Reviews,* 27**,** 724-737.

CARRILHO DA GRAÇA, G., CHEN, Q., GLICKSMAN, L. & NORFORD, L. 2002. Simulation of wind-driven ventilative cooling systems for an apartment building in Beijing and Shanghai. *Energy and buildings,* 34**,** 1-11.

CASTELLÓN, C., CASTELL, A., MEDRANO, M., MARTORELL, I. & CABEZA, L. 2009. Experimental study of PCM inclusion in different building envelopes. *Journal of Solar Energy Engineering,* 131**,** 041006.

CATALANOTTI, S., CUOMO, V., PIRO, G., RUGGI, D., SILVESTRINI, V. & TROISE, G. 1975. The radiative cooling of selective surfaces. *Solar Energy,* 17**,** 83-89.

CHAIYAT, N. 2015. Energy and economic analysis of a building air-conditioner with a phase change material (PCM). *Energy Conversion and Management,* 94**,** 150-158.

CHANDEL, S. & AGARWAL, T. 2017. Review of current state of research on energy storage, toxicity, health hazards and commercialization of phase changing materials. *Renewable and Sustainable Energy Reviews,* 67**,** 581-596.

CHIRAS, D. D. 2002. *The solar house: passive heating and cooling*, Chelsea Green Publishing.

CHOTIVISARUT, N. & KIATSIRIROAT, T. 2009. Cooling load reduction of building by seasonal nocturnal cooling water from thermosyphon heat pipe radiator. *International Journal of Energy Research,* 33**,** 1089-1098.

CHOTIVISARUT, N., NUNTAPHAN, A. & KIATSIRIROAT, T. 2012. Seasonal cooling load reduction of building by thermosyphon heat pipe radiator in different climate areas. *Renewable Energy,* 38**,** 188-194.

CIBSE, G. A. 2006. Environmental design. *The Chartered Institution of Building Services Engineers, London*.

CLARK, E. & BERDAHL, P. Radiative cooling: resource and applications. Proceedings of the Passive Cooling Workshop, 1980. Center for Energy Efficient Design Berkeley, Ca, 177-212.

CLARK, G. 1981. Passive/hybrid comfort cooling by thermal radiation. *Passive Cooling: American Section of the International Solar Energy Society, Miami Beach*.

CLARK, G. & ALLEN, C. The estimation of atmospheric radiation for clear and cloudy skies. Proc. 2nd National Passive Solar Conference (AS/ISES), 1978. 675-678.

CLARK, G. & BLANPIED, M. The effect of IR transparent windscreens on net nocturnal cooling from horizontal surfaces. Proceedings of the 4th National Passive Solar Conference, Kansas City, MO, 1979.

CLIMATOR. Available: <http://climator.com/?lang=en> [Accessed 06/07 2017,].

COSTA, M., BUDDHI, D. & OLIVA, A. 1998. Numerical simulation of a latent heat thermal energy storage system with enhanced heat conduction. *Energy Conversion and Management,* 39**,** 319-330.

COT-GORES, J., CASTELL, A. & CABEZA, L. F. 2012. Thermochemical energy storage and conversion: A-state-of-the-art review of the experimental research under practical conditions. *Renewable and Sustainable Energy Reviews,* 16**,** 5207-5224.

CRISTOPIA. Available: [<http://www.cristopia.com/>] [Accessed 06/07 2017,].

CUI, Y. Q. & RIFFAT, S. Review on Phase Change Materials for Building Applications. Applied Mechanics and Materials, 2011. Trans Tech Publ, 1958-1962.

DARKWA, K. & KIM, J. 2004. Heat transfer in neuron composite laminated phase-change drywall. *Proceedings of the Institution of Mechanical Engineers, Part A: Journal of Power and Energy,* 218**,** 83-87.

DARZI, A. R., MOOSANIA, S., TAN, F. & FARHADI, M. 2013. Numerical investigation of free-cooling system using plate type PCM storage. *International Communications in Heat and Mass Transfer,* 48**,** 155-163.

DAVIES, M. G. 2004. *Building heat transfer*, John Wiley & Sons.

DE GRACIA, A., NAVARRO, L., CASTELL, A. & CABEZA, L. F. 2015. Energy performance of a ventilated double skin facade with PCM under different climates. *Energy and Buildings,* 91**,** 37-42.

DIATEZUA, M., THIRY, P. & CAUDANO, R. 1995. Characterization of silicon oxynitride multilayered systems for passive radiative cooling application. *Vacuum,* 46**,** 1121-1124.

DIMOUDI, A. & ANDROUTSOPOULOS, A. 2006. The cooling performance of a radiator based roof component. *Solar energy,* 80**,** 1039-1047.

DINCER, I. 2002. On thermal energy storage systems and applications in buildings. *Energy and Buildings,* 34**,** 377-388.

DINCER, I. & DOST, S. 1996. A perspective on thermal energy storage systems for solar energy applications. *International Journal of Energy Research,* 20**,** 547-557.

DINCER, I., DOST, S. & LI, X. 1997. Performance analyses of sensible heat storage systems for thermal applications. *International Journal of Energy Research,* 21**,** 1157-1171.

DINCER, I. & ROSEN, M. 2002. *Thermal energy storage: systems and applications*, John Wiley & Sons.

DING, Y. 2014. *Investigation of high capacity heat energy storage for building applications.* University of Nottingham.

DING, Y. & RIFFAT, S. 2013. Thermochemical energy storage technologies for building applications: a state-of-the-art review. *International Journal of Low-Carbon Technologies,* 8**,** 106-116.

DOBSON, K., HODES, G. & MASTAI, Y. 2003. Thin semiconductor films for radiative cooling applications. *Solar energy materials and solar cells,* 80**,** 283-296.

DOLADO, P., LAZARO, A., MARIN, J. M. & ZALBA, B. 2011a. Characterization of melting and solidification in a real-scale PCM–air heat exchanger: Experimental results and empirical model. *Renewable Energy,* 36**,** 2906-2917.

DOLADO, P., LAZARO, A., MARIN, J. M. & ZALBA, B. 2011b. Characterization of melting and solidification in a real scale PCM-air heat exchanger: numerical model and experimental validation. *Energy Conversion and Management,* 52**,** 1890-1907.

DUAN, Z. 2011. *Investigation of a novel dew point indirect evaporative air conditioning system for buildings.* University of Nottingham.

DUTIL, Y., ROUSSE, D. R., SALAH, N. B., LASSUE, S. & ZALEWSKI, L. 2011. A review on phase-change materials: Mathematical modeling and simulations. *Renewable and Sustainable Energy Reviews,* 15**,** 112-130.

EICKER, U. & DALIBARD, A. 2011. Photovoltaic–thermal collectors for night radiative cooling of buildings. *Solar Energy*, 85**,** 1322-1335.

EPS. Available: [<http://www.pcmproducts.net/>] [Accessed 06/07 2017,].

ERELL, E. & ETZION, Y. 1996. Heating experiments with a radiative cooling system. *Building and Environment,* 31**,** 509-517.

ERELL, E. & ETZION, Y. 2000. Radiative cooling of buildings with flat-plate solar collectors. *Building and Environment,* 35**,** 297-305.

ERIKSSON, T., JIANG, S.-J. & GRANQVIST, C. 1985. Surface coatings for radiative cooling applications: silicon dioxide and silicon nitride made by reactive RF-sputtering. *Solar Energy Materials,* 12**,** 319-325.

ETZION, Y. & ERELL, E. 1991. Thermal storage mass in radiative cooling systems. *Building and Environment,* 26**,** 389-394.

FAMILY, R. & MENGÜÇ, M. P. 2017. Materials for radiative cooling: a review. *Procedia environmental sciences,* 38**,** 752-759.

FAN, L. & KHODADADI, J. 2011. Thermal conductivity enhancement of phase change materials for thermal energy storage: a review. *Renewable and Sustainable Energy Reviews,* 15**,** 24-46.

FANG, D., SUN, Z., LI, Y. & CHENG, X. 2016. Preparation, microstructure and thermal properties of MgBi alloys as phase change materials for thermal energy storage. *Applied Thermal Engineering,* 92**,** 187-193.

FARID, M. M. & KANZAWA, A. 1989. Thermal performance of a heat storage module using PCM's with different melting temperatures: mathematical modeling. *Journal of solar energy engineering,* 111**,** 152-157.

FARID, M. M., KHUDHAIR, A. M., RAZACK, S. A. K. & AL-HALLAJ, S. 2004. A review on phase change energy storage: materials and applications. *Energy conversion and management,* 45**,** 1597-1615.

FARMAHINI-FARAHANI, M. & HEIDARINEJAD, G. 2012. Increasing effectiveness of evaporative cooling by pre-cooling using nocturnally stored water. *Applied Thermal Engineering,* 38**,** 117-123.

FARMAHINI FARAHANI, M., HEIDARINEJAD, G. & DELFANI, S. 2010. A two-stage system of nocturnal radiative and indirect evaporative cooling for conditions in Tehran. *Energy and Buildings,* 42**,** 2131-2138.

FELDMAN, D., BANU, D. & HAWES, D. W. 1995. Development and application of organic phase change mixtures in thermal storage gypsum wallboard. *Solar Energy Materials and Solar Cells,* 36**,** 147-157.

FELDMAN, D., SHAPIRO, M. M., BANU, D. & FUKS, C. J. 1989. Fatty acids and their mixtures as phase-change materials for thermal energy storage. *Solar Energy Materials,* 18**,** 201-216.

FERNANDEZ, A., MARTÍNEZ, M., SEGARRA, M., MARTORELL, I. & CABEZA, L. 2010. Selection of materials with potential in sensible thermal energy storage. *Solar Energy Materials and Solar Cells,* 94**,** 1723-1729.

FIORENTINI, M., COOPER, P. & MA, Z. 2015. Development and optimization of an innovative HVAC system with integrated PVT and PCM thermal storage for a net-zero energy retrofitted house. *Energy and Buildings,* 94**,** 21-32.

FLUENT, A. 2013. 15-Theory Guide, ANSYS. *Inc., Canonsburg, PA.*

FOKAIDES, P. A., KYLILI, A. & KALOGIROU, S. A. 2015. Phase change materials (PCMs) integrated into transparent building elements: a review. *Materials for Renewable and Sustainable Energy,* 4**,** 6.

FOX, R. W., MCDONALD, A. T. & PRITCHARD, P. J. 1985. *Introduction to fluid mechanics*, John Wiley & Sons New York.

FRANCONI, E. M. & BRADFORD, J. B. 2000. 4.3 Ventilation and Air Handling Systems. *Handbook of Heating, Ventilation, and Air Conditioning***,** 67.

GEETHA, N. & VELRAJ, R. 2012. Passive cooling methods for energy efficient buildings with and without thermal energy storage–A review. *Energy Education Science and Technology Part A: Energy Science and Research,* 29**,** 913-946.

GENTLE, A., DYBDAL, K. & SMITH, G. 2013. Polymeric mesh for durable infra-red transparent convection shields: applications in cool roofs and sky cooling. *Solar Energy Materials and Solar Cells,* 115**,** 79-85.

GIL, A., MEDRANO, M., MARTORELL, I., LAZARO, A., DOLADO, P., ZALBA, B. & CABEZA, L. F. 2010. State of the art on high temperature thermal energy storage for power generation. Part 1—Concepts, materials and modellization. *Renewable and Sustainable Energy Reviews,* 14**,** 31-55.

GIRO-PALOMA, J., MARTÍNEZ, M., CABEZA, L. F. & FERNÁNDEZ, A. I. 2016. Types, methods, techniques, and applications for microencapsulated phase change materials (MPCM): A review. *Renewable and Sustainable Energy Reviews,* 53**,** 1059-1075.

GIVONI, B. 1977. Solar heating and night radiation cooling by a roof radiation trap. *Energy and buildings,* 1**,** 141-145.

GIVONI, B. 1994. *Passive low energy cooling of buildings*, John Wiley & Sons.

GIVONI, B. 1998. *Climate considerations in building and urban design*, John Wiley & Sons.

GIVONI, B. 2011. Indoor temperature reduction by passive cooling systems. *Solar Energy,* 85**,** 1692-1726.

GIVONI, B. & HOFFMAN, M. 1970. Preliminary Study of Cooling of Houses in Desert Regions by Utilizing Outgoing Radiation. *Haifa, Israel,(December, 1970).*

GOLAKA, A. & EXELL, R. H. B. 2007. An investigation into the use of a wind shield to reduce the convective heat flux to a nocturnal radiative cooling surface. *Renewable Energy,* 32**,** 593-608.

GONG, Z.-X. & MUJUMDAR, A. S. 1996. Enhancement of energy charge-discharge rates in composite slabs of different phase change materials. *International Journal of Heat and Mass Transfer,* 39**,** 725-733.

GRANQVIST, C. 1981. Radiative heating and cooling with spectrally selective surfaces. *Applied optics,* 20**,** 2606-2615.

GRANQVIST, C. & ERIKSSON, T. 1991. Materials for radiative cooling to low temperatures. *Materials Science for Solar Energy Conversion Systems", edited by Granqvist CG (Pergamon, Oxford, UK, 1991)***,** 168-203.

GRANQVIST, C. & HJORTSBERG, A. 1981. Radiative cooling to low temperatures: General considerations and application to selectively emitting SiO films. *Journal of Applied Physics,* 52**,** 4205-4220.

GULICH, M., GOMEZ, C., GOMEZ, A. & GIVONI, B. Radiant Cooling By Metal Roofs In Developing Countries. PROCEEDINGS OF THE NATIONAL PASSIVE SOLAR CONFERENCE, 1996. AMERICAN SOLAR ENERGY SOCIETY INC, 83-87.

H ABEDIN, A. & A ROSEN, M. 2011. A critical review of thermochemical energy storage systems. *The Open Renewable Energy Journal,* 4.

HALAWA, E., BRUNO, F. & SAMAN, W. 2005. Numerical analysis of a PCM thermal storage system with varying wall temperature. *Energy Conversion and Management,* 46**,** 2592-2604.

HANIF, M., MAHLIA, T., ZARE, A., SAKSAHDAN, T. & METSELAAR, H. 2014. Potential energy savings by radiative cooling system for a building in tropical climate. *Renewable and Sustainable Energy Reviews,* 32**,** 642-650.

HANSEN, J., RUEDY, R., SATO, M. & LO, K. 2010. Global surface temperature change. *Reviews of Geophysics,* 48.

HARIRI, A. S. & WARD, I. C. 1988. A review of thermal storage systems used in building applications. *Building and Environment,* 23**,** 1-10.

HARRIS, D. C. 1999. *Materials for infrared windows and domes: properties and performance*, SPIE press.

HASAN, A., ALNOMAN, H. & RASHID, Y. 2016. Impact of integrated photovoltaic-phase change material system on building energy efficiency in hot climate. *Energy and Buildings,* 130**,** 495-505.

HASNAIN, S. 1998. Review on sustainable thermal energy storage technologies, part I: heat storage materials and techniques. *Energy Conversion and Management,* 39**,** 1127-1138.

HASSE, C., GRENET, M., BONTEMPS, A., DENDIEVEL, R. & SALLÉE, H. 2011. Realization, test and modelling of honeycomb wallboards containing a phase change material. *Energy and Buildings,* 43**,** 232-238.

HAWES, D., FELDMAN, D. & BANU, D. 1993. Latent heat storage in building materials. *Energy and buildings,* 20**,** 77-86.

HAY, H. & YELLOTT, J. 1969. Natural air conditioning with roof ponds and movable insulation. *ASHRAE Trans.;(United States),* 75.

HAY, H. R. A passive heating and cooling system from concept to commercialization. Proceedings of the annual meeting of the International Section of the Solar Energy Society, 1978. 262-272.

HED, G. & BELLANDER, R. 2006. Mathematical modelling of PCM air heat exchanger. *Energy and Buildings,* 38**,** 82-89.

HEIDARI, S. & SHARPLES, S. 2002. A comparative analysis of short-term and long-term thermal comfort surveys in Iran. *Energy and Buildings,* 34**,** 607-614.

HEIDARINEJAD, G., FARAHANI, M. F. & DELFANI, S. 2010. Investigation of a hybrid system of nocturnal radiative cooling and direct evaporative cooling. *Building and Environment,* 45**,** 1521-1528.

HENNINGSON, D. S. & BERGGREN, M. 2005. Fluid dynamics: Theory and computation.

HOFFMAN, D. L. & SIMMONS, A. 2008. *The Resilient Earth: Science, Global Warming and the Future of Humanity*, BookSurge Pub.

HOSSAIN, R., MAHMUD, S., DUTTA, A. & POP, I. 2015. Energy storage system based on nanoparticle-enhanced phase change material inside porous medium. *International Journal of Thermal Sciences,* 91**,** 49-58.

HU, H., XIE, N., FANG, D. & ZHANG, X. 2018a. The role of renewable energy consumption and commercial services trade in carbon dioxide reduction: Evidence from 25 developing countries. *Applied Energy,* 211**,** 1229-1244.

HU, M., ZHAO, B., AO, X., SU, Y., WANG, Y. & PEI, G. 2018b. Comparative analysis of different surfaces for integrated solar heating and radiative cooling: A numerical study. *Energy,* 155**,** 360-369.

HUANG, M., EAMES, P. & NORTON, B. 2004. Thermal regulation of building-integrated photovoltaics using phase change materials. *International Journal of heat and mass transfer,* 47**,** 2715-2733.

HUANG, M., EAMES, P. & NORTON, B. 2006. Phase change materials for limiting temperature rise in building integrated photovoltaics. *Solar Energy,* 80**,** 1121-1130.

HULL, R. 1999. *Properties of crystalline silicon*, IET.

HUNGER, M., ENTROP, A., MANDILARAS, I., BROUWERS, H. & FOUNTI, M. 2009. The behavior of self-compacting concrete containing micro-encapsulated phase change materials. *Cement and Concrete Composites,* 31**,** 731-743.

IBRAHIM, N. I., AL-SULAIMAN, F. A., RAHMAN, S., YILBAS, B. S. & SAHIN, A. Z. 2017. Heat transfer enhancement of phase change materials for thermal energy storage applications: A critical review. *Renewable and Sustainable Energy Reviews,* 74**,** 26-50.

IEA 2017a. CO2 emissions from fuel combustion-highlights. *In:* HTTPS://WWW.IEA.ORG/PUBLICATIONS/FREEPUBLICATIONS/PUBLICATION/CO2EMISSIONSFROMFUELCOMBUSTIONHIGHLIGHTS2017.PDF (ed.) 2017 ed. International Energy Agency (IEA).

IEA 2017b. Key world energy statistics. *In:* HTTPS://WWW.IEA.ORG/PUBLICATIONS/FREEPUBLICATIONS/PUBLICATION/KEYWORLD2017.PDF (ed.) 2017 ed. International Energy Agency (IEA).

INCROPERA, F. P. 2011. *Fundamentals of heat and mass transfer,* John Wiley & Sons.

ISMAIL, K. & HENRıQUEZ, J. 2002. Parametric study on composite and PCM glass systems. *Energy conversion and management,* 43**,** 973-993.

ITEN, M. & LIU, S. 2015. Experimental Study on the Performance of RT 25 to be Used as Ambient Energy Storage. *Energy Procedia,* 70**,** 229-240.

ITEN, M., LIU, S. & SHUKLA, A. 2016. A review on the air-PCM-TES application for free cooling and heating in the buildings. *Renewable and Sustainable Energy Reviews,* 61**,** 175-186.

ITO, S. & MIURA, N. 1989. Studies of Radiative Cooling Systems for Storing Thermal-Energy. *Journal of Solar Energy Engineering-Transactions of the Asme,* 111**,** 251-256.

JABER, S. & AJIB, S. 2012. Novel cooling unit using PCM for residential application. *International Journal of Refrigeration,* 35**,** 1292-1303.

JACOB, R. & BRUNO, F. 2015. Review on shell materials used in the encapsulation of phase change materials for high temperature thermal energy storage. *Renewable and Sustainable Energy Reviews,* 48**,** 79-87.

JAMEKHORSHID, A., SADRAMELI, S. M. & FARID, M. 2014. A review of microencapsulation methods of phase change materials (PCMs) as a thermal energy storage (TES) medium. *Renewable and Sustainable Energy Reviews,* 31**,** 531-542.

JEGADHEESWARAN, S. & POHEKAR, S. D. 2009. Performance enhancement in latent heat thermal storage system: a review. *Renewable and Sustainable Energy Reviews,* 13**,** 2225-2244.

KALAISELVAM, S. & PARAMESHWARAN, R. 2014. *Thermal Energy Storage Technologies for Sustainability: Systems Design, Assessment and Applications,* Elsevier.

KALNÆS, S. E. & JELLE, B. P. 2015. Phase change materials and products for building applications: a state-of-the-art review and future research opportunities. *Energy and Buildings,* 94**,** 150-176.

KAMAL, M. A. 2012. An overview of passive cooling techniques in buildings: design concepts and architectural interventions. *Acta Technica Napocensis: Civil Engineering & Architecture,* 55**,** 84-97.

KAMALI, S. 2014. Review of free cooling system using phase change material for building. *Energy and Buildings,* 80**,** 131-136.

KARAIPEKLI, A., SARı, A. & BIÇER, A. 2016. Thermal regulating performance of gypsum/(C18–C24) composite phase change material

(CPCM) for building energy storage applications. *Applied Thermal Engineering,* 107**,** 55-62.

KENISARIN, M. & MAHKAMOV, K. 2007. Solar energy storage using phase change materials. *Renewable and Sustainable Energy Reviews,* 11**,** 1913-1965.

KENISARIN, M. & MAHKAMOV, K. 2016. Passive thermal control in residential buildings using phase change materials. *Renewable and sustainable energy reviews,* 55**,** 371-398.

KERSKES, H. 2016. Thermochemical Energy Storage. *Storing Energy: with Special Reference to Renewable Energy Sources***,** 345.

KHADIRAN, T., HUSSEIN, M. Z., ZAINAL, Z. & RUSLI, R. 2016. Advanced energy storage materials for building applications and their thermal performance characterization: A review. *Renewable and Sustainable Energy Reviews,* 57**,** 916-928.

KHARRUFA, S. N. & ADIL, Y. 2008. Roof pond cooling of buildings in hot arid climates. *Building and Environment,* 43**,** 82-89.

KIM, S.-E., CHOUDHURY, D. & PATEL, B. 1999. Computations of complex turbulent flows using the commercial code FLUENT. *Modeling complex turbulent flows.* Springer.

KONG, X., LU, S., LI, Y., HUANG, J. & LIU, S. 2014. Numerical study on the thermal performance of building wall and roof incorporating phase change material panel for passive cooling application. *Energy and Buildings,* 81**,** 404-415.

KONUKLU, Y., OSTRY, M., PAKSOY, H. O. & CHARVAT, P. 2015. Review on using microencapsulated phase change materials (PCM) in building applications. *Energy and Buildings,* 106**,** 134-155.

KOSCHENZ, M. & LEHMANN, B. 2004. Development of a thermally activated ceiling panel with PCM for application in lightweight and retrofitted buildings. *Energy and Buildings,* 36**,** 567-578.

KOTHANDARAMAN, C. 2006. *Fundamentals of heat and mass transfer*, New Age International.

KOUSKSOU, T., BRUEL, P., JAMIL, A., EL RHAFIKI, T. & ZERAOULI, Y. 2014. Energy storage: Applications and challenges. *Solar Energy Materials and Solar Cells,* 120, Part A**,** 59-80.

KUZNIK, F., DAVID, D., JOHANNES, K. & ROUX, J.-J. 2011. A review on phase change materials integrated in building walls. *Renewable and Sustainable Energy Reviews,* 15**,** 379-391.

KUZNIK, F. & VIRGONE, J. 2009. Experimental assessment of a phase change material for wall building use. *Applied Energy,* 86**,** 2038-2046.

KYLILI, A. & FOKAIDES, P. A. 2017. Numerical simulation of phase change materials for building applications: a review. *Advances in Building Energy Research,* 11**,** 1-25.

LA ROCHE, P. M. 2011. *Carbon-neutral architectural design,* CRC Press.

LAI, C.-M., CHEN, R. & LIN, C.-Y. 2010. Heat transfer and thermal storage behaviour of gypsum boards incorporating micro-encapsulated PCM. *Energy and Buildings,* 42**,** 1259-1266.

LANDRO, B. & MCCORMICK, P. 1980. Effect of surface characteristics and atmospheric conditions on radiative heat loss to a clear sky. *International Journal of Heat and Mass Transfer,* 23**,** 613-620.

LANE, G. A. & SHAMSUNDAR, N. 1983. Solar heat storage: Latent heat materials, Vol. I: Background and scientific principles. American Society of Mechanical Engineers.

LAROCHE & GIVONI 2001. Modeling Radiant Cooling systems for Developing Countries. *ISES World Conference.* Adelaide, Australia.

LAROCHE & GIVONI 2002. The Effect of Heat Gain on the Performance. *methods and tools for design-assistance.*

LAZARO, A., DOLADO, P., MARIN, J. M. & ZALBA, B. 2009a. PCM-air heat exchangers for free-cooling applications in buildings: Empirical model and application to design. *Energy Conversion and Management,* 50**,** 444-449.

LAZARO, A., DOLADO, P., MARÍN, J. M. & ZALBA, B. 2009b. PCM–air heat exchangers for free-cooling applications in buildings: experimental results of two real-scale prototypes. *Energy Conversion and Management,* 50**,** 439-443.

LIN, W., MA, Z., SOHEL, M. I. & COOPER, P. 2014. Development and evaluation of a ceiling ventilation system enhanced by solar photovoltaic thermal collectors and phase change materials. *Energy conversion and management,* 88**,** 218-230.

LIU, C., LI, F., MA, L. P. & CHENG, H. M. 2010. Advanced materials for energy storage. *Advanced Materials,* 22**,** E28-E62.

LIU, L., ALVA, G., HUANG, X. & FANG, G. 2016a. Preparation, heat transfer and flow properties of microencapsulated phase change materials for thermal energy storage. *Renewable and Sustainable Energy Reviews,* 66**,** 399-414.

LIU, L., SU, D., TANG, Y. & FANG, G. 2016b. Thermal conductivity enhancement of phase change materials for thermal energy storage: A review. *Renewable and Sustainable Energy Reviews,* 62**,** 305-317.

LIU, M., SAMAN, W. & BRUNO, F. 2012. Review on storage materials and thermal performance enhancement techniques for high temperature phase change thermal storage systems. *Renewable and Sustainable Energy Reviews,* 16**,** 2118-2132.

LIU, M., STEVEN TAY, N. H., BELL, S., BELUSKO, M., JACOB, R., WILL, G., SAMAN, W. & BRUNO, F. 2016c. Review on concentrating solar power plants and new developments in high temperature thermal energy storage technologies. *Renewable and Sustainable Energy Reviews,* 53**,** 1411-1432.

LIU, S. & LI, Y. 2015. Heating performance of a solar chimney combined PCM: A numerical case study. *Energy and Buildings,* 99**,** 117-130.

LORSCH, H. G., KAUFFMAN, K. W. & DENTON, J. C. 1975. Thermal energy storage for solar heating and off-peak air conditioning. *Energy conversion,* 15**,** 1-8.

LU, S.-M. & YAN, W.-J. 1995. Development and experimental validation of a full-scale solar desiccant enhanced radiative cooling system. *Renewable Energy,* 6**,** 821-827.

LU, X., XU, P., WANG, H., YANG, T. & HOU, J. 2016. Cooling potential and applications prospects of passive radiative cooling in buildings: The current state-of-the-art. *Renewable and Sustainable Energy Reviews,* 65**,** 1079-1097.

LUO, Y., ZHANG, L., WANG, X., XIE, L., LIU, Z., WU, J., ZHANG, Y. & HE, X. 2017. A comparative study on thermal performance evaluation of a new double skin façade system integrated with photovoltaic blinds. *Applied Energy,* 199**,** 281-293.

MA, T., YANG, H., ZHANG, Y., LU, L. & WANG, X. 2015. Using phase change materials in photovoltaic systems for thermal regulation and

electrical efficiency improvement: a review and outlook. *Renewable and Sustainable Energy Reviews,* 43**,** 1273-1284.

MAHLIA, T. M. I., SAKTISAHDAN, T. J., JANNIFAR, A., HASAN, M. H. & MATSEELAR, H. S. C. 2014. A review of available methods and development on energy storage; technology update. *Renewable and Sustainable Energy Reviews,* 33**,** 532-545.

MAN, Y., YANG, H., SPITLER, J. D. & FANG, Z. 2011. Feasibility study on novel hybrid ground coupled heat pump system with nocturnal cooling radiator for cooling load dominated buildings. *Applied Energy,* 88**,** 4160-4171.

MARÍN, J. M., ZALBA, B., CABEZA, L. F. & MEHLING, H. 2005. Improvement of a thermal energy storage using plates with paraffin–graphite composite. *International Journal of Heat and Mass Transfer,* 48**,** 2561-2570.

MARTIN, M. 1989. Radiative cooling. *Passive Cooling***,** 138-196.

MCCORMICK, P. & LANDRO, B. 1980. *Radiative Cooling for Air-conditioning Applications*, University of Western Australia, Department of Mechanical Engineering.

MEDVED, S. & ARKAR, C. 2008. Correlation between the local climate and the free-cooling potential of latent heat storage. *Energy and Buildings,* 40**,** 429-437.

MEHLING, H. Strategic project ‘‘Innovative PCM-Technology’’results and future perspectives. 8th expert meeting and work shop, Kizkalesi, Turkey, 2004.

MEHLING, H. & CABEZA, L. F. 2007. Phase change materials and their basic properties. *Thermal energy storage for sustainable energy consumption.* Springer.

MEHLING, H. & CABEZA, L. F. 2008. *Heat and cold storage with PCM*, Springer.

MEMON, S. A. 2014. Phase change materials integrated in building walls: A state of the art review. *Renewable and sustainable energy reviews,* 31**,** 870-906.

MERGHANI, A. 2001. *Thermal comfort and spatial variability: a study of traditional courtyard houses in the hot dry climate of Khartoum, Sudan.* University of Cambridge.

MERKER, O., HEPP, F., BECK, A. & FRICKE, J. A new solar shading system with phase change material (PCM). Proceedings of the World Renewable Energy Congress WII, Cologne (Germany), 2002.

MESALHY, O., LAFDI, K., ELGAFY, A. & BOWMAN, K. 2005. Numerical study for enhancing the thermal conductivity of phase change material (PCM) storage using high thermal conductivity porous matrix. *Energy Conversion and Management,* 46**,** 847-867.

MIHALAKAKOU, G. & BAGIORGAS, H. A low-energy innovative system for space cooling. Proceedings of the 34th AIVC-3rd TightVent-2nd Cool Roofs'-1st venticool Conference" Energy conservation technologies for mitigation and adaptation in the built environment: the role of ventilation strategies and smart materials", 25-26 September, 2013.

MIHALAKAKOU, G., FERRANTE, A. & LEWIS, J. 1998. The cooling potential of a metallic nocturnal radiator. *Energy and buildings,* 28**,** 251-256.

MILIÁN, Y. E., GUTIÉRREZ, A., GRÁGEDA, M. & USHAK, S. 2017. A review on encapsulation techniques for inorganic phase change materials and the influence on their thermophysical properties. *Renewable and Sustainable Energy Reviews,* 73**,** 983-999.

MILLER, W. & BRADLEY, J. Radiative cooling with selective surfaces in a desert climate. Proceedings of the 4th National Passive Solar Conference, 1979.

MIRAHMAD, A., SADRAMELI, S. & JAMEKHORSHID, A. 2016. A Comprehensive Study on a Latent Heat Thermal Energy Storage System and its Feasible Applications in Greenhouses. *Iranian Journal of Chemical Engineering,* 13.

MOFFAT, R. J. 1988. Describing the uncertainties in experimental results. *Experimental thermal and fluid science,* 1**,** 3-17.

MOHAMED, E., RIFFAT, S., OMER, S. & ZEINELABDIEN, R. 2019. A comprehensive investigation of using mutual air and water heating in multi-functional DX-SAMHP for moderate cold climate. *Renewable Energy,* 130**,** 582-600.

MOHAMED, S. A., AL-SULAIMAN, F. A., IBRAHIM, N. I., ZAHIR, M. H., AL-AHMED, A., SAIDUR, R., Yılbaş, B. S. & SAHIN, A. Z. 2017. A review on current status and challenges of inorganic phase change

materials for thermal energy storage systems. *Renewable and Sustainable Energy Reviews*.

MONDAL, S. 2008. Phase change materials for smart textiles – An overview. *Applied Thermal Engineering,* 28**,** 1536-1550.

MOORE, F. 1993. *Environmental control systems: Heating, cooling, lighting*, McGraw-Hill New York, NY.

MOSAFFA, A. & FARSHI, L. G. 2016. Exergoeconomic and environmental analyses of an air conditioning system using thermal energy storage. *Applied Energy,* 162**,** 515-526.

MOSAFFA, A., FERREIRA, C. I., ROSEN, M. & TALATI, F. 2013a. Thermal performance optimization of free cooling systems using enhanced latent heat thermal storage unit. *Applied Thermal Engineering*, 59**,** 473-479.

MOSAFFA, A., FERREIRA, C. I., TALATI, F. & ROSEN, M. 2013b. Thermal performance of a multiple PCM thermal storage unit for free cooling. *Energy Conversion and Management,* 67**,** 1-7.

MOSS, K. 2002. *Heat and mass transfer in building services design*, Routledge.

MOSTREL, M. & GIVONI, B. 1982. Windscreens in radiant cooling. *Passive Sol. J.;(United States),* 1.

MUNSON, B. R., OKIISHI, T. H., HUEBSCH, W. W. & ROTHMAYER, A. P. 2013. *Fluid mechanics*, Wiley Singapore.

MUTHUVELAN, T., PANCHABIKESAN, K., MUNISAMY, R., NIBHANUPUDI, K. M. & RAMALINGAM, V. 2016. Experimental investigation of free cooling using phase change material-filled air heat exchanger for energy efficiency in buildings. *Advances in Building Energy Research***,** 1-11.

NAGANO, K. 2007. Development of the PCM floor supply air-conditioning system. *Thermal Energy Storage for Sustainable Energy Consumption.* Springer.

NAGANO, K., TAKEDA, S., MOCHIDA, T. & SHIMAKURA, K. 2004. Thermal characteristics of a direct heat exchange system between granules with phase change material and air. *Applied Thermal Engineering*, 24**,** 2131-2144.

NAGANO, K., TAKEDA, S., MOCHIDA, T., SHIMAKURA, K. & NAKAMURA, T. 2006. Study of a floor supply air conditioning system using granular phase change material to augment building mass thermal

storage—heat response in small scale experiments. *Energy and Buildings,* 38**,** 436-446.

NASA. *Global Annual Mean Surface Air Temperature Change* [Online]. Available: https://data.giss.nasa.gov/gistemp/graphs/ [Accessed 24/8 2018].

NAVARRO, L., DE GRACIA, A., COLCLOUGH, S., BROWNE, M., MCCORMACK, S. J., GRIFFITHS, P. & CABEZA, L. F. 2016a. Thermal energy storage in building integrated thermal systems: A review. Part 1. active storage systems. *Renewable Energy,* 88**,** 526-547.

NAVARRO, L., DE GRACIA, A., NIALL, D., CASTELL, A., BROWNE, M., MCCORMACK, S. J., GRIFFITHS, P. & CABEZA, L. F. 2016b. Thermal energy storage in building integrated thermal systems: A review. Part 2. Integration as passive system. *Renewable Energy,* 85**,** 1334-1356.

NEJAT, P., JOMEHZADEH, F., TAHERI, M. M., GOHARI, M. & ABD. MAJID, M. Z. 2015. A global review of energy consumption, CO2 emissions and policy in the residential sector (with an overview of the top ten CO2 emitting countries). *Renewable and Sustainable Energy Reviews,* 43**,** 843-862.

NICOL, F. 1974. *An Analysis of some observations of thermal comfort in Roorkee, India and Baghdad, Iraq*.

NICOL, F., JAMY, G., SYKES, O., HUMPHREYS, M., ROAF, S. & HANCOCK, M. 1994. A survey of thermal comfort in Pakistan toward new indoor temperature standards. *Final Report to the Overseas Development, Administration Published by Oxford Brookes University, School of Architecture, UK*.

NICOL, J. F. & HUMPHREYS, M. A. 2002. Adaptive thermal comfort and sustainable thermal standards for buildings. *Energy and buildings,* 34**,** 563-572.

NILSSON, T. M. & NIKLASSON, G. A. 1995. Radiative cooling during the day: simulations and experiments on pigmented polyethylene cover foils. *Solar energy materials and solar cells,* 37**,** 93-118.

NOMURA, T., OKINAKA, N. & AKIYAMA, T. 2010. Technology of latent heat storage for high temperature application: a review. *ISIJ international,* 50**,** 1229-1239.

OKBA, E. Building envelope design as a passive cooling technique. Proceedings from the, 2005. Citeseer.

OLIVER, J. 1965. The climate of Khartoum province. *Sudan notes and records,* 46**,** 90-129.

OMER, A. 2002. Overview of renewable energy sources in the Republic of the Sudan. *Energy,* 27**,** 523-547.

OREL, B., GUNDE, M. K. & KRAINER, A. 1993. Radiative cooling efficiency of white pigmented paints. *Solar Energy,* 50**,** 477-482.

ORÓ, E., DE GRACIA, A., CASTELL, A., FARID, M. & CABEZA, L. 2012. Review on phase change materials (PCMs) for cold thermal energy storage applications. *Applied Energy,* 99**,** 513-533.

OROPEZA-PEREZ, I. & ØSTERGAARD, P. A. 2018. Active and passive cooling methods for dwellings: A review. *Renewable and Sustainable Energy Reviews,* 82**,** 531-544.

OSTERMAN, E., BUTALA, V. & STRITIH, U. 2015a. PCM thermal storage system for 'free'heating and cooling of buildings. *Energy and Buildings,* 106**,** 125-133.

OSTERMAN, E., HAGEL, K., RATHGEBER, C., BUTALA, V. & STRITIH, U. 2015b. Parametrical analysis of latent heat and cold storage for heating and cooling of rooms. *Applied Thermal Engineering,* 84**,** 138-149.

OSTERMAN, E., TYAGI, V., BUTALA, V., RAHIM, N. & STRITIH, U. 2012. Review of PCM based cooling technologies for buildings. *Energy and Buildings,* 49**,** 37-49.

PACHECO, R., ORDÓÑEZ, J. & MARTÍNEZ, G. 2012. Energy efficient design of building: A review. *Renewable and Sustainable Energy Reviews,* 16**,** 3559-3573.

PAKSOY, H. Ö. 2007. *Thermal energy storage for sustainable energy consumption: fundamentals, case studies and design,* Springer Science & Business Media.

PANAYIOTOU, G. P., KALOGIROU, S. A. & TASSOU, S. A. 2016. Evaluation of the application of Phase Change Materials (PCM) on the envelope of a typical dwelling in the Mediterranean region. *Renewable Energy,* 97**,** 24-32.

PANCHABIKESAN, K., ABARANJI, S., VELLAICHAMY, P. & RAMALINGAM, V. 2017a. Effect of direct evaporative cooling during the charging process of phase change material based storage system for building free cooling application—A real time experimental investigation. *Energy and Buildings,* 152**,** 250-263.

PANCHABIKESAN, K., VELLAISAMY, K. & RAMALINGAM, V. 2017b. Passive cooling potential in buildings under various climatic conditions in India. *Renewable and Sustainable Energy Reviews,* 78**,** 1236-1252.

PANCHABIKESAN, K., VINCENT, A. A. R., DING, Y. & RAMALINGAM, V. 2018. Enhancement in free cooling potential through PCM based storage system integrated with direct evaporative cooling (DEC) unit. *Energy,* 144**,** 443-455.

PANOFSKY, H. A. & DUTTON, J. 1984. Atmospheric Turbulence: Models and Methods for Engineering Applications, 397 pp. John Wiley, New York.

PARAMESHWARAN, R., KALAISELVAM, S., HARIKRISHNAN, S. & ELAYAPERUMAL, A. 2012. Sustainable thermal energy storage technologies for buildings: a review. *Renewable and Sustainable Energy Reviews,* 16**,** 2394-2433.

PARDO, P., DEYDIER, A., ANXIONNAZ-MINVIELLE, Z., ROUGÉ, S., CABASSUD, M. & COGNET, P. 2014. A review on high temperature thermochemical heat energy storage. *Renewable and Sustainable Energy Reviews,* 32**,** 591-610.

PASUPATHY, A. & VELRAJ, R. 2008. Effect of double layer phase change material in building roof for year round thermal management. *Energy and Buildings,* 40**,** 193-203.

PASUPATHY, A., VELRAJ, R. & SEENIRAJ, R. 2008. Phase change material-based building architecture for thermal management in residential and commercial establishments. *Renewable and Sustainable Energy Reviews,* 12**,** 39-64.

PASUPATHY, A. V. & VELRAJ, R. 2006. Phase Change Material Based ThermalStorage for Energy Conservation inBuilding Architecture. *International Energy Journal,* 7.

PATEL, J. H., DARJI, P. & QURESHI, M. 2017. Phase Change Material with Thermal Energy Storage System and Its Applications: A Systematic Review. *Indian Journal of Science and Technology,* 8.

PÉREZ-LOMBARD, L., ORTIZ, J. & POUT, C. 2008. A review on buildings energy consumption information. *Energy and buildings,* 40**,** 394-398.

PIELICHOWSKA, K. & PIELICHOWSKI, K. 2014. Phase change materials for thermal energy storage. *Progress in materials science,* 65**,** 67-123.

PINEL, P., CRUICKSHANK, C. A., BEAUSOLEIL-MORRISON, I. & WILLS, A. 2011. A review of available methods for seasonal storage of solar thermal energy in residential applications. *Renewable and Sustainable Energy Reviews,* 15**,** 3341-3359.

PLUSS. Available: [<http://www.pluss.co.in/>] [Accessed 06/07 2017,].

POMIANOWSKI, M., HEISELBERG, P. & ZHANG, Y. 2013. Review of thermal energy storage technologies based on PCM application in buildings. *Energy and Buildings,* 67**,** 56-69.

PRIETO, C., COOPER, P., FERNÁNDEZ, A. I. & CABEZA, L. F. 2016. Review of technology: Thermochemical energy storage for concentrated solar power plants. *Renewable and Sustainable Energy Reviews,* 60**,** 909-929.

PROMOPPATUM, P., YAO, S.-C., HULTZ, T. & AGEE, D. 2017. Experimental and numerical investigation of the cross-flow PCM heat exchanger for the energy saving of building HVAC. *Energy and Buildings,* 138**,** 468-478.

PY, X., OLIVES, R. & MAURAN, S. 2001. Paraffin/porous-graphite-matrix composite as a high and constant power thermal storage material. *International Journal of heat and mass transfer,* 44**,** 2727-2737.

RABANI, M., KALANTAR, V., FAGHIH, A. K., RABANI, M. & RABANI, R. 2013. Numerical simulation of a Trombe wall to predict the energy storage rate and time duration of room heating during the non-sunny periods. *Heat and Mass Transfer,* 49**,** 1395-1404.

RAJ, V. A. A. & VELRAJ, R. 2010. Review on free cooling of buildings using phase change materials. *Renewable and Sustainable Energy Reviews,* 14**,** 2819-2829.

RAJ, V. A. A. & VELRAJ, R. 2011. Heat transfer and pressure drop studies on a PCM-heat exchanger module for free cooling applications. *International Journal of Thermal Sciences,* 50**,** 1573-1582.

RAJAGOPAL, M. 2014. Studies on free cooling potential and PCM based heat exchanger for thermal management of buildings.

RAJAGOPAL, M., DINESH BABU, R., ANTONY AROUL RAJ, V. & VELRAJ, R. 2016. Investigation on phase change material-based flat plate heat exchanger modules for free cooling applications in energy-efficient buildings. *Advances in Building Energy Research***,** 1-23.

RAJAGOPAL, M., SOLOMON, G. R., JAYASUDHA, C. K. & VELRAJ, R. 2014. Free Cooling Potential and Technology Options for Thermal Energy Management of a Commercial Building in Bangalore City, India. *Energy Engineering,* 111**,** 11-24.

RAO, Z., WANG, S. & ZHANG, Z. 2012. Energy saving latent heat storage and environmental friendly humidity-controlled materials for indoor climate. *Renewable and Sustainable Energy Reviews,* 16**,** 3136-3145.

RATHOD, M. K. & BANERJEE, J. 2013. Thermal stability of phase change materials used in latent heat energy storage systems: a review. *Renewable and Sustainable Energy Reviews,* 18**,** 246-258.

RBIRADAR, N. & CHOUGALE, C. A. 2015. Review on Thermal Energy Storage using Phase Change Materials and Applications.

REARDON, C., MILNE, G., MCGEE, C. & DOWNTON, P. 2011. Your Home Technical Manual, Australia's guide to environmentally sustainable homes. *Institute for Sustainable Futures, University of Technology, Sydney, Australia*.

REGIN, A. F., SOLANKI, S. & SAINI, J. 2008. Heat transfer characteristics of thermal energy storage system using PCM capsules: a review. *Renewable and Sustainable Energy Reviews,* 12**,** 2438-2458.

RIFFAT, S., MEMPOUO, B. & FANG, W. 2013. Phase change material developments: a review. *International Journal of Ambient Energy***,** 1-14.

RIFFAT, S., MEMPOUO, B. & FANG, W. 2015. Phase change material developments: a review. *International Journal of Ambient Energy,* 36**,** 102-115.

RODRIGUES, L. T. 2009. *An Investigati0n Into the Use of Thermal Mass to Improve Comfort in British Housing.*

RODRIGUEZ-UBINAS, E., RUIZ-VALERO, L., VEGA, S. & NEILA, J. 2012. Applications of phase change material in highly energy-efficient houses. *Energy and Buildings,* 50**,** 49-62.

ROUAULT, F., BRUNEAU, D., SEBASTIAN, P. & LOPEZ, J. 2013. Numerical modelling of tube bundle thermal energy storage for free-cooling of buildings. *Applied Energy,* 111**,** 1099-1106.

ROZANNA, D., CHUAH, T., SALMIAH, A., CHOONG, T. S. & SA'ARI, M. 2005. Fatty acids as phase change materials (PCMs) for thermal energy storage: a review. *International Journal of Green Energy,* 1**,** 495-513.

RUBITHERM. Available: [<https://www.rubitherm.eu/>] [Accessed 09/11 2017,].

RUBITHERM. Available: [<https://www.rubitherm.eu/>] [Accessed 06/07 2017,].

RUNSHENG, T., ETZION, Y. & ERELL, E. 2003. Experimental studies on a novel roof pond configuration for the cooling of buildings. *Renewable Energy,* 28**,** 1513-1522.

SADINENI, S. B., MADALA, S. & BOEHM, R. F. 2011. Passive building energy savings: A review of building envelope components. *Renewable and Sustainable Energy Reviews,* 15**,** 3617-3631.

SAFFARI, M., DE GRACIA, A., USHAK, S. & CABEZA, L. F. 2017. Passive cooling of buildings with phase change materials using whole-building energy simulation tools: A review. *Renewable and Sustainable Energy Reviews,* 80**,** 1239-1255.

SALUNKHE, P. B. & SHEMBEKAR, P. S. 2012. A review on effect of phase change material encapsulation on the thermal performance of a system. *Renewable and Sustainable Energy Reviews,* 16**,** 5603-5616.

SAMUEL, D. G. L., NAGENDRA, S. M. S. & MAIYA, M. P. 2013. Passive alternatives to mechanical air conditioning of building: A review. *Building and Environment,* 66**,** 54-64.

SANTAMOURIS, M. 2007. *Advances in passive cooling,* Earthscan.

SANTAMOURIS, M. & ASIMAKOPOULOS, D. 1996. *Passive cooling of buildings,* Earthscan.

SATZGER, P., EXKA, B. & ZIEGLER, F. 1998. Matrix-heat-exchanger for a latent-heat cold-storage. *Proceedings of Megastock_98, Sapporo (Japan).*

SCHLICHTING, H. & GERSTEN, K. 2016. *Boundary-layer theory,* Springer.

SCHOSSIG, P., HENNING, H.-M., GSCHWANDER, S. & HAUSSMANN, T. 2005. Micro-encapsulated phase-change materials integrated into construction materials. *Solar Energy Materials and Solar Cells,* 89**,** 297-306.

SHAO, J., DARKWA, J. & KOKOGIANNAKIS, G. 2015. Review of phase change emulsions (PCMEs) and their applications in HVAC systems. *Energy and Buildings,* 94**,** 200-217.

SHARIFI, A. & YAMAGATA, Y. 2015. Roof ponds as passive heating and cooling systems: A systematic review. *Applied Energy,* 160**,** 336-357.

SHARMA, A., TYAGI, V., CHEN, C. & BUDDHI, D. 2009. Review on thermal energy storage with phase change materials and applications. *Renewable and Sustainable energy reviews,* 13**,** 318-345.

SHARMA, S., BUDDHI, D. & SAWHNEY, R. 1999. Accelerated thermal cycle test of latent heat-storage materials. *Solar Energy,* 66**,** 483-490.

SHARMA, S. D. & SAGARA, K. 2005. Latent heat storage materials and systems: a review. *International Journal of Green Energy,* 2**,** 1-56.

SHIH, T. 1995. A New–Eddy-Viscosity Model for High Reynolds Number Turbulent Flows–Model Development and Validation/T.-H. Shih, WW Liou, A. Shabbir, Z. Yang, J. Zhu. *Computers Fluids***,** 3.

SHRESTHA, S., MILLER, W., STOVALL, T., DESJARLAIS, A., CHILDS, K., PORTER, W., BHANDARI, M. & COLEY, S. Modeling PCM-enhanced insulation system and benchmarking EnergyPlus against controlled field data. Building Simulation 2011: 12th Conference of International Building Performance Simulation Association, Sydney, Australia, 2011.

SHUKLA, A., BUDDHI, D. & SAWHNEY, R. 2008. Thermal cycling test of few selected inorganic and organic phase change materials. *Renewable Energy,* 33**,** 2606-2614.

SILAKHORI, M., NAGHAVI, M. S., METSELAAR, H. S. C., MAHLIA, T. M. I., FAUZI, H. & MEHRALI, M. 2013. Accelerated thermal cycling test of microencapsulated paraffin wax/polyaniline made by simple preparation method for solar thermal energy storage. *Materials,* 6**,** 1608-1620.

SILVA, T., VICENTE, R. & RODRIGUES, F. 2016. Literature review on the use of phase change materials in glazing and shading solutions. *Renewable and Sustainable Energy Reviews,* 53**,** 515-535.

SIMA, J., SIKULA, O., KOSUTOVA, K. & PLASEK, J. 2014. Theoretical Evaluation of Night Sky Cooling in the Czech Republic. *Energy Procedia,* 48**,** 645-653.

SMIL, V. 2016. *Energy transitions: global and national perspectives*, ABC-CLIO.

SOARES, N., COSTA, J., GASPAR, A. & SANTOS, P. 2013. Review of passive PCM latent heat thermal energy storage systems towards buildings' energy efficiency. *Energy and buildings,* 59**,** 82-103.

SOCACIU, L., PLEŞA, A., UNGUREŞAN, P. & GIURGIU, O. 2014. Review on phase change materials for building applications. *Leonardo Electronic Journal of Practices and Technologies***,** 179-194.

SOHEL, M. I., MA, Z., L COOPER, P., ADAMS, J., NICCOL, L. & GSCHWANDER, S. A Feasibility Study of Night Radiative Cooling of BIPVT in Climatic Conditions of Major Australian Cities. Proceedings of Asia-Pacific solar research conference, 2014.

SOLÉ, A., NEUMANN, H., NIEDERMAIER, S., CABEZA, L. F. & PALOMO, E. 2014. Thermal stability test of sugar alcohols as phase change materials for medium temperature energy storage application. *Energy Procedia,* 48**,** 436-439.

SOLOMON, G. R. & VELRAJ, R. 2013. Analysis of the heat transfer mechanisms during energy storage in a Phase Change Material filled vertical finned cylindrical unit for free cooling application. *Energy Conversion and Management,* 75**,** 466-473.

SOUAYFANE, F., FARDOUN, F. & BIWOLE, P.-H. 2016. Phase change materials (PCM) for cooling applications in buildings: A review. *Energy and Buildings,* 129**,** 396-431.

STRITIH, U. & BUTALA, V. 2007. Energy saving in building with PCM cold storage. *International Journal of Energy Research,* 31**,** 1532-1544.

STRITIH, U. & BUTALA, V. 2010. Experimental investigation of energy saving in buildings with PCM cold storage. *International journal of refrigeration,* 33**,** 1676-1683.

STRITIH, U. & BUTALA, V. 2011. Energy savings in building with a PCM free cooling system. *Strojniški vestnik-Journal of Mechanical Engineering,* 57**,** 125-134.

SU, W., DARKWA, J. & KOKOGIANNAKIS, G. 2015. Review of solid–liquid phase change materials and their encapsulation technologies. *Renewable and Sustainable Energy Reviews,* 48**,** 373-391.

SUN, X., SUN, Y., ZHOU, Z., ALAM, M. A. & BERMEL, P. 2017. Radiative sky cooling: fundamental physics, materials, structures, and applications. *Nanophotonics,* 6**,** 997-1015.

SZOKOLAY, S. V. 2014. *Introduction to architectural science: the basis of sustainable design*, Routledge.

TABARES-VELASCO, P. C., CHRISTENSEN, C. & BIANCHI, M. 2012. Verification and validation of EnergyPlus phase change material model for opaque wall assemblies. *Building and Environment,* 54**,** 186-196.

TAKEDA, S., NAGANO, K., MOCHIDA, T. & SHIMAKURA, K. 2004. Development of a ventilation system utilizing thermal energy storage for granules containing phase change material. *Solar Energy,* 77**,** 329-338.

TATSIDJODOUNG, P., LE PIERRÈS, N. & LUO, L. 2013. A review of potential materials for thermal energy storage in building applications. *Renewable and Sustainable Energy Reviews,* 18**,** 327-349.

TEAP. Available: [<http://www.teappcm.com/>] [Accessed 06/07 2017,].

TELKES, M. Thermal storage for solar heating and cooling. Proceedings of the Workshop on Solar Energy Storage Subsystems for the Heating and Cooling of Buildings, Charlottesville (Virginia, USA), 1975.

TELKES, M. Trombe wall with phase change storage material. Proceedings of the 2nd National Passive Solar Conference, Philadelphia, PA, USA, 1978.

TEVAR, J. A. F., CASTAÑO, S., MARIJUÁN, A. G., HERAS, M. R. & PISTONO, J. 2015. Modelling and experimental analysis of three radioconvective panels for night cooling. *Energy and Buildings,* 107**,** 37-48.

THAMBIDURAI, M., PANCHABIKESAN, K. & RAMALINGAM, V. 2015. Review on phase change material based free cooling of buildings—The way toward sustainability. *Journal of Energy Storage,* 4**,** 74-88.

TURNPENNY, J., ETHERIDGE, D. & REAY, D. 2000. Novel ventilation cooling system for reducing air conditioning in buildings.: Part I: testing and theoretical modelling. *Applied Thermal Engineering,* 20**,** 1019-1037.

TURNPENNY, J., ETHERIDGE, D. & REAY, D. 2001. Novel ventilation system for reducing air conditioning in buildings. Part II: testing of prototype. *Applied thermal engineering,* 21**,** 1203-1217.

TYAGI, V. V. & BUDDHI, D. 2007. PCM thermal storage in buildings: a state of art. *Renewable and Sustainable Energy Reviews,* 11**,** 1146-1166.

TYAGI, V. V., BUDDHI, D., KOTHARI, R. & TYAGI, S. K. 2012. Phase change material (PCM) based thermal management system for cool energy storage application in building: An experimental study. *Energy and Buildings,* 51**,** 248-254.

TYAGI, V. V., KAUSHIK, S. C., TYAGI, S. K. & AKIYAMA, T. 2011. Development of phase change materials based microencapsulated technology for buildings: A review. *Renewable and Sustainable Energy Reviews,* 15**,** 1373-1391.

TYAGI, V. V., PANDEY, A. K., BUDDHI, D. & KOTHARI, R. 2016. Thermal performance assessment of encapsulated PCM based thermal management system to reduce peak energy demand in buildings. *Energy and Buildings,* 117**,** 44-52.

VALL, S. & CASTELL, A. 2017. Radiative cooling as low-grade energy source: A literature review. *Renewable and Sustainable Energy Reviews,* 77**,** 803-820.

VATS, G. & VAISH, R. 2014. Phase change materials selection for latent heat thermal energy storage systems (LHTESS): an industrial engineering initiative towards materials science. *Advanced Science Focus,* 2**,** 140-147.

VEERAKUMAR, C. & SREEKUMAR, A. 2016. Phase change material based cold thermal energy storage: Materials, techniques and applications–A review. *international journal of refrigeration,* 67**,** 271-289.

VELRAJ, R., SEENIRAJ, R., HAFNER, B., FABER, C. & SCHWARZER, K. 1999. Heat transfer enhancement in a latent heat storage system. *Solar energy,* 65**,** 171-180.

VENT-AXIA. Available: https://www.vent-axia.com/range/acm100-200-acm250-315 [Accessed 30/03 2018].

VERMA, P. & SINGAL, S. 2008. Review of mathematical modeling on latent heat thermal energy storage systems using phase-change material. *Renewable and Sustainable Energy Reviews,* 12**,** 999-1031.

VOELKER, C., KORNADT, O. & OSTRY, M. 2008. Temperature reduction due to the application of phase change materials. *Energy and Buildings,* 40**,** 937-944.

VOLLER, V. Modeling solidification processes. Mathematical Modeling of Metals Processing Operations Conference, American Metallurgical Society, 1987.

VOLLER, V., BRENT, A. & REID, K. 1988. Computational Modelling Framework for Analysis of Metallurgical Solidification Processes and Phenomena. *The Institute of Metals***,** 378-380.

VOLLER, V. R. & PRAKASH, C. 1987. A fixed grid numerical modelling methodology for convection-diffusion mushy region phase-change problems. *International Journal of Heat and Mass Transfer,* 30**,** 1709-1719.

WAHID, M. A., HOSSEINI, S. E., HUSSEN, H. M., AKEIBER, H. J., SAUD, S. N. & MOHAMMAD, A. T. 2017. An overview of phase change materials for construction architecture thermal management in hot and dry climate region. *Applied Thermal Engineering,* 112**,** 1240-1259.

WANG, X., LU, E., LIN, W., LIU, T., SHI, Z., TANG, R. & WANG, C. 2000. Heat storage performance of the binary systems neopentyl glycol/pentaerythritol and neopentyl glycol/trihydroxy methyl-aminomethane as solid–solid phase change materials. *Energy conversion and management,* 41**,** 129-134.

WANG, X., ZHANG, Y., XIAO, W., ZENG, R., ZHANG, Q. & DI, H. 2009. Review on thermal performance of phase change energy storage building envelope. *Chinese science bulletin,* 54**,** 920-928.

WAQAS, A., ALI, M. & UD DIN, Z. 2015. Performance analysis of phase-change material storage unit for both heating and cooling of buildings. *International Journal of Sustainable Energy***,** 1-19.

WAQAS, A. & DIN, Z. U. 2013. Phase change material (PCM) storage for free cooling of buildings—a review. *Renewable and sustainable energy reviews,* 18**,** 607-625.

WAQAS, A. & KUMAR, S. 2011a. Thermal performance of latent heat storage for free cooling of buildings in a dry and hot climate: An experimental study. *Energy and Buildings,* 43**,** 2621-2630.

WAQAS, A. & KUMAR, S. 2011b. Utilization of latent heat storage unit for comfort ventilation of buildings in hot and dry climates. *International Journal of Green Energy,* 8**,** 1-24.

WEINLÄDER, H., BECK, A. & FRICKE, J. 2005. PCM-facade-panel for daylighting and room heating. *Solar Energy,* 78**,** 177-186.

WMO. 2016. *World Meteorological Organization* [Online]. Available: http://worldweather.wmo.int/en/city.html?cityId=249 & ftp://ftp.atdd.noaa.gov/pub/GCOS/WMO-Normals/TABLES/REG__I/SU/62721.TXT [Accessed 12/5 2016].

XIANG, Y. & GAN, G. 2015. Optimization of building-integrated photovoltaic thermal air system combined with thermal storage. *International Journal of Low-Carbon Technologies,* 10**,** 146-156.

XU, J., WANG, R. Z. & LI, Y. 2014. A review of available technologies for seasonal thermal energy storage. *Solar Energy,* 103**,** 610-638.

XU, X., ZHANG, Y., LIN, K., DI, H. & YANG, R. 2005. Modeling and simulation on the thermal performance of shape-stabilized phase change material floor used in passive solar buildings. *Energy and Buildings,* 37**,** 1084-1091.

YANBING, K., YI, J. & YINPING, Z. 2003. Modeling and experimental study on an innovative passive cooling system—NVP system. *Energy and buildings,* 35**,** 417-425.

YONG, C., YIPING, W. & LI, Z. 2015. Performance analysis on a building-integrated solar heating and cooling panel. *Renewable Energy,* 74**,** 627-632.

YUAN, Y., ZHANG, N., TAO, W., CAO, X. & HE, Y. 2014. Fatty acids as phase change materials: A review. *Renewable and Sustainable Energy Reviews,* 29**,** 482-498.

ZALBA, B., MARíN, J. M., CABEZA, L. F. & MEHLING, H. 2003. Review on thermal energy storage with phase change: materials, heat transfer analysis and applications. *Applied thermal engineering,* 23**,** 251-283.

ZALBA, B., MARíN, J. M., CABEZA, L. F. & MEHLING, H. 2004. Free-cooling of buildings with phase change materials. *International Journal of Refrigeration,* 27**,** 839-849.

ZALEWSKI, L., JOULIN, A., LASSUE, S., DUTIL, Y. & ROUSSE, D. 2012. Experimental study of small-scale solar wall integrating phase change material. *Solar Energy,* 86**,** 208-219.

ZEINELABDEIN, R., OMER, S. & GAN, G. 2018. Critical review of latent heat storage systems for free cooling in buildings. *Renewable and Sustainable Energy Reviews,* 82**,** 2843-2868.

ZEYGHAMI, M., GOSWAMI, D. Y. & STEFANAKOS, E. 2018. A review of clear sky radiative cooling developments and applications in renewable power systems and passive building cooling. *Solar Energy Materials and Solar Cells,* 178**,** 115-128.

ZHANG, H., BAEYENS, J., CÁCERES, G., DEGRÈVE, J. & LV, Y. 2016a. Thermal energy storage: Recent developments and practical aspects. *Progress in Energy and Combustion Science,* 53**,** 1-40.

ZHANG, K., ZHAO, D., YIN, X., YANG, R. & TAN, G. 2018. Energy saving and economic analysis of a new hybrid radiative cooling system for single-family houses in the USA. *Applied Energy,* 224**,** 371-381.

ZHANG, P., XIAO, X. & MA, Z. W. 2016b. A review of the composite phase change materials: Fabrication, characterization, mathematical modeling and application to performance enhancement. *Applied Energy,* 165**,** 472-510.

ZHANG, S. & NIU, J. 2012. Cooling performance of nocturnal radiative cooling combined with microencapsulated phase change material (MPCM) slurry storage. *Energy and Buildings,* 54**,** 122-130.

ZHANG, Y., XU, X., DI, H., LIN, K. & YANG, R. 2006. Experimental study on the thermal performance of the shape-stabilized phase change material floor used in passive solar buildings. *Journal of solar energy engineering,* 128**,** 255-257.

ZHANG, Y., ZHOU, G., LIN, K., ZHANG, Q. & DI, H. 2007. Application of latent heat thermal energy storage in buildings: state-of-the-art and outlook. *Building and Environment,* 42**,** 2197-2209.

ZHAO, D., MARTINI, C. E., JIANG, S., MA, Y., ZHAI, Y., TAN, G., YIN, X. & YANG, R. 2017. Development of a single-phase thermosiphon for cold collection and storage of radiative cooling. *Applied Energy,* 205**,** 1260-1269.

ZHOU, D., ZHAO, C.-Y. & TIAN, Y. 2012. Review on thermal energy storage with phase change materials (PCMs) in building applications. *Applied Energy*, 92**,** 593-605.

ZHU, N., MA, Z. & WANG, S. 2009. Dynamic characteristics and energy performance of buildings using phase change materials: A review. *Energy Conversion and Management,* 50**,** 3169-3181.

ZIVKOVIC, B. & FUJII, I. 2001. An analysis of isothermal phase change of phase change material within rectangular and cylindrical containers. *Solar Energy,* 70**,** 51-61.

Appendix

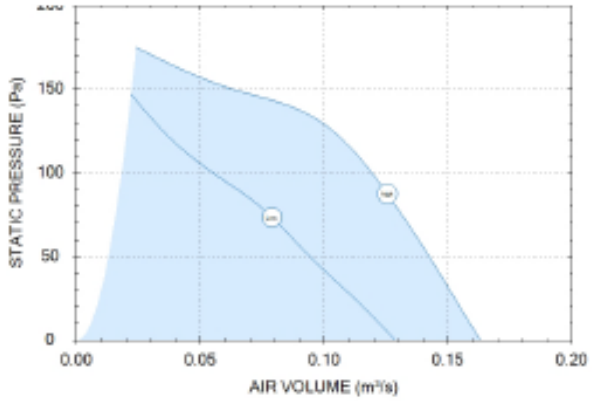
A: Fan specifications (17106010 Vent-Axia)

Vent-Axia®

Domestic & Commercial
Sales Tel: 0844 856 0590
Tech Support Tel: 0844 856 0594

Industrial
Sales Tel: 0844 856
Tech Support Tel: 08

Performance Chart





17106010

Tech Ref File:	
Stock Reference:	17106010
Product Type	Ventilation
Product Range:	In-Line Fans
Impeller:	Mixed Flow
Casing:	ABS thermoplastic
Speed:	2350 rpm
Airstream Temperature:	-30°C to 50°C
dBA:	36

Stated dB(A) levels at 3m with spherical propagation at a reference level of 2 x 1
Specific Fan Power & dB(A) shown are at duty point.

Warranty:	2 Years

Acoustic Information

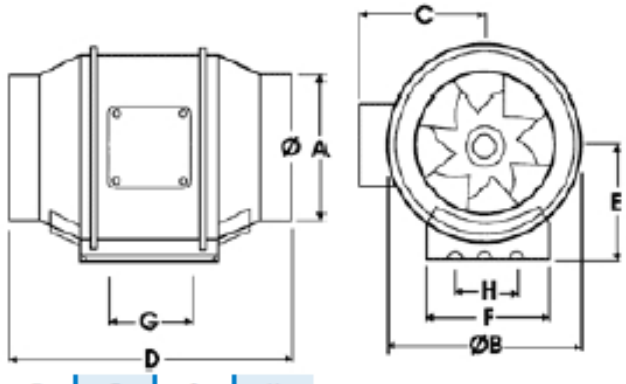
	63	125	250	500	1k	2k	4k	8k	Total	dBA@3m
Inlet	40	49	59	63	59	63	55	47	68	46
Outlet	36	48	54	60	58	61	54	46	65	44
Breakout	26	28	41	45	48	54	41	29	56	36

Sound Power Level Spectra dB (re 10^{-12} Watts) shown @ free air.

Electrical Information

Watts	48
Supply Voltage:	220-240V/1/50Hz
Full Load Current:	0.21 A
Motor Poles:	2
Insulation:	B
Motor IP Rating:	IP44
S.T.O.P. Protection:	Yes
Speed Controllable:	Yes

Dimensions



AØ	BØ	C	D	E	F	G	H
147	200	138	350	118	192	162	178